The RNA helicase Dbp5/DDX19 regulates the ribosomal entry of eRF1-eRF3 and Dom34-Hbs1 in translation termination and cytoplasmic mRNA quality control

Dissertation

for the award of the degree
"Doctor rerum naturalium"
of the Georg-August-Universität Göttingen

within the doctoral program "Biology"
of the Georg-August University School of Science (GAUSS)

submitted by

Christian Beißel

from Hürtgenwald-Bergstein

Göttingen 2020

Members of the Thesis Committee

Prof. Dr. Heike Krebber
Department of Molecular Genetics
Institute for Microbiology and Genetics

Prof. Dr. Ralf Ficner
Department of Molecular Structural Biology
Institute of Molecular Structural Biology

Prof. Dr. Marina Rodnina
Department of Physical Biochemistry
Max Planck Institute for Biophysical Chemistry

Members of the Examination Board

Referee: Prof. Dr. Heike Krebber
Department of Molecular Genetics
Institute for Microbiology and Genetics

2nd Referee: Prof. Dr. Ralf Ficner
Department of Molecular Structural Biology
Institute of Molecular Structural Biology

Further Members of the Examination Board

Prof. Dr. Marina Rodnina
Department of Physical Biochemistry
Max Planck Institute for Biophysical Chemistry

Prof. Dr. Jörg Stülke
Department of General Microbiology
Institute for Microbiology and Genetics

Dr. Oliver Valerius
Department of Molecular Microbiology and Genetics
Institute for Microbiology and Genetics

PD Dr. Wilfried Kramer
Department of Molecular Genetics
Institute for Microbiology and Genetics

Affidavit

I hereby declare that I prepared this doctoral thesis titled "The RNA helicase Dbp5/DDX19 regulates the ribosomal entry of eRF1-eRF3 and Dom34-Hbs1 in translation termination and cytoplasmic mRNA quality control" independently and with no other sources and aids than quoted.

Göttingen, April 2020

Christian Beißel

Table of contents

Table of figures

1.Abstract

Translation is a highly regulated and quality-controlled process ensuring the production of correct polypeptides. Although translation initiation is a major target of regulation, translational control occurs also at the end of translation. Both, translation termination and ribosome recycling are tightly connected and create a pool of ribosomal subunits necessary for multiple rounds of translation. Arriving mRNAs from the nucleus are controlled in the cytoplasm for the presence of correct open reading frames (ORFs). In cases where errors are detected, the regarding faulty mRNAs and the truncated proteins are degraded. The three cytoplasmic quality control pathways are nonsense mediated decay (NMD), no-stop decay (NSD) and no-go decay (NGD). NMD targets mRNAs that contain a premature termination codon (PTC), whereas NSD recognizes transcripts that lack a stop codon. NGD finally senses ribosomes that stall on regular codons, because of strong secondary structures or rare codons.

In this study, we have characterized the role of the DEAD-box RNA helicase 5 (Dbp5/DDX19) in translation termination. Moreover, we have identified a novel role of Dbp5 in the cytoplasmic mRNA quality control.

Current models anticipate that the translation termination factors eRF1 and eRF3 are recruited to terminating ribosomes in a complex. In our studies we used a combination of *in vivo* and *in vitro* experiments to shown that Dbp5 regulates a stepwise assembly of the termination complex. Our experiments indicate that the termination factor Rli1 and eRF3-GDP associate with the ribosome first. Subsequently, Dbp5-ATP delivers eRF1 to the stop codon. Dbp5 dissociates upon ATP-hydrolysis, allowing eRF1 to contact eRF3 and terminate translation. Upon GTP hydrolysis by eRF3, eRF1 is placed in the peptidyl transferase center to initiate peptidyl-tRNA hydrolysis. eRF3-GDP is displaced from the termination complex by Hcr1, which was delivered by eIF3. Rli1 can now bind to eRF1 to mediate the release of the peptide. The interaction of Rli1 and eRF1 enables ATP hydrolysis by Rli1, which leads to the splitting of the ribosomes into their subunits. Therefore, the delivery of eRF1 through Dbp5 prevents a premature dissociation of eRF1 from the ribosome through premature contact with eRF3. This is important, because defects in *DBP5* result in the readthrough of the stop codon and elongated polypeptides. Thus, the stepwise Dbp5 controlled termination complex assembly is essential for correct translation termination.

Defects in *DBP5* do not only affect normal translation. Our data furthermore show a function of this helicase in NMD, as an NMD-reporter construct accumulate in *RAT8* mutants. Importantly, we have shown that Dbp5 not only collaborates with eRF1 and eRF3 in regular translation and NMD, but we could also show that it regulates NSD through delivery of the non-canonical translation termination factors Dom34 and Hbs1. We show that Dbp5

interacts with Dom34 and Hbs1, which is different from regular termination, where Dbp5 does not contact eRF3. This suggests a different functional mode of Dbp5 in NSD and NGD than in regular termination. In fact, Dom34, and Hbs1 show a decreased interaction with each other and the ribosome when Dbp5 is not functional, supporting this view. Importantly, this binding defect culminates in the accumulation of NSD transcripts.

Therefore, Dbp5 does not only govern regular translation termination and NMD via controlling the eRF1 and eRF3 interaction, but it is also an important factor required for NSD and presumable also NGD, which require delivery of Dom34 and Hbs1.

2. Introduction

2.1. Eukaryotic translation termination and ribosome recycling

A rapidly dividing cell is estimated to synthesize 13,000 proteins per second (von der Haar, 2008) and contains ~200.000 ribosomes (Warner, 1999). In consideration of the tremendous resources cells use for translation, approximately more then the half of the energy is used for translation in a logarithmically growing yeast cell, it is important to understand this complex process to get insights into the biology of life. In accord with its critical role in protein synthesis, the translation apparatus adapts mRNA specific protein synthesis on growth conditions and external stimuli. The basic mechanism of translation is well conserved and involves the following steps: initiation, elongation, termination and ribosome recycling. The multiple players necessary for initiation and elongation are well described in several reviews (Dever and Green, 2012; Dever et al., 2016). This work focuses on translation termination and ribosome recycling, which were considered as distinct mechanisms for a long time. However, Shoemaker *et al.* (2011) highlight a key connection between eukaryotic translation termination and recycling, with which the mechanism clearly differs from the independently evolved and heterogeneous processes in bacteria.

2.1.1. Translation termination and recycling

Translation termination takes place as soon as the elongating ribosome reaches a stop codon (UAA, UAG or UGA) on the mRNA and involves stop codon recognition at the ribosomal A-site, subsequent hydrolysis of the P-site peptidyl-tRNA and finally the release of the polypeptide chain (Jackson et al., 2012). Subsequently, the post-termination complex is recycled and provides a pool of 40S and 60S subunits for additional rounds of translation (Dever and Green, 2012). In eukaryotes two essential release factors are well known to mediate translation termination. The eukaryotic release factor 1 (eRF1) and eukaryotic release factor 3 (eRF3) encoded by the *SUP45* and *SUP35*, respectively in *S. cerevisiae* are the main players in translation termination (von der Haar and Tuite, 2007). All three kinds of stop codons are recognized and bound by eRF1, which subsequently promotes hydrolysis of the peptidyl-tRNA in the ribosomal peptidyl transferase center (PTC). The interaction between eRF1 and eRF3 is critical for stop codon recognition (Wada and Ito, 2014) and GTP hydrolysis by eRF3 enhances translation termination efficiency (Salas-Marco and Bedwell, 2004). Upon GTP hydrolysis eRF3 dissociates from eRF1 and Ribonuclease L inhibitor 1 (Rli1) is able to bind to eRF1. Binding of Rli1 (ABCE1 in human), an ABC-family ATPase, promotes eRF1 mediated hydrolysis of the peptidyl-tRNA and ultimately leads to the release of the ribosomal subunits (Shoemaker and Green, 2011).

2.1.2. The eukaryotic release factors eRF1 and eRF3

In contrast to bacteria, which contain the two release factors RF1 and RF2, eRF1 is the only class I release factor in eukaryotes and as such capable of recognizing all three termination codons (Jackson et al., 2012).

The structure of eRF1 mimics a tRNA and is composed of three domains (Song et al., 2000; Taylor et al., 2012) (Fig 1). The N-terminal domain with its conserved TASNIKS and YxCxxF motifs is required for recognizing all three termination codons (Bertram et al., 2000). The central domain or domain M with its methylated GGQ motif promotes hydrolysis of the peptidyl-tRNA bond (Heurgué-Hamard et al., 2005) and the C-terminal domain interacts with the class II release factor eRF3 (Blanchet et al., 2015; Conard et al., 2012).

In yeast, a temperature sensitive mutant (*sup45-2*) of eRF1 was described, which loses the ribosome binding ability upon a temperature shift to the non-permissive temperature of 37°C. The temperature sensitivity of the mutant is caused by an Ile222Ser missense mutation, which is located within the β8 motif of the M domain (Song et al., 2000; Stansfield et al., 1995). This binding defect results in a translation termination defect as the peptidyl-tRNA hydrolysis is disturbed (Stansfield et al., 1997).
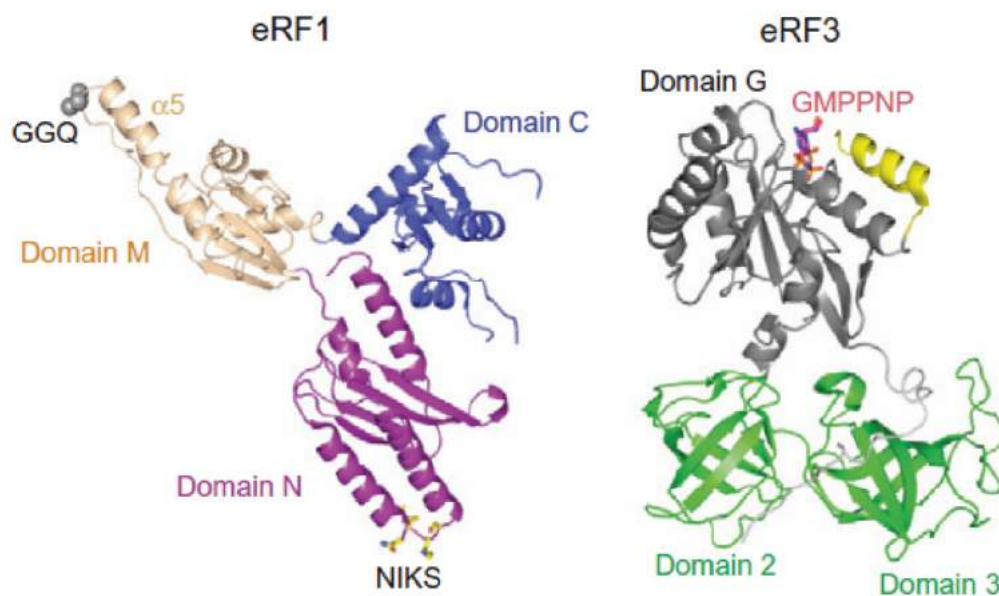
Figure 1 - Structure and domains of the eukaryotic release factors eRF1 and eRF3.
The ribbon structure of human eRF1 and eRF3 are shown. For both proteins, their different domains and important motifs are displayed. Adopted from Jackson *et al.* (2012)*.*

The eRF3 protein consists of an essential C-terminus and a dispensable N-terminus that is capable to elicit the prion [*PSI*+] activity of eRF3 (Jackson et al., 2012). The C-terminal region contains the domain 1 or G and the β-barrel domains 2 and 3 (Fig 1). Domain 1 is necessary for the binding of GTP and shows structural similarities to the corresponding domains in bacterial RF3 and in the eukaryotic elongation factor eEF1A (Kong et al., 2004). Domains 2 and 3 contribute to the binding to eRF1 (Paushkin et al., 1997). Interestingly,

the N-terminal domain is required for the interaction with the poly(A)-binding protein Pab1, although it is dispensable for termination (Kushnirov et al., 1988; Stansfield et al., 1997; Uchida et al., 2002). In mammals, the gene duplication of eRF3 leads to two different variants that differ in the length of their N-termini, called eRF3a (GSPT1) and eRF3b (GSPT2) (Hoshino et al., 1998). Binding of eRF3 to eRF1 increases its binding affinity to GTP (Pisareva et al., 2006). Because, both eRF1 and 80S ribosomes are required for the stimulation of the GTPase activity of eRF3 (Frolova et al., 1996), GTP hydrolysis should occur at the ribosome after eRF1 binding.

2.1.3. The iron sulfur containing ATP-binding cassette protein Rli1

Rli1 was originally identified as an inhibitor of the ribonuclease RNase L, which was characterized as a protein that is activated by the interferon system in response to viral infections in mammalian cells (Bisbal et al., 1995). However, an additional function of Rli1 in translation termination is described, where its main function was shown to be in splitting the ribosome into its subunits at the end of translation (Khoshnevis et al., 2010; Pisarev et al., 2010; Shoemaker et al., 2011).

The yeast Rli1 protein has 68% amino acid identity with human ABCE1 (Dean and Annilo, 2005). It comprises a cysteine-rich N-terminal domain, which carries two cubic [4FE-4S] clusters, followed by two nucleotide binding domains (NBDs) arranged in the typical head-to-tail orientation (Kispal et al., 2005). These two ATP binding cassettes (ABC) share high sequence homology with members of the ABC protein family and are connected by a unique hinge domain (Barthelme et al., 2011; Chen et al., 2006) (Fig 2). Rli1 is essential and mutations in conserved motifs involved in ATP binding and hydrolysis are lethal (Barthelme et al., 2007; Dong et al., 2004; Karcher et al., 2005). The ADP-bound and nucleotide-free states are in an open conformation and ATP binding induces a conformational change required for closure of the nucleotide binding site (Chen et al., 2003; Karpowich et al., 2001). It is assumed that Rli1 converts the chemical energy of ATP hydrolysis into a tweezers-like motion of the NBDs that could be transferred to interaction partners as this is characteristic for ABC-proteins (Chen et al., 2003; Karcher et al., 2005). Addition of the non-hydrolysable ATP analogue AMPPNP arrests Rli1 in a conformation that associates efficiently with the 40S but not with the 60S ribosomal subunit (Andersen and Leevers, 2007; Dong et al., 2004; Kispal et al., 2005).

There is no homolog of Rli1 known in bacteria, but the protein is highly conserved in eukaryotes and archaea (Chen et al., 2006; Kispal et al., 2005). However, for the known interaction partner of Rli1 in higher eukaryotes, RNase L, no orthologue is present in either lower eukaryotes or in archaebacteria.
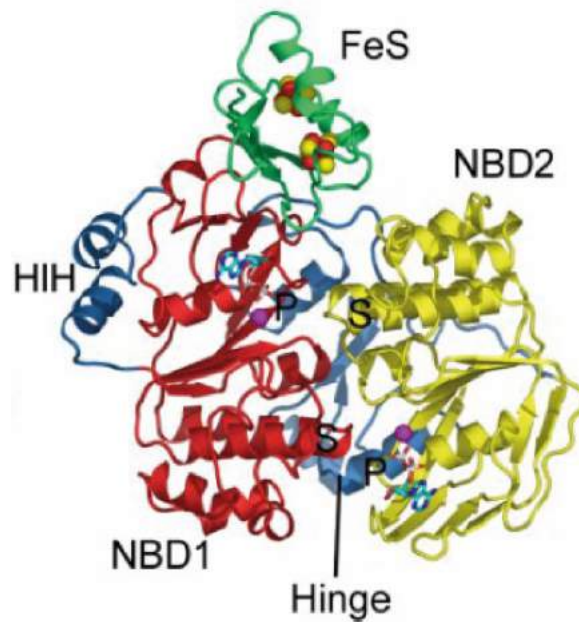
Figure 2 - Structural overview and conformation of *Pyrococcus abysii* ABCE1.
Top-view of *pab*ABCE1 in a stereo plot of a ribbon representation. The Fe-S domains bound to iron (red) and sulfur (yellow) are shown in green. The two nucleotide binding domains NBD1 and NBD2 are indicated in yellow (NBD2) and red (NBD2). The P-loop/Walker A motif is highlighted by **P**, while the signature motif is indicated by **S**. Furthermore, the helix-loop-helix insertion of NBD1 (blue) and the hinge domain (pale blue) are shown. Adopted from Karcher *et al.* (2008).

Yarunin *et al.* (2005) showed that the majority of Rli1 is bound to 40S subunits, 80S ribosomes and polysomes under low-salt conditions. Furthermore, depletion of Rli1 in yeast leads to processing and export defects of the large and small ribosomal subunits. In accord, depletion of Nar1, required for incorporation of Fe-S clusters into Rli1, affects nuclear accumulation of pre-ribosomal subunits. Taken together with the binding of Rli1 to late 20S and 7S pre-rRNAs, an additional function in late ribosome biogenesis of Rli1 is probable (Kispal et al., 2005; Yarunin et al., 2005).

A further possible function of Rli1 might be in translation initiation. Dong *et al.* (2004) showed that Rli1 in yeast associates with eukaryotic translation initiation factors *in vivo*, such as eukaryotic initiation factor 5 (eIF5), eukaryotic initiation factor 3 (eIF3) and with subunits of the eIF3. Moreover, depletion of Rli1 leads to reduced protein synthesis and polysome run-off, as well as to fewer polysomes. Additionally, the interaction of the 40S subunit with the eukaryotic initiation factor 2 (eIF2) and eukaryotic initiation factor 1 (eIF1) was markedly decreased if Rli1 is not functional, indicating a role in the assembly of 43S pre-initiation complexes (Dong et al., 2004; Kispal et al., 2005).

Its main function, however, is in ribosome splitting. Pisarev *et al.* (2010) showed that Rli1 is involved in the dissociation of the ribosome after translation termination, which is also termed ribosome recycling. For ribosomal splitting, Rli1 requires also the canonical translation termination factors eRF1 and eRF3 (Khoshnevis et al., 2010; Rodnina, 2010; Shoemaker et al., 2011). To separate the ribosomal subunits, Rli1 uses its tweezers-like

movement, which is generated through ATP-hydrolysis. In addition to its function in regular translation termination, Rli1 is also involved in separating the ribosomal subunits of empty or stalled ribosomes on mostly defective transcripts in no-go decay (NGD) and no-stop decay (NSD). In contrast to regular termination, in which Rli1 interacts with eRF1 and eRF3, here it requires the eRF1-eRF3 paralogues Dom34 (pelota in humans) and Hbs1 (Pisareva et al., 2011; Shoemaker et al., 2011).

2.1.4. Current model of translation termination and recycling

Termination occurs when the ribosome reaches the end of the open reading frame (ORF) and a stop codon enters the A-site. Upon arrival of the elongating ribosome at the stop codon current models assume that the ternary complex eRF1-eRF3-GTP binds to the A-site of pre-TCs (termination complex). This binding likely results in conformational changes in pre-TCs that induces a 2-nt forward shift of their toe-print (Alkalaeva et al., 2006) allowing the stop codon to reach the P1 pocket of eRF1 (Blanchet et al., 2015). This mode of rearrangements has been supported by crystal structures of pre-TCs (Cheng et al., 2009; Song et al., 2000). Binding of the complex to the 80S ribosome stimulates the GTPase activity of eRF3 (Frolova et al., 1996). GTP hydrolysis of eRF3 induces further conformational changes in eRF1 that enable the GGQ motif of its M domain to enter the PTC. This conformation is able to mediate the subsequent peptidyl-tRNA hydrolysis, which is abrogated if eRF3 is bound to GMPPNP instead of GTP (Alkalaeva et al., 2006). Effective peptidyl-tRNA hydrolysis, is further supported by an interaction of Rli1 with eRF1, which is conducted via the NBD2 of Rli1 and the C-terminus of eRF1 (Becker et al., 2012; Preis et al., 2014; Shoemaker et al., 2011). Moreover, depletion of Rli1 causes increased readthrough activity of stop codons in a dual reporter assay, indicating a connecting role of Rli1 in translation termination and recycling. This is further supported by nonsense suppression assays in which it was shown that overexpression of *RLI1* can compensate the readthrough activity of translation termination factor mutants (Khoshnevis et al., 2010). Interestingly, Rli1 cannot interact with eRF1 on ribosomal complexes, if eRF3 is sterically fixed in its GTP-bound form (e.g. with GMPPNP) (Pisarev et al., 2010). Thus, a model in which Rli1 is not able to bind to eRF1 before eRF3 leaves the post-TC complex is likely. In addition, even though Rli1 binds effectively to the 40S ribosomal subunit in its ATP-bound form, this interaction is not sufficient to enhance the NTPase activity of Rli1. This was only observed for the interaction with eRF1 bound to post- and pre-TCs (Pisarev et al., 2010). Furthermore, it was shown, that only in the presence of ATP but not ADP or AMPPNP, Rli1 is able to disassemble eRF1 bound post-TCs (Pisarev et al., 2010). This led to the suggestion, that the ATPase activity of Rli1 and its binding to eRF1 are requirements for splitting post-terminated ribosomes into their subunits and that the mechanical work of Rli1

is a prerequisite for efficient recycling (Pisarev et al., 2010). This model shows similarities between the eukaryotic and bacterial ribosome recycling, whereby bacteria use the recycling factor RRF/EG-G and its GTP hydrolysis for phosphate release and subunit dissociation (Savelsbergh et al., 2009). According to the presented data, the following model for translation termination and ribosome recycling mediated by eRF1, eRF3 and Rli1 was proposed:

As soon as the ribosome reaches a stop codon, it is assumed that eRF1-eRF3-GTP as a ternary complex is recruited to the free A-site of the ribosome (Fig 3). GTP hydrolysis by eRF3 causes a conformational change of eRF1 that places the GGQ motif in the PTC. Furthermore, dissociation of eRF3 allows Rli1 to take over the binding site of eRF1 and stabilize eRF1 in its favorable conformation (Brown et al., 2015). Subsequently, eRF1 acts as peptidyl-tRNAse and releases the peptide from the ribosome.
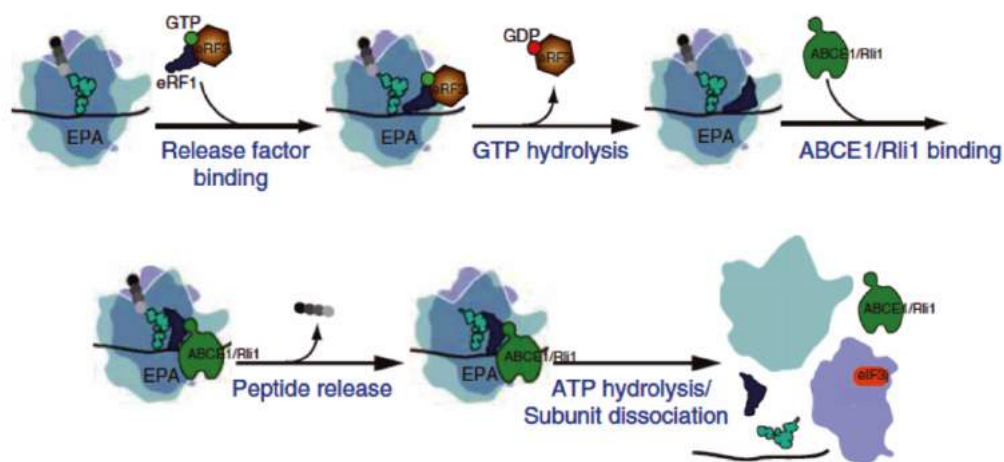
Figure 3 - Model of translation termination and ribosome recycling.
Upon arrival of the 80S ribosome at the stop codon the A-site is free. Thus, eRF1 (blue) and eRF3 (brown) together with GTP (green) are recruited in a ternary complex to the ribosomal A-site and eRF1 recognizes the stop codon. GTP-hydrolysis of eRF3 leads to the proper positioning of eRF1 in the peptidyl-transferase center. Subsequently, ABCE1/Rli1 (green) is able to bind to eRF1 at the same binding site of eRF3 and locks eRF1 in its favorable position. That allows eRF1 to hydrolyze the peptidyl-tRNA (cyan) and the polypeptide is released. Subsequently, Rli1 mediates the ATPase dependent splitting of the ribosomal subunits in association with eRF1. The subunits are directly occupied by eIF3j to avoid subunit rejoining. Modified from Dever and Green (2012).

While the binding of Rli1 to eRF1 and the ribosome induces its ATPase activity, the resulting tweezers-like motion of Rli1 separates the ribosomal subunits. In detail, those post-termination ribosomes are split into free 60S subunits, the deacylated tRNA and mRNA-bound 40S subunit. Therefore the mechanical driving force of Rli1 that disrupts some intersubunit bridges during recycling (Barthelme et al., 2011; Nürenberg and Tampé, 2013; Pisarev et al., 2010) and eRF1 and eRF3 are sufficient to mediate translation termination shown by a kinetic *in vitro* analysis (Shoemaker and Green, 2011). However, *in vivo* several additional factors have been identified to be involved in translation termination. Therefore, the situation in cells is more complicated and has additional layers of regulation.

Several findings point to a connection between initiation, termination and recycling in translation. Poly uridylate binding 1 (Pub1) was shown to interact with the N-terminal prion domain of eRF3, but it binds independently of eRF1 and eRF3 to the ribosome. Lack of Pub1 decreases the efficiency of nonsense readthrough in different nucleotide surroundings (Urakov et al., 2017). Furthermore, several mutations in eIF3 reduce the rate of stop codon readthrough and these mutants genetically interact with mutant eRFs (Beznosková et al., 2013). Moreover, deletion of the high copy suppressor of Rpg1 (Hcr1), which is not considered as a *bona fide* eIF3 subunit anymore, increases readthrough and accumulates eRF3 in heavy polysomes (Beznosková et al., 2013, 2015). Additionally, Schuller *et al.* (2017) described that ribosomes accumulate at stop codons and in the 3' UTR in the absence of the eukaryotic initiation factor 5 A (eIF5A). Moreover, adding recombinant eIF5A in a reconstituted translation system increases the rate of peptidyl-tRNA hydrolysis more than 17-fold. Another interesting finding is, that Rli1 can bind Hcr1 (Khoshnevis et al., 2010). Furthermore, the dissociation efficiency of Rli1 and the subsequent release of tRNA and mRNA from recycled 40S subunits is enhanced by the presence of eukaryotic initiation factor 6 (eIF6) and eukaryotic initiation factors 1, 1A and 3 (Jackson et al., 2010; Pisarev et al., 2010; Si et al., 1997). Most surprising, however was the discovery, that the mRNA-export factor Dbp5 is required for translation termination (Bolger et al., 2008; Gross et al., 2007) (see also chapter 2.3.2).

Taken together, it seems that not only translation termination and ribosome recycling are tightly connected steps in translation, but also initiation, termination and recycling are functionally linked. Thus, the identification of the functions of the additional factors required for translation in vivo is essential to get the full picture and the regulatory layers that are important in nature.

2.2. Cytoplasmic mRNA surveillance systems

Eukaryotic mRNAs have to pass several different quality control checkpoints to ensure the production of correct polypeptides. Nuclear quality control monitors 5' capping, 3' polyadenylation and splicing and allows nuclear export through recruitment of export factors (Doma and Parker, 2007; Soheilypour and Mofrad, 2018; Zander et al., 2016).

The cytoplasmic quality control of mRNAs is a co-translational process that tests the presence of an intact ORF. If a ribosome stalls because of secondary structures (e.g. sequence of rare codons or stem loops) or because a truncated mRNAs that lacks a stop codon altogether, the mRNA and truncated protein are degraded through NGD or NSD. If the mRNA contains a premature stop codon e.g. due to splicing defects, these transcripts are eliminated via the nonsense mediated decay (NMD) (Lykke-Andersen and Bennett, 2014; Mühlemann and Jensen, 2012).

If a ribosome never reaches a correct termination codon, it is useful that this error is detected at an early time point to avoid accumulation of defective proteins (Pechmann et al., 2013). To ensure this, cells tag such faulty proteins for degradation already during translation.

2.2.1. Nonsense mediated decay (NMD)

Nonsense mediated decay factors recognize and typically degrade mRNAs with translation termination codons that are classified as premature termination codon (PTC). A major group of transcripts containing a PTC originates from unspliced mRNAs, indicating that NMD might act as a fail-save mechanism for nuclear splicing (He et al., 1993; He et al., 2003). However, in multicellular organisms NMD is not only part of the cellular quality control system, but also necessary to dynamically adjust their transcriptomes to varying physiological conditions. It is part of the maturation pathway of lymphocytes (Wang et al., 2002) and plays a crucial role in several developmental stages (Medghalchi, 2001; Metzstein and Krasnow, 2006). Although several models of NMD are discussed, in yeast the model shown in Fig 4 is currently widely accepted.
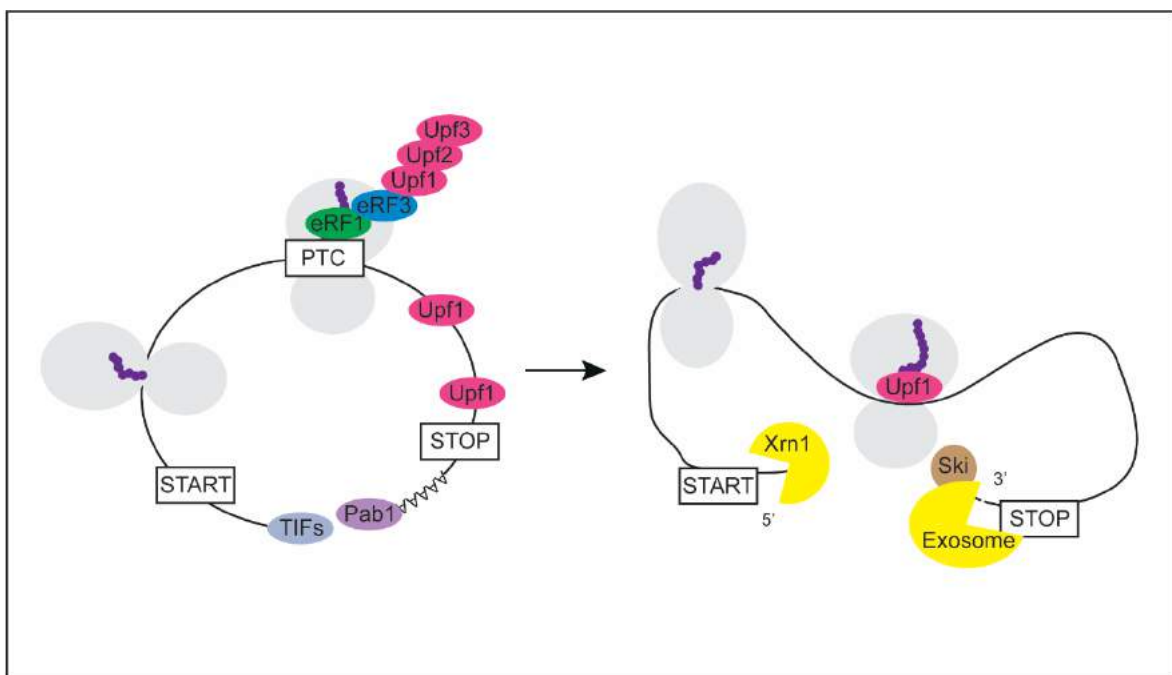
Figure 4 - NMD initiation in *S. cerevisiae*.
Upf1 binds nonspecifically to every mRNA and remains bound if the ribosome terminates at a PTC and not RTC (regular termination codon). Thus, eRF3 and Upf1 interact and thereby recruit Upf2 and Upf3. Recruitment of the Upf-complex inhibits further translation and recruit downstream factors that promote rapid degradation of the mRNA. Xrn1 act from 5' to 3' and the Ski complex and the exosome degrade the PTC-containing mRNA from 3' into 5' direction. Modified from Beißel *et al.* (2020).

The proteins <u>n</u>uclear <u>a</u>ccommodation of <u>m</u>itochondria 7, (NAM7 but more frequently called Upf1), <u>n</u>onsense <u>m</u>ediated mRNA <u>d</u>ecay 2 (NMD2, but more frequently named Upf2) and <u>up f</u>rameshift 3 (Upf3), are the master regulators of NMD and conserved in all studied

eukaryotes (Kervestin and Jacobson, 2012; Schweingruber et al., 2013). Upf1 is composed of a helicase domain, two RecA-like domains forming the helicase core and two regulatory domains called 1B and 1C. The ability of Upf1 to recognize PTC containing mRNAs depends on its ATPase and helicase activities (Franks et al., 2010; Kashima et al., 2006; Weng et al., 1996). It also has a cysteine histidine rich (CH) domain, which is essential for the interaction with the C-terminal domain of Upf2 (Dehecq et al., 2018). Upf2 instead connects Upf1 with Upf3 with the aid of one of its MIF4G domains that binds to Upf3 (He and Jacobson, 1995; He et al., 1997; Mendell et al., 2000). Upf3 contains both, a nuclear localization signals (NLSs) as well as a nuclear export signals (NESs) and shuttles between nucleus and cytoplasm (Shirley et al., 1998). Several groups could show that inhibition of translation elongation via cycloheximide treatment or translation mutants also affects NMD (Peltz et al., 1992; Zhang et al., 1997; Zuk and Jacobson, 1998). Additionally, stop codon recognition by eRF1 and eRF3 is a perquisite for activation of NMD. These results, corroborate that NMD requires translation termination as a starting point for its initiation (Kervestin and Jacobson, 2012).

Current models suggest that the PTC of nonsense mRNAs is initially recognized by the canonical translation termination factors eRF1 and eRF3. How the surveillance machinery distinguishes between a PTC and a regular termination codon (RTC) is still a matter of debate. Two models are considered as the most likely. The first is the faux-UTR model, which is based on the observation that elongated 3'UTRs of mRNAs are sensed by the cell (Muhlrad and Parker, 1999). In normal translation termination, the poly(A) binding protein Pab1 is in close proximity to eRF3, whereas in premature termination the lack of eRF3 and Pab1 interaction allows the binding of Upf1 to eRF3 (Brogna and Wen, 2009). The second proposed model is the marking model, that assumes that a PTC does not only differ from a regular termination codon (RTC) in its distance to the poly(A) tail but also in the protein composition on the 3' UTR. Downstream sequence elements (DSEs) in yeast are occupied by regulatory factors, which are removed by the translating ribosome (Peltz et al., 1993; Ruiz-Echevarría et al., 1998). If these regulatory factors are still bound to the mRNA, NMD is triggered. Similarly, intron splicing leads in higher eukaryotes to the deposition of exon junction complexes (EJCs), that have to be removed by the ribosome to prevent that NMD is triggered (Lykke-Andersen and Jensen, 2015). When a stop codon is reached, the Upf protein complex is recruited to the termination complex and stabilized to trigger mRNA degradation. He *et al.* (2003) and Muhlrad and Parker (1994) could show that NMD targets are degraded by the 5´-3´ decapping pathway and exoribonuclease 1 (Xrn1) catalyzed RNA degradation. Furthermore, deadenylation and 3'-5' decay by the exosome and the Ski complex were also reported to degrade NMD targets (Mitchell and Tollervey, 2003).

2.2.2. Dom34 and Hbs1

No-stop decay (NSD) and no-go decay NGD are part of the cytoplasmic mRNA co-translational quality control surveillance system and degrade mRNAs lacking a stop codon and mRNAs with translation inhibiting secondary structures. The yeast protein duplication of multilocus region (Dom34) and its co-factor HSP70 subfamily B suppressor (Hbs1) play a crucial role in NSD and NGD. As such, both proteins and their human homologs called Pelota and HBS1 are broadly conserved in archaea and eukaryotes, albeit with the exception that the translational GTPase Hbs1 seems to be functionally replaced by the related GTPase *a*EF1 in *archaea* (Kobayashi et al., 2010). Hbs1 is a member of the translational GTPase family that includes the eukaryotic eEF1A and eRF3 proteins. eEF1A delivers tRNAs to the ribosome and eRF3 was suggested to deliver eRF1 to the ribosome (Dever and Green, 2012; Jackson et al., 2012). These proteins bind their interaction partners (eEF1A + tRNA, eRF3 + eRF1 and Hbs1 + Dom34) in a GTP dependent manner at distinct states of the ribosome. Hbs1 has a paralogue, super killer 7 (Ski7), that arose from gene duplication in yeast (Marshall et al., 2018).
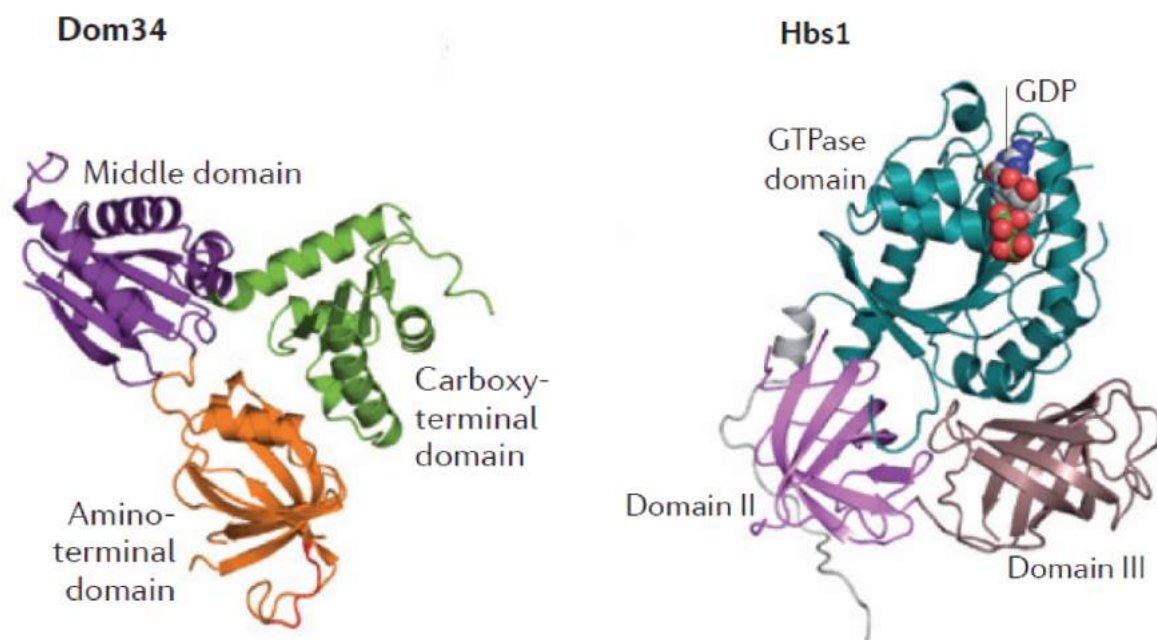
Figure 5 - Structures of Dom34 and Hbs1.
Ribbon representation of *Saccharomyces cerevisiae* Dom34 (left) and Hbs1 bound to GDP (right). Modified from Graille and Seraphin (2012).

As a member of the eEF1A protein family, it is not surprising that both Hbs1 and eRF3 share a conserved part consisting of the G domain, domain I and II and a nonconserved N-terminal domain (Becker et al., 2011).

Structural analyses of Pelota (Dom34) from *Thermoplasma acidophilum* (*Ta*Pelota) revealed that the protein possesses a tripartite structure that is organized in a cloverleaf-like shape (Lee et al., 2007) (Fig 5). The overall structure of the central and C-terminal

domain of Dom34 is similar to that of eRF1, but the two proteins differ in in their N-terminal domains (Lee et al., 2007). This indicates that the domains in eRF1, which are important for the interaction with eRF3, are structurally conserved in Dom34, and represent the binding domain for Hbs1. The binding of Dom34 to Hbs1 enhances the affinity of Hbs1 to GTP (Graille et al., 2008). However, as described earlier (chapter 2.1.2), the NTD of eRF1 is thought to recognize the stop codons in the ribosomal A-site via its conserved NIKS loop, while Dom34 lacks this loop. Furthermore, Dom34 misses the conserved GGQ motif required for catalysis of peptide release.

2.2.3. No-go-decay (NGD)

NGD leads to ribosome stalling, that can turn out to be harmful, because it might change protein expression or involves changes in protein conformation or function. It occurs due to secondary structures like stem-loops (SL), rare codons or positively charged nascent NCs polypeptides (Chen et al., 2010; Doma and Parker, 2006; Van Den Elzen et al., 2010; Kobayashi et al., 2010; Kuroha et al., 2010; Tsuboi et al., 2012). As soon as the ribosome stalls on an mRNA, the endonucleolytic cleavage in close proximity to the stalled ribosome results in two mRNA fragments (Van Den Elzen et al., 2010; Passos et al., 2009; Tsuboi et al., 2012). The 3' fragment is rapidly degraded via the 5'-3' directed Xrn1 exoribonuclease. The 5'-end of transcripts, however, requires in addition Dom34-Hbs1 and Rli1 action before degradation of the 3'-ends of the endonucleolytically cleaved mRNAs can occur. The released 3' end of the 5' fragment is subsequently degraded via the exosome (Tsuboi et al., 2012).

2.2.4. No-stop decay (NSD)

mRNA maturation, in particular splicing, is of importance for the generation of alternative splice variants and responsible for an increased variation of gene products. All processing events are highly regulated, but given the complexity of the reactions, errors can occur. For instance, polyadenylation usually occurs at the 3' end of mRNA, but can be incorporated within an open reading frame at cryptic sites, resulting in mRNAs that lack a stop codon. Such mRNAs are called nonstop mRNAs (Frischmeyer et al., 2002; Van Hoof et al., 2002; Ozsolak et al., 2010; Pelechano et al., 2013). Another source of non-stop mRNAs is generated through endonucleolytic cleavage during NMD in higher eukaryotes. These RNAs parts comprise a proper 5'-end, but lack both a stop codon and poly-(A)-tail (Lykke-Andersen and Jensen, 2015). NSD was first identified by using artificial model substrates. However, ribosome profiling in the presence and absence of Dom34, identified the *HAC1*,

the homologous of Aft/Crb1 encoding protein transcript as endogenous substrate for NSD (Guydosh and Green, 2014).

In general, if the ribosome translates to the end of a truncated mRNA, the A-site is not mRNA bound and leads to the degradation of this aberrant transcript and the ribosome-associated polypeptide. Biochemical analysis with a reconstituted translation system suggested a direct role of Dom34-Hbs1 in recognizing these complexes and in release of the mRNA, but found no indication for an influence of these proteins in peptide release (Pisareva et al., 2011; Shoemaker et al., 2010). Studies in cells of *Drosophila melanogaster* showed that Rli1 is also necessary for resolving stalled ribosomes on truncated mRNAs from the translation machinery (Frischmeyer et al., 2002). Additionally, the fungi specific GTPase Ski7, which recruits the Ski complex and subsequently the exosome is essential for 3'-5' mediated degradation (Frischmeyer et al., 2002; van Hoof et al., 2000; Van Hoof et al., 2002; Tsuboi et al., 2012).

2.2.5. Ribosome-associated quality control (RQC)

Considering that Dom34 lacks the GGQ motif required to hydrolyze the ester bond between the peptide and tRNA, an additional pathway is required to degrade the nascent peptidyl-tRNA. The ribosome-associated quality control (RQC) machinery recognizes nascent chains (NCs) associated with stalled ribosomes and promotes the ubiquitylation and degradation of stalled NCs at the 60S subunit (Bengtson and Joazeiro, 2010; Brandman et al., 2012; Shao and Hegde, 2014; Shao et al., 2015). The yeast E3 ubiquitin ligase, called RING domain mutant killed by Rft1 deletion (Rkr1, but more frequently called Lnt1), was identified to ubiquitinylate the product of nonstop mRNA. Ubiquitylation by Ltn1 (Listerin in mammals) makes the NC accessible for degradation by the proteasome (Bengtson and Joazeiro, 2010). In parallel, a search for genetic interactions with *LTN1* mutants and mRNA decay pathway mutants uncovered mutations in ribosome quality control 1 (Rqc1), ribosome quality control complex 2 (Rqc2) and the cell division cycle 48 (Cdc48) complex (Brandman et al., 2012; Defenouillère et al., 2013). Together with the 60S subunit, these factors form the 60S-associated ribosome quality control complex (RQC). Recruitment of Cdc48 to the ribosome requires Rqc1, Rqc2, Ltn1 and an ubiquitinylated NC, whereby Cdc48 finally delivers the NC to the proteasome for degradation (Brandman et al., 2012; Defenouillère et al., 2013).

2.2.6. Current model of no-go and no-stop decay

Shoemaker *et al.* (2011) could show that Rli1 is capable of stimulating ribosome subunit dissociation with either eRF1 or Dom34 in an ATP dependent manner. Furthermore, they revealed that ribosome recycling requires energy because it is inhibited by GTPase deficient eRF3 and Hbs1 or in the presence of a non-hydrolysable GTP analog, GDPPNP. Together with the finding that binding of Dom34 to Hbs1 promotes its GTP binding affinity, a model comparable to normal translation termination is probable. In this model, it is suggested that Dom34 and Hbs1 bind to the ribosome presumably together with GTP in a ternary complex (Becker et al., 2011) (Fig 6). In yeast, the ribosome is marked as stalled by the histone E3 ubiquitin ligase (Hel2, ZNF598 in mammals). Hel2 ubiquitinates uS10 at K6/8 and plays a crucial role in RQC (Garzia et al., 2017; Juszkiewicz and Hegde, 2017; Matsuo et al., 2017; Sundaramoorthy et al., 2017). GTP hydrolysis by Hbs1 accommodates Dom34 into the active site. Thereby, Dom34 could directly interact with the decoding center contacting mRNA, rRNA and uS7. As a consequence the mRNA-tRNA interaction with the ribosome is destabilized (Becker et al., 2011). Interestingly, cryoEM structures indicate that the N-terminal domain of Hbs1 contacts the mRNA entry site (Becker et al., 2011). Following GTP hydrolysis by Hbs1, GDP-Hbs1 dissociates from the complex and Rli1 can take over the binding site of Dom34. In NGD and NSD Rli1 might act with Dom34, like it does in regular termination with eRF1, to lock it in its favorable position for the ATP-dependent splitting of the ribosome. However, in contrast to regular termination, peptide release does not occur (Shoemaker et al., 2011). The released mRNA is rapidly degraded via the Ski complex and the exosome from its 3' end (Kashima et al., 2014). The Ski (Ski2-Ski3-Ski8) complex in yeast is recruited by Ski7 and is required for 3'-5' degradation (Schmidt et al., 2016). The nascent protein is degraded via the ribosome associated quality control pathway. This model coopts in general both NGD and NSD, but there are some notable differences. In NSD the A-site of the ribosome is empty and after recycling of the ribosomes, the mRNA is freely accessible for degradation. In no-go decay the mRNA is occupied by stalled ribosomes and an endonucleolytic cleavage event in close proximity to the ribosome is necessary to generate two different mRNA substrates (Doma and Parker, 2006). Recent work has identified Cue2 as a possible endonuclease involved in NGD (D'Orazio et al., 2019). The 3' fragment is rapidly degraded from the 5' end by Xrn1. After cleavage, Dom34-Hbs1-Rli1 is required for the degradation of the 5' fragment, which is then treated like a no-stop mRNA (Tsuboi et al., 2012).
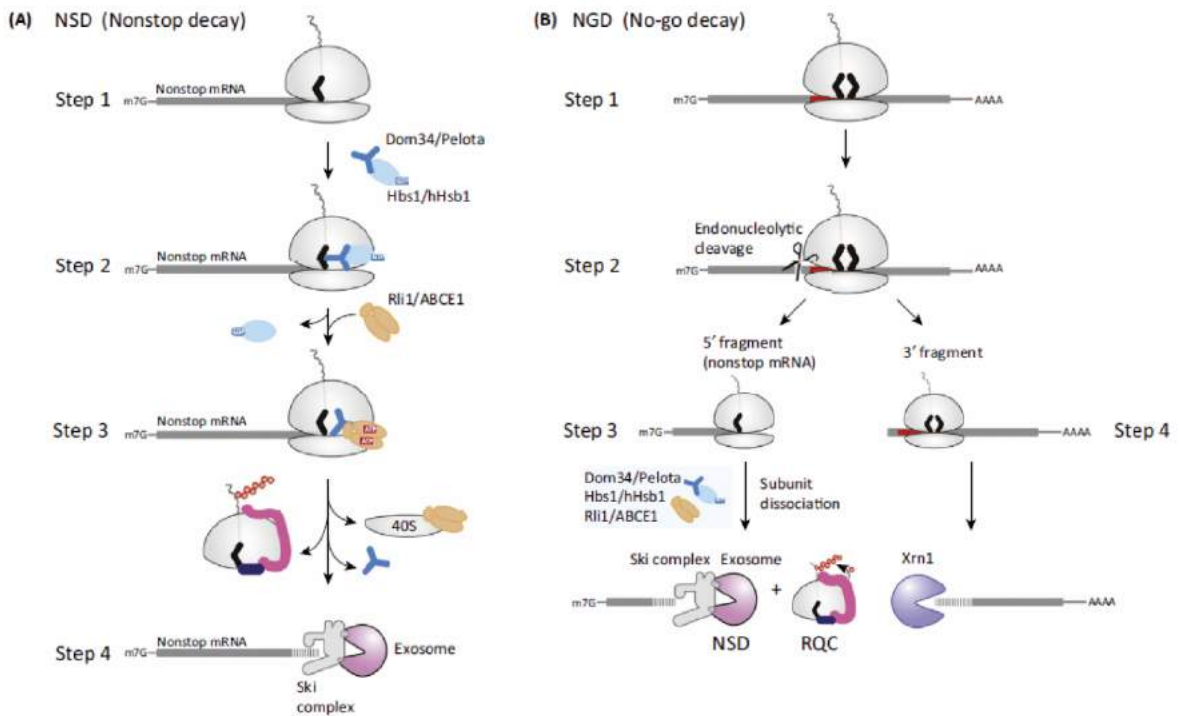
Figure 6- Model for no-stop and no-go decay.
(A) If a ribosome stalls in a poly(A) tail or truncated mRNA, Dom34 together with Hbs1 and GTP is recruited on a ternary complex. Subsequently, GTP hydrolysis by Hbs1 leads to the dissociation of Hbs1 and binding of Rli1 to Dom34. Ribosome splitting by Dom34 in a Rli1-ATP hydrolysis dependent manner leads to the degradation of the truncated protein via the ribosome associated quality control (RQC) system. The mRNA is degraded by the exosome, which is recruited by the Ski complex.
(B) In no-go decay ribosome stalling occurs because of e.g. stem loop structure or a sequence of rare codons within an mRNA. That leads to endonucleolytic cleavage of the mRNA by Cue2 in close proximity to the ribosome and results in two mRNA fragments. The 5' mRNA fragment and truncated protein are degraded similar to no-stop complexes. The 3' fragment of the mRNA is degraded via Xrn1. Modified from Inada (2017).

2.3. The DEAD-Box RNA-helicase Dbp5/Rat8

The DEAD-box protein 5 (Dbp5) is well known for its ATPase dependent remodeling activity on RNA-protein complexes and functions in mRNA export (Schmitt et al., 1999; Snay-Hodge et al., 1998; Tseng et al., 1998; Zhao et al., 2002). Furthermore, Dbp5 is described to mediate tRNA export and physically interacts with components of the transcription factor complex TFIIH in yeast (Estruch and Cole, 2003; Lari et al., 2019). Additionally, Dbp5 was identified to be involved in translation termination and ribosomal maturation (Gross et al., 2007; Neumann et al., 2016). Dbp5 (encoded by *RAT8* (ribonucleic trafficking protein 8) in yeast and *DDX19* in humans) belongs to the helicase superfamily 2 (SF2) and is conserved and essential in all eukaryotes. To fulfill its function, the stimulation by its co-factors GLFG lethal (Gle1) and inositol 1,2,3,4,5,6-hexakisphosphate (IP$_6$), is required (Alcázar-Román et al., 2006; Gross et al., 2007; Neumann et al., 2016; Weirich et al., 2006). The helicase core of Dbp5 is composed of two highly conserved Rec-A-like domains, which are connected by a linker region (Linder and Jankowsky, 2011) (Fig 7). Both RecA-like domains form a cleft

that is capable of ATP hydrolysis in its closed state, while the open state is required for ADP release (Tieg and Krebber, 2013).The helicase core of Dbp5 contains 13 characteristic sequence motifs and the eponymous sequence Asp-Glu-Ala-Asp (DEAD) in motif 2 (Fairman-Williams et al., 2010; Linder and Jankowsky, 2011). Additionally, the unique N-terminal extension of Dbp5 is important for its autoregulation and determines the specificity of the enzyme (Collins et al., 2009). In recent work, an Xpo1- dependent nuclear export signal has been identified in the N-terminal extension of the protein (Lari et al., 2019).
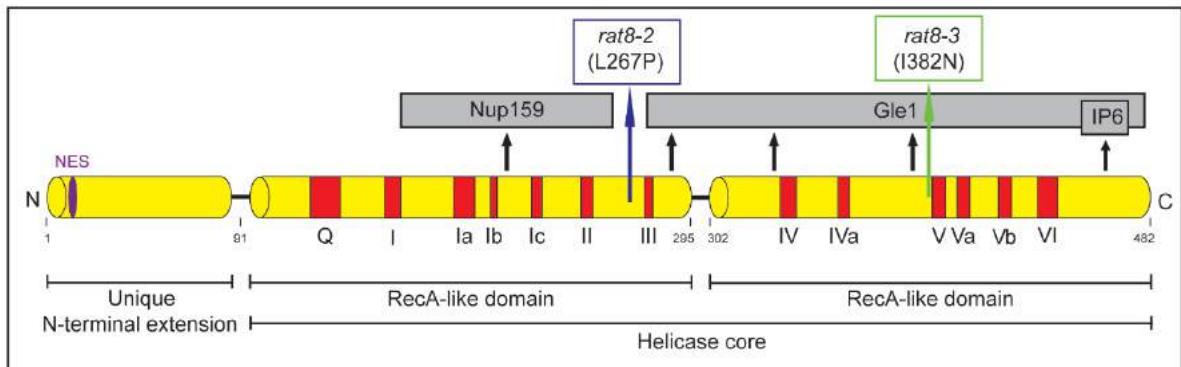
Figure 7- The domain structure of Dbp5.
Scheme of the domain structure of Dbp5 (yellow). The catalytic helicase core of Dbp5 consists of two RecA-like domains, which contain 13 conserved motifs for ATP and RNA binding (red). Furthermore, the regions for its co-factors binding (grey) and the unique N-terminal, extension that contains a nuclear export signal (NES, purple), are displayed. Additionally, the amino acid exchanges and their position in the helicase core, resulting in temperature sensitivity, for *rat8-2* (blue) and *rat8-3* (green) are indicated. Modified from Tieg and Krebber (2013).

Different temperature-sensitive mutants of *DBP5* are known. All of them contain point mutations, which lead to single amino acid exchanges in the two RecA-like domains of Dbp5 (Snay-Hodge et al., 1998). These mutants grow almost like wild type cells at the permissive temperature of 25°C, while shifts to 37°C lead to cell death (Snay-Hodge et al., 1998). All of these mutants show a rapid poly(A) accumulation and translation termination defects upon shift to the non-permissive temperature (Gross et al., 2007; Snay-Hodge et al., 1998). The *rat8-2* mutant is known to localize together with other export factors in cytoplasmic foci after shift to 37°C (Scarcelli et al., 2008).

2.3.1. Functions of Dbp5

Dbp5 is mainly localized at the nuclear rim and in the cytoplasm, but the protein is also found in the nucleus (Hodge et al., 1999; Zhao et al., 2002). Estruch and Cole (2003) suggested, that Dbp5 might have a function in transcription initiation in the nucleus, because they could show that Dbp5 genetically and physically interacts with components of the transcription factor complex TFIIH in yeast. It was also suggested that Dbp5 might shuttle with the mRNA into the cytoplasm. However, live cell imaging experiments showed that Dbp5 is not bound to messenger ribonucleoprotein (mRNPs) particles during nucleoplasmic

transport, indicating that Dbp5 is not part of transported mRNP (Zhao et al., 2002). Interestingly, Lari *et al.* (2019) showed that the nuclear shuttling of Dbp5 is not essential for mRNA export but rather important for tRNA export. They identified a physical interaction of Dbp5 and tRNAs and tRNA export defects were apparent in *DBP5* mutants after a temperature shift to 37°C.
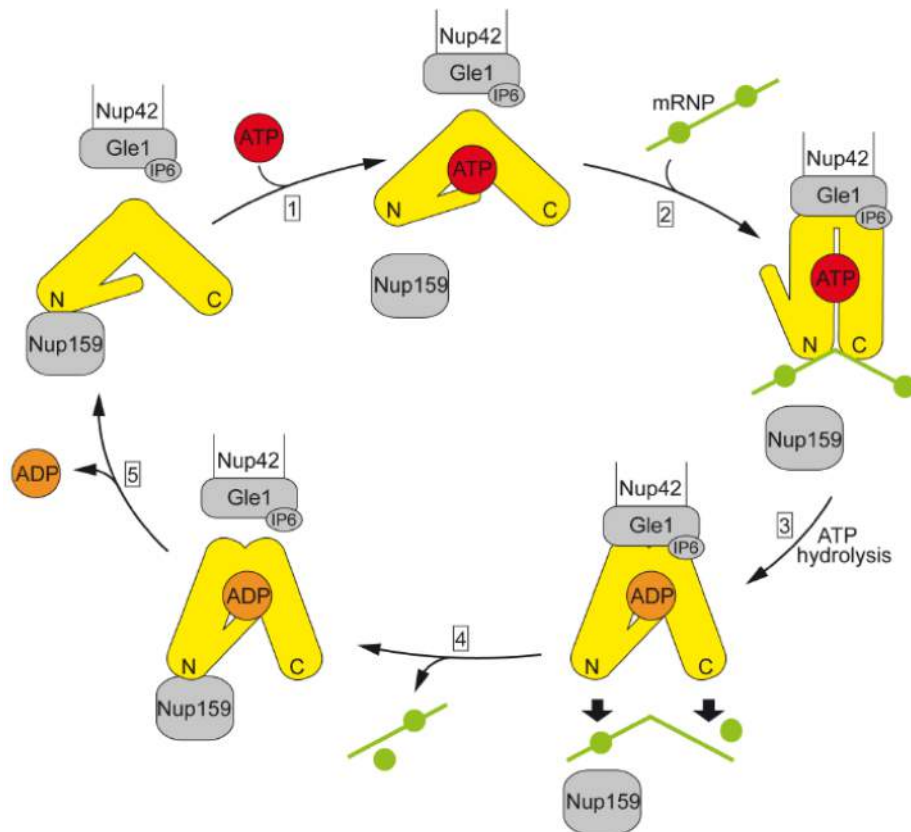
Figure 8 - The ATPase cycle of Dbp5 during nuclear mRNA export.
Dbp5 (yellow) appears in an open conformation with separated RecA-like domains in its nucleotide-free state. (1) Dbp5 first binds ATP (red). (2) Dbp5-ATP subsequently interacts with the mRNP (green) and with its co-factors IP_6 and Gle1 (grey). Hence, the catalytic center is remodeled into a close conformation, which is now competent to hydrolyze ATP. (3). ATP hydrolysis leads to a partial opening of the helicase core and simultaneously mRNA release and (4) displacement of the export reporter Mex67-Mtr2. (5) Subsequent binding of Dbp5 to Nup159 orchestrates a further opening of the helicase core leading to the release of ADP. Modified from Tieg and Krebber (2013).

At the nuclear pore complex (NPC), Dbp5 interacts with the cytoplasmic fibrils of the NPC by an association with the N-terminal domain (NTD) of the nucleoporin Nup159 (encoded by *RAT7* (ribonucleic acid trafficking protein 7) in yeast and *NUP214* in humans) (Hodge et al., 1999; Von Moeller et al., 2009; Napetschnig et al., 2009; Schmitt et al., 1999; Snay-Hodge et al., 1998; Weirich et al., 2004). Therefore, yeast strains lacking the NTD of Nup159 or *DBP5* mutants, which have lost their Nup159 binding ability, exhibit defects in the NPC association and show a solely cytoplasmic Dbp5 localization (Hodge et al., 2011; Schmitt et al., 1999; Weirich et al., 2004). However, Nup159 is not only needed to tether Dbp5 to the nuclear pore complex, but it also regulates its ATPase cycle and functions as an ADP-

release factor (Noble et al., 2011) (Fig 8). The binding site of Nup159 overlaps with the binding site of RNA and an Nup159 association with Dbp5 stimulates a conformational change in the helicase that culminates in ADP release and recycling of the enzyme. (Von Moeller et al., 2009; Montpetit et al., 2011; Napetschnig et al., 2009; Noble et al., 2011). For the ATPase activity itself, Dbp5 requires the stimulation by its co-factors Gle1 and IP$_6$ (Alcázar-Román et al., 2006; Weirich et al., 2006). The binding of Dbp5 and Gle1, is mainly mediated via their C-terminal domains and is stabilized by the binding of IP$_6$ (Alcázar-Román et al., 2010; Dossani et al., 2009; Montpetit et al., 2011; Weirich et al., 2006).

Temperature sensitive mutants of *DBP5* showed a rapid accumulation of mRNAs in the nucleus upon shift to their non-permissive temperatures (Snay-Hodge et al., 1998; Tseng et al., 1998). Additionally, temperature sensitive mutants of *GLE1*, *NUP159* and strains lacking the N-terminal β-propeller domain of Nup159, exhibit mRNA export defects and show increased amounts of Mex67 that remains bound to the mRNA (Lund and Guthrie, 2005; Murphy and Wente, 1996; Del Priore et al., 1996). During transcription and maturation mRNAs are packed with proteins into messenger ribonucleoprotein complexes (mRNPs) that are exported to the cytoplasm. Correctly processed mRNAs contain a 3' poly(A) tail and a 5' cap structure and are competent for export and every step is quality controlled by e.g. by the guard proteins (Grünwald et al., 2011; Stewart, 2010; Zander and Krebber, 2017). This group of proteins include the shuttling serine, arginine (SR) containing proteins Npl3, Gbp2, Hrb1 and the poly(A) binding proteins Nab2 (Hackmann et al., 2014; Stewart, 2010; Zander and Krebber, 2017). Upon quality control they recruit the export receptor heterodimer Mex67-Mtr2 (TAP-p15 in metazoans), which interacts with all FG-repeat containing nucleoporins of the NPC and channels the messenger ribonucleoprotein mRNP through the NPC (Sträßer et al., 2000). Dbp5 displaces the mRNP bound export factor Mex67-Mtr2 at the NPC that leads to directionality of mRNA export (Lund and Guthrie, 2005; Tran et al., 2007).

An additional function for Dbp5 is described for the nuclear export of pre-ribosomal subunits, which is independent of its ATPase activity (Neumann et al., 2016). Yeast temperature sensitive *DBP5* mutants accumulate both ribosomal subunits in the nucleus and Dbp5 interacts with the well-described ribosomal transport factor NMD3. Interestingly, *GLE1* mutants and ATPase deficient *DBP5* mutants show no defect in ribosomal maturation (Neumann et al., 2016), suggesting a different export mechanism for ribosomal subunits than for mRNAs.

2.3.2. Role of Dbp5 in translation termination

Dbp5 is located at the cytoplasmic side of the NPC, creating a typical rim staining of the nuclear envelope (Snay-Hodge et al., 1998). However, a remarkable fraction of Dbp5 is also present in the cytoplasm, reflecting its function in translation termination (Gross et al., 2007). This function was first identified through growth analyses showing that mutants of *DBP5* were hypersensitive to translational inhibitors (Gross et al., 2007). Subsequently, Bolger *et al*. (2008) revealed that also temperature sensitive mutants of *GLE1* are hypersensitive to translation inhibitors. Furthermore, it was shown that Dbp5 and Gle1 are part of polysomal fractions in sucrose-density gradient analysis, indicating that Dbp5 is part of actively translating ribosomes (Gross et al., 2007). In agreement, *DBP5* mutants showed increased readthrough activities in a dual reporter assay (Gross et al., 2007).

Additionally, *GLE1* mutants lacking the interaction domain for IP_6 and cells deleted for *IPK* (inositol phosphate kinase; phosphorylates IP_6), exhibit defects in sufficient stop codon recognition (Alcázar-Román et al., 2010; Bolger et al., 2008). It is of interest to note that temperature sensitive mutants of *DBP5* and *GLE1* showed an increased readthrough activity comparable to that of the *SUP35* mutant *sup35-1* (Alcázar-Román et al., 2010; Bolger et al., 2008). Taking into account, that overexpression of *DBP5*, but not of the ATP-deficient mutant *dbp5 (e240Q)*, rescues the increased stop codon readthrough of *sup45-2* mutants, it became clear that the ATPase activity of Dbp5 is necessary for efficient stop-codon recognition by eRF1 (Gross et al., 2007). Accordingly, a physical interaction between Dbp5 and eRF1 was detected and that the binding of eRF1 and eRF3 is decreased in *rat8-2* mutants (Gross et al., 2007). Moreover, also Gle1 was identified as an interaction partner of eRF1 (Bolger et al., 2008). Likewise, it was recently shown that the human protein DDX19 stabilizes translation termination complexes and participate in translation (Mikhailova et al., 2017). In summary, the ATPase dependent remodeling activity of Dbp5, which is stimulated via Gle1 and IP_6, is possibly required for the proper positioning of eRF1 in the ribosomal A-site. (Baierlein et al., 2010). These data could suggest that Dbp5 might help eRF1 for its proper positioning at the A-site of the ribosome. Also, it seems to mediate the interaction of eRF1 and eRF3. However, it is currently unknown if Dbp5 might also have a function with the non-canonical termination factors Dom34 and Hbs1 in NSD and/or NGD. To be able to generate a comprehensive *in vivo* translation termination model including novel translation termination factors and their order of action and addressing their function in NGD and NSD additional research is needed.

3. Material and Methods

3.1. Materials

Solutions and media were autoclaved at 121 °C for 20 min and sensitive compounds sterile-filtered. Glassware was autoclaved, or sterilized at 180 °C for 6 h.

Table 1 - List of consumable materials

Materials	Source
Amersham™ Protran® 0.45 µm Nitrocellulose Membranes	GE Healthcare
cOmplete™, EDTA-free Protease Inhibitor	Roche
Cozy™ Prestained Protein Ladder	HighQu
Cycloheximide	Carl Roth
Difco Skim Milk	Becton, Dickinson and Co.
GFP-Trap®-A Beads	ChromoTek GmbH
Glass Beads Type S 0.4-0,6 mm	Carl Roth
Glutahtione Sepharose 4B Beads	GE Healthcare
GSTrap 4B Gluthathione Sepharose	GE Healthcare
HDGreen™ Plus DNA Stain	Intas Science Imaging
Isopropyl-β-D-thiogalactopyranosid (IPTG)	Carl Roth
MYC-Trap®-A Beads	ChromoTek GmbH
Lambda DNA/*EcoR1+HindIII* Marker	Thermo Fisher Scientific
Oligonucleotides	Sigma-Aldrich
PageRuler™ Prestained Protein Ladder	Thermo Fisher Scientific
PageRuler™ Unstained Protein Ladder	Thermo Fisher Scientific
Ponceau S	Carl Roth
qPCRBIO SyGreen Mix Lo-ROX	Nippon Genetics
Rotiophorese Gel 30 (37.5:1) Acrylamide	Carl Roth
RiboLOCK RNAse Inhibitor	Thermo Fisher Scientific
TRIzol™ Reagent	Thermo Fisher Scientific
Salomon Sperm-Carrier DNA	AppliChem GmbH
WesternBright™ Quantum™ Western Blotting HRP Substrate	Advansta
Whatman® Blotting Paper	Hahnemühle

Enzymes	Source
DreamTaq DNA Polymerase	Thermo Fisher Scientific
FastAP Alkaline Phosphatase	Thermo Fisher Scientific
Gibson Assembly® Master Mix	New England Biolabs
Phusion® High-Fidelity DNA Polymerase	New England Biolabs
Q5® High-Fidelity DNA Polymerase	New England Biolabs
Restriction Enzymes	New England Biolabs
Restriction Enzymes	Thermo Fisher Scientific
RNase A	AppliChem
RNase-Free DNase	Quiagen
Zymolase 20T	Zymo Research

Kits	Source
Nucleospin® Gel and PCR Clean-up	
Nucleospin® Plasmid	MACHERY-NAGEL
Nucleospin® RNA	
Nucleospin® Xtra Midi	

Table 2 - List of equipment

Equipment	Source
ÄKTAprime Plus	GE Healthcare
BioPhotometer	Eppendorf
CFX Connect 96FX2 qPCR Cycler	Bio-Rad Laboratories
Eclipse E400 Tetrad Microscope	Nikon
FastPrep-24® Cell Homogenizer	MP Biomedicals
Fusion-SL-3500.WL	Peqlab
Foxy Jr. ® Fraction Collector, Optical Unit Type 11, Absorbance Detector UA-6	Teledyne Isco
Gene Pulser Xcell™ Electroporation System	Bio-Rad Laboratories
Gradient Master 108	BioComp Instruments
UV Gel Detection System	INTAS
Heraeus™ Pico™ 21	Thermo Fisher Scientific
Heraeus™ Fresco™ 21	Thermo Fisher Scientific
Heraeus™ Multifuge™ X3R with TX750 or F15-8x50cy Rotor	Thermo Fisher Scientific
Light Microscope Leitz Biomed Typ 020-507-010	Leica Microsystems
Microfluidizer™ LM10	Unitronics
Milli-Q® Water Purification System	Millipore
My Cycler 1,065	Bio-Rad Laboratories
Nano Drop 2000 Spectrophotometer	Thermo Fisher Scientific
Neubauer Improved Hemocytometer	Carl Roth
PerfectBlue Semi-Dry Electro Blotter Sedec M	Peqlab
Sonifierer Cell Disrupter S-250A	Branson Ultrasonics
Sorvall™ WX80 Ultracentrifuge with TH-641 rotor	Thermo Fisher Scientific
T100™ Thermal Cycler	Bio-Rad Laboratories

Table 3 - List of software

Software	Source
Adobe Illustrator CS6/2020	Adobe Systems
Adobe Photoshop CS6/CC 2019	Adobe Systems
ApE Plasmid Editor	M. Wayne Davis
Bio-1D	Peqlab
CFX Manager 3,1	Bio-Rad Laboratories
Snapgene	GSL Biotech
Office® 2011/2019	Microsoft
PrimeView 8.0	GE Healthcare
Prism8	GraphPad
QuickCalcs Outlier Calculator	GraphPad

Table 4 - List of *Escherichia coli* media

LB	Conc.	2YT	Conc.
Ampicillin* (if added)	100 µg/ml	Ampicillin* (if added)	100 µg/ml
Kanamycin* (if added)	20 µg/ml	Kanamycin* (if added)	20 µg/ml
Chloramphenicol * (if added)	34 µg/ml	Chloramphenicol * (if added)	34 µg/ml
Agar-Agar (for plates only)	1.5 % (w/v)	NaCl	85 mM
NaCl	85 mM	Tryptone	1.6 % (w/v)
Tryptone	1 % (w/v)	Yeast Extract	1 % (w/v)
Yeast Extract	0.5 % (w/v)		

Auto Inducing Medium	Conc.	SOC	Conc.
LB Media		Glucose	20 mM
Ampicillin* (if added)	100 µg/ml	KCl	2.5 mM
Kanamycin* (if added)	20 µg/ml	MgCl$_2$	10 mM
Chloramphenicol * (if added)	34 µg/ml	MgSO$_4$	10 mM
Glucose	0.05 % (v/v)	NaCl	10 mM
Glycerol	0.5 % (v/v)	Peptone	2 % (w/v)
Lactose	0.2 % (v/v)	Yeast Extract	0.5 % (w/v)
K$_2$HPO$_4$	25 mM		
NaH$_2$PO$_4$	25 mM		
Na$_2$SO$_4$	0.5 mM		
NH$_4$Cl	50 mM		

(Sambrook 1989 modified)   *Sterile antibiotics were added separately

Table 5 – List of *Saccharomyces cerevisiae* media

YPD	Conc.	B-plates	Conc.
Agar-Agar (for plates only)	1.8 % (w/v)	Agar-Agar*	3 % (w/v)
Glucose	2 % (w/v)	Ammonium Sulphate	3 mM
Peptone	2 % (w/v)	Glucose*	2 % (w/v)
Yeast Extract	1 % (w/v)	Nitrogen Base	0.17 % (w/v)

Sporulation Medium	Conc.	Selective Media	Conc.
Glucose**	0.05 % (w/v)	Agar-Agar* (for plates only)	1.8 % (w/v)
Potassium Acetate**	150 mM	Ammonium Sulphate	40 mM
Yeast Extract**	0.25 % (w/v)	Glucose*	2 % (v/v)
Adenine**	40 mg/ml	Nitrogen Base	0.17 % (w/v)
Arginine**	20 mg/ml	Yeast Dropout Mix	0.2 % (w/v)
Histidine**	20 mg/ml		
Leucine**	20 mg/ml	FOA	Conc.
Lysine**	20 mg/ml	5-Fluoroorotic Acid (FOA)	0.1 % (w/v)
Methionine**	20 mg/ml	Agar	1.8 % (w/v)
Phenylalanine**	100 mg/ml	Ammonium Sulphate	0.51 % (w/v)
Threonine**	350 mg/ml	Glucose	2 % (w/v)
Tryptophan**	20 mg/ml	Yeast Dropout Mix	0.2 % (w/v)
Tyrosine**	40 mg/ml	Nitrogen Base	0.17 % (w/v)
Uracil**	40 mg/ml		

(Sherman, 1991 modified)   * autoclaved separately   **sterile filtered

Table 6 – List of *Saccharomyces cerevisiae* strains

Name	Genotype	Source	Parental Strains
HKY36	*his3Δ200; leu2Δ1; ura3-52;*	(Winston et al., 1995)	
HKY128	*RAT8::HIS3; ura3-52; leu2Δ1; trp1Δ63; his3Δ200*	(Snay-Hodge et al., 1998)	
HKY314	*his3Δ1; leu2Δ0; ura3Δ0; met15Δ0*	Euroscarf	
HKY456	*RAT8::HIS3; leu2Δ1; trp1Δ63; his3Δ200*	(Neumann et al., 2016)	128
HKY477	*RAT8::HIS3; his3Δ200; leu2Δ1; ura3-52; trp1Δ63*	(Beißel et al., 2019)	36 x 456
HKY492	*UPF1::kanMX4; his3Δ1; leu2Δ0; lys2Δ0; ura3Δ0*	Euroscarf	
HKY1631	*DOM34-GFP:HIS3MX6; his3Δ1; leu2Δ0; ura3Δ0; met15Δ0*	Invitrogen	
HKY1632	*HBS1-GFP:HIS3MX6; his3Δ1; leu2Δ0; ura3Δ0; met15Δ0*	Invitrogen	
HKY1646	*RAT7ΔN(1-500); ura3-52; leu2Δ1; his3Δ200; trp1Δ63*	(Hodge et al., 1999)	
HKY1797	*DOM34::kanMX4; ura3Δ0; leu2Δ0; met15Δ0; his3Δ1*	Euroscarf	
HKY1798	*Hbs1::kanMX4; ura3Δ0; leu2Δ0; met15Δ0; his3Δ1*	Euroscarf	
HKY1693	*DOM34-GFP:HIS3MX6; RAT8::HIS3; leu2Δ0; ura3Δ0*	This study	477x 1631
HKY1694	*HBS1-GFP:HIS3MX6; RAT8::HIS3; leu2Δ0; ura3Δ0*	This study	477x 1632
HKY1888	*Dom34::kanMX4; RAT8::HIS3; leu2Δ0; his3Δ1; ura3Δ0*	This study	477x 1797
HKY1890	*Hbs1::kanMX4; RAT8::HIS3; leu2Δ0; his3Δ1; ura3Δ0*	This study	477x 1798

Table 7– List of *Escherichia coli* strains

Name	Gentotype	Application
DH5α	*F⁻Φ80lacZΔM15Δ (lacZYA-argF) U169 recA1 end A1 hsdR17 (rK-, mK+) phoA supE44λ-thi-1 gyr96 relA1*	Cloning and amplification of plasmid-DNA
Rosetta 2 (DE3)	*F- ompT gal dcm lon hsdS$_B$ (r$_B$-,m$_B$-) λ(DE3) pRARE2(CAM^R)*	Expression of recombinant proteins

Table 8 – List of Plasmids

Name	Genotype	Source
pHK88	*URA3; CEN; AMP^R*	(Sikorski and Hieter, 1989)
pHK630	*P$_{RAT8}$RAT8 LEU2; 2µ; AMP^R*	(Snay-Hodge et al., 1998)
pHK638	*P$_{RAT8}$ RAT8-3 LEU2; 2µ; AMP^R*	(Snay-Hodge et al., 1998)
pHK693	*P$_{RAT8}$ RAT8-2-MYCLEU2; 2µ; AMP^R*	(Snay-Hodge et al., 1998)
pHK1282	*P$_{TAC}$GST in pGEX-6P-1; AMP^R*	(Beißel et al., 2019)
pHK1288	*P$_{TAC}$GST-DBP5 in pGEX-4T-1; KAN^R*	(Beißel et al., 2019)
pHK1414	*P$_{TAC}$GST-RLI1 in pGEX-6P-1; AMP^R*	(Beißel et al., 2019)
pHK1574	*P$_{CBP80}$CBP80-MYC; URA3; CEN; AMP^R*	This study
pHK1578	*P$_{CBP80}$CBP80^{PTC}-MYC; URA3; CEN; AMP^R*	This study
pHK1631	*P$_{ADH}$MYC-HBS1; URA3; CEN; AMP^R*	This study
pHK1640	*P$_{ADH}$DOM34; URA3; CEN; AMP^R*	This study
pHK1647	*P$_{ADH}$DOM34-MYC; URA3; CEN; AMP^R*	This study
pHK1653	*P$_{GAL}$-GFP-GGN12-FLAG-HIS3; URA3; CEN; AMP^R*	(Tsuboi et al., 2012)
pHK1654	*P$_{GAL}$-GFP-SL-FLAG-HIS3; URA3; CEN; AMP^R*	(Tsuboi et al., 2012)
pHK1655	*P$_{GAL}$-GFP-FLAG-HIS3; URA3; CEN; AMP^R*	(Tsuboi et al., 2012)
pHK1656	*P$_{GAL}$-GFP-FLAG-HIS3; URA3; CEN; AMP^R*	(Tsuboi et al., 2012)

Table 9 – List of Oligonucleotides

Name	Genotype	Origin/Purpose
HK2507	*ACTCACTATAGGGCGAATTTGGAGCTGACGATTCTTCGAGTGTGTC*	*CBP80* pHK755 fw
HK2508	*ACTTTTGTTCACCTCTAGAGGAATTAACTTCCTTTGTTTCTTGAATCC*	*CBP80* pHK755 rev
HK2625	*GCCTAAATGACAGAGAATCCCACCTGTTGTAC*	*CBP80* muta. fw
HK2626	*GATTCTCTGTCATTTAGGCATGCGAGGCC*	*CBP80* muta. rev
HK3179	*TCTGCACAATATTTCAAGCTATACCAAGCATACAATAAGCATCGATATGAAGGTTATTAGTCTGAAAAGGATTCT*	*DOM34* GA fw
HK3180	*TTCACCGTTCAAATCTTCTTCAGAAATCAACTTTTGTTCCATCGATCTACTCCTCACCATCGTCTTCA*	*DOM34* GA rev
HK3219	*AATTGTAATACGACTCACTATAGGGCGAATTGGAGCTCCACCGCGGTCTTCAGTCTCCTCCAAGTCG*	*DOM34-MYC* GA rev
HK2134	*ATGCCCGAAGGTTATGTACAGG*	*GFP* qPCR fw
HK2135	*CATTCTTTTGTTTGTCTGCCATG*	*GFP* qPCR rec
HK3089	*AGTTACGCTAGGGATAACAGGG*	*21S* qPCR fw
HK3090	*AGTTACGCTAGGGATAACAGGG*	*21S* qPCR rev
HK2696	*AGTTACGCTAGGGATAACAGGG*	*CBP80* qPCR fw
HK2697	*AGTTACGCTAGGGATAACAGGG*	*MYC* qPCR rev

3.2. Methods

3.2.1. Cell Culture

3.2.1.1. Escherichia coli cell culture

Cultivation of *E. coli* was performed compliant to standard protocols (Sambrook et al., 1989). DH5α bacteria cells were standardly cultivated in LB media (see Table 4) containing the corresponding antibiotics for specific resistance genes encoded in the plasmid-DNA (100 µg/ml Ampicillin, 20 µg/ml Kanamycin or 34 µg/ml Chloramphenicol).

After transformation (see 3.2.2.5.), liquid media was inoculated with a single colony from an agar plate and cultivated with gently rotating at 37 °C over night. To determine the cell yield, the optical density of the cells was measured at 600 nm by using a photometer. For expression and/or protein purification *Rosetta 2* bacterial cells were inoculated and cultivated in 10 ml LB media over night. The LB medium was supplemented with the corresponding antibiotics for specific resistance genes encoded in the plasmid-DNA. Subsequently, 2 ml of the saturated cell suspension was used to inoculate 2 l auto inducing medium (AIM see Table 4) and incubated at 16 °C for 3 days.

3.2.1.2. Cultivation of Saccharomyces cerevisiae cells

Yeast cells without plasmid-DNA were grown in YPD medium (see Table 5). The selective medium was chosen regarding the plasmid- or genome-encoded selection marker gene. The used yeast drop out mix contained all other amino acids needed and ingredients required for cell growth (Sherman and Hicks, 1991). For long time storage, the yeast strains were kept in 50 % glycerol at -80 °C. These stocks were streaked out on YPD plates and grown for 1 day. Subsequently, cells were re-streaked on YPD plates again and incubated for 1 day at 25 °C. Yeast strains were either transformed (see 3.2.3.2.) or kept on YPD plates at 4 °C. Positive transformants that grew on selective media were stored at 4 °C. Cells were freshly inoculated in liquid media, according to experimental purposes. In regular intervals, the yeast strains were re-streaked onto fresh agar plates or streaked out from frozen stocks. For experiments, cell material from the agar plate was used to inoculate 200 ml of YPD or selective media and grown overnight at 25 °C. The next day, the cell number was determined by counting them with a hemocytometer and diluted in at last 400 ml media to 0.5-1.0x 10^7 cells/ml. As soon as the cells reached the log-phase (2-3x10^7 cells/ml), they were either shifted for the indicated time period to the non-permissive temperature and/or immediately harvested by centrifugation at 4100x g and 4 °C for 5 min. The cell pellet was resuspended in 5 ml distilled water, transferred in a 15 ml falcon tube and centrifuged again under the same conditions and either immediately used, or the cell pellet was frozen in liquid nitrogen and stored at -20 °C. If the yeast

encoded a galactose- inducible promotor, cells were grown to log-phase in 2 % (v/v) sucrose as carbon source. For galactose induction of mRNA expression, 2 % (v/v) galactose was added and cells were harvested after the indicated time periods.

3.2.2. Construction of plasmid DNAs

3.2.2.1. Polymerase chain reaction (PCR)

In general, all polymerase chain reactions (PCRs), were performed by amplification of particular DNA-fragments from plasmid-DNA or genomic DNA with appropriate primer pairs. For analytic PCRs, DNA was amplified using the Dream *Taq* polymerase (Thermo Fisher Scientific). For DNA, which was later used for cloning purposes, proof-reading polymerases (New England Biolabs) were preferred. The reaction conditions varied for each enzyme based on the manufacture's protocols. Subsequently, the sizes of the produced PCR products were quality controlled by agarose gel electrophoresis.

Table 10 – PCR reaction composition

Polymerase:	Dream *Taq*	Phusion	Q5
dNTPs	200 µM each	200 µM each	200 µM each
Primers	0.2 µM each	0.5 µM each	0.5 µM each
Polymerase	0.025 U/µl	0.02 U/µl	0.02 U/µl
Template DNA	0.5 µg genomic DNA or 20 ng plasmid		

Table 11 – PCR program

Polymerase:	Dream *Taq*	Phusion	Q5
Initial Denaturation	95 °C - 3 min	98 °C - 30 s	98 °C - 30 s
Denaturation	95 °C – 30 s	98 °C – 10 s	98 °C – 10 s
Annealing	30 s	30 s	30 s
	According to melting temperature of primers		
Extension	72 °C – 1 min/kb	72 °C – 30 s/kb	72 °C – 30 s/kb
Final Extension	72 °C – 10 min	72 °C – 10 min	72 °C – 10 min

3.2.2.2. Restriction digestion and DNA separation

Restriction digestion was conducted to analyze plasmid-DNA or to produce linearized DNA-fragments from plasmids. Restriction enzymes and their appropriate buffers were chosen as proposed from the manufacture. For the digestion, 2-5 µg of plasmid-DNA were mixed with buffer and enzyme in a total volume of 20 µl and incubated over night at 37 °C. To avoid rapid re-ligation of linearized plasmids that were linearized only by a single restriction enzyme, the 5' and 3' phosphate groups of the DNA were dephosphorylated. Dephosphorylation was carried out by adding 1 U of Fast AP alkaline phosphatase (Thermo Fisher Scientific) to the sample and incubation took place at 37 °C for 10 min. In the final

step, the enzymes were deactivated by heating for 15 min at 65 °C. The DNA was visualized by agarose gel electrophoresis.

3.2.2.3. Agarose gel electrophoresis and DNA extraction

DNA was analyzed and separated by agarose gel electrophoresis. To prepare a 1 % gel, 1 g agarose was added to 100 ml TAE buffer (40 nM Tris-acetate, 1 mM EDTA) and heated in a microwave until the mixture was homogenized and the agarose melted. After letting the solution cool down under constant stirring, either 4 µl of ethidium bromide (10 mg/ml) or 10 µl HD Green Plus DNA Stain (Intas Science Imaging) was added. Afterwards, the agarose solution was poured into a gel chamber and a comb was added to form sample pockets. After this, the polymerized gel was placed in an electrophoresis chamber flooded with 1x TAE buffer. The DNA samples were mixed with a 6x DNA loading dye and loaded into the gel in parallel with a DNA size standard (Thermo Fisher Scientific). Subsequently a voltage of 120 V was applied and after 30 - 90 min the DNA bands were visualized with an UV transilluminator. If necessary, the desired DNA fragments were purified with the Nucleospin Gel and PCR clean-up kit (MACHEREY-NAGEL). Finally, the DNA was eluted in the provided elution buffer (5 nM Tris/HCl, pH 8.5) and measured with the NanoDrop spectrophotometer (Thermo Fisher Scientific).

3.2.2.4. Gibson Assembly

For the Gibson assembly (GA), inserts with 30-40 bp overhangs were created by using primers, which have beside their annealing sequence to the insert, an overhang that correspond to the plasmid backbone. For the GA reaction, 100 ng linearized vector fragment and a two-fold molar excess of insert were mixed in a total volume of 10 µl. This solution was then mixed with 10 µl of 2x GA-master mix (New England Biolabs) and incubated at 50 °C for 1 h. The 5' exonuclease shortens the 5' ends of the vector and thereby generates 3' overhangs. Due to the generated overlaps in the insert sequence, the insert can anneal. Finally, the Phusion DNA-polymerase extends the 3' ends and the gaps are filled by the *Taq* DNA ligase (Gibson et al., 2009).

3.2.2.5. Transformation of *Escherichia coli*

For all cloning purposes, the DH5α *Escherichia coli* strain was used. For protein purification and *in vitro* assays, the Rossetta 2 strain was used.

3.2.2.6. Heat shock transformation

To get chemically ultra-competent cells, the protocol provided by Inou *et al.* (1990) was followed. For transformation 100 µl cell suspension were placed on ice and mixed with 200-300 ng plasmid or 10 µl GA reaction mix and incubated on ice for 30 min. Subsequently, the cells were exposed to a heat shock at 42 °C for 2 min and after that immediately placed on ice. 1 ml SOC medium was added. After 45-60 min incubation at 37 °C, the cells were precipitated at 3500 x g for 1 min and resuspended in 100 µl of the residual liquid. The suspension was plated on LB plates containing the corresponding antibiotic(s) and incubated at 37 °C overnight.

3.2.2.7. Electroporation

For electroporation, the DNA suspension had to be free of ions that would otherwise elicit a bypass for the current. Therefore, the DNA suspension was dialyzed on a nitrocellulose membrane in a deionized water containing petri-dish prior to transformation. Electro competent cells were prepared according to Dower *et al.* (1988) and 50 µl of them were mixed with 10 µl of the dialyzed DNA sample. Then this mixture was pipetted between the electrodes of an electroporation cuvette (1 mm gap), which was cooled on ice. The cuvette was placed in the electroporator (Bio-Rad Laboratories), which generates a pulse (exponential decay, 155 V, 50 µF, 150 Ω) for penetration of the DNA through the cell wall. After electroporation, 1 ml SOC was immediately added. After 45-60 min in the incubator at 37 °C, the cells were centrifuged at 3500x g for 1 min and resuspended in 100 µl residual liquid. The suspension was plated on LB plates containing the corresponding antibiotic(s) and incubated at 37 °C overnight.

3.2.2.8. Plasmid Extraction from *E. coli* cultures

To determine the genotype of the generated plasmid-DNA construct after Gibson assembly (see 3.2.2.4.), plasmid-DNA was extracted from 10 ml bacteria cultures by using the NucleoSpin Plasmid purification kit (MACHEREY-NAGEL), following the manufacturer's instructions. For plasmid-DNA amplification, 100 to 200 ml bacteria cultures were prepared and plasmid-DNAs were isolated with the NucleoBond Xtra midi kit (MACHEREY-NAGEL) as described in the manufacturer's protocol. In both cases, the *E. coli* were grown in LB medium containing the corresponding antibiotic(s) until saturation. The yield and quality of

the isolated plasmid-DNA was determined with the NanoDrop spectrophotometer (Thermo Fisher Scientific).

3.2.2.9. *E. coli* colony PCR

For determine successfully generate Gibson assembly products, several *E. coli* colonies were picked from the transformed antibiotic containing LB-plate. The whole cell lysate was then transferred into an PCR tube and in addition streaked onto a fresh LB-plate containing the same antibiotic. The PCR tube was filled with 10 µl Dream *Taq* reaction mix and a PCR run was performed as described in (see 3.2.2.1.). Positive clones, regarding to positive results in the colony-PCR, inoculated from the LB-plate in 10 ml liquid LB medium containing the corresponding antibiotic and incubated overnight. Plasmids were isolated as described in chapter 3.2.2.8..

3.2.2.10. Sequencing of plasmid-DNA

Altered DNA constructs were sequenced to screen for the gene of interest and sent to LGC Genomics for Sanger sequencing.

3.2.3. Manipulation of Saccharomyces cerevisiae

3.2.3.1. Crossing of yeast strains

Crossing of yeast strains was performed as described by Sherman (1991) and Sherman and Hicks (1991). In general, all yeast strains in this study are haploid strains. For the generation of diploid strains, two haploid strains with the mating types *MATa* or *MATα* were mixed on YPD-plates and incubated at 25° C for 1 day. Afterwards, the strains were plated onto selective agar plates containing the selective markers of both haploid strains and selected for diploids. To induce sporulation, the diploid cells were transferred into 2 ml sporulation medium (see Table 5) and incubated in a rotator under agitation at 25 °C for 5 days. The presence of tetrads (asci with 4 spores), was verified using a light microscope and the tetrads were prepared for dissection. For that, a cell culture (100 µl) was centrifuged at 16200x g for 1 min and washed once with 1 ml distilled water and diluted in 100 µl distilled H_2O. For digestion of the cell wall, the cell suspension was incubated with 1 µg/µl zymolase (Zymo Research) at room temperature for 10 min. Afterwards, the cells were washed with 100 µl P-solution to stop digestion and subsequently diluted in 1 ml water, from which 100 µl were pipetted on one third of a YPD plate. The tetrads were picked and separated from the plate with the tetrad microscope attached to a micromanipulator (Nikon). After 2-3 days growth at 25°C, the tetrads were plated onto different selective agar plates to determine the genotypes. Additionally, colony PCR was used to identify certain markers

and/or genes. Candidates were further analyzed for mating types, by re-plating the spores onto plates that contained lawns of *MATa* or *MATα* reference strains. After 1 day of growth they were transferred to selective B-plates (Sprague, 1991). The references strains were isoleucine and valine auxotroph, which was complemented by the tested tetrads. Thus, only cells that had a different mating type were able to form diploids and grew on B-plates. All knockout strains contained either a *KanMX4* cassette or *HIS3* marker. To select for *KanMX4*, 100 µl geneticin (40 µg/µl) was mixed with the medium for a YPD plate. For selection for *HIS3,* selective media plates lacking histidine were used. The same procedure was used to select for GFP tagged proteins that are fused to a *HIS3MX6* cassette.

3.2.3.2. Yeast cell transformation

Yeast cells were treated with lithium acetate and heat shocked to introduce plasmid-DNA into the cells following the protocol of Gietz *et al.* (1992). Cells were grown in liquid media at 25 °C to a density of approx. $1\text{-}2\text{x}10^7$ cells/ml and harvested by centrifugation at 4100x g for 5 min. The cell pellet was washed once with distilled water and once with TE lithium acetate buffer (10 mM Tris, 1 mM EDTA, 100 mM lithium acetate, pH 7.5). After every washing step, the cells were collected by centrifugation at 3500x g for 2 min. Finally, the cell pellet was resuspended in 100 µl of lithium acetate buffer. For transformation, 50 µl of this cell suspension ($\sim0.5\text{x}10^8$ cells) were mixed with 1 µg plasmid-DNA and 50 µg (5 µL) *Salmon sperm*-carrier DNA (AppliChem GmbH) and 300 µl PEG-TE lithium acetate buffer (10 mM Tris, pH 7.5, 1 mM EDTA, 100 mM lithium acetate, 40 % (v/v) poly ethylene glycol 4000). Prior to use, the carrier DNA was boiled at 95 °C for 5 min and rapidly cooled on ice to generate single DNA strands. Subsequently, the cell suspension was incubated under agitation at 25 °C for 30-60 min and then heat-shocked to 42 °C for 15 min. Afterwards, cells were centrifuged at 16200x g for 1 min and washed with 1 ml distilled water. After a second centrifugation step, the cell pellet was resuspended in 100 µl residual water and plated onto a selective agar plate. Finally, the plate was incubated at 25 °C for 2-3 days until single colonies could be picked, which were then streaked onto new selective agar plates.

3.2.4. Cell biology methods

3.2.4.1. Growth analysis of yeast strains

To determine potential growth defects of certain gene knock-outs, or tagging of certain gene products, temperature sensitive strains, strains containing a tagged version of a protein or different combinations of these were analyzed. Cell suspension were prepared in 10-fold serial dilutions. For this, yeast cells from agar plates were solved in water and the cell density was determined by cell counting with a hemocytometer. The cells were diluted 10-fold from 1×10^7 to 1×10^3 and pipetted in 15 µl rows onto a plate. The cells were grown at 16 °C, 25 °C, 30 °C, 35 °C or 37 °C for 2-5 days and images were taken by scanning. In this study, only dilution series, that showed a growth defect or rescue effect of growth defects by overexpression of a gene, are shown. Additionally, to increase the growth defect of strains combined with NSD and NGD reporters, the medium was supplemented with 1 mM diamide as described earlier (Jamar et al., 2017).

3.2.4.2. Loss of *URA3* gene selection

To lose *URA3* gene containing plasmid-DNA, FOA plates (see Table 5) were used. On FOA plates, cells expressing *URA3* produce the toxic compound 5-fluorouracil, which is lethal to the cells. Selection of cells that loss *URA3* containing plasmid-DNA was performed before (non-essential protein) or after (essential protein) transformation of the strain with a substituting plasmid-DNA that contained a different marker gene such as *LEU2*.

3.2.5. Protein biochemical methods

3.2.5.1. Preparation of yeast whole cell lysates

For experimental approaches, yeast cells were grown in 400-600 ml cultures to log-phase ($2-3 \times 10^7$ cells/ml) and harvested by centrifugation at 4 °C and 4100 g for 5 minutes. The cell precipitates were washed with distilled water, transferred into a 2 ml screw top tube or 15 ml falcon tube and centrifuged again. For cell lysis, the same amount of glass beads type S 0.4-0,6 mm (Carl Roth) and assay specific lysis buffer supplemented with cOmplete™ EDTA-free protease inhibitor cocktail (5 µl per 100 ml cell lysate) were added to the cell pellets. Afterwards, the cells were disrupted by using the FastPrep-24®
(MP Biomedicals) machine with the settings of 5.0 m/s for 30 seconds, at least 2 times. The lysate was purified from cell debris by centrifugation at 4 °C and 16200x g for 10 minutes and the supernatant was used directly for the experimental approach. To avoid protein degradation all steps were performed on ice.

3.2.5.2. Co-Immunoprecipitation (Co-IP) analysis

For the analysis of protein interactions *in vivo*, co- immunoprecipitation (co-IP) experiments were conducted. In general, a protein fused to a protein tag is immunoprecipitated by the corresponding antibody bound to beads. Pulling down of the tagged protein leads to the co-precipitation of all proteins bound directly or indirectly to the tagged protein. The co-precipitated proteins were separated via SDS Page and analyzed on western blot. In this study, co-immunoprecipitation experiments were performed with cells expressing either GFP- or myc-tagged proteins, as described earlier (Gross et al., 2007). For immobilization of the tagged proteins, GFP-Trap®-A beads and MYC- Trap®-A beads (ChromoTek), which covalently bind the antibodies, were used. The GFP- or MYC- beads were homogenized by vigorous shaking and 10 µl of this suspension (slurry) was washed 5 times with 1 ml PBSKMT buffer (1x (10x PBS, pH 7.5), 2 mM KCl 2.5 mM MgCl$_2$ and 0.5 % (v/v) Trition -X-100) and always collected by centrifugation each time at 500x g for 2 minutes. After the last washing step, the beads were resuspended with the lysate and incubated at 8 °C for 2 h to precipitate the tagged protein. The beads were washed at least 3 times with 1 ml lysate buffer and centrifuged at 500x g for 2 minutes. In the last step, the supernatant was removed completely and exchanged by 30 µl 2x sample buffer (125 mM Tris/HCl, pH 6.8, 25 % (v/v) glycerol, 2 % (w/v) sodium dodecyl sulfate (SDS), 5 % (v/v) β-mercaptoethanol and a tip of bromophenol blue). Control aliquots were collected from the lysate fractions before Co-IP.

3.2.5.3. Expression of recombinant proteins

For the expression and purification of recombinant proteins, *E. coli* Rosetta 2 (DE3) cells were transformed with the required plasmid-DNA. Rosetta 2 cells contain a genome encoded T7-polymerase expression system, which can easily be used as an *E. coli* expression system for recombinant protein expression. Furthermore, Rosetta 2 (DE3) harbor a plasmid that expresses tRNAs for infrequently used codons in *E. coli* and additionally encodes for a chloramphenicol resistance. Moreover, the low incubation temperature of 16 °C increase the folding capacity of eukaryotic proteins. The expression of glutathione s-transferase (GST)- tagged recombinant yeast proteins its affinity purification were performed regarding the standard protocols (Harper and Speicher, 2011). For the expression of GST-Dbp5, a preculture of 10 ml LB medium was mixed with 100 µg/ml of ampicillin and 34 µg/ml of chloramphenicol and inoculated with Rosetta 2 cells containing GST-DBP5 expressing plasmid-DNA. The pre-culture was incubated at 37 °C overnight and 2 ml of pre-culture was used to inoculate 2 L of auto inducing medium the next day (AIM). AIM contains glucose, glycerol and lactose as carbon source. The main culture was incubated at 16 °C for 3 days. During the growth phase of the bacterial cells, glucose and

glycerol were used as carbon source, whereas lactose induced the expression of the recombinant protein. Furthermore, the low temperature induced chaperone expression, which support a better folding capacity of the protein. After 3 days of growth, the cells were harvested by centrifugation at 4100x g and 4 °C for 10 minutes and washed once with distilled water. After an additional identical centrifugation step the pellet was resuspended in binding buffer (10 mM PBS (10 mM Na_2HPO_4, 140 mM NaCl, 2,7 mM KCl, 1.8 mM KH_2PO_4), pH 7.4, 20 mM DTT) complemented with cOmplete™ EDTA-free protease inhibitor cocktail (5µl per 100 ml cell lysate) to prevent protein degradation. Then cells were disrupted by using a Microfluidizer LM10 (Unitronics) through applying a pressure of 700 MPa. The lysate was centrifuged at 4 °C and 30.000 x g for 30 min in a Sorvall WX Ultra Series Centrifuge (Thermo Scientific) attached with the Ti50 rotor (Beckmann). The supernatant was loaded on two 1 ml GSTrap™ FF (GE Healthcare) column with a flow rate of 5 ml/min using the ÄKTAprime plus (GE Healthcare). After loading of the lysate, the column was washed with binding buffer, until the absorbance reached the baseline. GST-Dbp5 was eluted from the column with elution buffer (50 mM Tris-HCl, 40 mM reduced Glutathione, 20 mM DTT, pH 8.0) and finally dialyzed (10 mM Na_2HPO_4, 140 mM NaCl, pH 7.4) at 8 °C for 2 days including a change of buffer twice. All fractions were collected and protein containing fractions were determined via SDS-PAGE (see 3.2.5.7.) and subsequent Coomassie staining (see 2.5.5.8.). The final protein concentration was determined with the Nano Drop 2000 spectrophotometer (Thermo Fisher Scientific) and the protein was stored at -80°C.

GST-Rli1 and GST-tag alone were expressed as described in this section, but not purified by 1 ml GSTrap™ FF columns. Instead, the cells were pelleted (50 ml cell suspension) and either stored at -20 °C or directly used after cell harvesting. For experimental approaches, the cells were resuspended in lysis buffer (20 mM HEPES, pH 7.5, 100 mM NaCl, 4 mM $MgCl_2$, 20% (v/v) Glycerol, 0.5% (v/v) NP-40, 1mM DTT) supplemented with cOmplete™, EDTA-free protease inhibitor cocktail (5µl per 100 ml cell lysate) and lysed on ice through sonification with the sonifierer cell disrupter S-250A (Branson Ultrasonics). For lysis, the cells were resuspended in 5 ml lysis buffer and sonified twice for 5 min to open the cells up. Subsequently, the crude extracts were centrifuged at 16000x g and 4 °C for 20 minutes. The lysates were used for *in vitro* assays or in combined *in vivo* and *in vitro* studies.

3.2.5.4. Combined *in vivo* and *in vitro* studies

The *in vivo* produced GFP tagged proteins are immobilized as described in chapter 3.2.5.2.. After immobilization, the co-purified proteins are detached from the protein of interest by harsh washing. For this, the proteins bound to the GFP beads are washed 5 times with PBSKMT buffer, incubated with *in vitro* lysis buffer and agitation at 8 °C for 20 min. The

samples were washed again 3 times with *in vitro* lysis buffer. Afterwards, either purified protein or clear cell lysate containing the expressed recombinant protein (see 3.2.5.3.), were added to the immobilized protein bound to GFP beads for 2 h. Subsequently, the beads were washed again 3 times with *in vitro* lysis buffer, finally mixed with 30 µl 2x SDS buffer and in the last step the proteins were separated by SDS-PAGE.

3.2.5.5. Displacement assay

The displacement assay used in this study is a combination of an *in vivo* and *in vitro* study. After binding of the first recombinant protein to the immobilized GFP tagged protein, the precipitated tagged protein was washed like as described in chapter 3.2.5.2.. Subsequently, a second recombinant protein was added to the preformed complex and incubated for 2 h. The second protein was added in the indicated increasing concentrations to investigate a possible competition or disassembly ability of the preformed complex. Finally, the beads were washed 3 times with *in vitro* lysis buffer and the samples were then applied to SDS-PAGE. The displacement activity was evaluated by detection of all proteins via western-blot.

3.2.5.6. Sucrose-density gradient fractionation

To analyze protein binding to different ribosomal complexes, sucrose-density gradient fractionation experiments were conducted according to Frey *et al*. (2001) and Masek *et al*. (2011). Yeast cells were inoculated in 200 ml of medium and incubated overnight at 25 °C to obtain a pre-culture. On the next day, the cells were counted and diluted in 400 ml medium to $0.5x10^7$ cells/ml. After additional incubation reaching the logarithmic growth phase ($2x10^7$ cells/ml), the cells were shifted to their non-permissive temperature (37 °C) for 1 h. To avoid a polysome run-off, the cells were treated with 100 µg/ml of the translational inhibitor cycloheximide (Carl Roth) on ice for 15 minutes. Afterwards, the cells were harvested, washed once with ice-cold distilled water and then lysed in pre-cooled lysis buffer (20 mM HEPES-KOH, pH 7.5, 10 mM KCl, 2.5 mM $MgCl_2$, 1 mM EGTA, 1 mM DTT and 100 µg/ml cycloheximide) supplemented with cOmplete™, EDTA-free protease inhibitor cocktail (5µl per 100 ml cell lysate). To estimate the protein concentration of each sample, absorption of the lysates was measured at 260 nm with the NanoDrop spectrophotometer. For ribosome gradients and subsequent protein analysis, 15 OD_{260} of lysates were loaded on top of each linear-sucrose gradient. To prepare linear sucrose-gradients, 7 % (w/v) sucrose and 47 % (w/v) (%sucrose, 20 mM HEPES-KOH, pH 7.5, 10 mM KCl, 2.5 mM $MgCl_2$) were mixed, poured with the gradient master 108 (BioComp Instruments) and stored on ice until usage.

The lysates were separated in the sucrose-gradients by centrifugation at ~200000x g at 4°C for 3 h in a Sorvall WX80 ultracentrifuge with the TH-641 rotor (Thermo Fisher Scientific). Thereafter, the gradients were collected in 700 µl fractions with a fraction collector (Teledyne Isco). For that, 60 % (w/v) sucrose was pumped to the bottom of the gradient upwards to push the gradient past a spectrophotometer into collection tubes. The spectrophotometer plotted the ribosomal rRNA by measuring the absorbance at 254 nm. For western-blot analysis of the proteins, all proteins were precipitated with 20 % trichloroacetic acid (TCA, Carl Roth). For this 700 µl of TCA was mixed with each sample, the proteins were pelleted through centrifugation at 16200x g and 4 °C for 15 minutes. The supernatant was removed and the pellets were washed twice with 80 % (v/v) acetone and afterwards dried at room temperature and resuspended in 30 µl of 2x SDS-sample buffer.

3.2.5.7. SDS-polyacrylamide gel-electrophoresis (SDS-PAGE)

Proteins were denaturized and separated by size using standard, vertical, discontinuous SDS- polyacrylamide- gel- electrophoresis (SDS-PAGE) (Garfin, 2009).

Table 12 - Formula of SDS-polyacrylamide-gels

Ingredient	Stacking Gel	Separation gel
Bis-/Acrylamide Mixture 37.5:1	5 % (v/v)	10 % (v/v)
Tris/HCl pH 8.8	-/-	0.375 mM
Tris/HCl pH 6.8	125 mM	-/-
SDS	0.1 % (v/v)	0.1 % (v/v)
APS	0.1 % (v/v)	0.1 % (v/v)
TEMED	0.1 % (v/v)	0.04 % (v/v)

The components listed in table 12 for separation gel were mixed and poured between two approx. 25 x 20 cm glass plates, detached by approx. 2 mm thick spacers. The separation gel mix was covered with a layer of 1 ml isopropanol. After polymerization, the isopropanol was washed off with water and the water was removed. The components of the stacking gel were mixed (Table 12) and poured on top of the separation gel. To form sample pockets, a comb was inserted immediately. After polymerization, the comb and the spacer at the bottom were removed and the gel was placed into a running chamber. The chamber was filled with SDS running buffer (25 mM Tris Base, 0.1% (w/v) SDS, 190 mM glycine) and the sample wells were washed with running buffer. Before loading, the samples were boiled at 95 °C for 5 minutes and then loaded side by side with a protein marker
(PageRuler Prestained protein ladder (Thermo Fisher Scientific) or Cozy Prestained Protein Ladder (highQu)) into the sample pockets. The power current was set to 14 mA and the gel run was performed over night.

3.2.5.8. Coomassie staining

For the determination of protein containing fractions and protein expression, SDS-polyacrylamide gels were stained with Coomassie brilliant blue. Upon SDS-polyacrylamide-electrophoresis, the gels were stained with staining solution (50 % (v/v) methanol, 0.25 % (w/v) coomassie brilliant blue R250) for 10 min. Subsequently, the stained gels were incubated with de-staining solution (5 % (v/v) Methanol, 10 % (v/v) glacial acetic acid), until clear protein bands were visible. For a faster de-staining, a tissue was placed in the solution and the gel was heated until boiling in a microwave. For documentation, the gels were scanned.

3.2.5.9. Western blot analysis

Following protein separation via SDS-PAGE, the proteins were transferred to a nitrocellulose membrane to make the proteins accessible for antibodies and chemiluminescent substrates. This method was first described by Towbin *et al.* (1979). Essentially, for Semi-Dry western blotting, two pieces Whatman® Blotting Paper (Hahnemühle) and one piece of Amersham™ Protran® 0.45 µm nitrocellulose Membranes (GE Healthcare), both in the size of the gel, were soaked in blotting buffer (25 mM Tris-Base, pH 8.3, 192 nM Glycine, 20 % (v/v) Methanol). The composition was placed in the following order beginning at the anode: Whatman paper, nitrocellulose membrane, SDS-gel and Whatman paper. Afterwards, the cathode was installed. The Semi-Dry western-blotter was run at 1.5 mA/cm^2 for 1.5 h. After that, the blot was incubated with Ponceau S solution (0.2 % (w/v) Ponceau S, 5 % (v/v) Glacial acetic acid) for ~10 min to stain rapidly aromatic amino acids. After de-staining with distilled water, the protein bands were visible and, in this way, confirmed the successful blotting procedure. If required, the membrane was cut into pieces to be able to use different antibodies and the stripes were blocked in blocking buffer (5% (w/v) non-fat dried milk powder in TBS-T (50 mM Tris-Base pH 7.4, 150 mM NaCl, 0.1 % (v/v) Tween-20)) for 1 h.

Table 13 - Antibodies for western blot analysis

Primary Antibodies	Dilution	Source
Mouse α GFP (Monoclonal, GF28R)	1:5000	Pierce Protein Biology
Rabbit α GFP	1:2000	Prof. Dr. Heike Krebber, University of Göttingen
Rabbit α GFP (Polyclonal, PABG1)	1:4000	ChromoTek GmbH
Rabbit α Dbp5	1:3000	Prof. Dr. Heike Krebber, University of Göttingen
Rabbit α Asc1	1:2000	Dr. Oliver Valerius, University of Göttingen
Rabbit α uS3 Peptide Antibody	1:3000	Prof. Dr. Heike Krebber, University of Göttingen
Rabbit α Zwf1	1:5000	Prof. Dr. Ulrich Mühlenhoff, University of Marburg
Mouse α c-MYC (Monoclonal, 9E10)	1:750	Santa Cruz Biotechnology
Mouse α GST (Monoclonal sc-138)	1:2000	Santa Cruz Biotechnology

Secondary Antibodies	Dilution	Source
Goat α Rabbit – HRP Conjugated	1:10000	Dianova
Goat α Mouse – HRP Conjugated	1:10000	Dianova

The primary antibody was diluted (Table 13) in 2 % non-fat dried milk powder solved in TBS-T and incubated with the membrane in agitation for 1.5 h at RT or at 8 °C overnight. Subsequently, the membrane was washed 3 times with TBS-T and then incubated with the secondary antibody, diluted in 2% non-fat dried milk powder in TBS-T for 1.5 h at RT. Upon 2 times washing with TBS-T, the membrane was washed 2 times in distilled water. Then, detection was achieved by WesternBright™ Quantum™ Western Blotting HRP Substrate (Advansta), which was converted by the enzyme Horseradish Peroxidase (HRP) coupled to the secondary antibody. The resulting chemiluminescence was detected by the Fusion-SL-3500.WL (Peqlab) chemiluminescence detection system.

3.2.6. Molecular biological methods

3.2.6.1. Extraction of genomic DNA from *S. cerevisiae* cells

For isolation of yeast genomic DNA, cells were grown in 10 ml liquid culture. The saturated cell culture was harvested by centrifugation at 4100x g and 4 °C for 5 min. Subsequently, the pellet was washed with 1 ml distilled water and resuspended in 300 µl detergent lysis buffer (2 % (v/v) Triton X-100, 1 % (w/v) SDS, 100 mM NaCl, 10 mM Tris-HCl pH 8, 1mM EDTA) and 300 µl of phenol/chloroform/isoamyl alcohol (P/C/I, 25:24:1). After adding glass beads type S 0.4-0,6 mm in the same volume as the sample pellet, the mixture was disrupted using the FastPrep-24 machine at 5 m/s for 30 sec. The samples were centrifuged at 16200x g and 4 °C for 5 min to separate the organic and the aquatic phase. The aquatic

phase was carefully separated from the interlayer and the organic phase and mixed again with the same volume of P/C/I and centrifuged again. These steps were repeated until the interlayer appeared clear. Then the genomic DNA was precipitated from the aquatic phase by treatment with 6 µl of 7.5 M ammonium acetate and 1 ml 100 % ethanol. This mixture was vortexed and then centrifuged again at 16200x g and 4 °C for 10 min to precipitate the DNA. In the final step, the DNA pellet was washed twice with 70% ethanol and dried at 65 °C for 5 min, before it was resolved in 100 µl water.

3.2.6.2. RNA Isolation

RNA from whole cell lysate was purified with silica membrane based NucleoSpin® RNA kit (MACHEREY-NAGEL) according to the manufacturer's instructions, with the modification that DNase digest was extended from 15 min to 30 min for an entire DNA removal. Alternatively, RNA was purified with TRIzol® reagent (Thermo Fisher Scientific), following the manufacturer's instructions (with modifications). 1 ml TRIzol® was added to the cell lysate and incubated with agitation at 65°C for 10 min. In the next step, 200 µl chloroform was added and mixed thoroughly. After centrifugation at 16200x g for 10 min, the resulting upper phase was transferred into a fresh tube and 1 µl glycogen and 500 µl isopropanol were added and mixed for RNA precipitation. The mixture was stored at -20 °C overnight and then centrifuged at 16200x g and 4°C for 30 min. After removing the supernatant, the RNA pellet was washed twice with 70 % ice-cold ethanol made with DEPC water (0.1% (v/v) diethyl pyrocarbonate). Finally, the RNA was dried at 65 °C for 10 min and subsequently resuspended in 30 µl DEPC water and dissolved at 65 °C for 10 min and then stored at -20 °C or -80 °C. The yield and quality of the isolated RNA was determined with the NanoDrop spectrophotometer.

3.2.6.3. cDNA synthesis from RNA

For the synthesis of cDNA from RNA, the FastGene Scriptase II Kit (NIPPON Genetics) was used according to the manufacturer's instructions. Isolated RNA was diluted to 200 ng and then reverse transcribed with random hexamer primers and reverse transcription at a temperature of 42 °C. After reverse transcription, the cDNA was diluted to 0.5 ng/µl to be suitable for qPCR analysis. For every experiment, a control was prepared in the same way, but without addition of the reverse transcriptase (-RT).

3.2.6.4. Quantitative polymerase chain reaction (qPCR)

Quantitative polymerase chain reaction was used to determine the quantitative amount of different RNAs in whole cell lysates and relies on fluorescent labeling with molecules that bind specifically to double stranded DNA. The fluorescence is measured after each PCR cycle and the increase of fluorescence depends on the efficiency of the amplification reaction, which can also depend in the chosen primers. The PCR cycle (Cq) in which the fluorescent signal exceeds the threshold was used for the calculation of the starting amount of DNA. In this study, the primer pairs were designed with the GeneScript Real-time PCR (TaqMan) primer designer (Genescript.com) to reach amplification efficiencies of 0.8 -1. All samples, except the -RT and negative controls, were prepared in triplicates. Each sample was prepared in 10 µl consisting of 5 µl 2x qPCR master mix (qPCRBIO SyGreen Mix Lo-Rox, Nippon genetics), 4µl cDNA (0.5 ng/µl), 0.08 µl (1000 ng/µl) of forward and reverse primers and 0.86 µl nuclease free water. The qPCR was executed in a two-step protocol with 95 °C initial denaturation and 45 cycles with 30 s at 60 °C and 10 s at 95 °C. For the verification that only one specific product was amplified, the qPCR cycler CFX connect (BioRad) recorded a melting curve starting from 65 °C to 95 °C.

The target cDNA was normalized to 21S cDNA and calculated using the $2^{-\Delta\Delta Cq}$ method (Livak and Schmittgen, 2001).

3.2.7. Statistical analysis

All experiments were performed at least in three independent biological replicates. The mean ± standard deviations are shown. All data were finally analyzed for significance by Student's two tailed, two-sample, unequal variance *t*-test. Significant *P*-values below 0.05 were indicated by asterisk (*P<0.05; **P<0.01, ***P<0.001)

4. Results

Christian Beißel, Bettina Neumann, Simon Uhse, Irene Hampe, Prajwal Karki, Heike Krebber, Translation termination depends on the sequential ribosomal entry of eRF1 and eRF3, *Nucleic Acids Research*, Volume 47, Issue 9, 21 May 2019, Pages 4798–4813, https://doi.org/10.1093/nar/gkz177

My contributions to this project are the results presented in figures 1 C-F, 2 G+H, 3 C-E, 4 D-H, 5, 6, 7 and the model in Fig 8.

In the following results section of this thesis the figures are listed as paper figures e.g. Fig P1, Fig P2, Fig P3 et cetera.

This publication identifies Dbp5 as a protein that controls a shielded entry of eRF1 into translation termination. This prevents a premature eRF1 and eRF3 contact and thus readthrough of the stop codon.

Ariyachet, C., Beißel, C., Li, X., Lorrey, S., Mackenzie, O., Martin, P.M., O'Brien, K., Pholcharee, T., Sim, S., Krebber, H. and McBride, A.E. (2017), Post-translational modification directs nuclear and hyphal tip localization of *Candida albicans* mRNA-binding protein Slr1. Molecular Microbiology, 104: 499-519. doi:10.1111/mmi.13643

My contributions to this project are the results presented in figure 7.

This publication confirms a function of the RNA binding protein Slr1 from *Candida albicans*, a homolog of yeast Npl3, in translation by sucrose density fractionation experiments.

Beißel, C*.; Grosse, S*.; Krebber, H. Dbp5/DDX19 between Translational Readthrough and Nonsense Mediated Decay. *Int. J. Mol. Sci.* **2020**, *21*, 1085.

*These authors contributed equally.

This review discusses the function of Dbp5 in translation termination and a potential function of this RNA helicase in nonsense mediated decay (NMD).

The published papers are attached in the 9. Appendix section.

Currently unpublished additional results are listed below:

4.1. Dbp5 is involved in nonsense mediated decay

We have shown that Dbp5 is involved in regular translation termination, where it controls the eRF1-eRF3 interaction and we speculated that it might have a possible function in NMD (Beißel et al., 2019, 2020). The following experiment addressed, whether Dbp5 is required for the recognition of premature termination codons (PTCs). For this, we used a PTC containing reporter construct, which derived from the intron containing gene *CBP80* (Figure 9 A). *CBP80* is a typically spliced mRNA in yeast, which contain an intron that is located very close to the start codon.
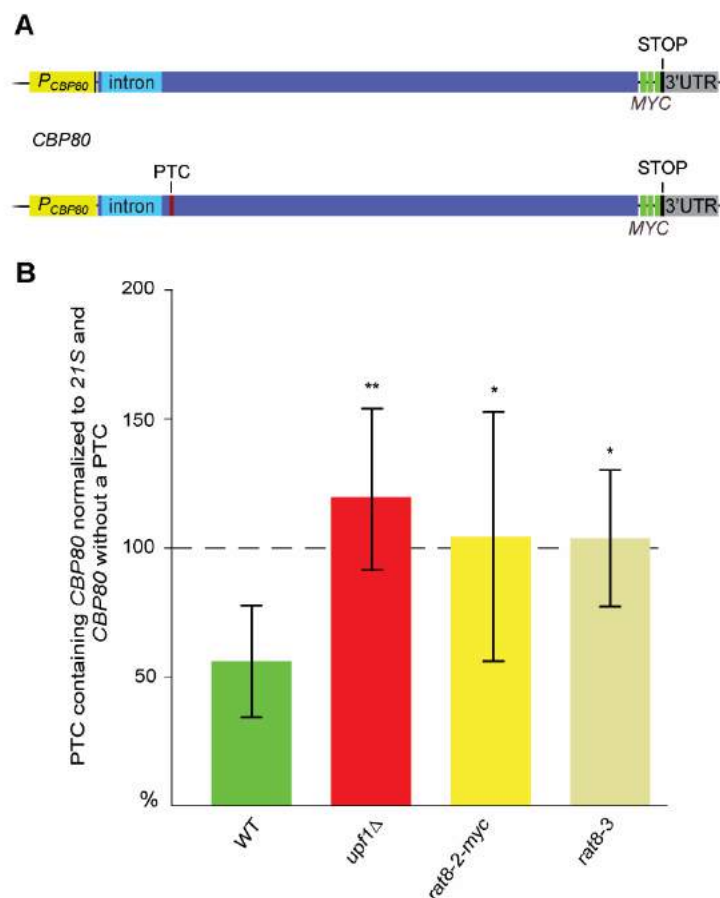
Figure 9 - Dbp5 is required for PTC induced destabilization of *CBP80* mRNA.
(A) Scheme of *CBP80* reporter constructs with and without a premature termination codon (PTC). (B) RNA levels of *CBP80^{PTC}* reporter construct in percent to *CBP80* without a PTC. The *MYC* sequence was used to discriminate between the reporter transcripts and endogenous *CBP80* mRNA. RNA levels were determined from the indicated strains containing the PTC-containing or a PTC-free NMD reporter. Both mRNA concentrations were normalized to the mitochondrial *21S* rRNA and quantified by qPCR. In each experiment the NMD reporter sample was normalized to the control reporter sample of the same strain. All strains were shifted to 37 °C for 1 h. (wild type (WT) and *rat8-2-myc* n=6; *upf1Δ* and *rat8-3* n=4, * indicate significances compared to WT).

In yeast, mis- or unspliced transcripts are thought to be a major source of NMD targets upon leakage of these faulty transcripts into the cytoplasm. Such pre-mRNAs typically contain a PTC that is close to the start codon (Christie, 2004). As it is known that Dbp5 plays a crucial role in mRNA export, we used a control reporter without a PTC to discriminate between co-

translational and mRNA export effects. Furthermore, the PTC is frame dependent and can only be recognized during translation. We found that the PTC reduced the RNA level of the reporter construct in wild type cells to 56 % after a temperature shift to 37 °C for 1 h (Figure 9 B). In contrast to that, our internal positive control, cells lacking *UPF1,* showed a significant stabilization of the PTC containing mRNA to 120 % after 1h at 37 °C. These results were comparable to unshifted wild type and *upf1Δ* cells (unpublished data, Laboratory of Prof. Dr. Heike Krebber). Interestingly, temperature sensitive mutants of *DBP5* that were incubated at 37 °C for 1 h showed a similar significant stabilization of the PTC-reporter as *upf1Δ*. We found an accumulation of the reporter mRNA to approximately 104 % in both, *rat8-2-myc* and *rat8-3* strains. These results indicate, that Dbp5 is involved in the PTC dependent destabilization of NMD targets. Given that the effect of the *DBP5* mutants was comparable to *upf1Δ* cells, it is possible that Dbp5 is required for NMD detection, because termination has to occur in order to trigger NMD via Upf1.

4.2. Dbp5 is involved in NSD and NGD

4.2.1. Dbp5 mediates the interaction of Dom34 and Hbs1 and their interaction with the ribosome

For regular translation it is known that Dbp5 mediates the interaction of the canonical translation termination factors eRF1 and eRF3. Furthermore, the interaction of both factors with the ribosome was reduced in temperature sensitive *DBP5* mutants (Fig P3 D+C). Interestingly, the decreased Dom34 and Hbs1 interaction was not only seen in *DBP5* mutant strains but also in strains mutated in the Dbp5 recycling factor Nup159 (Fig P4 F+G). These findings suggest that Dbp5 might not only mediate the interaction between eRF1 and eRF3 but also the binding between their orthologues Dom34 and Hbs1. To investigate this in more detail, we immunoprecipitated Dom34-GFP (Figure 10 A) or myc-Hbs1 (Figure 10 B) in either wild type cells or strains mutated in *DBP5/RAT8* and detected the co-immuno-precipitated proteins after a temperature shift to 37 °C for 1 h. In this experiment, absence of growth suppressor of Cyp1 (Asc1) served as an indicator for a ribosomal interaction. Asc1 is a ribosome binding protein that can be detected with ribosomes in wild type strains (Kouba et al., 2012). Indeed, we could clearly determine an interaction of Dom34-GFP with myc-Hbs1 and Asc1 in wild type cells.
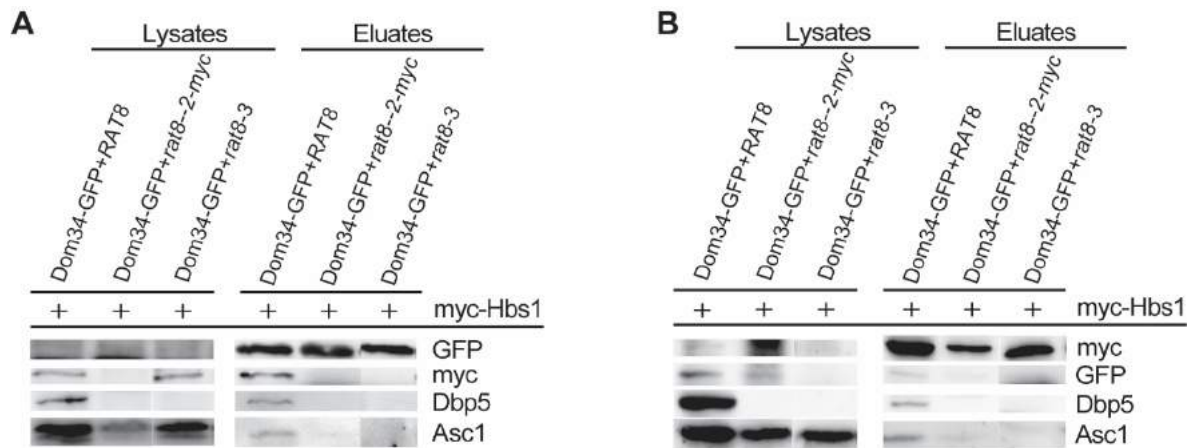
Figure 10 -The interaction of Dom34 and Hbs1 is decreased in *DBP5* mutants.
Western-blot analysis of co- immunoprecipitations of Dom34-GFP or myc-Hbs1 are displayed. (A) Detection of Dom34-GFP pull down and co-immunoprecipitated proteins (myc-Hbs1, Dbp5, Asc1) in different strain backgrounds (*RAT8*, *rat8-2-myc* and *rat8-3*). (B) Detection of co-immunoprecipitated proteins (Dom34-GFP, Dbp5, Asc1) of myc-Hbs1 pull downs in different strain backgrounds (*RAT8*, *rat8-2-myc* and *rat8-3*). The displayed results were seen in four (left) and three (right) independent experiments.

Interestingly, these interactions were diminished in *rat8-2-myc* and *rat8-3 cells*

(Figure 10 A). A similar decrease in the interaction was detected for the interaction with Dom34-GFP and Asc1, when we immunoprecipitated myc-Hbs1 in *RAT8* mutant cells (Figure 10 B). In wild type cells we detected a clear interaction of myc-Hbs1 with Dom34-GFP and Asc1 (Figure 10 B). In both experiments, the interaction of Dom-GFP or myc-Hbs1 with Dbp5 was abolished in *RAT8* mutants. (Figure 10 A+B). In contrast, in wild type cells Dbp5 co-precipitated with Dom34-GFP and Hbs1-myc. Interestingly, in *nup159Δ* cells, which specifically lack the interaction domain of Dbp5, the binding defect between Dom34-GFP and its co-purified proteins, myc-Hbs1, Dbp5 and Asc1, was also detectable (unpublished data, laboratory of Prof. Dr. Krebber). In summary, Dom34 and Hbs1 require Dbp5 for their interaction and association with the ribosome, and they share this behavior with the canonical release factor eRF1 and eRF3.

4.2.2. Dbp5 interacts directly with Dom34 and Hbs1

For canonical translation termination, a direct interaction of eRF1 and Dbp5 was shown. This interaction depends on the nucleotide status of Dbp5 (Fig P5 A). In contrast, however, a direct interaction of Dbp5 and eRF3 was not detectable, neither in *in vivo* nor in *in vitro* studies (Fig P5 A) (Gross et al., 2007). Contrary to that, an *in vivo* interaction of Dbp5 to both, Dom34-GFP and myc-Hbs1 was visible (Figure 10). To further investigate the binding preference of Dbp5 to Dom34 and Hbs1, we performed combined *in vivo* and *in vitro* studies. We first immobilized either Dom34-GFP (Figure 11 A) or myc-Hbs1 (Figure 11 B) from whole yeast lysate to beads and added recombinant GST-Dbp5.

We determine the nucleotide status of GST-Dbp5 by supplying 1 mM AMPPNP. As shown in Fig 11 A, keeping it in its ATP-bound state was necessary for the interaction with Dom34-GFP but not with myc-Hbs1, as GST-Dbp5 was only able to bind to Dom34 when it is bound to AMPPNP.
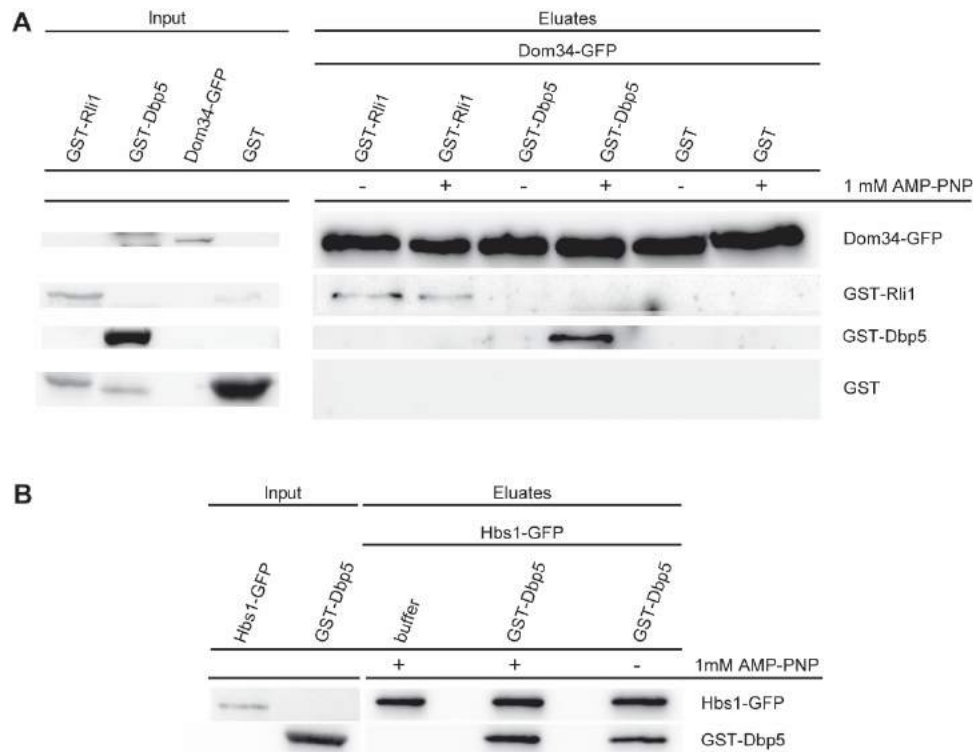
Figure 11 - Binding of Dbp5 to Dom34 and Hbs1 in regard to its nucleotide associated status. Western-Blot analysis of combined *in vivo* and *in vitro* studies are depicted. (A) Binding of either recombinant GST-Rli1, GST or GST-Dbp5 to immobilized Dom34-GFP is shown. All binding studies are performed once with 1 mM AMPPNP and once without 1 mM AMPPNP. (B) Nucleotide (1 mM AMPPNP) dependent binding of Dbp5 to immobilized myc-Hbs1 or to MYC-beads incubated with buffer only. The displayed results were seen in four (top) and two (bottom) independent experiments.

Interestingly, our positive control GST-Rli1 could interact with Dom34-GFP independently of its bound nucleotide (Figure 11 A). Moreover, the binding of Dbp5 to Hbs1 was independent of the nucleotide bound status of Dbp5. These findings reveal that Dbp5 might interact with Dom34 in the same manner as with eRF1, but in contrast to eRF3 it also binds to Hbs1, independent of its ATP binding.

4.2.3. Binding of Dbp5 and Hbs1 to Dom34 is not mutually exclusive

Taking into account that we were able to detect an interaction of Dbp5 with Dom34 and Hbs1, we investigated whether the binding of Dbp5 and Hbs1 to Dom34 is mutually exclusive. For this, we immobilized Dom34-GFP from whole yeast lysate and added 350 µg recombinant GST-Dbp5, which was supplemented with 1 mM AMPPNP. To this pre-formed complex, we added increasing concentrations of yeast lysate containing myc-Hbs1. The positive controls showed that GST-Dbp5 and myc-Hbs1 alone are able to bind to Dom34-GFP respectively (Figure 12). Interestingly, even high concentrations of myc-Hbs1 did not disrupt this complex, but rather presumably formed a bigger complex composed of Dom34-GFP, GST-Dbp5-AMPPNP and myc-Hbs1 (Figure 12). This is in contrast to the canonical translation termination factors eRF1 and eRF3 and their binding to Dbp5, where the binding of either eRF3 or Dbp5 to eRF1 is mutually exclusive (Fig P5 B). The addition of eRF3 did not result in its association with eRF1 and Dbp5.
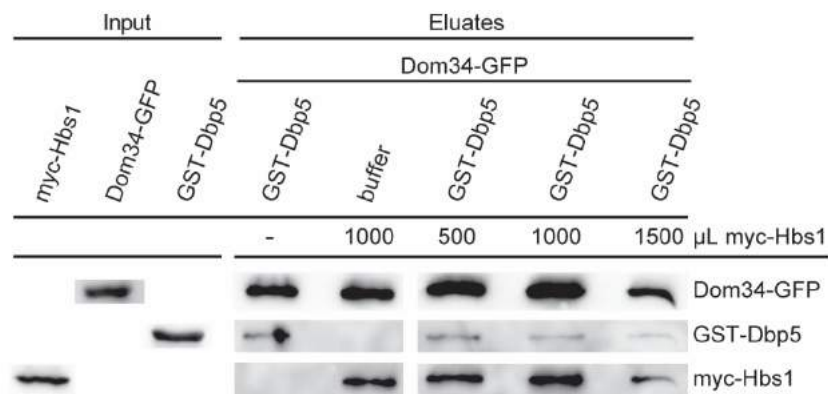
Figure 12 - Dbp5 and Hbs1 interaction with Dom34 is not mutually exclusive.
Western blot analysis of competition assay is displayed. Increasing concentrations of myc-Hbs1 were not able to disrupt a preformed complex of Dom34-GFP and GST-Dbp5, supplemented with 1 mM AMPPNP, but rather additionally associated with Dom34-GFP, GST-Dbp5 and AMPPNP.
The displayed results were seen in four independent experiments.

4.2.4. Dom34 and Hbs1 co-migrate with Dbp5 and Asc1 in polysomes of sucrose-density gradients

To investigate how Dbp5 might influence the binding of Dom34 and Hbs1 to translating ribosomes, we performed sucrose-density fractionation experiments. The experiment was either carried out in wild type cells or *rat8-2* and *rat7ΔN* mutants. All strains were shifted to the non-permissive temperature of 37°C for 1 h and treated with 100 µg/ml cycloheximide to avoid polysome run-off. Polysome profiles of wild type cells showed after 100 µg/ml cycloheximide treatment, a non-ribosomal peak of proteins not bound to ribosomes, a peak for the 40S and 60S ribosomal subunits, a peak for 80S ribosomes and polysomes reflecting actively translating ribosomes (Figure 13 A, left). Also, in *rat8-2* and *rat7ΔN* mutants, comparable amounts of non-ribosomal, 40S and 60S ribosomal subunits were detected.

However, in contrast to wild type cells these mutants showed increased 80S peaks and fewer polysomes (Figure 13 A middle and right). Consistently, Asc1, as a ribosome associated protein, reflects this altered distribution in western blots of the gradient fractions (Figure 13 B, bottom). Asc1 was found in all polysomal fractions, and in the 80S and 40S peaks in wild type cells.
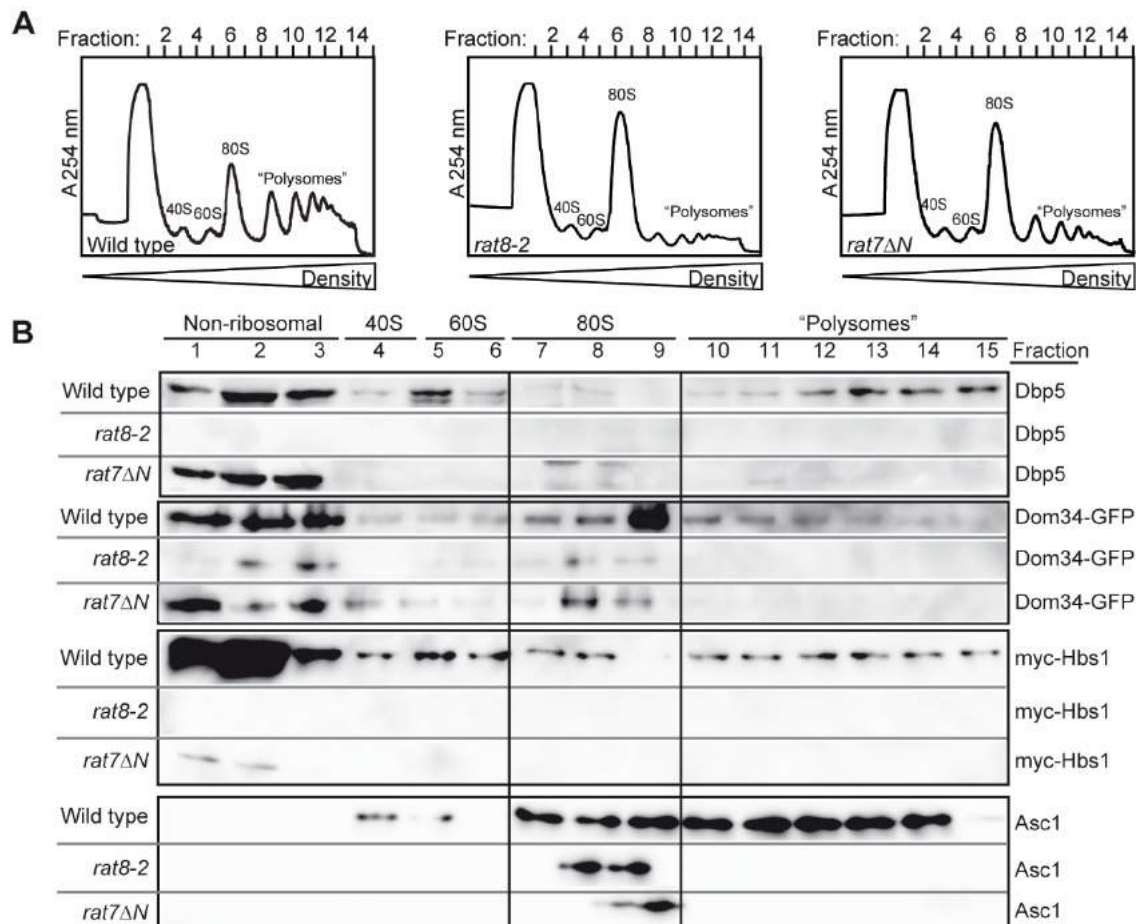
Figure 13 - Stability of Hbs1 and binding of Dom34 to polysomes depends on functional Dbp5.
(A) Ribosome profiles of wild type, *rat8-2* and *rat7ΔN* strains after sucrose density gradients are displayed. Ribosome profiles were recorded via measuring the absorbance at 254 nm.
(B) Western blot analysis of precipitated proteins after ribosome fractionation are shown. Proteins of each fraction are precipitated and detected via different antibodies (GFP, MYC, Dbp5 and Asc1). Similar results were obtained in three independent experiments.

In contrast, in *rat8-2* and *rat7ΔN* mutants, Asc1 was only visible in the 80S fractions of ribosomes. Dbp5 migrated with the non-ribosomal, 60S and polysomes fractions in wild type cells. Interestingly, in the *rat7ΔN* mutant the fraction of Dbp5 shifted to the non-ribosomal fraction, while in *rat8-2* mutants Dbp5 was not longer detectable (Figure 13 B, top), suggesting that the helicase is absent from ribosomes or even degraded, respectively. For myc-Hbs1, we uncovered its presence in all fraction of the ribosome gradient in wild type cells. In contrast, myc-Hbs1 was only slightly detectable in the non-ribosomal fractions of *rat7ΔN* cells and not detectable at all in *rat8-2* mutants (Figure 13 B; middle-bottom).

Furthermore, Dom34-GFP was detectable in the polysomes fractions, as well as in the 80S and non ribosomal fraction in the wild type strain. Contrary to that, Dom34-GFP was only present in 80S and non-ribosomal fractions in *rat8-2* and *rat7ΔN* strains (Figure 13 B, middle-top). Together, these data suggest that the stability of Hbs1 might depend on functional Dbp5, while Dom34 shows a different behavior. Like Hbs1, it co-migrates with Dbp5, but in contrast to Hbs1, Dom34 is able bind to the 80S ribosomes independently of Dbp5.

4.2.5. *rat8-3 dom34Δ* double mutant strains are hypersensitive to oxidative stress

To gain insights into how Dbp5 might act together with Dom34 in NSD and NGD, growth analysis of a *DOM34* knock out strain combined with *rat8-3* mutants was performed. Taking into account that *dom34Δ* showed no growth defect under normal conditions, we supplemented the medium with 1 mM of the oxidizing reagent diamide. This drug was shown to increase the growth defect of the *dom34Δ* strain (Jamar et al., 2017). For an even stronger phenotype of reduced growth, we combined this experimental setup with NSD and NGD reporter constructs (Tsuboi et al., 2012). The general composition of these reporter constructs expressed from a *GAL1* promoter are depicted in figure 14 A. The reporters are composed of a GFP ORF (green) followed by the sequence that is recognized by NSD or NGD (red). These sequences are a stem loop (SL) structure, sequence of rare codons $(GGN)_{12}$ or a sequence with an autocatalytically acting self cleavage ribozyme (*hammerhead ribozyme*) (*Rz)* (Forster and Symons, 1987). Additionally, the NGD and NSD sequence is each followed by a FLAG-tag and *HIS3* gene. Furthermore, a reporter with the same composition, but lacking an NSD or NGD evoking sequence was used as a control reporter. The combination of 1 mM diamide with the transcription of NSD and NGD mRNAs reporters had no negative effect on the growth of *rat8-3* mutants compared to cells that contained wild typical *RAT8*, neither at 25 nor at 35 °C. Rather a small general growth rescue effect was visible (Figure 14 B, middle-bottom). Interestingly, in both strains *dom34Δ RAT8* or *DOM34 rat8-3* the presence of the reporter constructs did not negatively affect the growth of the strains. Only the double mutant of *dom34Δ* and *rat8-3* was sensitive to the presence of the reporter constructs at 35°C (Figure 14 B, bottom).
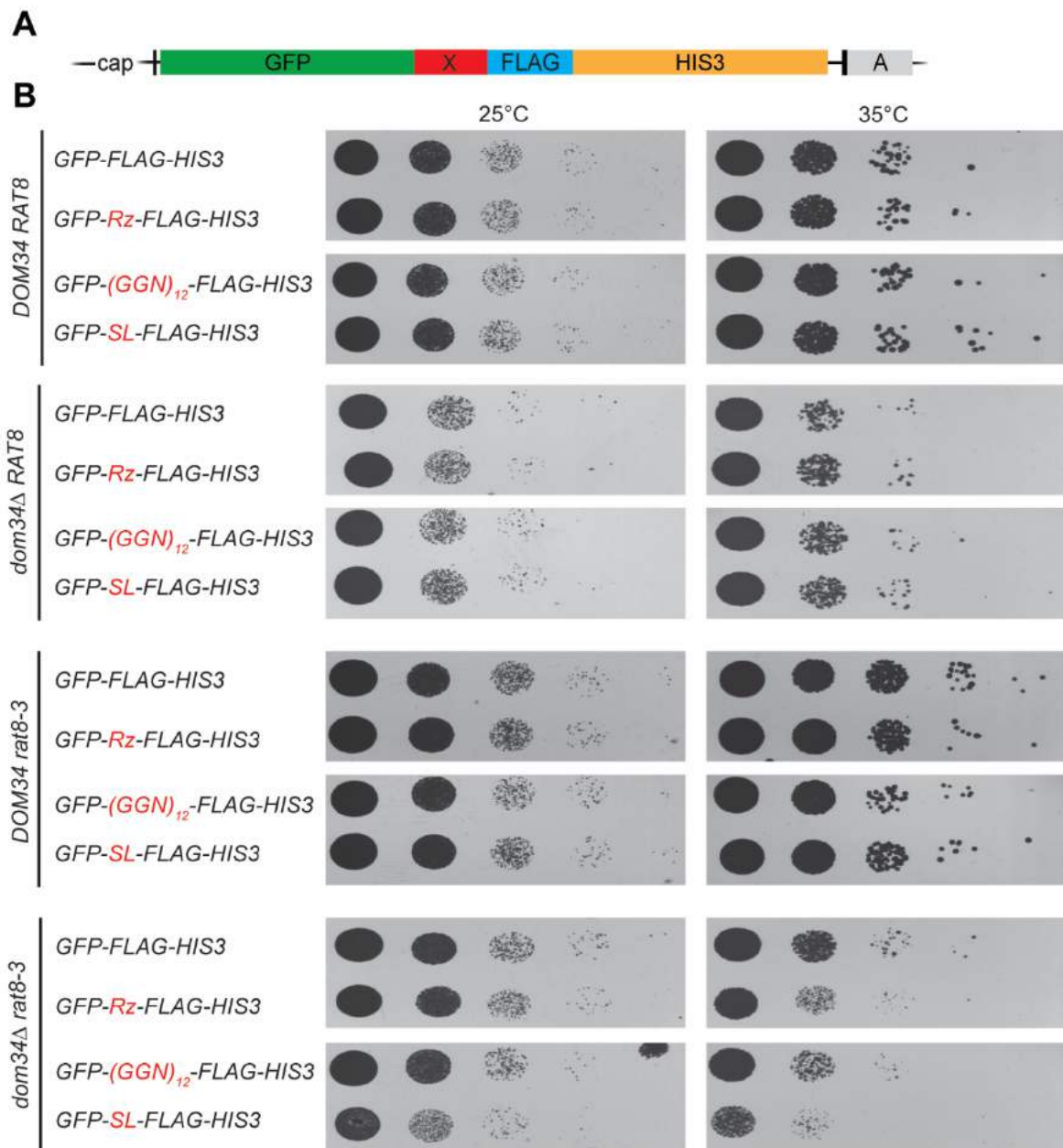
Figure 14 - *dom34Δ* and *rat8-3* double mutants are sensitive to increased amounts of NGD and NSD substrates.

(A) The general composition of the NSD and NGD reporter constructs is displayed. The GFP ORF (green) is followed by X (red), which reflects either a stem loop structure (SL), rare codons (GGN)$_{12}$, or a hammerhead ribozyme (*Rz*). The control reporter had no additional sequence but the *FLAG*-tag sequence directly followed the GFP sequence.

(B) Growth analysis of wild type, *dom34Δ*, *rat8-3* and a combination of both are shown. The media was supplemented with 1 mM diamide and strains were transformed with the indicated reporter constructs. The displayed results were seen in three independent experiments.

4.2.6.NSD reporter construct accumulate in *dom34Δ* and *rat8-3* single and double mutant strains

To investigate whether the growth defect of *dom34Δ rat8-3* double mutants, arose from potential defects in the degradation of the reporter mRNA, we analyzed the RNA levels via qPCRs.
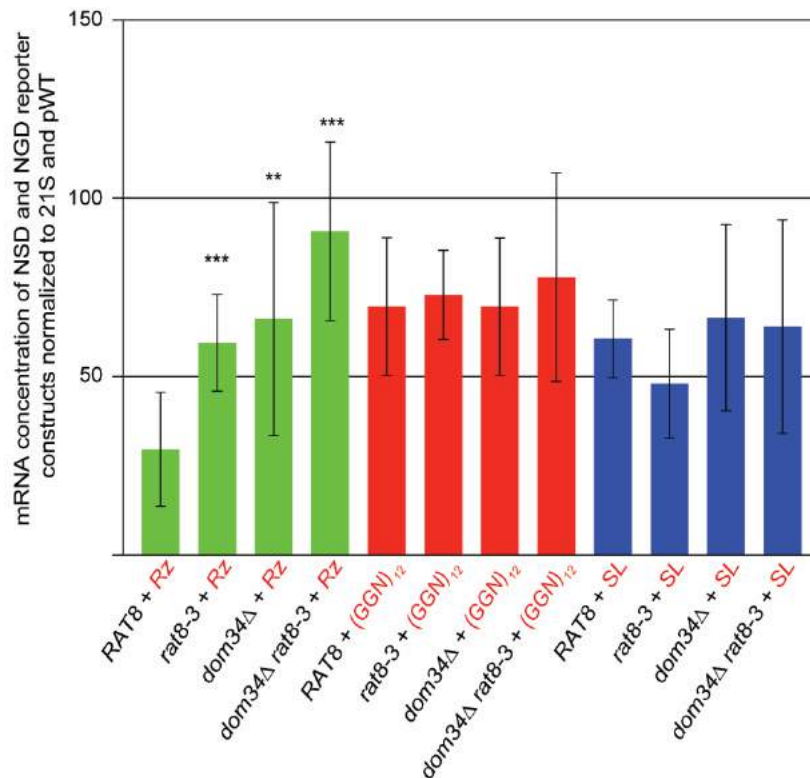
Figure 15 - Accumulation of NSD and NSG reporter constructs in *dom34, rat8-3* and the double mutant strains.
All reporter constructs, including the control reporter (pWT) were detected by primers that amplify the GFP sequence. All constructs were normalized to *21S* rRNA and the control reporter. (n=8).

After expressing the reporter constructs for 24 h in medium containing 2% galactose, the reporter mRNA was detected via qPCR with primers targeting the GFP sequence in the middle of the ORF. All measured cDNA concentrations of the reporter constructs were first normalized to *21S* rRNA and additionally to the wild typical construct that lacks an NSD or NGD response sequence. In the wild typical strain with the *Rz* reporter (NSD) construct the mRNA mostly degraded and only ~30 % of it was detectable. In contrast *rat8-3* cells showed a stabilization of the Rz reporter construct (Figure 15, green bars) to ~60 % compared to wild type cells and a similar increase to ~66 % was detectable in *dom34Δ* cells, indicating that Dbp5, like Dom34, functions in NSD. Strikingly, the double mutant of *dom34Δ* and *rat8-3* stabilized the reporter construct to ~91 %, suggesting additive effects of Dbp5 and Dom34 in NSD. For the NGD sensed reporters (GGN)$_{12}$ (Figure 15, red bars) and SL (Figure 15, blue bars) the faulty reporter mRNAs did not accumulate. Their expression levels ~56 % in

case of the $(GGN)_{12}$ sequence and ~60 % for the stem loop structure were comparable to the control construct in all tested strains.

These results indicate that the growth defect of the *dom34Δ rat8-3* double mutant (Fig 14) might originate from mRNA accumulation of the NSD reporter, which indicate problems in their degradation, either through direct or indirect effects.

4.2.7. Overexpression of *DOM34* suppresses the growth defect of the *rat8-2* mutant

To address, whether Dbp5 and Dom34 act in the same pathway, we investigated if growth defects of one of the mutants would be rescued by overexpression of the other. Therefore, we overexpressed either *DOM34* or *DOM34-MYC* from the strong *ADH1* promoter in wild type and *rat8-2* mutant strains. The sequences were encoded on plasmids that contain the *URA3* gene. To control, that the rescue effect originates from overexpression of *DOM34*, we spotted all tested strains also on FOA plates (Figure 16). Additionally, we included an empty vector in our studies that only encoded *URA3*. Overexpression of *DOM34* did not affect the growth rates of the wild type strain. Interestingly, the growth defect of the *rat8-2* strain, was rescued by overexpression of *DOM34* at 30 °C and 35 °C. This rescue effect was not longer detectable on FOA plates, on which the cells had lost the URA3 marked *DOM34* plasmids (Figure 16, right). No effects of the *DOM34* overexpression plasmids were detectable at the permissive temperature of 25 °C and at the non-permissive temperature of 37 °C. These finding indicate that mutant strains of Dbp5 that has access to more Dom34 molecules show a better survival.
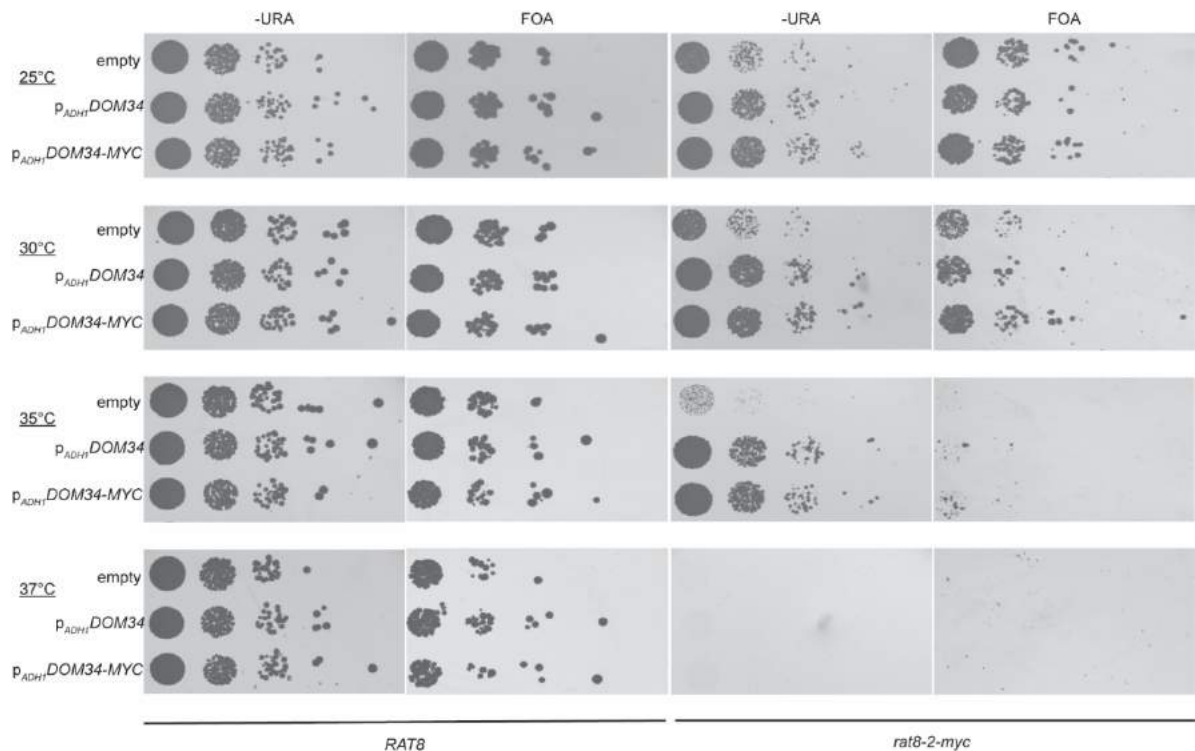
Figure 16 - Overexpression of *DOM34* rescues growth defect of *rat8-2* mutants.
Wild type and *rat8-2* mutants containing either P$_{ADH}$*DOM34* or P$_{ADH}$*DOM34-myc* were spotted in 10-fold serial dilutions onto -URA or FOA plates. Scanned pictures of plates are displayed after an incubation at the indicated temperatures for 3 days (URA) or 5 days (FOA).

Taken together, we have identified a novel function of Dbp5 in the cytoplasmic quality control pathways NSD and NGD. Dbp5 can interact with both, Dom34 and Hbs1. Importantly, defects in *DBP5* lead to growth defects with *dom34Δ* in the presence increased amounts of both NSD and NGD reporter mRNAs, although only an increase of an NSD reporter RNA was indeed detectable. Strikingly, overexpression of *DOM34* partially rescued the growth defect of a *DBP5* mutants that supports a function of Dbp5 with Dom34.

5. Discussion

5.1. Translation termination depends on the sequential ribosomal entry of eRF1 and eRF3

5.1.1. Dbp5 binding to the ribosome, depends on functional eRF1

Previous studies revealed that Rli1 is involved in translation termination, recycling and initiation (Dong et al., 2004; Khoshnevis et al., 2010; Pisarev et al., 2010). However, it is not clear when Rli1 is recruited to the ribosome. A further involvement of Rli1 in ribosome biogenesis suggested that Rli1 might stay associated with the ribosome during its complete life cycle (Kispal et al., 2005). Instead, Dbp5 seems to act only in translation termination and it might also interact with the ribosome only at late steps of translation (Gross et al., 2007). In our study we accumulated evidence that the binding of Rli1 to the termination complex is independent of eRF1, while the binding of Dbp5 to the ribosome clearly depends on functional eRF1. Quantitative analysis (Fig P1 D) of co-immunoprecipitation experiments (Fig P1 C) revealed that binding of mutant sup45-2 protein to the ribosome was significantly decreased to about ~50% after a temperature shift to the non-permissive temperature for 1 hour. This is consistent with earlier findings in which it was shown that the mutated sup45-2 protein loses its ribosome binding ability (Song et al., 2000; Stansfield et al., 1995). However, the binding of Rli1 to the ribosome was not negatively affected by the binding defect of sup45-2 (Fig P1 A+D). In contrast, we detected an even stronger binding of Rli1 to the 40S ribosomal subunit. Given the fact, that AMPPNP arrests Rli1 in a conformation that mainly binds to the 40S but not the 60S subunit (Andersen and Leevers, 2007), it is tempting to speculate that a large fraction of Rli1 is ATP-bound in *sup45-2* mutants. Interestingly, the binding of Dbp5 to the ribosome decreased in *sup45-2* mutants similar to eRF1 (Fig P1 B-D), indicating that Dbp5 requires functional eRF1 for its association with the ribosome. Taken together, these findings indicate that Rli1 is bound to the ribosome before eRF1 is recruited and binding of Dbp5 with the ribosome requires the binding of eRF1.

To get further evidence for such a sequential recruitment, we took advantage of the *tef2-9* mutant, encoding mutant *eEF1A*. Mutations of *eEF1A* lead to defects in translation elongation, causing a detectable polysome fraction in strains that were not treated with cycloheximide (Fig P1 E and (Dinman and Kinzy, 1997)). In contrast to that the ribosome run off the mRNA in wild type cells, which is represented by no detectable polysomes. Quantitative analysis (Fig P1 G) of Rli1 binding to the polysomes in wild type and *tef2-9* (Fig P1 F) demonstrated that Rli1 was present in the arrested polysomes in *tef2-9* mutants, to an even greater extend than of Asc1. Taking earlier findings into account in which it was shown that human ABCE1 and *archaea* EF1 bind to the same inter-subunit space of the

ribosome (Becker et al., 2012), it is possible that their binding might be mutually exclusive and Rli1 takes over the binding site of eEF1A. In contrast to that, Dbp5 binding to the polysomes was almost not detectable in wild type and *tef2-9* strains (Fig P1 G), indicating that Dbp5 binds to the ribosome after translation elongation.

5.1.2. Dbp5 and Rli1 interact in translation termination

It is known for more than a decade that Rli1 and Dbp5 act in translation termination (Gross et al., 2007; Khoshnevis et al., 2010), but it was still unclear whether they interact during translation termination. Our results showed, that Rli1 interacts with Dbp5 and Gle1 in wild type cells (Fig P2 A and Fig P1S). However, both proteins are also involved in ribosome biogenesis (Dong et al., 2004; Kispal et al., 2005; Neumann et al., 2016). To distinguish between a possible interaction during ribosome maturation and translation termination, we investigated whether Dbp5 and Rli1 interact in *sup45-2* mutants and upon cycloheximide treatment of wild type cells. In fact, the interaction of Dbp5 and Rli1 was diminished to ~42% in *sup45-2* cells (Fig P2 B+C) in which eRF1 and Dbp5 are not able to enter the ribosome (Fig P1 D). Furthermore, the treatment of wild type cells with cycloheximide led to ribosome stalling during elongation and the interaction of Dbp5 and Rli1 was decreased to approximately 41% (Fig P2 D+E). Thus, most of the interaction of Dbp5 and Rli1 presumably takes place during translation termination. Interestingly, the interaction of Rli1 with the small ribosomal subunit was not affected in cycloheximide treated cells (Fig P2 D). This stays in contrast to earlier findings showing that mutations in *SUP45* lead to an increased binding of Rli1 to the 40S subunit (Fig P1 D and P2 B). This phenomenon indicates that the accumulation of Rli1, presumably in its ATP bound state, to the small ribosomal subunit increases if eRF1 is not able to hydrolyze the peptidyl-tRNA (Stansfield et al., 1997). However, as Rli1 might be the earliest translation termination factor to be recruited to the ribosome, it could be possible that Rli1 helps to fetch other translation termination factors. Indeed, we detected that overexpression of *RLI1* could partially rescue the growth defect of *sup45-2* mutants (Fig P2 F). This rescue defect might have two possible reasons. Either, Rli1 might help the residually bound sup45-2 protein (~44%) to hydrolyze the peptidyl-tRNA or it might recover the binding defect of sup45-2 to the ribosome, or both. However, our results rather indicate that the latter assumption is more likely, because overexpression of Rli1 also rescued the binding defect of sup45-2 to the 40S ribosomal particle from 24 % to 63 % (Fig P2 G+H).

5.1.3. eRF1 and eRF3 enter the termination complex independently

In contrast to Rli1, the binding of Dbp5 to the ribosome requires functional eRF1 (Fig P1). It was already suggested earlier that Dbp5 might mediate the positioning of eRF1 at stop codons and dissociate from the termination complex to facilitate the interaction of eRF1 and eRF3 (Gross et al., 2007). To get further evidence for this idea, we took advantage of the s*up45-2* mutant, in which mutant eRF1 has lost its ability to bind to the ribosome. In this mutant, eRF1 is freely available in the cytoplasm at the non-permissive temperature (Fig P1 C+D). Strikingly, in this mutant the binding between Dbp5 and eRF1 was increased to ~217 % (Fig P3 A+C) and the interaction of eRF3 and eRF1 was diminished to ~32 % (Fig P3 B+C). Moreover, this increased binding of Dbp5 and eRF1 was visible, although the stability of eRF1 was impaired in *sup45-2* mutants (Fig P1 A+B, lysate lanes). These results indicate, that the cytoplasmic eRF1 is preferentially bound to Dbp5 and that the interaction of eRF1 and eRF3 is rather prevented by Dbp5 in the cytoplasm or only takes place upon eRF1 entry to the stop-codon bound ribosome. If the interaction of eRF1 and eRF3 would indeed be blocked by a pre-formed eRF1-Dbp5 complex, we expected to see a similar outcome for a disturbed eRF1 and eRF3 interaction, in *rat8-2* mutants. If mutant Dbp5 would not be able to deliver eRF1, an accidental contract of eRF1 and eRF3 might immediately lead to a GTP recruitment of eRF3, its subsequent hydrolysis and the consecutive dissociation of the two proteins.

Indeed, in the *DBP5* mutant strain *rat8-2*, we detected a decreased interaction of eRF1 with eRF3 to ~ 30 % and to ~34% with the ribosomal subunit (Fig P3 D+E). This finding supports the hypothesis that ribosome delivery of eRF1 through Dbp5 is important for correct translation termination. In fact, eRF3 and Dbp5 do not interact *in vivo* (Gross et al., 2007). Thus, a model is probable in which the binding of eRF1 and eRF3 takes place only at the ribosome and after Dbp5 release. In line with our model, a previous study showed that the interaction of eRF1 and eRF3 in *rat8-2* mutants is decreased after a temperature shift to 37 °C for 20 minutes (Gross et al., 2007). This observed binding defect was not as prominent as in our study, which might originate from the shorter shifting time.

5.1.4. The function of Dbp5 in translation termination requires its ATPase cycle

The ATPase activity of Dbp5 is essential for its function in mRNA export, but not for its role in ribosomal export (Hodge et al., 2011; Neumann et al., 2016; Tieg and Krebber, 2013). However, for translation termination Gross *et al.* (2007) showed that only the overexpression of wild type *DBP5* and not of the ATPase deficient *DBP5* mutant (*E240Q*) was able to rescue the readthrough defect of the *sup45-2* mutant.

Furthermore, Dbp5 requires its co-factors Gle1 and IP$_6$ for its ATPase cycle and mutations of both showed increased readthrough of stop codons (Alcázar-Román et al., 2010; Bolger et al., 2008). For mRNA export, Nup159 was identified as the recycling factor of Dbp5 at the nuclear pore complex (Noble et al., 2011). Indeed, by using a dual reporter ß-galactosidase luciferase assay (Fig P4 A) our study revealed that different mutants of *NUP159* (*RAT7*) showed increased readthrough defects. Both the temperature sensitive *rat7-1* mutant and the *rat7ΔN* mutant, which specifically lacks the interaction domain of Dbp5, showed a ~20 % and 21 % reduced stop codon recognition, respectively. The observed readthrough defects are comparable to those detected in *rat8-2* mutant, which showed ~25 % readthrough activity (Fig P4 B). Although wild type cells were not fully readthrough resistant for the reporter construct, readthrough was really low with ~13 %. Similarly, an independent mutant of the karyopherin that is not involved in mRNA export or translation, *kap123Δ* (karyopherin 123), was also unaffected in its stop codon recognition and equal to wild type with ~13 % (Fig P4 B). Interestingly, overexpression of wild type *DBP5* could rescue the increased readthrough defects seen in *rat7ΔN* mutants from approximately 25 % to wild typical levels (~12 %). These findings indicate that Nup159 is required to recycle Dbp5 and maintain the functionality of Dbp5 in translation termination. When Dbp5 is not recycled, as it is the case at the non-permissive temperature of *RAT7*, elevated amounts of Dbp5, which thereby also provide elevated levels of ATP-bound Dbp5, sustain a larger pool of active Dbp5, which can function in translation termination. This explains why an overexpression of *DBP5* in this recycling defective mutant suppresses the Nup159 defect. Further insight into the role of Nup159 in sustaining active Dbp5 were obtained from co-immunoprecipitation experiments. In *rat7ΔN* strains, the binding of Dbp5 to eRF1 is reduced to ~54 % and the interaction of eRF1 to eRF3 decreases even further to ~12 % as compared to wild type cells (Figure P4 D-G). These results suggest that only recycled, probably ATP bound Dbp5 is able to interact with eRF1 and regiment the interaction of eRF1 and eRF3. To investigate more directly whether Dbp5 in only its ATP bound form can interact with eRF1, we performed an *in vitro* binding study. Clearly, only in the presence of 1 mM AMPPNP Dbp5 was able to interact with eRF1 (Fig P4 H). In contrast, the binding affinity of eRF3 to eRF1 was not affected by the presence or absence of the ATP-analogon (Fig P4 H). Taken together, these *in vivo* and *in vitro* assays led to a model in which eRF1 and Dbp5-ATP interact in the cytoplasm. Dbp5 delivers eRF1 to the ribosome and places eRF1 correctly in the termination complex. Subsequent dissociation of Dbp5 allows eRF1 and eRF3 contact on the ribosome (Fig P3 B+C) and the completion of the termination reaction.

5.1.5. Binding of Dbp5 and eRF3 to eRF1 is mutually exclusive

We have shown that ATP-bound Dbp5 and eRF1 interact in the cytoplasm (Fig P3 A+C, Fig P4 H) and our results further indicate that the interaction of eRF1 and eRF3 is Dbp5-ATP dependent (Fig P3 D+E; Fig P4 F+G) and it is conceivable that the function of Dbp5 is to prevent an early contact between eRF1 and eRF3. In this case, the binding of Dbp5 and eRF3 to eRF1 would be mutually exclusive. Indeed, our results from an *in vitro* binding assay clearly showed that eRF1 lacking the last 25 amino acids of its C-terminus (His-eRF1Δ25C) neither interacts with Dbp5 nor with eRF3 (Fig P5 A). These findings indicate, that eRF3 and Dbp5 share the same binding site within eRF1 and that the last C-terminal amino acids of eRF1 mediate the interaction with both, the helicase and eRF3. The interaction domain of eRF1, responsible for the eRF3 contact, was already determined earlier to be within the last 25 amino acids residues (Eurwilaichitr et al., 1999). Given that Dbp5 does not interact with eRF3 *in vivo* (Gross et al., 2007), and Dbp5 and eRF3 share the same binding site on eRF1, eRF3 should not be able to disrupt a preformed complex of Dbp5 and eRF1. This was indeed the case as shown in our *in vitro* displacement assay. Even high amounts of eRF3 were not able to disrupt a preformed Dbp5-eRF1 complex (Fig P5 B).

5.1.6. Dbp5 mediates the interaction of eRF1 and eRF3

In a model, in which one function of Dbp5 in translation termination prevent an early eRF1-eRF3 contact, one has to assume that eRF3 enters the termination complex in a different way and should already be present when eRF1 is delivered. Indeed, in the elongation factor mutant *tef2-9* (see 5.1.1.) the binding of eRF3 to the polysomal fraction was even stronger than the binding of Asc1 to the polysomes when compared to wild type cells (Fig P6 A+B). However, eRF1 was almost absent in the polysomes in both wild type and *tef2-9* strains (Fig P6 A+B). These findings suggest, that eRF3 binds to the ribosome prior to eRF1 and is already bound to the ribosome during translation elongation. This is in line with the finding, that the binding of eRF3 to the small (uS3-GFP) and large (uL23-GFP) ribosomal subunits was increased in *sup45-2* mutants compared to wild type cells (Fig S6 C+D). Taken together, these findings indicate that eRF3 is already bound to the ribosome prior to eRF1 and Dbp5 association. Furthermore, the data also show that binding of eRF1 is necessary for the release of eRF3 from the termination complex. Since we could also detect a binding for Rli1 to the ribosome at that early time point (Fig P1 G+F), we investigated a potential direct interaction of eRF3 and Rli1. In our *in vitro* binding study, we detected that GDP-bound but not GTP bound eRF3 directly interacts with Rli1 (Fig P6 E). This finding corroborates with the work of Pisarev *et al.* (2010), who suggested that eRF3-GDP can

productively interact with ABCE1/Rli1. Moreover, they found that Rli1 in its nucleotide free state is only partially bound to the 40S ribosomal subunit. In our *in vitro* assay (Fig P6 E), we did not supplement the buffer system with ATP. Thus, Rli1 is in its nucleotide free state when it interacts with eRF3. Furthermore, the binding might take place prior to the binding of Rli1 to the 40S ribosomal subunit, leading to a model in which Rli1 changes its position during translation termination through the stepwise entry of eRF3 and eRF1. Indeed, conformational changes in Rli1 upon its binding to eRF1 increases the binding affinity of Rli1 to the 80S ribosome (Pisarev et al., 2010). Such a model implicates that eRF1 and eRF3 would not enter the termination complex together and their premature contact must be prevented. Therefore, we analyzed situations in which this sequential entry is impaired. This could either be the case when Dbp5 itself is defective, or when its re-charging with ATP is impaired, such as in *RAT7* mutants, because the helicase needs ATP-hydrolysis for its function (Fig P4 B-G). Therefore, we investigated the binding of eRF3, Dbp5 and eRF1 to the small ribosomal subunit (uS3-GFP) in *rat7ΔN* and *rat8-2* mutants after a temperature shift to 37°C for 1h (Fig P6 F-I). In both cases, the binding of eRF1, eRF3 and Dbp5 to the ribosome was significantly decreased, indicating that recycled (*rat7ΔN)* and functional (*rat8-2*) Dbp5 is required to form the termination complex at the ribosome. Possibly, eRF1 and eRF3 are less present at the ribosome, because the termination complex disassembles instantly upon the uncontrolled contact of eRF1 and eRF3. Generally, interaction of eRF1 and eRF3 initiate GTP-binding of eRF3 (Pisareva et al., 2006). Premature contact stimulates GTP binding of eRF3 prematurely and culminates in the subsequent GTP hydrolysis by eRF3, which in turn triggers the dissociation of eRF1 and eRF3 from each other and the ribosome. Such a model is strongly supported by the observed readthrough defects, seen in both Dbp5-impaired strains (Fig P4 B+C).

Not only canonical, but also near cognate stop codons such as the UGG tryptophan codon that is comparable to the stop codon UGA, can erroneously lead to translation termination. For this type of codons, it was often observed that translation elongation stalls or is slowed down and increased rate of translation termination occurs. In this context, it might be conceivable that increased readthrough defects seen in yeast strains with impaired Dbp5, might suppress the growth defects of strains disturbed in their UGG-recognizing tRNA synthesis. To investigate this, we combined a *rat8-2* mutant with the knock out of the tryptophan synthetase gene (*trp5Δ*) and monitored the growth at different temperatures (Fig P6 J). Indeed, we found a partial rescue effect of the double mutant strain at 16°C and 37°C, suggesting that mutations in *DBP5*, which reduce the termination efficiently, provide more time for the incorporation of near cognate stop codons.

5.1.7. Hcr1 and eIF3 enter at late steps of translation termination

In addition to eRF1, eRF3, Rli1, Dbp5 and some additional factors (see 2.1.4.), eIF3 and Hcr1 participate in translation termination (Beznosková et al., 2013, 2015). Mutations in eIF3 reduce the rate of stop codon readthrough, while *hcr1Δ* shows the opposite effect. Interestingly, the increased readthrough defects seen in *HCR1* deletion strain are fully suppressed by overexpression of Rli1 (Beznosková et al., 2013). From these data a model was proposed in which Hcr1 promotes the ejection of GDP-eRF3 from the ribosome. Because Hcr1, in such a model, joins the termination complex at late stages, it should not interact with Dbp5 because in our studies no interaction of eRF3 and Dbp5 was detected an we suggested that Dbp5 has to leave the complex to allow eRF1 to interact with eRF3 (Beißel et al., 2019; Gross et al., 2007). Indeed, co-immunoprecipitation experiments with eRF1 and Hcr1 showed that both proteins bind eRF3. Moreover, only eRF1 but not Hcr1 interacts with Dbp5 (Fig P7 A). It was also suggested that eIF3 acts in late steps of translation termination and might promote ribosome recycling. As such it would be an additional factor that connects translation termination and ribosome recycling (Beznosková et al., 2015). Furthermore, Beznoskova *et al.* (2015) were able to show an interaction of eRF1, eRF3 and Rli1 with subunits of eIF3 *in vivo*. In our co-immunoprecipitation assay we chose Prt1 as one protein from the eIF3 complex and in co-IPs we could clearly verify the interaction of Prt1 with Rli1, eRF1 and eRF3. Indeed, their interactions were clearly diminished in *sup45-2* mutants in which the termination event does not occur (Fig P7 B). Interestingly, neither in wild type nor in *sup45-2* mutants an interaction of Prt1 with Dbp5 could be detected, indicating that eIF3 binds to the termination complex after Dbp5 has delivered eRF1. If eIF3, like Rli1, connects late steps of translation termination and ribosome recycling it should bind to Rli1 independently of the nucleotide status of Rli1, which was indeed the case (Fig P7 C).

5.1.8. Dbp5 ensures the stepwise entry of eRF1 and eRF3 to translation termination complexes

Translation termination is a highly regulated process that depends on the three key factors eRF1, eRF3 and Dbp5 (Gross et al., 2007; von der Haar, 2007). Moreover, translation termination is connected with ribosome recycling by the factors Rli1 and eIF3 (Beznosková et al., 2015; Khoshnevis et al.; Shoemaker et al., 2011). However, the order in which the termination complex assembles was unclear. Polysome gradient fractionation experiments and co-immunoprecipitation assays revealed that nucleotide free Rli1 and eRF3 are bound to the ribosome prior to stop codon recognition through eRF1 (Fig P1+P6). Together with the finding, that binding of Rli1 to Dbp5 was diminished in strains with impaired translation

termination (Fig P2 A-E), these results suggest that Rli1 might help to recruit eRF1 and Dbp5 to termination complexes. Indeed, we could show that overexpression of *RLI1* rescues the binding defect of the sup45-2 protein (Fig P2 G+H). For this function, it is tempting to speculate that Rli1 is still bound to ADP, because it was shown that translation termination occurs independently of the ATPase activity of Rli1. (Khoshnevis et al., 2010; Shoemaker et al., 2011). This correlates with our finding that Rli1 interacts with eRF3 even in the absence of ATP (Fig P6 E). Binding of Rli1 in its nucleotide free state to the ribosome and to eRF3 are in agreement with other models in which Rli1 takes over the position of eRF3 upon GTP hydrolysis, because eRF1 interaction with Rli1 increases its binding affinity to ATP and to the 80S ribosome (Pisarev et al., 2010).

In earlier models it was suggested, that eRF1 and eRF3 together with GTP enters the termination complex as a ternary complex once the ribosome reaches a stop codon (Jackson et al., 2010). However, we have shown that eRF3 is already bound to the ribosome prior to the eRF1-entry at a stop codon in the A-site (Fig P6 A-D). This early binding of eRF3 to the ribosome lead to the speculation that an additional factor might be present that regulate the interaction of eRF3 and eRF1 only if a stop codon is reached. Considering the total protein abundance of Dbp5:eRF1:eRF3 of ~1:2:4 (yeastgenome.org), it is tempting to speculate that Dbp5 which is also involved in other cellular process, is the limiting regulator of the interaction between eRF1 and eRF3. Excess of eRF1 over Dbp5 might be required, because eRF1 also participates in ribosome recycling (Preis et al., 2014; Shoemaker et al., 2011). The high amount of eRF3 might be explained in a model in which eRF3 binds to all ribosomes engaged in translation, to wait for entry of eRF1. Such a model is supported by the finding that a 20 % reduction of basal Dbp5 and eRF1 protein concentration impairs protein synthesis, while a 60 % decrease of eRF3 had no effect (Mikhailova et al., 2017). Interestingly, our *in vivo* results indicate that Dbp5 is not bound to the ribosome during translation elongation (Fig P1 F+G, Fig P2 D+E). This seems to be in contrast to findings with the human homolog DDX19, which was shown to stabilize translation elongation *in vitro* (Mikhailova et al., 2017). This might either be due to functional differences of the yeast and human helicase, or might simply not reflect the *in vivo* situation, because Dbp5 binding to elongating ribosomes was *in vivo* not detected and recruitment might only be possible together with eRF1. Our results furthermore indicate that Dbp5-ATP and eRF1 interact already in the cytoplasm (Fig P3 A+C, Fig P4 D) and that the decoding capability of eRF1 is necessary to recruit the Dbp5-eRF1 complex to the ribosome. Either placement of eRF1 on the stop codon might in turn require the ATPase activity of Dbp5 or the dissociation of the helicase from the termination complex might require the energy. Finally, however, Dbp5-ADP dissociates and needs to be recycled at the NPC via Nup159 (Fig P4). This mode of action has the advantage that a premature interaction of eRF1 and eRF3 is prevented.
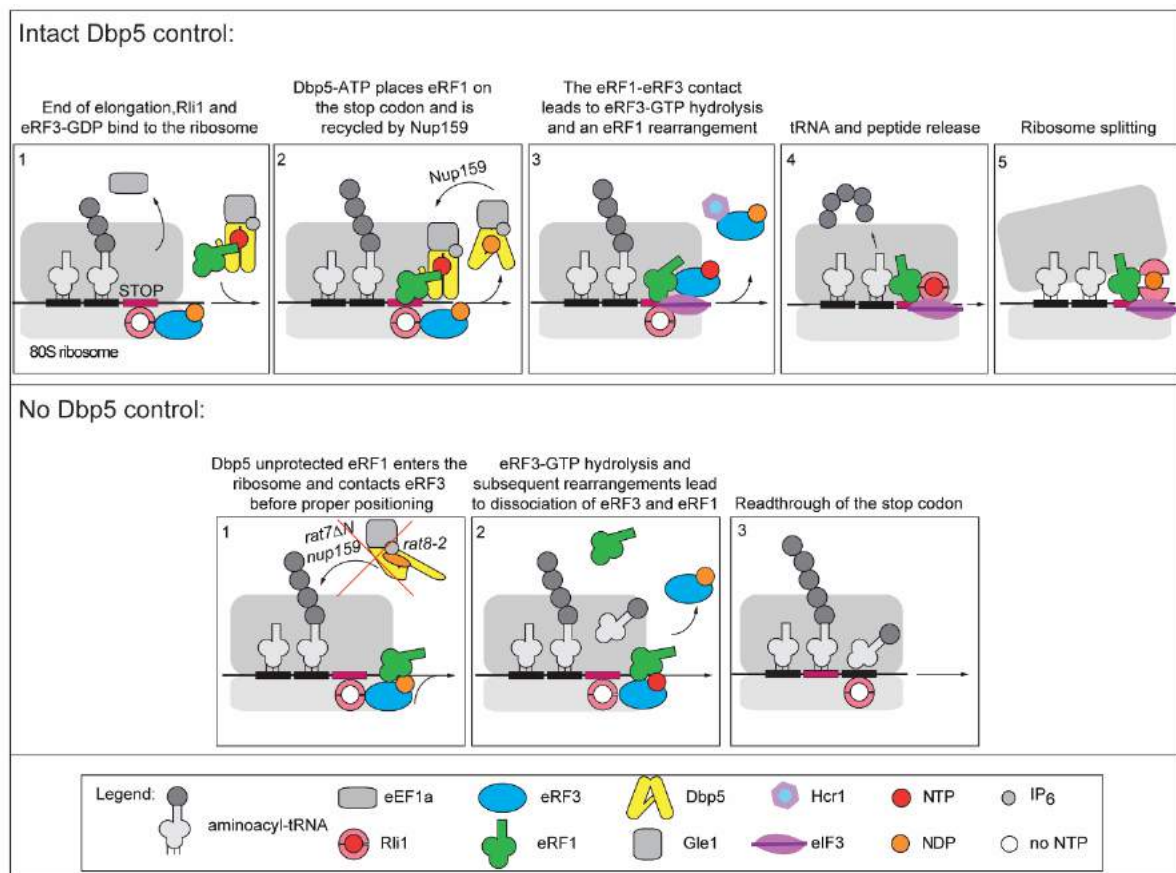
Figure 17 - Stepwise entry model for translation termination.
(Top) Step 1: Nucleotide free Rli1 is already bound to the ribosome and eRF3-GDP as soon as the ribosome reaches a stop codon and the A-site is free. eRF3 joins Rli1 in its GDP-bound form Step 2: Rli1 supports the entry of ATP-Dbp5-eRF1 and Gle1/IP$_6$ stimulated ATP-hydrolysis of Dbp5 leads to proper positioning of eRF1 on the stop codon. ATP-hydrolysis also leads to the dissociation of Dbp5-ADP. Recycling of the helicase occurs at the NPC by Nup159. Step 3: Dissociation of Dbp5-ADP allows the controlled interaction of eRF1 and eRF3, which in turn triggers the GTP binding of eRF3. Subsequent GTP hydrolysis leads to a conformational change in eRF1 that places the GGQ motif in the peptidyl-transferase center. eRF3-GDP is displaced by Hcr1, which was initially delivered by eIF3. Step4: After eRF3-GDP dissociation, eRF1 binds to Rli1-ATP and locks it in a position required for peptidyl-tRNA hydrolysis. Step5: Upon peptide release, Rli1 and its ATPase activity separates the ribosomal subunits from each other and in this way recycle them for further translation events.
(Bottom) Situation in which Dbp5 does not control the eRF1-eRF3 interaction.
Step1: Nucleotide free Rli1 and eRF3-GDP are already bound to the ribosome when the ribosome reaches a stop codon and the A-site is free. Step2: Premature binding of eRF1 to eRF3 is not protected by Dbp5. eRF3 binds to eRF1 before it was properly positioned, leading to GTP binding, subsequent hydrolysis of the nucleotide and their dissociation from each other and the ribosome. This occurs before the polypeptide and the tRNA was released. Step 3: A near cognate tRNA gets access to the A-site, the stop codon is wrongly translated and elongation continues until the next stop codon is reached. Adopted from Beißel *et al.* (2019).

Indeed, in our study, we could show that the last 25 amino acid residues are important for the interaction of eRF1 with either Dbp5 or eRF3 and their binding to eRF1 is mutually exclusive (Fig P5). Moreover, a separated entry of eRF1 and eRF3 is supported by the finding that decreased eRF3 expression does not impair the ribosomal association of eRF1 (Salas-Marco and Bedwell, 2004). In situations, in which the sequential entry is impaired due to dysfunctional Dbp5, as it is the case in *rat8-2* cells or because of a disturbed Dbp5

recycling as seen in the *rat7ΔN* strain, a premature interaction of eRF1 and eRF3 leads to a rapid disassembly of the termination complex (Fig P6 F-I, Fig P3 D+E Fig P4 F+G). This might be because eRF1 is not properly placed and rearranged on the stop codon prior to its interaction with eRF3 and/or because it has to pass eRF3 to get into the A-site and the random contact without the Dbp5-shield provokes premature GTP binding and subsequent hydrolysis and dissociation. Such a model seems plausible, because it was shown earlier that the binding of eRF3 to eRF1 increases the binding affinity of eRF3 to GTP (Frolova et al., 1996; Pisareva et al., 2006). Therefore, we suggested that Dbp5 is an important regulator of the eRF1-eRF3 interaction and as such responsible for the timely trigger of translation termination (Fig 15). Notably, a reduced binding of eRF3 to the polysomal fraction was already described in *rat8-2* mutants after a relatively short temperature shift to 37 °C for 20 min (Gross et al., 2007). Moreover, *gle1-4* temperature sensitive mutants of the Dbp5 co-factor Gle1 likewise exhibit polysome binding defects of eRF3 (Bolger et al., 2008). In our model, a premature interaction of eRF1 and eRF3 leads to their immediate dissociation and thus shorter time, bound to the ribosomes. This model also explains that both *NUP159* and *RAT8* mutants showed increased readthrough activity.

5.2. Dbp5 plays a crucial role in cytoplasmic mRNA quality control

5.2.1. Dbp5 is required for initial steps of NMD

NMD is activated after the recognition of a premature termination codon. This requires the action of the regular termination factors eRF1 and eRF3 (Amrani et al., 2006; Kervestin and Jacobson, 2012). We found that Dbp5 is required for the stop-codon recognition, which suggests also an involvement of the helicase in NMD (Beißel et al., 2019, 2020). We investigated that assumption by using NMD reporter constructs (Fig 9 A), and indeed detected a stabilization of the PTC containing reporter construct in *rat8-2-myc* and *rat8-3* mutants (Fig 9 B). Remarkably, the stabilization effect reached similar levels of our *upf1Δ* strain which was shown to be essential for NMD (Kervestin and Jacobson, 2012). These findings indicate that Dbp5 and Upf1 are both required for NMD (Fig 9). Since NMD leads to PTC-containing RNA degradation, we investigated the effects only on mRNA level. However, it would be interesting to analyze if a similar effect through stabilization of NMD transcripts would also be detectable on protein level. There we expected to detect full-length proteins which might be expressed from PTC containing transcripts that were not eliminated through the Upf-pathway. However, we found that Hsp104-RFP accumulates in *rat8-2-myc* and *rat8-3* mutants, which indicates a high number of defective proteins (unpublished data, Laboratory Heike Krebber). In fact, mutations in cytoplasmic quality control factors lead to an increased number of protein aggregated, which are bound by the chaperone protein Hsp104 and visibly accumulate in cytoplasmic foci (Jamar et al., 2018). Cytoplasmic mRNA quality control not only includes defects in NMD, but also in NSD and NGD. Presumably, the detected Hsp104 foci in the *RAT8* mutants might also result from impaired function of Dbp5 in Dom34-Hbs1 regulated functions on NSD and NGD. Nevertheless, our results show that the Dbp5-mediated delivery of eRF1 is not only important for regular termination, but also for termination at PTCs.
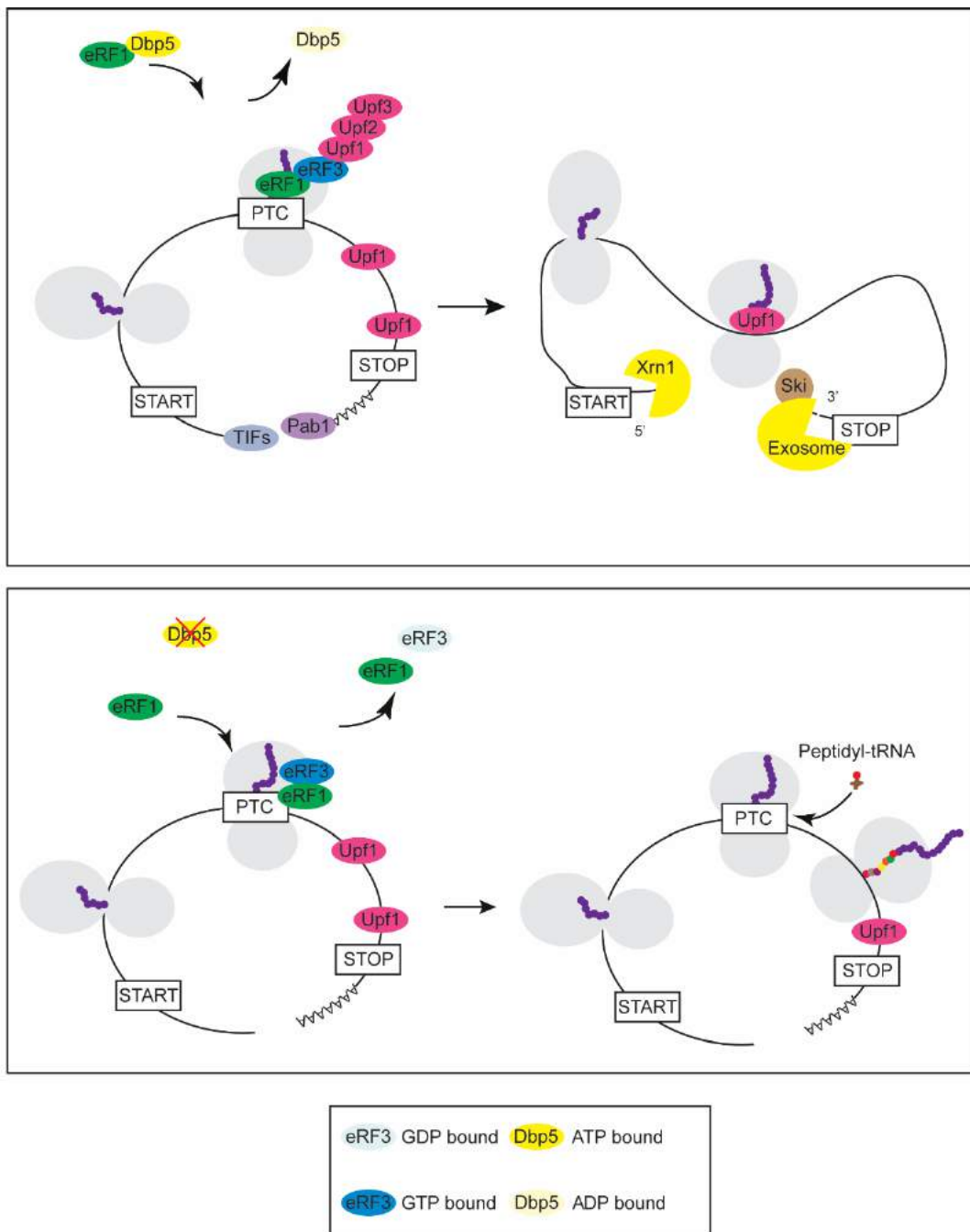
Figure 18 - Initial NMD activation with and without the Dbp5 mediated control of the eRF1-eRF3 interaction.
(Top) The Initial PTC recognition requires Dbp5, which controls the eRF1 and eRF3 interaction. Dbp5 promotes the stop codon recognition of a PTC by eRF1 and eRF3. UPF1 that is bound to the 3' region of the transcript can interact with eRF3 and recognize that termination occurs prematurely. Upf1 assembles the Upf1-2,3 complex, which is responsible for the degradation of the faulty transcript. Translation is inhibited and downstream factors are recruited to promote mRNA decay. Xrn1 acts in 5' to 3' direction and the Ski complex recruits the exosome which degrades the PTC mRNA in 3' to 5' direction.
(Bottom) Loss of Dbp5 mediated delivery of eRF1, as it is the case in the *RAT8* mutants, leads to readthrough of the PTC and the generation of a full-length protein. A near cognate peptidyl-tRNA enters the A site of the ribosome and translation elongation continues. Translation is terminated at a regular termination codon (RTC). The resulting full-length protein has at most one amino acid exchange. Modified from Beißel *et al.* (2020).

5.2.2. Dbp5 promotes no-stop mRNA detection by Dom34 and Hbs1

It is known that Dom34 and Hbs1 as well as Rli1 are necessary to separate ribosomal subunits stalled on mRNAs that are truncated or contain translation inhibiting sequences or secondary structures (Shoemaker et al., 2011; Tsuboi et al., 2012). Furthermore, Dom34-Hbs1 mediates the dissociation of inactive 80S-like ribosomes to restart translation after stress (Van Den Elzen et al., 2014). During stress, ribosomes are stored in 80S-like complexes to avoid subunit degradation and provide a pool of translation competent ribosomes after stress release. Interestingly, van den Elzen *et al*. (2014) observed that mutations of *HBS1* located within the binding domain of Dom34 has a lesser impact on recovery from stress then a mutation in *DOM34,* which was located within the binding site of Hbs1. To explain the observed phenomenon, they speculated that an additional factor might be required to separate 80S-like ribosomes and may bind to the same domain in Dom34 as Hbs1 or to an additional binding sequence of the protein. Furthermore, the similarities of Dom34 and eRF1 in their sequence and structure at their C-termini (Lee et al., 2007) led us to postulate that Dbp5 might be the missing factor. To investigate that, we carried out co- immunoprecipitation experiments and found that Dom34 and Hbs1 interact with Dbp5 (Fig 10). Importantly, the binding of Dom34 to Dbp5, Hbs1 and the ribosome, as determined by interaction with Asc1, is abolished in *rat8-2-myc* and *rat8-3* mutants (Fig 10 A). The same interaction pattern was also detected when the co-IP was done with Hbs1. While Hbs1 pull downs precipitated Dom34, Dbp5 and Asc1 in wild type cells, mutations in *RAT8* disassembled the complex (Fig 10 B). This stays in contrast to the formed Dbp5 complex with the canonical release factors, where Dbp5 interacts only with eRF1 and protects if from premature eRF3 contact. However, van den Elzen *et al.* (2010) could show that only domain 3 of Hbs1 participates in Dom34 binding. This is different from eRF3, in which domains 2 and 3 are necessary for eRF1 binding (Paushkin et al., 1997). In an additional experiment, we could confirm the interaction of Dbp5 and Hbs1 in a combined *in vivo* and *in vitro* assay (Fig 11 B). We could show that immobilized Hbs1 bound to recombinant Dbp5, independently of the nucleotide status of Dbp5. In contrast, the binding of Dbp5 to immobilized Dom34 was only detectable if 1 mM AMPPNP was present (Fig 11 A). Furthermore, we found that the binding of Dom34 to Rli1 was independent of its ATP bound state (Fig 11 A). These results suggest, that the function of Dbp5 in NSD and NGD might be similar to that in regular translation termination. In both processes, the helicase (Dbp5) delivers the proteins Dom34 and eRF1, respectively. However, in regular termination Dbp5 prevents through its presence an early eRF1-eRF3 contact, while in NSD and NGD this does not seem necessary and Dbp5 delivers both proteins (Dom34 and Hbs1) to the ribosome, which might make this process more efficient, as the protein abundance of Hbs1 in the cell with ~3580 proteins/cell (yeastgenome.org) is very low. With such low

numbers Hbs1 is unlikely to binds continuously to all translating ribosomes and waits for the entry of Dom34 on approximately 200.000 ribosomes per cell (Warner, 1999)). Such a model would suggest that Dbp5 does not interact with Dom34 and Hbs1 in separate complexes. To test this, we performed a displacement assay and found that a preformed complex of Dom34 and Dbp5 was not disrupted by increasing concentrations of Hbs1. Instead, Hbs1, Dom34, and Dbp5 rather formed a ternary complex (Fig 12). This finding suggests, that Dbp5 delivers Dom34 and Hbs1 together to the ribosome. Moreover, the binding ability of Hbs1 to ribosomes, detected via Asc1, and its overall stability were significantly decreased in *rat8-2* and *rat7ΔN* mutants (Fig 13 B). This finding cannot be explained by a secondary effect, such as defects in the function of Dbp5 in translation termination or mRNA export, because the half-life time of Hbs1 is ~10,4 h (Christiano et al., 2014). It seems more likely that Dbp5 has a stabilizing effect on Hbs1, maybe due to mediating the interaction with Dom34. Another possibility is that Hbs1 co-migrates with Dbp5 into cytoplasmic foci, as it is described for Dbp5 in *rat8-2* mutants (Scarcelli et al., 2008). The foci might not be accessible for antibody-based detection, because the foci were not disrupted by SDS treatment and the proteins were not accessible for antibody binding. For Dom34 we did not detect such a strong decrease in overall protein abundance and in the Dbp5 affecting mutants, Dom34 was still bound to the 80S ribosomes (Fig 13 B). This 80S-accumulation of Dom34 seems to independent of Dbp5, because Dbp5 was hardly detectable in 80S ribosomes in the examined mutant strains (Fig 13 B). This finding shows that Dom34 accumulates on 80S ribosomes if Dbp5 is absent, which could also suggest that Dom34 requires the helicase and ATPase activity of Dbp5 also for its dissociation. It is likely that the observed 80S ribosomes are 80S-like ribosomes which form because the translational shutdown evokes cellular stress (Van Den Elzen et al., 2014). This finding is corroborated by the observation that overexpression of *DOM34* rescues the growth defect of *rat8-2* mutants at 35°C (Fig 16). Overexpression of *DOM34* might release more 80S-like ribosomes into translational competent 40S and 60S ribosomal subunits. To analyze this more directly, polysome gradient fractionation experiments of *rat8-2* and *rat7ΔN* mutants in the presence of high copy *DOM34* would be helpful. Interestingly, overexpression of *HBS1* showed no rescue of the growth defect of *rat8-2* mutants (unpublished data, AG Prof. Dr. Heike Krebber), indicating that Dom34 is the main player in releasing of 80S-like ribosomes into their subunits, which was already suggested elsewhere (Van Den Elzen et al., 2014). Additional support for a novel role of Dbp5 in NSD and NSD came from growth analyses that were carried out in the presence of 1 mM diamide, which enhances the phenotype of growth defect in *dom34Δ* (Jamar et al., 2017). To provoke even more NSD and NGD events we additionally expressed NGD and NSD reporter containing plasmids (Tsuboi et al., 2012) (Fig 14). While the investigated single mutants of *dom34Δ* and *rat8-3* showed no growth

defect when expressing the reporter constructs on diamide plates, growth of the double mutant *rat8-3 dom34Δ,* at 35°C was inhibited in contrast to the strain without any reporter construct (Fig 14). These findings suggest that mutations in one of the genes can be compensated through the presence of the other. To investigate, whether this growth defect originates from defects in the degradation of the reporter mRNA, we analyzed the GFP transcript levels of the reporter in qPCR. It was already described that both, the NSD and NGD reporter transcripts accumulated in *dom34Δ* knock out strains, in particular when dom34Δ was combined with knock outs of other factors required to degrade the truncated mRNA, such as mutants of *SKI2*, *XRN1* and *HBS1* (Tsuboi et al., 2012). Indeed, the mRNA of the NSD reporter *Rz* accumulated already in the *RAT8* and *DOM34* single mutants. Interestingly, this stabilization effect was even stronger in the double mutants of *rat8-3 dom34Δ*, indicating that Dbp5 and Dom34 act in concert to sense and degrade truncated NSD mRNA. Surprisingly, the NGD reporter constructs showed no accumulation, neither in the single mutants nor in the double mutant. This might originates from the fact that our primer pair bind to the middle domain of the GFP ORF, while Tsuboi *et al.* (2012) showed that particularly the 5'- intermediate of the NGD reporters were stabilized in either *DOM34* or *HBS1* knock outs. To further investigate if this might also be the case for our experimental setup a primer pair that specifically binds to the 5'- end of the GFP ORF could be used. In addition to the detection of the increased transcript levels Tsuboi *et al.*(2012) were also able to show that not only truncated mRNA but also truncated proteins that originate from the reporter construct were stabilized in mutated NSD and NGD genes. Thus, it would be interesting to investigate whether the growth defect detectable in *DOM34* and *RAT8* mutants might originate from the accumulation of 5'- intermediates of NGD reporters or stabilization of the resulting truncated proteins. Furthermore, it would be worthwhile to combine *DBP5* mutants with mutants of late acting factors in NGD and NSD e.g. *SKI2*, *SKI7* or *XRN1*, to get a more global view of the function of Dbp5 in NGD and NSD. From the data presented so far, a model comparable to canonical translation termination, in which Dbp5 recruits Dom34 to the stalled ribosome is likely but in contrast Dbp5 might in addition also recruit Hbs1 to the ribosome (Figure 19). From our data, only a function of Dbp5 in NSD could be confirmed, but due to the functional similarities of the processes an involvement of Dbp5 also in NGD is likely.

In particular, because only the 5' fragment of NGD mRNAs are sensed, repetition with appropriate primes is necessary. Although, additional experiments as discussed above might further elucidate the function of Dbp5 in NGD and NSD, this work has uncovered a novel function of the DEAD-box RNA helicase in the cytoplasmic ribosome-dependent mRNA quality control that is executed via Dom34 and Hbs1.
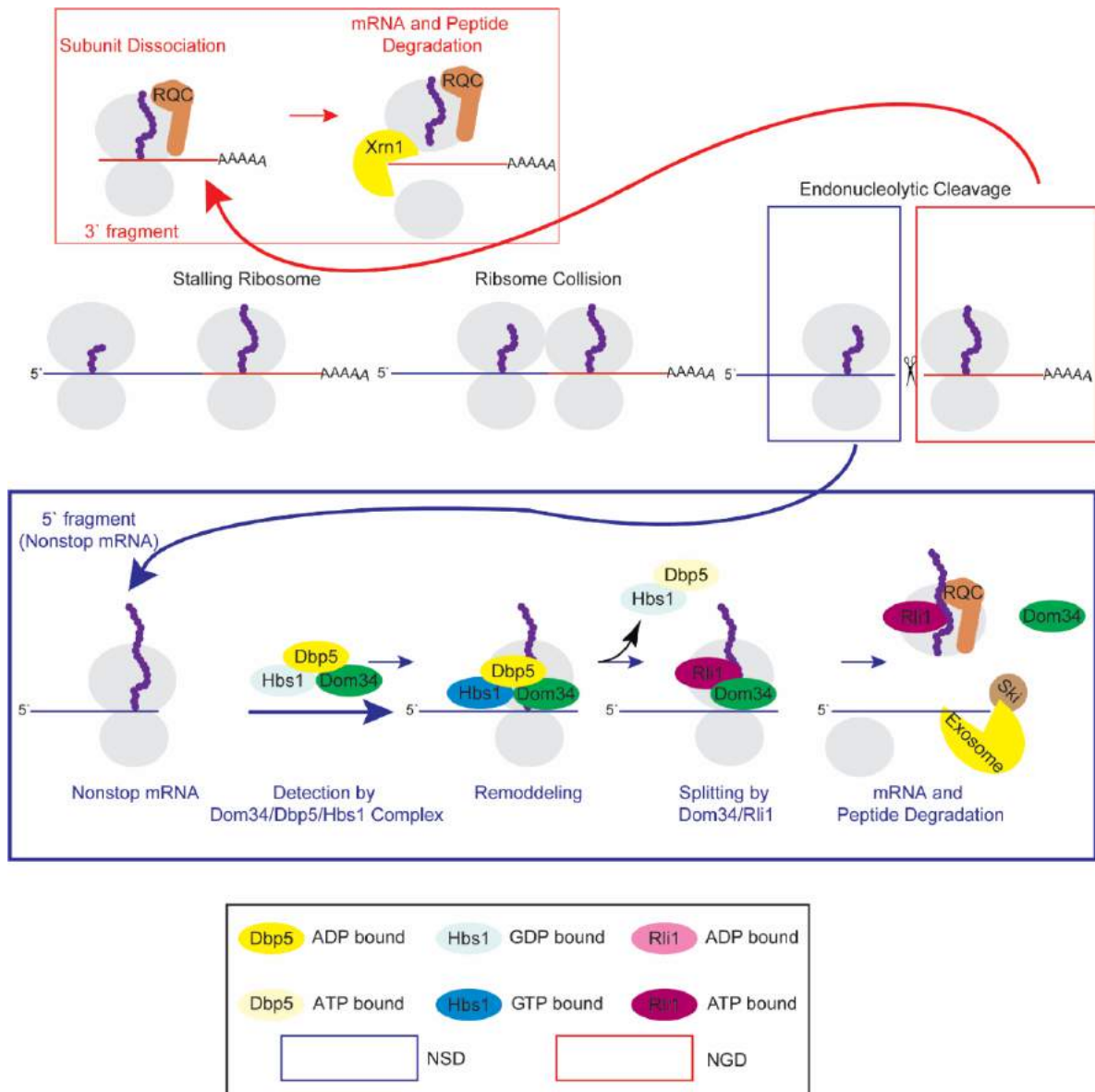
Figure 19 - New Model of no-stop decay and no-go decay.
The ribosome stalls because of e.g. a stem loop or sequence of rare codons. The mRNA is endonucleolytically cleaved, probably via Cue2, which leads to emerging of 3' and 5' fragments. The ribosome on the 3' fragment is dissociated by the ribosome quality control (RQC) machinery. The mRNA is rapidly degraded by Xrn1 and the truncated protein is degraded via the RQC pathway. The 5' fragment is recognized as non-stop mRNA, which can also be originated from e.g. truncated transcripts. However, the mRNA is still occupied by stalled ribosomes which are marked as faulty by ubiquitination of the stalled ribosomes via Hel2. This is recognized by a complex of Dom34 and Hbs1, which is delivered through the helicase Dbp5, which places the complex in the A-site of the ribosome. ATP-hydrolysis of Dbp5 and GTP hydrolysis by Hbs1 accommodates Dom34 into the active site and lead to the subsequent dissociation of Dbp5 and Hbs1. This allows Rli1 to bind to Dom34. This contact might trigger ATP hydrolysis of Rli1, which initiates the splitting of the ribosome into ribosomal subunits. The mRNA is rapidly degraded by the Ski complex and exosome. The non-released truncated protein is degraded via the RQC pathway.

6. References

Alcázar-Román, A.R., Tran, E.J., Guo, S., and Wente, S.R. (2006). Inositol hexakisphosphate and Gle1 activate the DEAD-box protein Dbp5 for nuclear mRNA export. Nat. Cell Biol. *8*, 711–716.

Alcázar-Román, A.R., Bolger, T.A., and Wente, S.R. (2010). Control of mRNA export and translation termination by inositol hexakisphosphate requires specific interaction with Gle. J. Biol. Chem. *285*, 16683–16692.

Alkalaeva, E.Z., Pisarev, A. V., Frolova, L.Y., Kisselev, L.L., and Pestova, T. V. (2006). In Vitro Reconstitution of Eukaryotic Translation Reveals Cooperativity between Release Factors eRF1 and eRF3. Cell *125*, 1125–1136.

Amrani, N., Sachs, M.S., and Jacobson, A. (2006). Early nonsense: mRNA decay solves a translational problem. Nat. Rev. Mol. Cell Biol.

Andersen, D.S., and Leevers, S.J. (2007). The essential drosophila ATP-binding cassette domain protein, pixie, binds the 40 S ribosome in an ATP-dependent manner and is required for translation initiation. J. Biol. Chem.

Baierlein, C., Krebber, H., Baierlein, C., and Krebber, H. (2010). Translation termination: new factors and insights (Taylor and Francis Inc.).

Barthelme, D., Scheele, U., Dinkelaker, S., Janoschka, A., MacMillan, F., Albers, S.V., Driessen, A.J.M., Stagni, M.S., Bill, E., Meyer-Klaucke, W., et al. (2007). Structural organization of essential iron-sulfur clusters in the evolutionarily highly conserved ATP-binding cassette protein ABCE1. J. Biol. Chem. *282*, 14598–14607.

Barthelme, D., Dinkelaker, S., Albers, S.-V.V., Londei, P., Ermler, U., and Tampé, R. (2011). Ribosome recycling depends on a mechanistic link between the FeS cluster domain and a conformational switch of the twin-ATPase ABCE1. Proc. Natl. Acad. Sci. U. S. A. *108*, 3228–3233.

Becker, T., Armache, J.P., Jarasch, A., Anger, A.M., Villa, E., Sieber, H., Motaal, B.A., Mielke, T., Berninghausen, O., and Beckmann, R. (2011). Structure of the no-go mRNA decay complex Dom34-Hbs1 bound to a stalled 80S ribosome. Nat. Struct. Mol. Biol.

Becker, T., Franckenberg, S., Wickles, S., Shoemaker, C.J., Anger, A.M., Armache, J.P., Sieber, H., Ungewickell, C., Berninghausen, O., Daberkow, I., et al. (2012). Structural basis of highly conserved ribosome recycling in eukaryotes and archaea. Nature *482*, 501–506.

Beißel, C., Neumann, B., Uhse, S., Hampe, I., Karki, P., and Krebber, H. (2019). Translation termination depends on the sequential ribosomal entry of eRF1 and eRF3. Nucleic Acids Res. *47*, 4798–4813.

Beißel, C., Grosse, S., and Krebber, H. (2020). Dbp5/DDX19 between Translational Readthrough and Nonsense Mediated Decay (NLM (Medline)).

Bengtson, M.H., and Joazeiro, C.A.P. (2010). Role of a ribosome-associated E3 ubiquitin ligase in protein quality control. Nature.

Bertram, G., Bell, H.A., Ritchie, D.W., Fullerton, G., and Stansfield, I. (2000). Terminating eukaryote translation: Domain 1 of release factor eRF1 functions in stop codon recognition. RNA *6*, 1236–1247.

Beznosková, P., Cuchalová, L., Wagner, S., Shoemaker, C.J., Gunišová, S., von der Haar, T., and Valášek, L.S. (2013). Translation Initiation Factors eIF3 and HCR1 Control Translation Termination and Stop Codon Read-Through in Yeast Cells. PLoS Genet. *9*.

Beznosková, P., Wagner, S., Jansen, M.E., Von Der Haar, T., and Valášek, L.S. (2015). Translation initiation factor eIF3 promotes programmed stop codon readthrough. Nucleic Acids Res. *43*, 5099–5111.

Bisbal, C., Martinand, C., Silhol, M., Lebleu, B., and Salehzada, T. (1995). Cloning and characterization of a RNase L inhibitor. A new component of the interferon-regulated 2-5A pathway. J. Biol. Chem.

Blanchet, S., Rowe, M., Von Der Haar, T., Fabret, C., Demais, S., Howard, M.J., and Namy, O. (2015). New insights into stop codon recognition by eRF1. Nucleic Acids Res. *43*, 3298–3308.

Bolger, T.A., Folkmann, A.W., Tran, E.J., and Wente, S.R. (2008). The mRNA Export Factor Gle1 and Inositol Hexakisphosphate Regulate Distinct Stages of Translation.

Brandman, O., Stewart-Ornstein, J., Wong, D., Larson, A., Williams, C.C., Li, G.W., Zhou, S., King, D., Shen, P.S., Weibezahn, J., et al. (2012). A ribosome-bound quality control complex triggers degradation of nascent peptides and signals translation stress. Cell *151*, 1042–1054.

Brogna, S., and Wen, J. (2009). Nonsense-mediated mRNA decay (NMD) mechanisms. Nat. Struct. Mol. Biol.

Brown, A., Shao, S., Murray, J., Hegde, R.S., and Ramakrishnan, V. (2015). Structural basis for stop codon recognition in eukaryotes. Nature.

Chen, J., Lu, G., Lin, J., Davidson, A.L., and Quiocho, F.A. (2003). A tweezers-like motion of the ATP-binding cassette dimer in an ABC transport cycle. Mol. Cell *12*, 651–661.

Chen, L., Muhlrad, D., Hauryliuk, V., Cheng, Z., Lim, M.K., Shyp, V., Parker, R., and Song, H. (2010). Structure of the Dom34-Hbs1 complex and implications for no-go decay. Nat. Struct. Mol. Biol. *17*, 1233–1240.

Chen, Z.Q., Dong, J., Ishimura, A., Daar, I., Hinnebusch, A.G., and Dean, M. (2006). The essential vertebrate ABCE1 protein interacts with eukaryotic initiation factors. J. Biol. Chem. *281*, 7452–7457.

Cheng, Z., Saito, K., Pisarev, A. V., Wada, M., Pisareva, V.P., Pestova, T. V., Gajda, M., Round, A., Kong, C., Lim, M., et al. (2009). Structural insights into eRF3 and stop codon recognition by eRF1. Genes Dev. *23*, 1106–1118.

Christiano, R., Nagaraj, N., Fröhlich, F., and Walther, T.C. (2014). Global Proteome Turnover Analyses of the Yeasts S.cerevisiae and S.pombe. Cell Rep. *9*, 1959–1965.

Christie, K.R. (2004). Saccharomyces Genome Database (SGD) provides tools to identify and analyze sequences from Saccharomyces cerevisiae and related sequences from other organisms. Nucleic Acids Res.

Collins, R., Karlberg, T., Lehtiö, L., Schütz, P., van den Berg, S., Dahlgren, L.G., Hammarström, M., Weigelt, J., and Schüler, H. (2009). The DEXD/H-box RNA helicase DDX19 is regulated by an α-helical switch. J. Biol. Chem. *284*, 10296–10300.

Conard, S.E., Buckley, J., Dang, M., Bedwell, G.J., Carter, R.L., Khass, M., and Bedwell, D.M. (2012). Identification of eRF1 residues that play critical and complementary roles in stop codon recognition. RNA *18*, 1210–1221.

D'Orazio, K.N., Wu, C.C.C., Sinha, N., Loll-Krippleber, R., Brown, G.W., and Green, R. (2019). The endonuclease Cue2 cleaves mRNAs at stalled ribosomes during No Go Decay. Elife.

Dean, M., and Annilo, T. (2005). EVOLUTION OF THE ATP-BINDING CASSETTE (ABC) TRANSPORTER SUPERFAMILY IN VERTEBRATES. Annu. Rev. Genomics Hum. Genet.

Defenouillère, Q., Yao, Y., Mouaikel, J., Namane, A., Galopier, A., Decourty, L., Doyen, A., Malabat, C., Saveanu, C., Jacquier, A., et al. (2013). Cdc48-associated complex bound to 60S particles is required for the clearance of aberrant translation products. Proc. Natl. Acad. Sci. U. S. A. *110*, 5046–5051.

Dehecq, M., Decourty, L., Namane, A., Proux, C., Kanaan, J., Le Hir, H., Jacquier, A., and Saveanu, C. (2018). Nonsense-mediated mRNA decay involves two distinct Upf1-bound complexes . EMBO J.

Dever, T.E., and Green, R. (2012). The elongation, termination, and recycling phases of translation in eukaryotes. Cold Spring Harb. Perspect. Biol. *4*, 1–16.

Dever, T.E., Kinzy, T.G., and Pavitt, G.D. (2016). Mechanism and regulation of protein synthesis in Saccharomyces cerevisiae. Genetics *203*, 65–107.

Dinman, J.D., and Kinzy, T.G. (1997). Translational misreading: Mutations in translation elongation factor 1α differentially affect programmed ribosomal frameshifting and drug sensitivity. RNA.

Doma, M.K., and Parker, R. (2006). Endonucleolytic cleavage of eukaryotic mRNAs with stalls in translation elongation. Nature *440*, 561–564.

Doma, M.K., and Parker, R. (2007). RNA Quality Control in Eukaryotes. Cell.

Dong, J., Lai, R., Nielsen, K., Fekete, C.A., Qiu, H., and Hinnebusch, A.G. (2004). The essential ATP-binding cassette protein RLI1 functions in translation by promoting preinitiation complex assembly. J. Biol. Chem. *279*, 42157–42168.

Dossani, Z.Y., Weirich, C.S., Erzberger, J.P., Berger, J.M., and Weis, K. (2009). Structure of the C-terminus of the mRNA export factor Dbp5 reveals the interaction surface for the ATPase activator Gle1.

Dower, W.J., Miller, J.F., and Ragsdale, C.W. (1988). High efficiency transformation of E.coli by high voltage electroporation. Nucleic Acids Res.

Van Den Elzen, A.M.G., Henri, J., Lazar, N., Gas, M.E., Durand, D., Lacroute, F., Nicaise, M., Van Tilbeurgh, H., Séraphin, B., and Graille, M. (2010). Dissection of Dom34gHbs1 reveals independent functions in two RNA quality control pathways. Nat. Struct. Mol. Biol. *17*, 1446–1452.

Van Den Elzen, A.M.G., Schuller, A., Green, R., and Séraphin, B. (2014). Dom34-Hbs1 mediated dissociation of inactive 80S ribosomes promotes restart of translation after stress. EMBO J. *33*, 265–276.

Estruch, F., and Cole, C.N. (2003). An early function during transcription for the yeast mRNA export factor Dbp5p/Rat8p suggested by its genetic and physical interactions with transcription factor IIH components. Mol. Biol. Cell *14*, 1664–1676.

Eurwilaichitr, L., Graves, F.M., Stansfield, I., and Tuite, M.F. (1999). The C-terminus of eRF1 defines a functionally important domain for translation termination in Saccharomyces cerevisiae. Mol. Microbiol. *32*, 485–496.

Fairman-Williams, M.E., Guenther, U.P., and Jankowsky, E. (2010). SF1 and SF2 helicases: Family matters. Curr. Opin. Struct. Biol. *20*, 313–324.

Forster, A.C., and Symons, R.H. (1987). Self-cleavage of virusoid RNA is performed by the proposed 55-nucleotide active site. Cell.

Franks, T.M., Singh, G., and Lykke-Andersen, J. (2010). Upf1 ATPase-dependent mRNP disassembly is required for completion of nonsense-mediated mRNA decay. Cell.

Frey, S., Pool, M., and Seedorf, M. (2001). Scp160p, an RNA-binding, Polysome-associated Protein, Localizes to the Endoplasmic Reticulum of Saccharomyces cerevisiae in a Microtubule-dependent Manner. J. Biol. Chem.

Frischmeyer, P.A., Van Hoof, A., O'Donnell, K., Guerrerio, A.L., Parker, R., and Dietz, H.C. (2002). An mRNA surveillance mechanism that eliminates transcripts lacking termination codons. Science (80-.).

Frolova, L., Goff, X.L.E., Zhouravleva, G., Davydova, E., Philippe, M., and Kisselev, L. (1996). Eukaryotic polypeptide chain release factor eRF3 is an eRF1- and ribosome-dependent guanosine triphosphatase. RNA.

Garfin, D.E. (2009). Chapter 29 One-Dimensional Gel Electrophoresis1. In Methods in Enzymology, p.

Garzia, A., Jafarnejad, S.M., Meyer, C., Chapat, C., Gogakos, T., Morozov, P., Amiri, M., Shapiro, M., Molina, H., Tuschl, T., et al. (2017). The E3 ubiquitin ligase and RNA-binding protein ZNF598 orchestrates ribosome quality control of premature polyadenylated mRNAs. Nat. Commun.

Gibson, D.G., Young, L., Chuang, R.Y., Venter, J.C., Hutchison, C.A., and Smith, H.O. (2009). Enzymatic assembly of DNA molecules up to several hundred kilobases. Nat. Methods 6, 343–345.

Gietz, D., Jean, A.S., Woods, R.A., and Schiestl, R.H. (1992). Improved method for high efficiency transformation of intact yeast cells. Nucleic Acids Res.

Graille, M., and Séraphin, B. (2012). Surveillance pathways rescuing eukaryotic ribosomes lost in translation. Nat. Rev. Mol. Cell Biol.

Graille, M., Chaillet, M., and Van Tilbeurgh, H. (2008). Structure of Yeast Dom34: A protein related to translation termination factor Erf1 and involved in No-Go decay. J. Biol. Chem. 283, 7145–7154.

Gross, T., Siepmann, A., Sturm, D., Windgassen, M., Scarcelli, J.J., Seedorf, M., Cole, C.N., and Krebber, H. (2007). The DEAD-box RNA helicase Dbp5 functions in translation termination.

Grünwald, D., Singer, R.H., and Rout, M. (2011). Nuclear export dynamics of RNA-"protein complexes. Nature 475, 333–341.

Guydosh, N.R., and Green, R. (2014). Dom34 rescues ribosomes in 3′ untranslated regions. Cell.

von der Haar, T. (2007). Optimized protein extraction for quantitative proteomics of yeasts. PLoS One 2.

von der Haar, T. (2008). A quantitative estimation of the global translational activity in logarithmically growing yeast cells. BMC Syst. Biol. 2, 87.

von der Haar, T., and Tuite, M.F. (2007). Regulated translational bypass of stop codons in yeast. Trends Microbiol. 15, 78–86.

Hackmann, A., Wu, H., Schneider, U.M., Meyer, K., Jung, K., and Krebber, H. (2014). Quality control of spliced mRNAs requires the shuttling SR proteins Gbp2 and Hrb1. Nat. Commun.

Harper, S., and Speicher, D.W. (2011). Purification of proteins fused to glutathione S-transferase. Methods Mol. Biol.

He, F., and Jacobson, A. (1995). Identification of a novel component of the nonsense-mediated mRNA decay pathway by use of an interacting protein screen. Genes Dev.

He, F., Peltz, S.W., Donahue, J.L., Rosbash, M., and Jacobson, A. (1993). Stabilization and ribosome association of unspliced pre-mRNAs in a yeast upf1- mutant. Proc. Natl. Acad. Sci. U. S. A.

He, F., Brown, A.H., and Jacobson, A. (1997). Upf1p, Nmd2p, and Upf3p are interacting components of the yeast nonsense-mediated mRNA decay pathway. Mol. Cell. Biol.

He, F., Li, X., Spatrick, P., Casillo, R., Dong, S., and Jacobson, A. (2003). Genome-Wide Analysis of mRNAs Regulated by the Nonsense-Mediated and 5′ to 3′ mRNA Decay Pathways in Yeast. Mol. Cell.

Heurgué-Hamard, V., Champ, S., Mora, L., Merkoulova-Rainon, T., Kisselev, L.L., and Buckingham, R.H. (2005). The glutamine residue of the conserved GGQ motif in Saccharomyces cerevisiae release factor eRF1 is methylated by the product of the YDR140w gene. J. Biol. Chem. *280*, 2439–2445.

Hodge, C.A., Colot, H. V., Stafford, P., and Cole, C.N. (1999). Rat8p/Dbp5p is a shuttling transport factor that interacts with Rat7p/Nup159p and Gle1p and suppresses the mRNA export defect of xpo1-1 cells. EMBO J. *18*, 5778–5788.

Hodge, C.A., Tran, E.J., Noble, K.N., Alcazar-Roman, A.R., Ben-Yishay, R., Scarcelli, J.J., Folkmann, A.W., Shav-Tal, Y., Wente, S.R., and Cole, C.N. (2011). The Dbp5 cycle at the nuclear pore complex during mRNA export I: Dbp5 mutants with defects in RNA binding and ATP hydrolysis define key steps for Nup159 and Gle1. Genes Dev. *25*, 1052–1064.

van Hoof, A., Staples, R.R., Baker, R.E., and Parker, R. (2000). Function of the Ski4p (Csl4p) and Ski7p Proteins in 3'-to-5' Degradation of mRNA. Mol. Cell. Biol.

Van Hoof, A., Frischmeyer, P.A., Dietz, H.C., and Parker, R. (2002). Exosome-mediated recognition and degradation of mRNAs lacking a termination codon. Science (80-.).

Hoshino, S.I., Imai, M., Mizutani, M., Kikuchi, Y., Hanaoka, F., Ui, M., and Katada, T. (1998). Molecular cloning of a novel member of the eukaryotic polypeptide chain-releasing factors (eRF): Its identification as eRF3 interacting with eRF1. J. Biol. Chem.

Inada, T. (2017). The Ribosome as a Platform for mRNA and Nascent Polypeptide Quality Control. Trends Biochem. Sci.

Inoue, H., Nojima, H., and Okayama, H. (1990). High efficiency transformation of Escherichia coli with plasmids. Gene.

Jackson, R.J., Hellen, C.U.T., and Pestova, T. V. (2010). The mechanism of eukaryotic translation initiation and principles of its regulation. Nat. Rev. Mol. Cell Biol. *11*, 113–127.

Jackson, R.J., Hellen, C.U.T., and Pestova, T. V. (2012). Termination and post-termination events in eukaryotic translation. In Advances in Protein Chemistry and Structural Biology, (Academic Press Inc.), pp. 45–93.

Jamar, N.H., Kritsiligkou, P., and Grant, C.M. (2017). The non-stop decay mRNA surveillance pathway is required for oxidative stress tolerance. Nucleic Acids Res. *45*, 6881–6893.

Jamar, N.H., Kritsiligkou, P., and Grant, C.M. (2018). Loss of mRNA surveillance pathways results in widespread protein aggregation. Sci. Rep.

Juszkiewicz, S., and Hegde, R.S. (2017). Initiation of Quality Control during Poly(A) Translation Requires Site-Specific Ribosome Ubiquitination. Mol. Cell.

Karcher, A., Büttner, K., Märtens, B., Jansen, R.P., and Hopfner, K.P. (2005). X-ray structure of RLI, an essential twin cassette ABC ATPase involved in ribosome biogenesis and HIV capsid assembly. Structure *13*, 649–659.

Karcher, A., Schele, A., and Hopfner, K.P. (2008). X-ray structure of the complete ABC enzyme ABCE1 from Pyrococcus abyssi. J. Biol. Chem. *283*, 7962–7971.

Karpowich, N., Martsinkevich, O., Millen, L., Yuan, Y.R., Dai, P.L., MacVey, K., Thomas, P.J., and Hunt, J.F. (2001). Crystal structures of the MJ1267 ATP binding cassette reveal an induced-fit effect at the ATPase active site of an ABC transporter. Structure *9*, 571–586.

Kashima, I., Yamashita, A., Izumi, N., Kataoka, N., Morishita, R., Hoshino, S., Ohno, M., Dreyfuss, G., and Ohno, S. (2006). Binding of a novel SMG-1-Upf1-eRF1-eRF3 complex (SURF) to the exon junction complex triggers Upf1 phosphorylation and nonsense-mediated mRNA decay. Genes Dev.

Kashima, I., Takahashi, M., Hashimoto, Y., Sakota, E., Nakamura, Y., and Inada, T. (2014). A functional involvement of ABCE1, eukaryotic ribosome recycling factor, in nonstop mRNA decay in Drosophila melanogaster cells. Biochimie *106*, 10–16.

Kervestin, S., and Jacobson, A. (2012). NMD: A multifaceted response to premature translational termination. Nat. Rev. Mol. Cell Biol. *13*, 700–712.

Khoshnevis, S., Gross, T., Rotte, C., Baierlein, C., Ficner, R., and Krebber, H. (2010). The iron-sulphur protein RNase L inhibitor functions in translation termination. EMBO Rep. *11*, 214–219.

Kispal, G., Sipos, K., Lange, H., Fekete, Z., Bedekovics, T., Janáky, T., Bassler, J., Aguilar Netz, D.J., Balk, J., Rotte, C., et al. (2005). Biogenesis of cytosolic ribosomes requires the essential iron-sulphur protein Rli1p and mitochondria. EMBO J. *24*, 589–598.

Kobayashi, K., Kikuno, I., Kuroha, K., Saito, K., Ito, K., Ishitani, R., Inada, T., and Nureki, O. (2010). Structural basis for mRNA surveillance by archaeal Pelota and GTP-bound EF1α complex. Proc. Natl. Acad. Sci. U. S. A. *107*, 17575–17579.

Kong, C., Ito, K., Walsh, M.A., Wada, M., Liu, Y., Kumar, S., Barford, D., Nakamura, Y., and Song, H. (2004). Naka-mura and Ito.

Kouba, T., Rutkai, E., Karásková, M., and Valášek, L.S. (2012). The eIF3c/NIP1 PCI domain interacts with RNA and RACK1/ASC1 and promotes assembly of translation preinitiation complexes. Nucleic Acids Res.

Kuroha, K., Akamatsu, M., Dimitrova, L., Ito, T., Kato, Y., Shirahige, K., and Inada, T. (2010). Receptor for activated C kinase 1 stimulates nascent polypeptide-dependent translation arrest. EMBO Rep.

Kushnirov, V. V., Ter-Avanesyan, M.D., Telckov, M. V., Surguchov, A.P., Smirnov, V.N., and Inge-Vechtomov, S.G. (1988). Nucleotide sequence of the SUP2 (SUP35) gene of Saccharomyces cerevisiae. Gene.

Lari, A., Arul Nambi Rajan, A., Sandhu, R., Reiter, T., Montpetit, R., Young, B.P., Loewen, C.J., and Montpetit, B. (2019). A nuclear role for the DEAD-box protein Dbp5 in tRNA export. Elife *8*.

Lee, H.H., Kim, Y.S., Kim, K.H., Heo, I., Kim, S.J.S.K., Kim, O., Kim, H.S.H.K., Yoon, J.Y., Kim, H.S.H.K., Kim, D.J., et al. (2007). Structural and Functional Insights into Dom34, a Key Component of No-Go mRNA Decay. Mol. Cell *27*, 938–950.

Linder, P., and Jankowsky, E. (2011). From unwinding to clamping ĝ€" the DEAD box RNA helicase family. Nat. Rev. Mol. Cell Biol. *12*, 505–516.

Livak, K.J., and Schmittgen, T.D. (2001). Analysis of relative gene expression data using real-time quantitative PCR and the 2-ΔΔCT method. Methods.

Lund, M.K., and Guthrie, C. (2005). The DEAD-box protein Dbp5p is required to dissociate Mex67p from exported mRNPs at the nuclear rim. Mol. Cell *20*, 645–651.

Lykke-Andersen, J., and Bennett, E.J. (2014). Protecting the proteome: Eukaryotic cotranslational quality control pathways. J. Cell Biol.

Lykke-Andersen, S., and Jensen, T.H. (2015). Nonsense-mediated mRNA decay: An intricate machinery that shapes transcriptomes. Nat. Rev. Mol. Cell Biol. *16*, 665–677.

Marshall, A.N., Han, J., Kim, M., and Van Hoof, A. (2018). Conservation of mRNA quality control factor Ski7 and its diversification through changes in alternative splicing and gene duplication. Proc. Natl. Acad. Sci. U. S. A.

Mašek, T., Valášek, L., and Pospíšek, M. (2011). Polysome analysis and RNA purification from sucrose gradients. Methods Mol. Biol.

Matsuo, Y., Ikeuchi, K., Saeki, Y., Iwasaki, S., Schmidt, C., Udagawa, T., Sato, F., Tsuchiya, H., Becker, T., Tanaka, K., et al. (2017). Ubiquitination of stalled ribosome triggers ribosome-associated quality control. Nat. Commun.

Medghalchi, S.M. (2001). Rent1, a trans-effector of nonsense-mediated mRNA decay, is essential for mammalian embryonic viability. Hum. Mol. Genet.

Mendell, J.T., Medghalchi, S.M., Lake, R.G., Noensie, E.N., and Dietz, H.C. (2000). Novel Upf2p Orthologues Suggest a Functional Link between Translation Initiation and Nonsense Surveillance Complexes. Mol. Cell. Biol.

Metzstein, M.M., and Krasnow, M.A. (2006). Functions of the nonsense-mediated mRNA decay pathway in Drosophila development. PLoS Genet.

Mikhailova, T., Shuvalova, E., Ivanov, A., Susorov, D., Shuvalov, A., Kolosov, P.M., and Alkalaeva, E. (2017). RNA helicase DDX19 stabilizes ribosomal elongation and termination complexes. Nucleic Acids Res. *45*, 1307–1318.

Mitchell, P., and Tollervey, D. (2003). An NMD pathway in yeast involving accelerated deadenylation and exosome-mediated 3′→5′ degradation. Mol. Cell.

Von Moeller, H., Basquin, C., and Conti, E. (2009). The mRNA export protein DBP5 binds RNA and the cytoplasmic nucleoporin NUP214 in a mutually exclusive manner. Nat. Struct. Mol. Biol. *16*, 247–254.

Montpetit, B., Thomsen, N.D., Helmke, K.J., Seeliger, M.A., Berger, J.M., and Weis, K. (2011). A conserved mechanism of DEAD-box ATPase activation by nucleoporins and InsP6 in mRNA export. Nature *472*, 238–244.

Mühlemann, O., and Jensen, T.H. (2012). MRNP quality control goes regulatory. Trends Genet.

Muhlrad, D., and Parker, R. (1994). Premature translational termination triggers mRNA decapping. Nature.

Muhlrad, D., and Parker, R. (1999). Aberrant mRNAs with extended 3' UTRs are substrates for rapid degradation by mRNA surveillance. RNA.

Murphy, R., and Wente, S.R. (1996). An RNA-export mediator with an essential nuclear export signal. Nature *383*, 357–360.

Napetschnig, J., Kassube, S.A., Debler, E.W., Wong, R.W., Nter Blobel, G., Hoelz, A., Blobel, G., and Hoelz, A. (2009). Structural and functional analysis of the interaction between the nucleoporin Nup214 and the DEAD-box helicase Ddx19.

Neumann, B., Wu, H., Hackmann, A., and Krebber, H. (2016). Nuclear export of pre-ribosomal subunits requires Dbp5, but not as an RNA-helicase as for mRNA export. PLoS One *11*.

Noble, K.N., Tran, E.J., Alcázar-Román, A.R., Hodge, C.A., Cole, C.N., and Wente, S.R. (2011). The Dbp5 cycle at the nuclear pore complex during mRNA export II: Nucleotide cycling and mRNP remodeling by Dbp5 are controlled by Nup159 and Gle1. Genes Dev. *25*, 4065–1077.

Nürenberg, E., and Tampé, R. (2013). Tying up loose ends: Ribosome recycling in eukaryotes and archaea. Trends Biochem. Sci. *38*, 64–74.

Ozsolak, F., Kapranov, P., Foissac, S., Kim, S.W., Fishilevich, E., Monaghan, A.P., John, B., and Milos, P.M. (2010). Comprehensive polyadenylation site maps in yeast and human reveal pervasive alternative polyadenylation. Cell *143*, 1018–1029.

Passos, D.O., Doma, M.K., Shoemaker, C.J., Muhlrad, D., Green, R., Weissman, J., Hollien, J., and Parker, R. (2009). Analysis of Dom34 and its function in No-Go decay. Mol. Biol. Cell.

Paushkin, S. V, Kushnirov, V. V, Smirnov, V.N., and Ter-Avanesyan, M.D. (1997). Interaction between Yeast Sup45p (eRF1) and Sup35p (eRF3) Polypeptide Chain Release Factors: Implications for Prion-Dependent Regulation.

Pechmann, S., Willmund, F., and Frydman, J. (2013). The Ribosome as a Hub for Protein Quality Control. Mol. Cell *49*, 411–421.

Pelechano, V., Wei, W., and Steinmetz, L.M. (2013). Extensive transcriptional heterogeneity revealed by isoform profiling. Nature *497*, 127–131.

Peltz, S.W., Donahue, J.L., and Jacobson, A. (1992). A mutation in the tRNA nucleotidyltransferase gene promotes stabilization of mRNAs in Saccharomyces cerevisiae. Mol. Cell. Biol.

Peltz, S.W., Brown, A.H., and Jacobson, A. (1993). mRNA destabilization triggered by premature translational termination depends on at least three cis-acting sequence elements and one trans-acting factor. Genes Dev.

Pisarev, A. V., Skabkin, M.A., Pisareva, V.P., Skabkina, O. V., Rakotondrafara, A.M., Hentze, M.W., Hellen, C.U.T., and Pestova, T. V. (2010). The Role of ABCE1 in Eukaryotic Posttermination Ribosomal Recycling. Mol. Cell *37*, 196–210.

Pisareva, V.P., Pisarev, A. V., Hellen, C.U.T., Rodnina, M. V., and Pestova, T. V. (2006). Kinetic analysis of interaction of eukaryotic release factor 3 with guanine nucleotides. J. Biol. Chem. *281*, 40224–40235.

Pisareva, V.P., Skabkin, M.A., Hellen, C.U.T.T., Pestova, T. V., and Pisarev, A. V. (2011). Dissociation by Pelota, Hbs1 and ABCE1 of mammalian vacant 80S ribosomes and stalled elongation complexes. EMBO J. *30*, 1804–1817.

Preis, A., Heuer, A., Barrio-Garcia, C., Hauser, A., Eyler, D.E., Berninghausen, O., Green, R., Becker, T., and Beckmann, R. (2014). Cryoelectron microscopic structures of eukaryotic translation termination complexes containing eRF1-eRF3 or eRF1-ABCE1. Cell Rep. *8*, 59–65.

Del Priore, V., Snay, C.A., Bahr, A.A., Cole, C.N., Priore, V. Del, Snay, C.A., Bahr, A.A., and Cole, C.N. (1996). The product of the Saccharomyces cerevisiae RSS1 gene, identified as a high-copy suppressor of the rat7-1 temperature-sensitive allele of the RAT7/NUP159 nucleoporin, is required for efficient mRNA export.

Rodnina, M. V. (2010). Protein synthesis meets ABC ATPases: New roles for Rli1/ABCE1. EMBO Rep. *11*, 143–144.

Ruiz-Echevarría, M.J., González, C.I., and Peltz, S.W. (1998). Identifying the right stop: Determining how the surveillance complex recognizes and degrades an aberrant mRNA. EMBO J.

Salas-Marco, J., and Bedwell, D.M. (2004). GTP Hydrolysis by eRF3 Facilitates Stop Codon Decoding during Eukaryotic Translation Termination. Mol. Cell. Biol. *24*, 7769–7778.

Sambrook, J., Fritsch, E.F., and Maniatis, T. (1989). Molecular Cloning: A Laboratory Manual, Second Edition.

Savelsbergh, A., Rodnina, M. V., and Wintermeyer, W. (2009). Distinct functions of elongation factor G in ribosome recycling and translocation. RNA *15*, 772–780.

Scarcelli, J.J., Viggiano, S., Hodge, C.A., Heath, C. V., Amberg, D.C., and Cole, C.N. (2008). Synthetic genetic array analysis in Saccharomyces cerevisiae provides evidence for an interaction between RAT8/DBP5 and genes encoding P-body components. Genetics *179*, 1945–1955.

Schmidt, C., Kowalinski, E., Shanmuganathan, V., Defenouillère, Q., Braunger, K., Heuer, A., Pech, M., Namane, A., Berninghausen, O., Fromont-Racine, M., et al. (2016). The cryo-EM structure of a ribosome-Ski2-Ski3-Ski8 helicase complex. Science (80-.).

Schmitt, C., Von Kobbe, C., Bachi, A., Panté, N., Rodrigues, J.P., Boscheron, C., Rigaut, G., Wilm, M., Séraphin, B., Carmo-Fonseca, M., et al. (1999). Dbp5, a DEAD-box protein required for mRNA export, is recruited to the cytoplasmic fibrils of nuclear pore complex via a conserved interaction with CAN/Nup159p.

Schuller, A.P., Wu, C.C.C., Dever, T.E., Buskirk, A.R., and Green, R. (2017). eIF5A Functions Globally in Translation Elongation and Termination. Mol. Cell *66*, 194-205.e5.

Schweingruber, C., Rufener, S.C., Zünd, D., Yamashita, A., and Mühlemann, O. (2013). Nonsense-mediated mRNA decay - Mechanisms of substrate mRNA recognition and degradation in mammalian cells. Biochim. Biophys. Acta - Gene Regul. Mech. *1829*, 612–623.

Shao, S., and Hegde, R.S. (2014). Reconstitution of a Minimal Ribosome-Associated Ubiquitination Pathway with Purified Factors. Mol. Cell.

Shao, S., Brown, A., Santhanam, B., and Hegde, R.S. (2015). Structure and assembly pathway of the ribosome quality control complex. Mol. Cell *57*, 433–444.

Sherman, F. (1991). Getting Started with Yeast. Methods Enzymol.

Sherman, F., and Hicks, J. (1991). Micromanipulation and Dissection of Asci. Methods Enzymol.

Shirley, R.L., Lelivelt, M.J., Schenkman, L.R., Dahlseid, J.N., and Culbertson, M.R. (1998). A factor required for nonsense-mediated mRNA decay in yeast is exported from the nucleus to the cytoplasm by a nuclear export signal sequence. J. Cell Sci.

Shoemaker, C.J., and Green, R. (2011). Kinetic analysis reveals the ordered coupling of translation termination and ribosome recycling in yeast. Proc. Natl. Acad. Sci. U. S. A. *108*, E1392–E1398.

Shoemaker, C.J., Eyler, D.E., and Green, R. (2010). Dom34:Hbs1 promotes subunit dissociation and peptidyl-tRNA drop-off to initiate no-go decay. Science (80-.). *330*, 369–372.

Shoemaker, C.J., Green, R., and Doudna, J.A. (2011). Kinetic analysis reveals the ordered coupling of translation termination and ribosome recycling in yeast. *108*.

Si, K., Chaudhuri, J., Chevesich, J., and Maitra, U. (1997). Molecular cloning and functional expression of a human cDNA encoding translation initiation factor 6. Proc. Natl. Acad. Sci. U. S. A. *94*, 14285–14290.

Sikorski, R.S., and Hieter, P. (1989). A system of shuttle vectors and yeast host strains designed for efficient manipulation of DNA in Saccharomyces cerevisiae. Genetics.

Snay-Hodge, C.A., Colot, H. V., Goldstein, A.L., and Cole, C.N. (1998). Dbp5p/Rat8p is a yeast nuclear pore-associated DEAD-box protein essential for RNA export.

Soheilypour, M., and Mofrad, M.R.K. (2018). Quality control of mRNAs at the entry of the nuclear pore: Cooperation in a complex molecular system. Nucleus.

Song, H., Mugnier, P., Das, A.K., Webb, H.M., Evans, D.R., Tuite, M.F., Hemmings, B.A., and Barford, D. (2000). The crystal structure of human eukaryotic release factor eRF1 - Mechanism of stop codon recognition and peptidyl-tRNA hydrolysis. Cell *100*, 311–321.

Sprague, G.F. (1991). Assay of yeast mating reaction. Methods Enzymol.

Stansfield, I., Jones, K.M., Kushnirov1, V. V, Ter-Avanesyan, M.D., and Tuite5, M.F. (1995). The products of the SUP45 (eRF1) and SUP35 genes interact to mediate translation termination in Saccharomyces cerevisiae.

Stansfield, I., Kushnirov, V. V., Jones, K.M., and Tuite, M.F. (1997). A conditional-lethal translation termination defect in a sup45 mutant of the yeast Saccharomyces cerevisiae. Eur. J. Biochem. *245*, 557–563.

Stewart, M. (2010). Nuclear export of mRNA. Trends Biochem. Sci. *35*, 609–617.

Sträßer, K., Baßler, J., and Hurt, E. (2000). Binding of the Mex67p/Mtr2p heterodimer to FXFG, GLFG, and FG repeat nucleoporins is essential for nuclear mRNA export. J. Cell Biol.

Sundaramoorthy, E., Leonard, M., Mak, R., Liao, J., Fulzele, A., and Bennett, E.J. (2017). ZNF598 and RACK1 Regulate Mammalian Ribosome-Associated Quality Control Function by Mediating Regulatory 40S Ribosomal Ubiquitylation. Mol. Cell.

Taylor, D., Unbehaun, A., Li, W., Das, S., Lei, J., Liao, H.Y., Grassucci, R.A., Pestova, T. V., and Frank, J. (2012). Cryo-EM structure of the mammalian eukaryotic release factor eRF1-eRF3-associated termination complex. Proc. Natl. Acad. Sci. U. S. A. *109*, 18413–18418.

Tieg, B., and Krebber, H. (2013). Dbp5 - From nuclear export to translation. Biochim. Biophys. Acta - Gene Regul. Mech. *1829*, 791–798.

Towbin, H., Staehelin, T., and Gordon, J. Electrophoretic transfer of proteins from polyacrylamide gels to nitrocellulose sheets: procedure and some applications. 1979.

Tran, E.J., Zhou, Y., Corbett, A.H., and Wente, S.R. (2007). The DEAD-Box Protein Dbp5 Controls mRNA Export by Triggering Specific RNA:Protein Remodeling Events. Mol. Cell *28*, 850–859.

Tseng, S.S.I., Weaver, P.L., Liu, Y., Hitomi, M., Tartakoff, A.M., Chang, T.-H.H., S-I Tseng, S., LWeaver, P., Liu, Y., Hitomi, M., et al. (1998). Dbp5 a cytosolic RNA helicase, is required for poly(A)+ RNA export.

Tsuboi, T., Kuroha, K., Kudo, K., Makino, S., Inoue, E., Kashima, I., and Inada, T. (2012). Dom34: Hbs1 Plays a General Role in Quality-Control Systems by Dissociation of a Stalled Ribosome at the 3' End of Aberrant mRNA. Mol. Cell *46*, 518–529.

Uchida, N., Hoshino, S. ichi, Imataka, H., Sonenberg, N., and Katada, T. (2002). A novel role of the mammalian GSPT/eRF3 associating with poly(A)-binding protein in cap/poly(A)-dependent translation. J. Biol. Chem. *277*, 50286–50292.

Urakov, V.N., Mitkevich, O. V., Safenkova, I. V., and Ter-Avanesyan, M.D. (2017). Ribosome-bound Pub1 modulates stop codon decoding during translation termination in yeast. FEBS J. *284*, 1914–1930.

Wada, M., and Ito, K. (2014). A genetic approach for analyzing the co-operative function of the tRNA mimicry complex, eRF1/eRF3, in translation termination on the ribosome. Nucleic Acids Res. *42*, 7851–7866.

Wang, J., Vock, V.M., Shulin Li, O., Olivas, R., and Wilkinson, M.F. (2002). A quality control pathway that down-regulates aberrant T-cell receptor (TCR) transcripts by a mechanism requiring UPF2 and translation. J. Biol. Chem.

Warner, J.R. (1999). The economics of ribosome biosynthesis in yeast. Trends Biochem. Sci.

Weirich, C.S., Erzberger, J.P., Berger, J.M., and Weis, K. (2004). The N-terminal domain of Nup159 forms a β-propeller that functions in mRNA export by tethering the helicase Dbp5 to the nuclear pore. Mol. Cell *16*, 749–760.

Weirich, C.S., Erzberger, J.P., Flick, J.S., Berger, J.M., Thorner, J., and Weis, K. (2006). Activation of the DExD/H-box protein Dbp5 by the nuclear-pore protein Gle1 and its coactivator InsP6 is required for mRNA export. Nat. Cell Biol. *8*, 668–676.

Weng, Y., Czaplinski, K., and Peltz, S.W. (1996). Genetic and biochemical characterization of mutations in the ATPase and helicase regions of the Upf1 protein. Mol. Cell. Biol.

Winston, F., Dollard, C., and Ricupero-Hovasse, S.L. (1995). Construction of a set of convenient saccharomyces cerevisiae strains that are isogenic to S288C. Yeast.

Yarunin, A., Panse, V.G., Petfalski, E., Dez, C., Tollervey, D., and Hurt, E.C. (2005). Functional link between ribosome formation and biogenesis of iron-sulfur proteins. EMBO J. *24*, 580–588.

Zander, G., and Krebber, H. (2017). Quick or quality? How mRNA escapes nuclear quality control during stress. RNA Biol. *14*, 1642–1648.

Zander, G., Hackmann, A., Bender, L., Becker, D., Lingner, T., Salinas, G., and Krebber, H. (2016). MRNA quality control is bypassed for immediate export of stress-responsive transcripts. Nature.

Zhang, S., Welch, E.M., Hagan, K., Brown, A.H., Peltz, S.W., and Jacobson, A. (1997). Polysome-associated mRNAs are substrates for the nonsense-mediated mRNA decay pathway in Saccharomyces cerevisiae. RNA.

Zhao, J., Jin, S.B., Björkroth, B., Wieslander, L., and Daneholt, B. (2002). The mRNA export factor Dbp5 is associated with Balbiani ring mRNP from gene to cytoplasm. EMBO J. *21*, 1177–1187.

Zuk, D., and Jacobson, A. (1998). A single amino acid substitution in yeast eIF-5A results in mRNA stabilization. EMBO J.

7.Acknowledgement – Danksagung

8. Curriculum Vitae

Christian Beißel

Date of Birth: 1st October 1985

Place of Birth: Düren, Germany

2016 – present	PhD student in the group of Prof. Dr. Heike Krebber, Department of Molecular Genetics, Institute for Microbiology and Genetics, Georg-August University Göttingen Member of the Georg-August University School of Science (GAUSS)
2012-2015	Master of Science (M.Sc.) – Biology with the specialization in Neuroscience at the RWTH-Aachen University Master Thesis in the group of Prof. Dr. Markus Kipp, Institute for Neuroanatomy, Uniklinik RWTH-Aachen "Relevance of the transcription factor CHOP for oligodendrocyte death, a combined *in vivo* and *in vitro* approach"
2009-2012	Bachelor of Science (B.Sc.) – Biology at the RWTH-Aachen University Bachelor Thesis in the group of Prof. Dr. Wagner, Institute for Biology II, RWTH-Aachen University "Orientation pop-out of free viewing barn owls"
2009-2013	Student Employee, Preclinical Drug Safety, Gruenenthal GmbH, Aachen
2009	Professional, Preclinical Drug Safety, Gruenenthal GmbH, Aachen
2006-2009	Apprenticeship as Biological Laboratory Technician; Gruenenthal GmbH, Aachen
1996-2006	Abitur, Gymnasium der Gemeinde Kreuzau

Publications

Ariyachet, C., Beißel, C., Li, X., Lorrey, S., Mackenzie, O., Martin, P.M., O'Brien, K., Pholcharee, T., Sim, S., Krebber, H. and McBride, A.E. (2017), Post-translational modification directs nuclear and hyphal tip localization of Candida albicans mRNA-binding protein Slr1. Molecular Microbiology, 104: 499-519. doi:10.1111/mmi.13643

Christian Beißel, Bettina Neumann, Simon Uhse, Irene Hampe, Prajwal Karki, Heike Krebber, Translation termination depends on the sequential ribosomal entry of eRF1 and eRF3, *Nucleic Acids Research*, Volume 47, Issue 9, 21 May 2019, Pages 4798–4813, https://doi.org/10.1093/nar/gkz177

Beißel, C*.; Grosse, S*.; Krebber, H. Dbp5/DDX19 between Translational Readthrough and Nonsense Mediated Decay. *Int. J. Mol. Sci.* **2020**, *21*, 1085.
(* these authors contributed equally)

9. Appendix

Post-translational modification directs nuclear and hyphal tip localization of *Candida albicans* mRNA-binding protein Slr1

Chaiyaboot Ariyachet,[1†] **Christian Beißel,**[2]
Xiang Li,[1‡] **Selena Lorrey,**[1§] **Olivia Mackenzie,**[1]
Patrick M. Martin,[1] **Katharine O'Brien,**[1]
Tossapol Pholcharee,[1] **Sue Sim,**[1¶] **Heike Krebber**[2]
and Anne E. McBride (ID)[1]*

[1] *Biology Department, Bowdoin College, Brunswick, ME 04011, USA.*
[2] *Abteilung für Molekulare Genetik, Institut für Mikrobiologie und Genetik, Göttinger Zentrum für Molekulare Biowissenschaften, Georg-August Universität Göttingen, Göttingen, Germany.*

Summary

The morphological transition of the opportunistic fungal pathogen *Candida albicans* from budding to hyphal growth has been implicated in its ability to cause disease in animal models. Absence of SR-like RNA-binding protein Slr1 slows hyphal formation and decreases virulence in a systemic candidiasis model, suggesting a role for post-transcriptional regulation in these processes. SR (serine–arginine)-rich proteins influence multiple steps in mRNA metabolism and their localization and function are frequently controlled by modification. We now demonstrate that Slr1 binds to polyadenylated RNA and that its intracellular localization is modulated by phosphorylation and methylation. Wildtype Slr1-GFP is predominantly nuclear, but also co-fractionates with translating ribosomes. The non-phosphorylatable slr1-6SA-GFP protein, in which six serines in SR/RS clusters are substituted with alanines, primarily localizes to the cytoplasm in budding cells. Intriguingly, hyphal cells display a slr1-6SA-GFP focus at the tip near the Spitzenkörper, a vesicular structure involved in molecular trafficking to the tip. The presence of slr1-6SA-GFP hyphal tip foci is reduced in the absence of the mRNA-transport protein She3, suggesting that unphosphorylated Slr1 associates with mRNA–protein complexes transported to the tip. The impact of *SLR1* deletion on hyphal formation and function thus may be partially due to a role in hyphal mRNA transport.

Introduction

Candida albicans is a common human commensal fungus as well as an opportunistic pathogen that can cause a wide range of diseases from relatively mild mucosal infections to systemic infections with mortality rates up to 37% (Wisplinghoff *et al.*, 2004). *C. albicans* pathogenicity is linked to a switch between budding yeast and filamentous hyphal morphologies (Lo *et al.*, 1997; Saville *et al.*, 2003). While the compact yeast form may facilitate dissemination in the bloodstream, interaction of yeast cells with host epithelia leads to a transition to the hyphal form, which increases host–cell adherence and promotes invasion into host tissues (Filler *et al.*, 1995; Dalle *et al.*, 2010). The yeast-to-hyphal transition is accompanied by many changes in gene expression that facilitate invasive infection such as the upregulation of cell-surface adhesins and secreted hydrolases (De Groot *et al.*, 2013; Schaller *et al.*, 2005). Whereas the signaling molecules and transcription factors required for this transition have been studied intensively (Nantel *et al.*, 2002; Kadosh and Johnson, 2005; Whiteway and Bachewich, 2007; Bruno *et al.*, 2010; Sellam *et al.*, 2010), much less is known about proteins with roles in post-transcriptional events that could influence hyphal development and function.

Post-transcriptional processes are critical for cellular differentiation in diverse eukaryotic systems, from mRNA transport and turnover during *Drosophila* embryogenesis (Lasko, 2011), to splicing during meiosis

in *Saccharomyces cerevisiae* (Spingola and Ares, 2000), to hyphal mRNA transport during filamentation of the corn smut fungus *Ustilago maydis* (Becht *et al.*, 2005, 2006). The eukaryotic serine–arginine (SR) family of RNA-binding proteins has numerous roles in the control of gene expression, from ubiquitous roles in splicing to impacts on mRNA transport, translation and stability (Shepard and Hertel, 2009; Long and Caceres, 2009; Zhong *et al.*, 2009) and SR protein activity can influence metazoan cellular differentiation (Baker *et al.*, 1989; Sen *et al.*, 2013). SR proteins are characterized by the presence of one or two RNA-recognition motifs (RRMs) and clusters of serine–arginine/arginine–serine (SR/RS) dipeptides. SR protein function and localization are frequently modulated by phosphorylation of the SR/RS dipeptides (Long and Caceres, 2009). While *Schizosaccharomyces pombe* has SR proteins (Srp1 and Srp2), neither *S. cerevisiae* nor *C. albicans* has canonical SR proteins; rather, these yeasts encode SR-like proteins that also include one or two RRMs, but which have repetitive arginine (R)-rich domains with fewer SR/RS dipeptides (Plass *et al.*, 2008). These R-rich domains are often targets for arginine methylation (Henry and Silver, 1996; McBride *et al.*, 2007; Ariyachet *et al.*, 2013). The most thoroughly studied yeast SR-like protein, *S. cerevisiae* Npl3, has been implicated in many aspects of mRNA metabolism from transcription and splicing to mRNA export and translation (Kadowaki *et al.*, 1994; Lee *et al.*, 1996; Bucheli and Buratowski, 2005; Dermody *et al.*, 2008; Kress *et al.*, 2008; Baierlein *et al.*, 2013). Both ScNpl3* and its *S. pombe* ortholog, SpSrp2, are essential, whereas SpSrp1 is not essential (Bossie *et al.*, 1992; Gross *et al.*, 1998; Lutzelberger *et al.*, 1999).

Our recent work identified a *C. albicans* SR-like RNA-binding protein, Slr1, that lacks an apparent ortholog in *S. cerevisiae* (Ariyachet *et al.*, 2013). Absence of this *C. albicans* SpSrp1 ortholog decreases *C. albicans* growth rate more than deletion of the *ScNPL3*/*SpSRP2* ortholog *CaNPL3*. *SLR1* deletion slows hyphal formation, leads to a defect in host cell damage *in vitro* and lowers virulence in a murine model of disseminated candidiasis (Ariyachet *et al.*, 2013). Absence of Slr1 also increases exposure of hyphal-specific adhesin Als3 on the cell surface, suggesting the importance of Slr1 for proper hyphal structure (Ariyachet *et al.*, 2013).

Given the importance of Slr1 for *C. albicans* hyphal formation and virulence and its sequence similarity to other yeast SR and SR-like proteins, we sought to

*As this study focuses on *C. albicans*, for clarity when discussing other proteins from different species, the first letters of genus and species names are included before protein names.

address whether the sequence similarities reflect functional similarities, including identifying the molecular interactions and modifications of Slr1 and testing the impact of post-translational modifications on Slr1 intracellular localization. Interestingly, we find that C-terminal S-to-A mutations that block Slr1 phosphorylation also cause Slr1 to accumulate not only in the cytoplasm of yeast-form cells, but also at the hyphal tip in a region close to the Spitzenkörper, a vesicular structure involved in trafficking lipids and proteins to the tip. The hyphal tip localization of mutant Slr1 is also partially dependent on the presence of mRNA transport protein She3. Combined with additional evidence that wildtype Slr1 interacts with polyadenylated RNA and mRNA-binding proteins, these results suggest a model in which unphosphorylated Slr1 associates with mRNA–protein complexes transported to the hyphal tip where the mRNA is locally translated and that phosphorylation facilitates release of Slr1 from such transport complexes. In fact, Slr1 is detected in polysomes, supporting a potential role in translation. The impact of *SLR1* deletion on hyphal formation and function thus may be due in part to a role in hyphal mRNA transport and translation.

Results

Structural and functional similarity of Slr1 and SR-like proteins

The amino acid sequence of *C. albicans* Slr1 shows distinct similarity to that of other fungal SR-like proteins, including the presence of an RNA-recognition motif (RRM) N-terminal to an arginine (R)-rich region (Fig. 1A). BLASTP searches with the RRM of Slr1 revealed its similarity to RRMs of SR-like proteins *S. pombe* Srp1 and *Aspergillus nidulans* SwoK (Fig. 1B); similar RRMs were also identified in other fungi from *Lachancea thermotolerans* to *Ustilago maydis* (Supporting Information Fig. S1), but not in *S. cerevisiae*. A motif common to many metazoan SR proteins that overlaps with RNP-1 (EFEDxRDAEDA), however, is better conserved in AnSwoK and SpSrp1 than in CaSlr1 (Fig. 1B, boldface). The amino acid composition within the low complexity R-rich region also differs among these proteins: RG dipeptides predominate in Slr1, RD dipeptides in AnSwoK and RS dipeptides in SpSrp1 (Fig. 1C). In addition, AnSwoK and SpSrp1 have regions C-terminal to this R-rich domain (Fig. 1A and C). Thus, the RRM is more highly conserved among Slr1-related proteins than the C-terminal region.

Whereas *S. cerevisiae* does not encode a protein with an Slr1-like RRM, the predominance of glycine and bulky hydrophobic residues in the R-rich region of Slr1
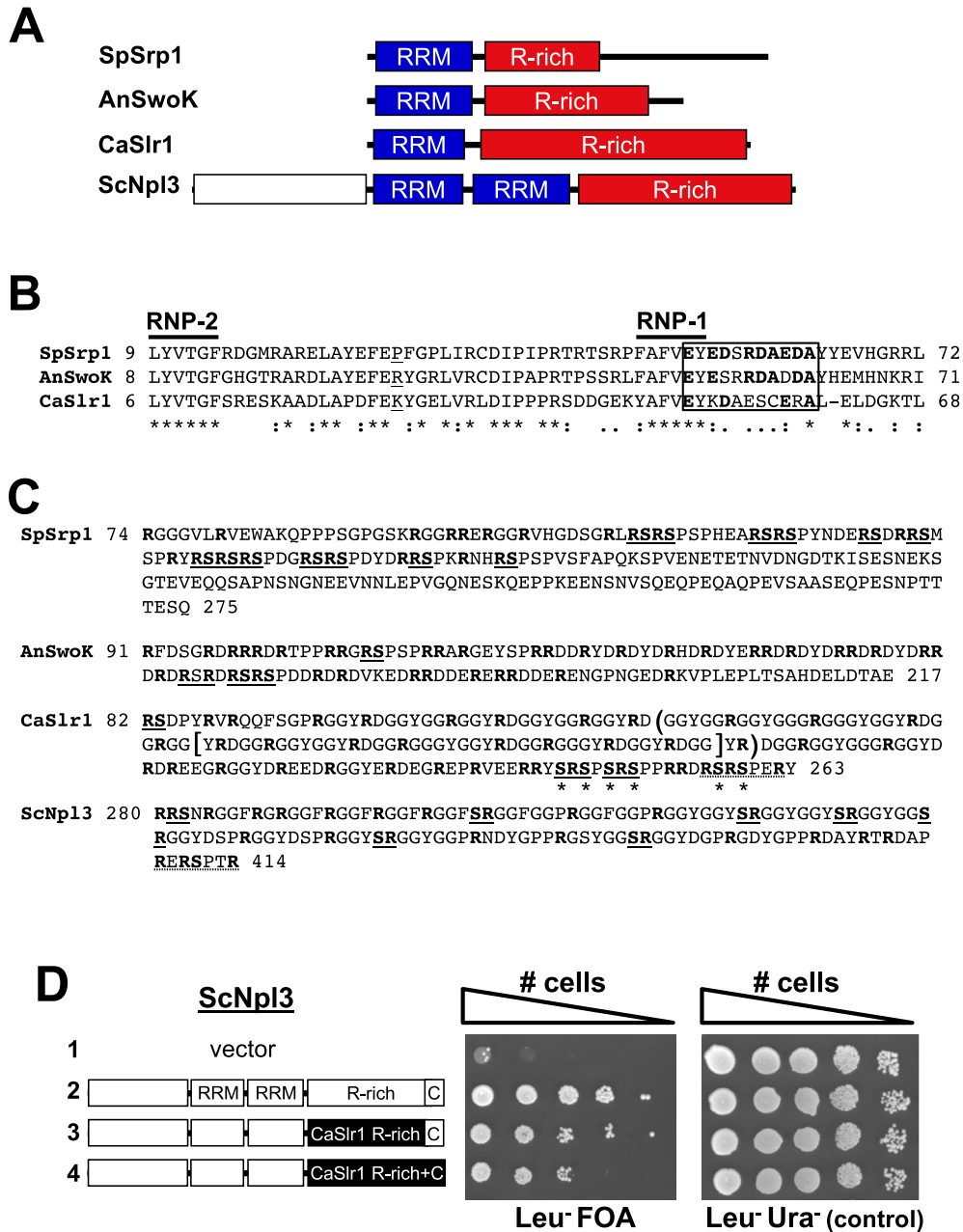
Fig. 1. *C. albicans* Slr1 sequence similarity to fungal SR-like proteins.
A. *Domain comparison of* S. pombe *Srp1,* A. nidulans *SwoK,* C. albicans *Slr1 and* S. cerevisiae *Npl3.* RNA-recognition motifs (RRM) and arginine-rich (R-rich) domains, as well as non-conserved N- and C-terminal domains, are shown.
B. *ClustalW sequence alignment of Slr1, AnSwoK and SpSrp1 RRM domains.* Conserved RNP-2 and RNP-1 motifs are indicated. Residues in boldface within the boxed region are identical to a conserved motif found in metazoan SR proteins (Birney *et al.*, 1993). The 5′ splice site for the first intron in Sp*SRP1*, An*swoK* and *SLR1* genes is located after the second nucleotide in the codon for the underlined residue. Identical (*) and conserved (:) residues are indicated.
C. *Comparison of arginine-rich C-termini.* C-terminal sequences starting at the first arginine following the RRM are shown. Arginine-rich (boldface) regions, SR/RS dipeptides (solid underlining) and a C-terminal SR/RS-containing heptapeptide (dashed underlining) are indicated. Note the similarity between ScNpl3 and Slr1 C-termini. Amino acids deleted in mutant Slr1 proteins are marked with brackets [slr1Δ151-192] and parentheses (slr1Δ123-194); asterisks mark serines mutated to alanine in slr1-6SA.
D. *Partial functionality of the* C. albicans *Slr1 C-terminus in* S. cerevisiae *Npl3.* S. cerevisiae *cells lacking chromosomal* NPL3 *and bearing a* ScNPL3 URA3 CEN *plasmid were transformed with* LEU2 *plasmids expressing chimeric forms of ScNpl3 or the vector plasmid without* NPL3*. White boxes indicate ScNpl3 domains; black boxes indicate equivalent CaSlr1 domains that are replaced within ScNpl3 (C=C-terminus). To test for chimeric ScNpl3 function, cells were grown to mid-log-phase and serial ten-fold dilutions plated on medium lacking leucine and containing 5-FOA (selecting for loss of the* ScNPL3 URA3 *plasmid). Cells were also plated on medium lacking leucine and uracil to confirm equal cell numbers. Plates were incubated at 30°C for 2 days prior to imaging.

does resemble this region of *S. cerevisiae* Npl3 (Fig. 1C). In addition, the C-terminus of ScNpl3 (ReRSPtR) (Fig.1C), which influences cellular localization of ScNpl3 through its phosphorylation (Yun and Fu, 2000; Gilbert *et al.*, 2001), resembles that of Slr1 (RsRSPeRy). This region is critical for ScNpl3 function: deletion of the R-rich region and C-terminus severely abrogates *S. cerevisiae* growth (McBride *et al.*, 2009). Therefore, to determine whether this sequence similarity is function-ally relevant, the ability of the R-rich region of Slr1 to substitute for that of ScNpl3 was tested. As shown in Fig. 1D, chimeric ScNpl3 proteins bearing the Slr1 R-rich domain supported growth of *S. cerevisiae* cells lacking Npl3 (*npl3Δ*). The Slr1 R-rich region linked to the ScNpl3 C-terminus supported only slightly more growth of *npl3Δ* cells than when it was linked to the Slr1 C-terminus (Fig. 1D, compare rows 3 and 4). These results suggest that the Slr1 R-rich region can mediate similar molecular interactions to those mediated by the ScNpl3 R-rich region, but that these regions of the two proteins are not functionally identical.

Slr1 is present in mRNPs

Given the structural similarity of Slr1 to proteins with known roles in mRNA metabolism, we tested whether Slr1 interacts physically with polyadenylated mRNA and mRNA-binding proteins. To assess whether Slr1 associ-ates with poly(A) RNA, cells expressing Slr1 with a C-terminal tandem affinity purification (TAP) tag were exposed to UV light to crosslink RNA with bound pro-teins. Poly(A) RNAs were purified from cell lysates through two rounds of binding to oligo(dT) sepharose. Proteins bound to poly(A) RNAs were released by RNase treatment and Slr1-TAP was detected by anti-Protein A immunoblot. As shown in Fig. 2A, Slr1-TAP did co-purify when crosslinked to poly(A) RNA. In con-trast, Slr1-TAP was not purified from untreated cell lysates (Fig. 2A), indicating that Slr1-TAP does not bind non-specifically to the oligo (dT) resin. Therefore, *C. albicans* Slr1 associates with poly(A) RNA and is likely an mRNA-binding protein.

To test whether Slr1 interacts with known RNA-binding proteins, we isolated proteins bound to Slr1-TAP from lysates of yeast-form *C. albicans* cells by purifica-tion on IgG-sepharose and subsequent elution by cleav-age of the tag with tobacco etch virus (TEV) protease (Fig. 2B). Lysates from cells expressing untagged Slr1 were used to detect background binding to the beads. Zinc staining of purified proteins revealed two major pro-teins that co-purify specifically with Slr1-TAP (Fig. 2B). Mass spectrometric analysis identified the lower band as Slr1-calmodulin-binding protein, the expected product
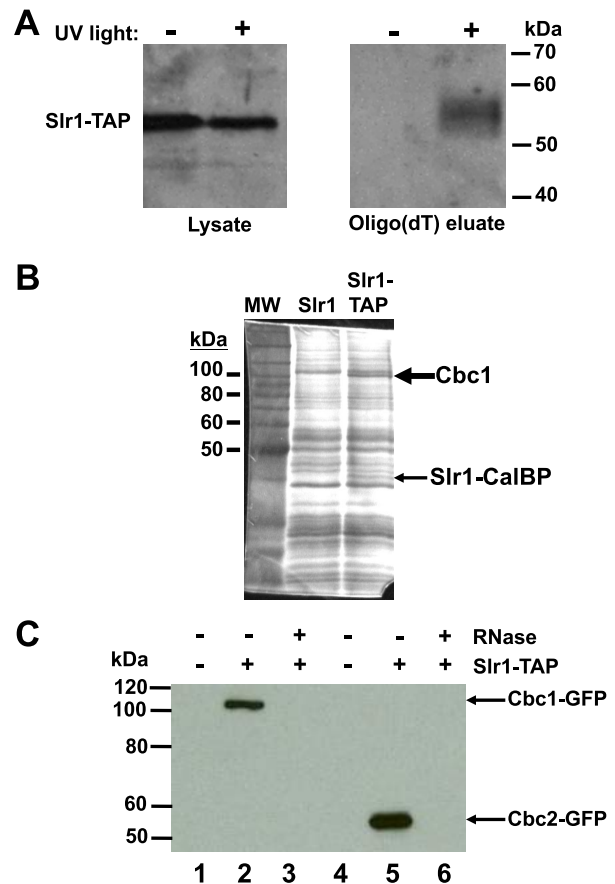

Fig. 2. Slr1 binds to mRNA.
A. *Slr1-TAP binds to polyadenylated RNA*. Cells expressing Slr1-TAP (*SLR1-TAP/slr1Δ*) were exposed to UV light to crosslink RNA with bound proteins. Following lysis, polyadenylated RNA was isolated through two rounds of isolation with oligo(dT)-sepharose. Proteins were released from the RNA by RNase digestion and resolved by SDS-PAGE; the presence of Slr1-TAP was determined by anti-Protein A (PrA) immunoblotting. Samples not exposed to UV light were processed in parallel to test for non-specific binding of Slr1-TAP to the oligo(dT) resin.
B. *Cap-binding complex protein 1 (Cbc1; Orf19.387) co-precipitates with Slr1-TAP*. Protein lysates (65 mg total protein) from *C. albicans* strains expressing untagged Slr1 (*SLR1/slr1Δ*) or Slr1-TAP (*SLR1-TAP/slr1Δ*) were incubated with IgG beads. Bound proteins were eluted with TEV protease and resolved by SDS-10% PAGE. Proteins were visualized by zinc staining and identified by mass spectrometry.
C. *RNA dependence of Slr1-cap-binding complex interaction*. Protein lysates (5 mg total protein) were prepared from cells expressing Slr1-TAP and Cbc1-GFP (lanes 2–3; *ORF19.387-GFP/ORF19.387 SLR1-TAP/slr1Δ*) or Cbc2-GFP (lanes 5–6; *ORF19.763-GFP/ORF19.763 SLR1-TAP/slr1Δ*). Lysates were either treated with RNase (lane 3, 6) or not treated (lane 2, 5) before IgG bead incubation. Slr1-TAP-bound proteins were eluted and analyzed by anti-GFP immunoblotting. Lysates from Cbc-GFP-expressing strains that did not express Slr1-TAP (*ORF19.387-GFP/ORF19.387 SLR1/slr1Δ* and *ORF19.763-GFP/ORF19.763 SLR1/slr1Δ*) were also incubated with IgG beads to test for non-specific binding of Cbc-GFP proteins to the beads (Cbc1, lane 1; Cbc2, lane 4).

following cleavage of the TAP-tagged protein from the IgG beads. The other specific protein (∼100 kDa) corre-sponded to the *C. albicans* ortholog of Cbc1/Cbp80, the

large subunit of the nuclear mRNA cap-binding complex (CBC) (Lewis *et al.*, 1996).

To confirm the interaction of Slr1 with the nuclear cap-binding complex, large and small subunits of the complex were tagged with green fluorescent protein (GFP) in the Slr1-TAP-expressing strain. Anti-GFP immuno-blots following IgG purification of Slr1-TAP from these strains supported an interaction between Slr1 and the CBC (Fig. 2C). The mRNA-binding activity of Slr1 (Fig. 2A) suggested that the co-purification of the cap-binding complex proteins might be due to simultaneous binding of Slr1 and the CBC to the same mRNA. Consistent with this model, RNase treatment of lysates prior to Slr1-TAP isolation eliminated co-purification of the Cbc-GFP proteins (Fig. 2C). Slr1 therefore interacts indirectly with Cbc proteins in an RNA-dependent manner, supporting the conclusion that Slr1 can interact with mRNA.

The C-terminus of Slr1 influences its subcellular localization

To begin to address which mRNA metabolic processes might involve Slr1, we sought to determine the steady-state subcellular localization of Slr1 by integrating a *GFP* tag at the 3′ end of *SLR1*. Wild type Slr1-GFP expressed from its native promoter localizes predominantly to the nucleus of *C. albicans*, as detected by colocalization with DAPI (Fig. 3A, panel c). This steady state nuclear localization contrasts with the whole cell localization of SpSrp1 (Tang *et al.*, 2007), but is similar to that seen for ScNpl3-family proteins and the CBC (Shen *et al.*, 2000; Yun and Fu, 2000; Gilbert *et al.*, 2001; McBride *et al.*, 2007; Tang *et al.*, 2007). In addition, Slr1-GFP appears in brighter puncta with slightly fainter fluorescence throughout the nucleus (Fig. 3B), reminiscent of the localization of metazoan SR proteins to nuclear speckles (Gui *et al.*, 1994). This localization supports a model in which Slr1 has functions within the nucleus, but does not rule out cytoplasmic functions, as many SR-like proteins are dynamic and shuttle between the nucleus and cytoplasm (Flach *et al.*, 1994; Hacker and Krebber, 2004; Tang *et al.*, 2007).

The arginine-rich domain of ScNpl3 modulates its nucleocytoplasmic transport (Senger *et al.*, 1998; McBride *et al.*, 2005; Baierlein *et al.*, 2013). To test whether the R-rich domain influences the nuclear localization of Slr1, we deleted parts of this domain in Slr1-GFP. Removal of 42 amino acids in the middle of this domain decreased the percentage of Slr1-GFP found in the nucleus (%N) and the ratio of mean nuclear to mean cytoplasmic fluorescence intensity (N/C), indicating a slight shift to the cytoplasm at steady state (Fig. 3A, C, slr1Δ151-192). Slr1 lacking an additional 30

residues primarily within the N-terminal half of this domain, however, showed more distinct cytoplasmic localization than slr1Δ151-192 (Fig. 3A, C; slr1Δ123-194). These results were confirmed in two additional independent experiments. The increased detection of the mutant proteins in the cytoplasm did not result from protein instability: the mutant proteins were expressed at comparable levels to wildtype Slr1-GFP (Supporting Information Fig. S2). In addition, the slight cytoplasmic localization of wildtype Slr1-GFP was not due to autofluorescence: cells that did not express GFP had significantly lower mean cytoplasmic fluorescence than Slr1-GFP-expressing cells (Supporting Information Fig. S3). These results indicate the importance of the C-terminal R-rich domain in proper Slr1 localization.

Post-translational modification of Slr1

Throughout eukaryotes, SR protein function and localization are modulated by phosphorylation at RS/SR dipeptides (Long and Caceres, 2009); in addition, arginine methylation within R-rich domains influences subcellular localization and molecular interactions of many RNA-binding proteins (Thandapani *et al.*, 2013). The extensive R-rich domain and the clustering of SR/RS dipeptides at the C-terminus of Slr1 suggest that this region could be a target for modification.

To test for Slr1 phosphorylation, we constructed cells that expressed two different GFP-tagged Slr1 proteins from the endogenous *SLR1* promoter. In one set of strains, GFP was linked to the C-terminus of wild type Slr1 (Slr1-GFP); in the second set of strains, GFP integration was coupled with the introduction of mutations to substitute all six serines in C-terminal SR/RS dipeptides with alanines (slr1-6SA-GFP; Fig. 1C, asterisks). These mutations did not affect log-phase growth of *C. albicans* in rich medium at 30°C or 37°C (30°C generation time: WT $= 198 \pm 6$ min (standard error of the mean SEM); 6SA $= 203 \pm 8$ min SEM; 37°C generation time: WT $= 182 \pm 6$ min SEM; 6SA $= 190 \pm 8$ min SEM; $n = 11$, unpaired student's *t*-test, $p > 0.05$). Anti-GFP immunoblot analysis of Slr1-GFP isolated from mid-log phase yeast-form cells revealed faster migration of the slr1-6SA-GFP mutant protein than the Slr1-GFP wild type protein (Fig. 4A, compare lanes 1 and 4); the apparent difference ($\sim$8 kDa) was much greater than would be expected based solely on the molecular weights of serine and alanine (difference <0.1 kDa) and could reflect phosphorylation of the wild type protein. The S-to-A mutations also led to an apparent increase in steady-state levels of slr1-6SA-GFP compared with Slr1-GFP (Fig. 4A, compare lanes 2 and 7).
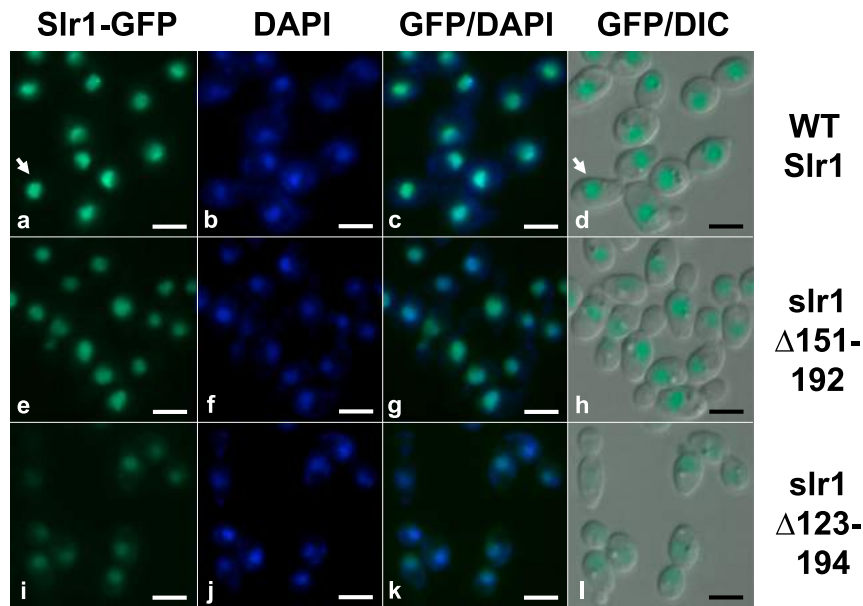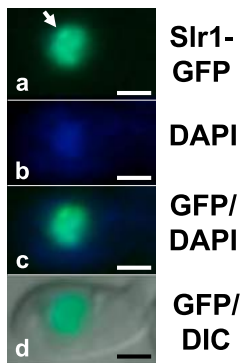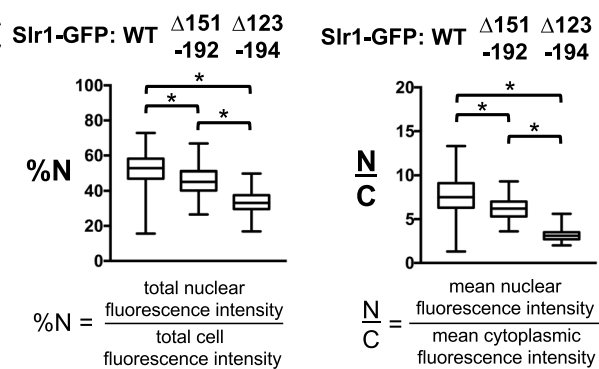
A

B

C

$$\%N = \frac{\text{total nuclear fluorescence intensity}}{\text{total cell fluorescence intensity}}$$

$$\frac{N}{C} = \frac{\text{mean nuclear fluorescence intensity}}{\text{mean cytoplasmic fluorescence intensity}}$$

Fig. 3. The C-terminal arginine-rich domain affects Slr1 nuclear localization.
A. *Localization of WT and mutant Slr1-GFP proteins*. Cells expressing Slr1-GFP were grown to mid-log phase at 30°C and stained with DAPI in PBS prior to fluorescence microscopy. Wildtype Slr1-GFP (panels a–d; *SLR1-GFP/slr1Δ*) and slr1-GFP proteins with deletions within the arginine-rich domain from tyrosine 151 to glycine 192 (panels e–h; *slr1Δ151-192-GFP/slr1Δ*) or from aspartate 123 to arginine 194 (panels i–l; *slr1Δ123-194-GFP/slr1Δ*) were expressed from the native locus. Exposure times were equivalent for all strains and GFP images were merged with DAPI and DIC images in Adobe Photoshop CS5. Arrow = cell enlarged in B. Scale bar = 5 μm.
B. *WT Slr1-GFP is present in nuclear puncta*. The cell indicated by an arrow in panels a–d of (A), is shown. The arrow indicates one region of brighter GFP fluorescence. Scale bar = 2 μm.
C. *Quantification of subcellular localization*. GFP, DAPI and DIC images of cells from the experiment in (A) were stacked in ImageJ (Schneider et al., 2012), the mean GFP fluorescence intensity and area of each cell (defined by DIC) and nucleus (defined by DAPI) were measured and used to calculate percent nuclear GFP fluorescence (%N) and the ratio of mean nuclear and mean cytoplasmic fluorescence intensity (N/C). Significant differences were detected among the cells of different genotypes ($n = 100$–110 per genotype; Kruskal–Wallis test, $p < 0.0001$). Significant differences by pairwise Mann–Whitney–Wilcoxon tests (*$p < 0.0001$) and the minimum, maximum, median and first and third quartiles are shown.

To test phosphorylation directly, immunopurified GFP-tagged proteins were incubated at 37°C with or without calf intestinal phosphatase. Phosphatase treatment of Slr1-GFP resulted in two additional bands, one of which comigrated with untreated slr1-6SA-GFP (Fig. 4A, lanes 3 and 4), whereas no change in the migration of slr1-6SA-GFP was detected following phosphatase treatment

(Fig. 4A, lanes 5 and 6). These results support a model where the phosphorylation of SR/RS dipeptides occurs in the C-terminus of Slr1.

Purification of arginine-methylated proteins from yeast-form *C. albicans* cells also indicated that Slr1 is methylated (Fig. 4B). Anti-methylarginine immunoprecipitation of proteins from wildtype *C. albicans* cell lysates
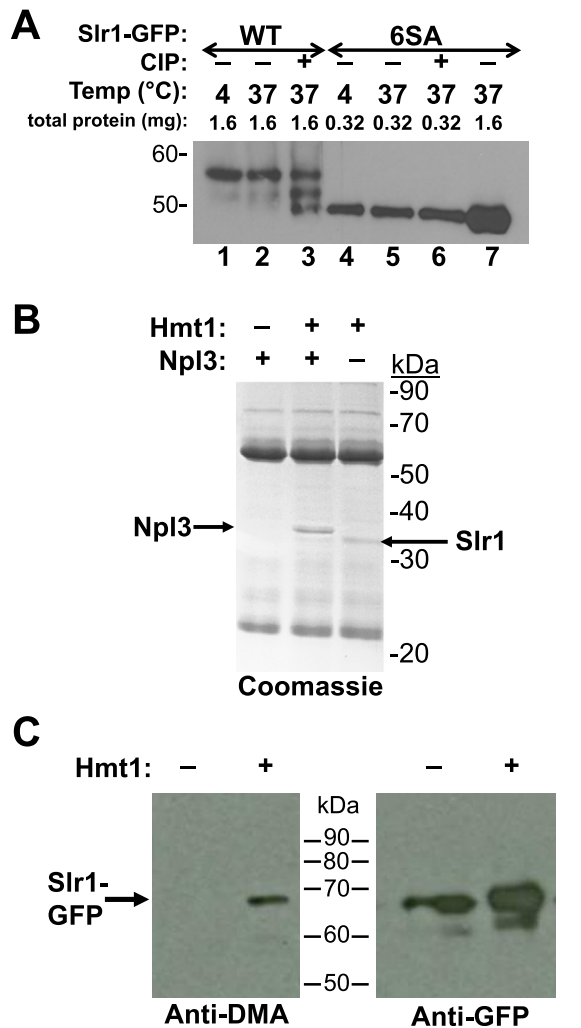
Fig. 4. Slr1 post-translational modification.
A. *Slr1 phosphorylation.* Slr1-GFP and slr1-6SA-GFP were immunoprecipitated from *SLR1-GFP/slr1Δ* and *slr1-6SA-GFP/slr1Δ* yeast-cell lysates and incubated with or without calf intestinal phosphatase for 1 h at 4°C or 37°C. Treated (+) and untreated (−) samples (precipitated from 1.6 mg or 0.32 mg total protein) were resolved by SDS-PAGE and relative migration of Slr1 proteins detected by immunoblotting with anti-GFP antibodies.
B. *SR-like proteins Npl3 and Slr1 are major targets for arginine methylation in* C. albicans. Lysates from yeast cells expressing the major arginine methyltransferase Hmt1 with (*HMT1/hmt1Δ*) or without (*HMT1/hmt1Δ npl3Δ/Δ*) Npl3 were incubated with anti-methylarginine antibody Ab412 (Abcam) and bound proteins purified with Protein G-sepharose. Proteins were resolved by SDS-PAGE and visualized by Coomassie staining. Cells lacking Hmt1 (*hmt1Δ/Δ*) were used to detect non-specifically bound proteins.
C. *Slr1-GFP is arginine-methylated.* Cells expressing Slr1-GFP with (+) and without (−) Hmt1 (*SLR1-GFP/slr1Δ* and *SLR1-GFP/slr1Δ hmt1Δ/Δ*) were lysed and Slr1-GFP precipitated with anti-GFP antibody. Methylation of Slr1-GFP was detected by immunoblot with Ab412.

2007). Immunoprecipitation from *npl3Δ/Δ* lysates, however, increased detection of a second, slightly smaller arginine-methylated protein, which was identified by mass spectrometry as Slr1 (Fig. 4B, lane 3). This modification of Slr1 was confirmed by immunoprecipitating Slr1-GFP from strains with and without the methyltransferase and immunoblotting with the anti-dimethylarginine antibody (Fig. 4C). The recognition of Slr1-GFP by the anti-methylarginine antibody in strains with Hmt1 indicated that its precipitation in Fig. 4B did not result from coprecipitation with another arginine-methylated protein. Therefore, Slr1 is both phosphorylated and arginine-methylated in *C. albicans*.

Modification of Slr1 influences its subcellular localization

Post-translational modifications affect subcellular localization of a number of yeast SR proteins including SpSrp1 and ScNpl3-family proteins ScNpl3, CaNpl3 and SpSrp2. All these RNA-binding proteins move between the nucleus and the cytoplasm, but phosphorylation of ScNpl3-family proteins facilitates their nuclear import (Yun and Fu, 2000; Gilbert *et al.*, 2001; McBride *et al.*, 2007; Tang *et al.*, 2007), whereas phosphorylation of SpSrp1 enhances its nuclear export (Tang *et al.*, 2007). In light of the sequence similarities between the N-termini of Slr1 and SpSrp1 and the C-termini of Slr1 and ScNpl3 proteins, we tested the impact of post-translational modifications on Slr1 localization using mutational approaches.

Given the multiplicity of kinases that target SR proteins in other species (Yun and Fu, 2000; Gilbert *et al.*, 2001; Tang *et al.*, 2007; Dermody *et al.*, 2008), to determine whether phosphorylation of Slr1 impacts its intracellular localization, localization of wildtype Slr1-GFP was compared with that of slr1-6SA-GFP. Introduction of the 6SA mutations caused a shift in the steady-state localization: slr1-6SA-GFP is more cytoplasmic than wildtype Slr1-GFP (Fig. 5A, compare panels a-c and e-g), with a significantly lower percent nuclear localization (%N) and ratio of mean nuclear to cytoplasmic fluorescence intensity (N/C) than WT Slr1-GFP (Fig. 5D). These findings were confirmed in two additional independent experiments. The increased cytoplasmic localization of slr1-6SA-GFP was not due to the release of GFP from the fusion protein, as indicated by the absence of < 40 kDa proteins detected by an anti-GFP antibody (Fig. 5E). In addition, slr1-6SA-GFP appeared in cytoplasmic foci, most notably at the bud neck of post-mitotic cells (Fig. 5B and C). These results suggested that Slr1 phosphorylation may facilitate nuclear import, but may also have roles beyond regulation of Slr1 nucleocytoplasmic transport.

revealed one major protein (Fig. 4B, lane 2) that was not seen in immunoprecipitates from cells lacking the major arginine methyltransferase, Hmt1 (lane 1). Mass spectrometric analysis identified this protein as CaNpl3, a known target of arginine methylation (McBride *et al.*,

A

B *HMT1/HMT1*   **C** *hmt1Δ/hmt1Δ*

D

$$\%N = \frac{\text{total nuclear fluorescence intensity}}{\text{total cell fluorescence intensity}}$$

$$\frac{N}{C} = \frac{\text{mean nuclear fluorescence intensity}}{\text{mean cytoplasmic fluorescence intensity}}$$
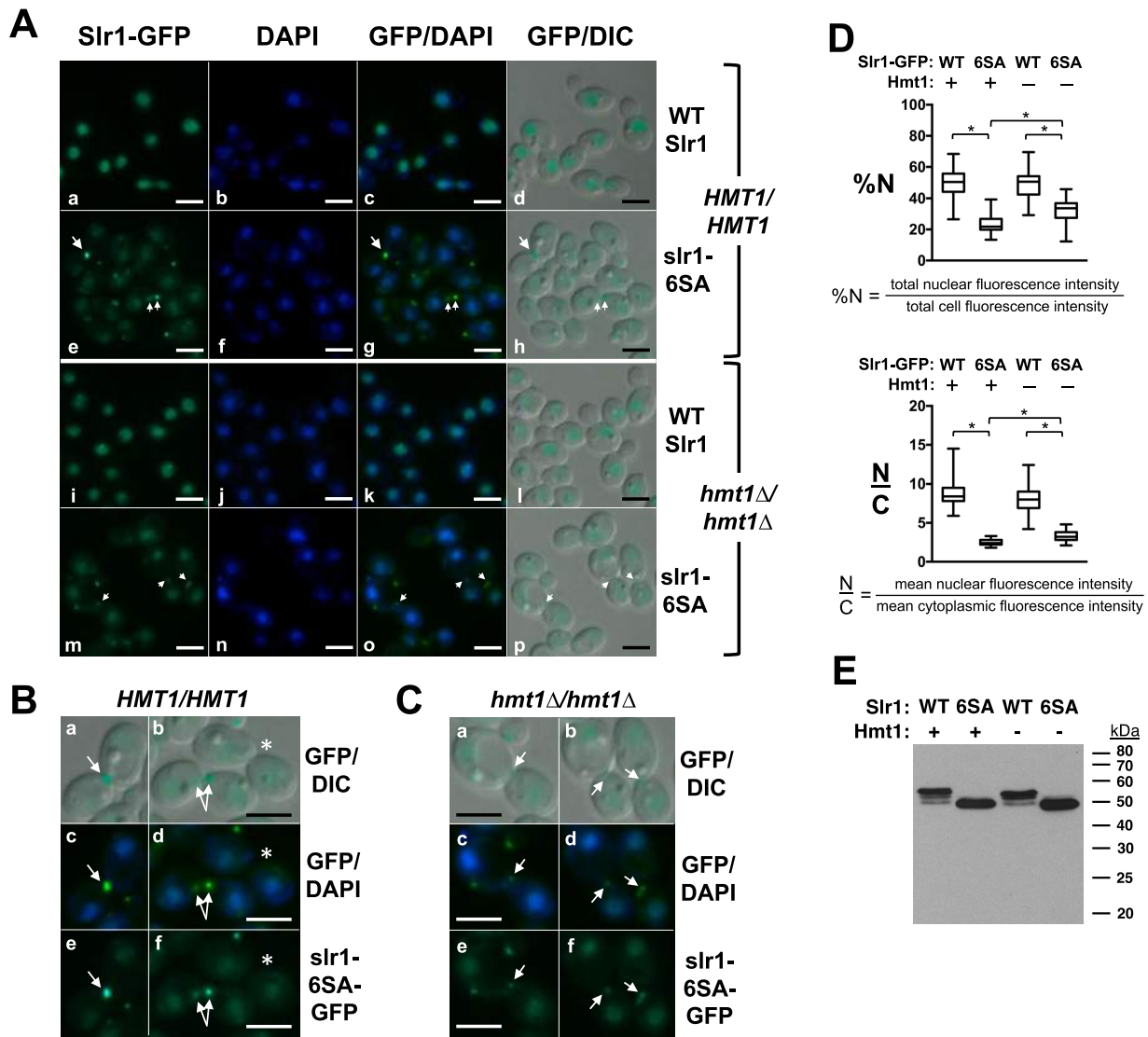
E

Fig. 5. Serine mutation and arginine methylation affect Slr1 localization.

A. *Localization of WT and mutant Slr1-GFP proteins.* Slr1-GFP and slr1-6SA-GFP were expressed in cells with (*SLR1-GFP/slr1Δ, panels a–d; slr1-6SA-GFP/slr1Δ, panels e–h*) or without (*SLR1-GFP/slr1Δ hmt1Δ/Δ, panels i–l; slr1-6SA-GFP/slr1Δ hmt1Δ/Δ, panels m–p*) the arginine methyltransferase Hmt1 and visualized as in Fig. 3A. Exposure times were equivalent for all genotypes. Arrows indicate examples of post-mitotic cells with slr1-6SA-GFP foci at the bud neck. Scale bar = 5 μm.

B. *Bud-neck localization of slr1-6SA-GFP in post-mitotic cells with Hmt1.* Examples of cells with 1 (arrow, panels a, c, e), 2 (arrows, panels b, d, f) or no (asterisk, panels b, d, f) bud-neck slr1-6SA-GFP focus from panels h, g and e in Fig. 5A are shown. Scale bar = 5 μm.

C. *Bud-neck localization of slr1-6SA-GFP in post-mitotic cells without Hmt1.* Examples of cells from panels p, o and m in Fig. 5A are shown (arrow = bud-neck focus). Scale bar = 5 μm.

D. *Quantification of subcellular localization.* GFP, DAPI and DIC images of cells from the experiment in Fig. 5A were analyzed as in Fig. 3C to determine percent nuclear GFP fluorescence (%N) and the ratio between the mean nuclear and mean cytoplasmic GFP fluorescence intensity (N/C). Significant differences were detected among the cells of different genotypes ($n = 59$–66 for each genotype; Kruskal–Wallis test, $p < 0.0001$). Significant differences by pairwise Mann–Whitney–Wilcoxon tests (*$p < 0.0001$) and the minimum, maximum, median and first and third quartiles are shown. WT = wildtype Slr1-GFP, 6SA = slr1-6SA-GFP.

E. *Absence of arginine methylation does not decrease Slr1 protein levels.* Cells in Fig. 5A were grown to mid-log phase in YPD, lysed and levels of GFP proteins in 17 μg total protein analyzed by SDS-10% PAGE and anti-GFP immunoblot.

Arginine methylation facilitates nuclear export of both ScNpl3 and CaNpl3 (Shen *et al.*, 1998; McBride *et al.*, 2007). To test whether methylation affects nucleocytoplasmic transport of Slr1, Slr1-GFP was expressed in cells lacking the methyltransferase Hmt1 (Fig. 5). The predominantly nuclear localization of Slr1-GFP in the absence of Hmt1 indicates that methylation is not required for nuclear import (Fig. 5A, panels i–k). No significant difference in the
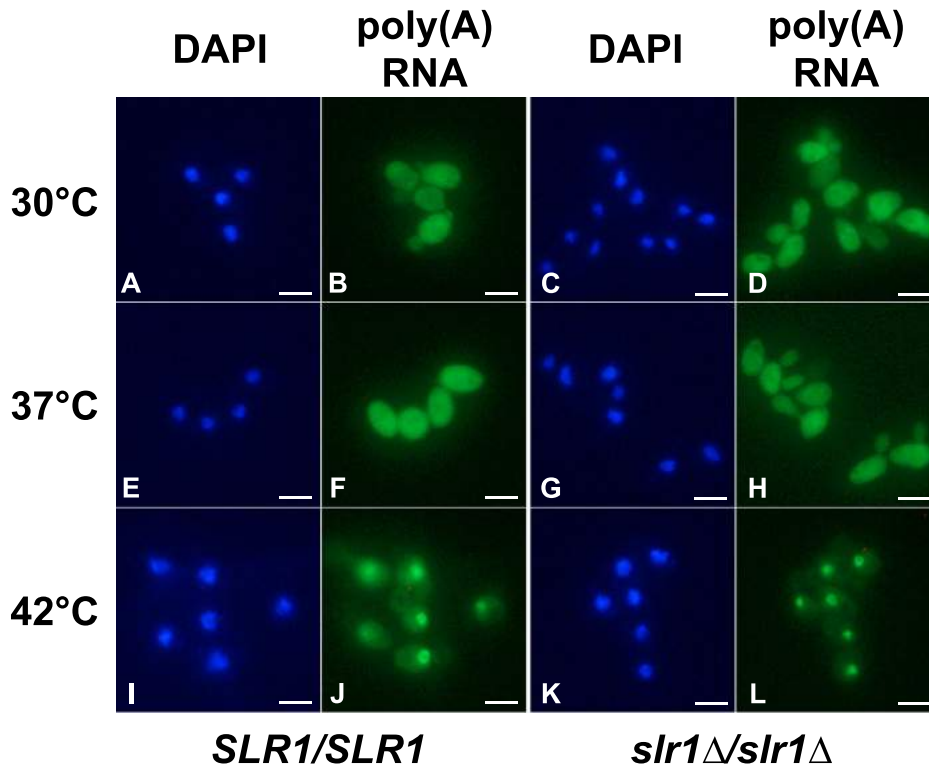
Fig. 6. *SLR1* deletion does not block bulk mRNA export. Cells with (*SLR1/SLR1*; AMC79) and without (*slr1Δ/slr1Δ*; AMC89) Slr1 were grown at 30°C, 37°C, or shifted to 42°C for 30 min. after growth at 30°C before fixation. Fixed cells were hybridized with digoxigenin-conjugated oligo(dT), and stained with DAPI and FITC-conjugated anti-digoxigenin antibody. Nuclei and bulk poly(A) mRNAs were visualized by fluorescence microscopy using the DAPI and GFP filters respectively. Exposure times were equivalent for all strains and growth conditions. Scale bar = 5 μm.

%N and N/C ratio of WT Slr1-GFP was detected between cells with and without Hmt1 (Fig. 5A, compare panels a–c and i–k; Fig. 5D). Both measures of nuclear slr1-6SA-GFP localization, however, were significantly increased by deletion of *HMT1* (Fig. 5D). This subtle increase in nuclear slr1-6SA-GFP in the absence of Hmt1 was confirmed in two additional independent experiments (N/C) and one of two additional experiments (%N). The apparent decrease in cytoplasmic slr1-6SA-GFP was not due to lower levels of expression of slr1-6SA-GFP in the absence of Hmt1 (Fig. 5E, compare lanes 2 and 4). The percentage of post-mitotic cells with slr1-6SA-GFP foci at the bud neck, however, was not significantly different in the presence (53% ± 8%SEM) and absence (47% ± 1%SEM) of arginine methylation (> 55 cells per strain in three independent experiments; $p >$ 0.05, student's *t*-test). Thus, the R-rich domain, arginine methylation and phosphorylation of Slr1 affect its intracellular localization.

Slr1 is not required for bulk mRNA export

The binding of Slr1 to mRNA in a complex with the CBC, combined with its ability to move between the nucleus and cytoplasm, suggested that Slr1, like ScNpl3, might play a role in nuclear export of mRNA (Singleton *et al.*, 1995; Lee *et al.*, 1996; Shen *et al.*, 2000). We, therefore, developed a fluorescence *in situ* hybridization (FISH) assay with an oligo(dT) probe to detect the localization of bulk mRNA in cells with and without Slr1 (Fig. 6). In *S. cerevisiae*, such assays detect the cytoplasmic localization of polyadenylated mRNA, which becomes predominantly nuclear in the presence of mutations that block mRNA export (Singleton *et al.*, 1995). In addition, heat shock treatment of *S. cerevisiae* at 42°C blocks bulk mRNA export while not affecting export of heat shock mRNAs (Saavedra *et al.*, 1996; Tani *et al.*, 1996).

To ascertain that our assay could detect a block to nuclear mRNA export, we tested whether heat shock treatment at 42°C also resulted in nuclear localization of bulk poly(A) RNA in *C. albicans* (Fig. 6). Polyadenylated RNA was found throughout *C. albicans* cells at 30°C and 37°C (Fig. 6, panels B, F), but accumulated in the nucleus at 42°C (panel J). In the absence of Slr1, however, no nuclear accumulation of bulk poly(A) RNA was detected (Fig. 6, panels D, H) except during heat-shock conditions (panel L). Therefore, although Slr1 moves between nuclear and cytoplasmic compartments, it is dispensable for nuclear export of the majority of polyadenylated mRNAs under standard conditions.

Slr1 co-fractionates with translating ribosomes

The detection of a fraction of wildtype Slr1-GFP outside the DAPI-stained nucleus (Fig. 5D), in addition to the cytoplasmic localization of slr1-6SA-GFP, suggested that
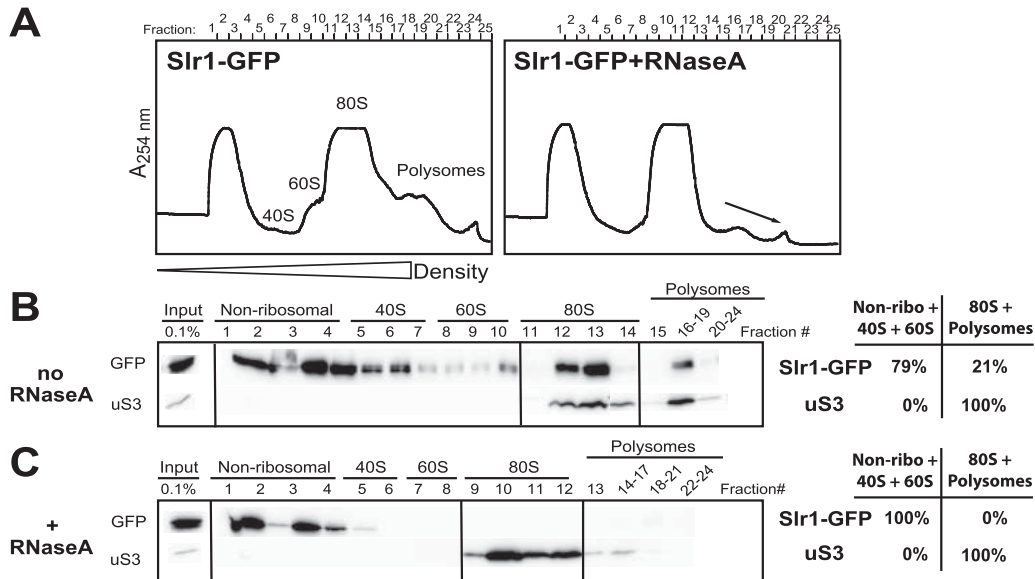
A

Fraction: 1 2 3 4 5 6 7 8 9 10 11 12 13 14 15 16 17 18 19 20 21 22 23 24 25   1 2 3 4 5 6 7 8 9 10 11 12 13 14 15 16 17 18 19 20 21 22 23 24 25

Slr1-GFP   **Slr1-GFP+RNaseA**

A254 nm

80S

60S

40S

Polysomes

Density

B

no RNaseA

	Input 0.1%	Non-ribosomal 1 2 3 4	40S 5 6 7	60S 8 9 10	80S 11 12 13 14	Polysomes 15 16-19 20-24	Fraction #		Non-ribo + 40S + 60S	80S + Polysomes
GFP								**Slr1-GFP**	79%	21%
uS3								**uS3**	0%	100%

C

+ RNaseA

	Input 0.1%	Non-ribosomal 1 2 3 4	40S 5 6	60S 7 8	80S 9 10 11 12	Polysomes 13 14-17 18-21 22-24	Fraction#		Non-ribo + 40S + 60S	80S + Polysomes
GFP								**Slr1-GFP**	100%	0%
uS3								**uS3**	0%	100%

Fig. 7. Slr1-GFP co-fractionates with 80S and translating ribosomes.
A. Log-phase yeast cells expressing Slr1-GFP (*SLR1-GFP/slr1Δ*) were treated with cycloheximide prior to lysis. Lysates were loaded on linear 7%–47% sucrose gradients and fractionated following centrifugation. RNA absorbance at 254 nm was measured during fractionation to detect 40S and 60S ribosomal subunits, 80S ribosomes and polysomes.
B. TCA-precipitated fractions were resolved by SDS-10% PAGE and tested for the presence of Slr1-GFP and ribosomal protein Rps3 by immunoblot (GFP, uS3). The percent of each protein present in non-ribosomal and ribosomal fractions was determined using Image StudioLite software (LI-COR).
C. Lysates were treated with RNase A prior to sucrose-density gradient centrifugation and then analyzed as in (B).

Slr1 might function in part in the cytoplasm. *S. cerevisiae* SR-like protein Npl3 is required for monosome formation during translation initiation and co-fractionates with polysomes (Windgassen *et al.*, 2004; Baierlein *et al.*, 2013). We, therefore, compared the migration of wildtype Slr1-GFP with that of ribosomal protein Rps3 through sucrose density gradients (Fig. 7). While the majority of Slr1-GFP was detected in non-ribosomal and ribosomal subunit fractions (79%; Fig. 7B), 21% was found in fractions that contained the 80S ribosome and polysomes. This association of Slr1-GFP with 80S and translating ribosomes was abrogated by treatment of lysates with RNase A prior to centrifugation (Fig. 7C). These results indicated that wildtype Slr1 is present in the cytoplasm and suggested that wildtype Slr1 may play a role in translation through binding to mRNA (Fig. 2A).

slr1-6SA localizes to the hyphal tip

The deletion of *SLR1* decreases hyphal growth and function (Ariyachet *et al.*, 2013), raising the question of whether Slr1 is present in hyphal cells. When cells were induced to form hyphae, wildtype Slr1-GFP localized to both mother cell and hyphal nuclei (Fig. 8A, panels c–e). Interestingly, slr1-6SA-GFP appeared not only in the nuclei and cytoplasm, but also in cytoplasmic foci along

the hypha, including an intense spot near the tip of the hypha (Fig. 8B, panel c–e, arrow). In addition, slr1-6SA-GFP accumulated at the tip of hyphal branches (Fig. 8C, arrowhead), another region of polarized growth, and at some septa (Fig. 8D, arrowhead), similar to its appearance at the bud neck of yeast-form cells (Fig. 5B). The predominant slr1-6SA-GFP hyphal tip focus was reminiscent of the Spitzenkörper, a structure found near hyphal tips of filamentous fungi (Riquelme, 2013). The vesicles that comprise the Spitzenkörper deliver protein and lipid cargoes to the growing hyphal tip (Riquelme, 2013).

We therefore tested for colocalization of the hyphal tip slr1-6SA-GFP focus and the Spitzenkörper (Fig. 9, Table 1). Cells incorporate the lipophilic dye FM4-64 into endocytic vesicles, leading to rapid accumulation in vacuolar membranes (Vida and Emr, 1995). In growing hyphae, however, FM4-64 can be seen in the Spitzenkörper in a brief window after exposure to the dye (Crampin *et al.*, 2005). Yeast-form cells expressing slr1-6SA-GFP were diluted in hyphal-inducing medium, incubated at 37°C and exposed to FM4-64 three hours after hyphal induction. In 65% of cells with distinct Spitzenkörper FM4-64 staining, this fluorescence partially colocalized with a slr1-6SA-GFP focus at the hyphal tip (Fig. 9A, panels b–d) and in 4%–8% of hyphae, an slr1-6SA-GFP focus was adjacent to the Spitzenkörper
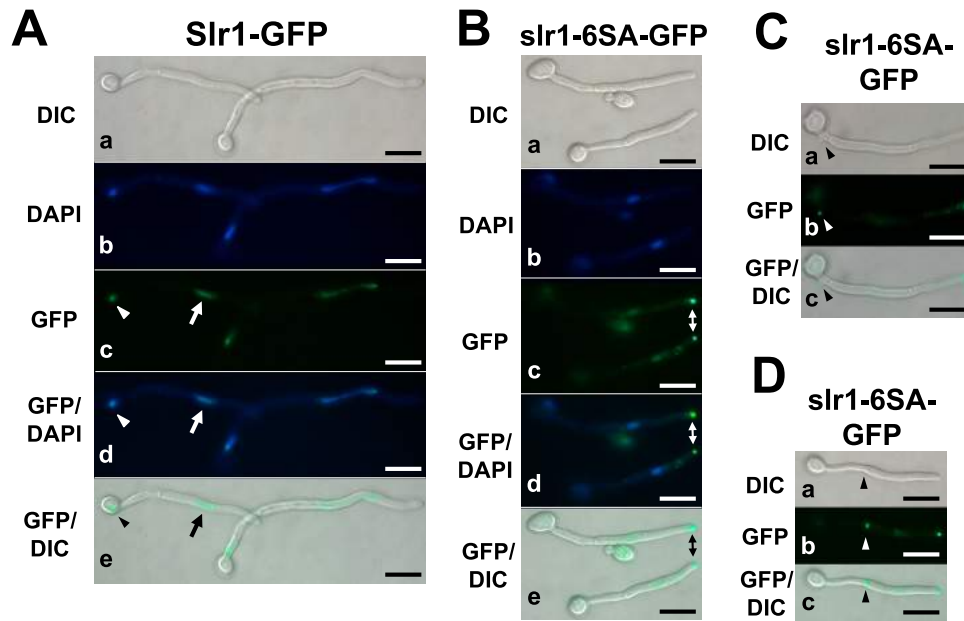
Fig. 8. Serine mutations shift localization of Slr1-GFP to hyphal foci.
A. Cells expressing wildtype Slr1-GFP (*SLR1-GFP/slr1Δ*) were grown in RPMI at 37°C to induce hyphal formation. After 3 h, cells were stained with DAPI to visualize nuclei and localization of Slr1-GFP proteins was determined by fluorescence microscopy using GFP and DAPI filters. Arrowhead = mother cell nucleus; arrow = hyphal nucleus.
B. Cells expressing slr1-6SA-GFP (*slr1-6SA-GFP/slr1Δ*) were grown and imaged as in (A). Arrow = hyphal tip focus.
C. Cells expressing slr1-6SA-GFP were grown and imaged as in (B). Arrowhead = hyphal branch focus.
D. Cells expressing slr1-6SA-GFP were grown and imaged as in (B). Arrowhead = septal focus. Exposure times were equivalent for both genotypes. Scale bar = 10 μm.

(Table 1). The ability of FM4-64 to stain the Spitzenkörper was confirmed by hyphal tip colocalization of FM4-64 with a fluorescent myosin light-chain 1 fusion protein (Mlc1-YFP), a known Spitzenkörper protein (Crampin *et al.*, 2005) (Fig. 9B, Table 1). Line scans

demonstrating the partial colocalization of slr1-6SA-GFP and Mlc1-YFP with the Spitzenkörper are shown in Supporting Information Fig. S4. The localization of slr1-6SA-GFP to a region of the hypha near the Spitzenkörper suggested that this protein might associate with
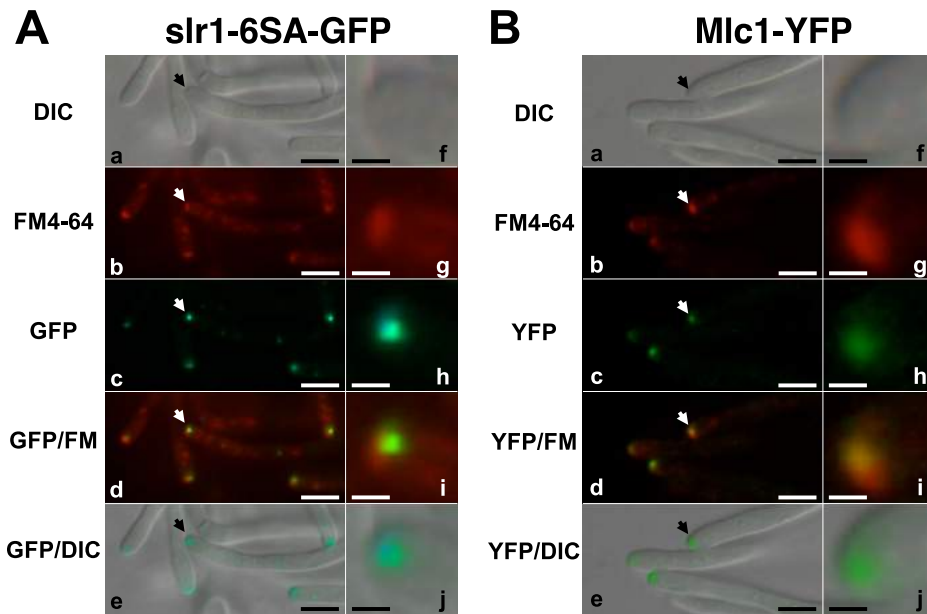
Fig. 9. The slr1-6SA-GFP hyphal tip focus partially overlaps with the Spitzenkörper.
A. Cells expressing slr1-6SA-GFP (*SLR1-GFP/slr1Δ*) were induced to form hyphae as in Fig. 8. After 3 h, FM4-64 was added and cells incubated at 37°C for 4 min. Cells were quickly washed with warm PBS and visualized by fluorescence microscopy with Texas Red (FM4-64) and GFP (slr1-6SA-GFP, Mlc1-YFP) filters. Arrows in panels a–e indicate hyphal tips enlarged in panels f–j. Scale bars: panels a–e = 5 μm, panels f–j = 1 μm.
B. Cells expressing Mlc1-YFP (*MLC1/MLC1-YFP*) were grown, stained, visualized and labeled as in (A).

Table 1. Partial overlap of slr1-6SA-GFP hyphal tip foci with the Spitzenkörper.

Experiment[a]	slr1-6SA-GFP		Mlc1-YFP	
	A	B	A	B
GFP/YFP focus[b]				
Partial overlap with Spitzenkörper	65% (43)	65% (15)	98% (63)	95% (21)
Adjacent to Spitzenkörper	8% (5)	4% (1)	0% (0)	0% (0)
No GFP/YFP focus at hyphal tip	27% (18)	30% (7)	2% (1)	5% (1)
Total # hyphae scored	66	23	64	22

a. FM4-64 staining of the Spitzenkörper was compared with slr1-6SA-GFP and Mlc1-YFP hyphal tip fluorescence in two experiments (A, B).
b. GFP/YFP foci for all hyphae with distinct FM4-64 staining of the Spitzenkörper were scored as partially overlapping with or adjacent to the Spitzenkörper, or absent from the hyphal tip. The absolute number of hyphae in each category is noted in parentheses.

transport complexes, for example by binding to mRNAs that are transported to the hyphal tip.

In *S. cerevisiae*, the She3 protein complex transports a set of mRNAs to the bud tip (Shepard *et al.*, 2003). The *C. albicans* She3 ortholog binds to at least 37 mRNAs during hyphal growth (Elson *et al.*, 2009). At least 12 of these transcripts localize to the hyphal tip and this localization requires the CaShe3 protein (Elson *et al.*, 2009). We hypothesized that the accumulation of the mRNA-binding protein slr1-6SA at the hyphal tip might depend on mRNA transport to the tip. We therefore expressed slr1-6SA-GFP in *C. albicans* strains without CaShe3 (Fig. 10). In cells lacking She3, many fewer cells contained slr1-6SA-GFP foci at the hyphal tip (Fig. 10A, panels g–l); the percentage of hyphal tips containing slr1-6SA-GFP foci is over three times lower in strains without She3 than in strains bearing a single copy of *SHE3* (Fig. 10B). In contrast, slr1-6SA-GFP formed cytoplasmic foci in the presence or absence of She3 (Fig. 10A). The average percentage of hyphal tips with slr1-6SA-GFP foci in the presence of She3 ($70.3\% \pm 2.6\%$ SEM) was consistent with the average percentage of hyphae with slr1-6SA-GFP foci that partially overlapped with (65%) or were adjacent to (4%–8%) the Spitzenkörper (Table 1). These results indicated that slr1-6SA-GFP localization specifically to the hyphal tip is partially dependent on She3, suggesting the association of slr1-6SA-GFP with She3-transported mRNAs.

Discussion

Post-transcriptional regulation of gene expression has been linked to cellular differentiation throughout eukaryotes. The absence of putative RNA-binding protein Slr1 delays hyphal formation in *C. albicans*, lowers virulence and alters exposure of a hyphal cell-wall-associated protein involved in host–cell interactions, suggesting the involvement of Slr1 in post-transcriptional processes that influence hyphal formation and function (Ariyachet *et al.*, 2013). We now demonstrate that Slr1 is a

component of an mRNP complex and is found in both the nucleus and the cytoplasm. Slr1 shares primary structural features with two different fungal SR-like RNA-
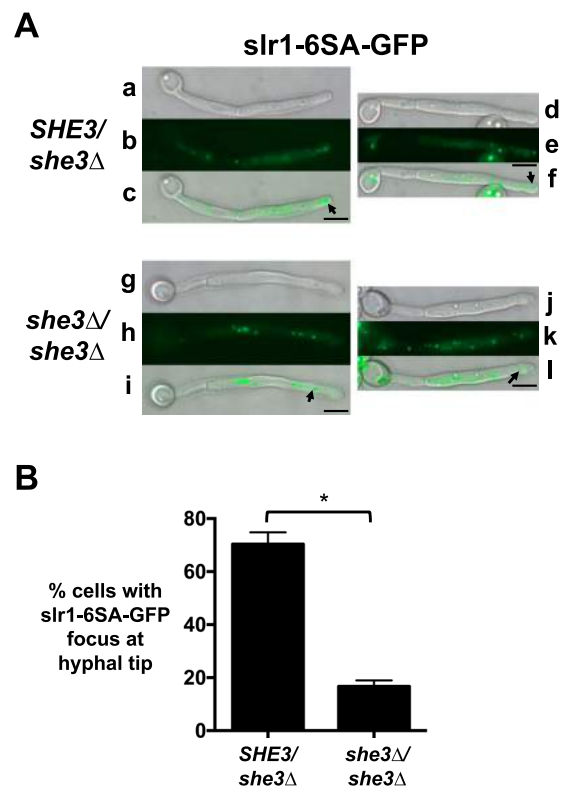
Fig. 10. Absence of RNA-binding protein She3 decreases slr1-6SA-GFP hyphal tip localization.
A. *Deletion of SHE3 decreases hyphal tip localization of slr1-6SA-GFP.* Cells expressing slr1-6SA-GFP in the presence (*slr1-6SA-GFP/SLR1 SHE3/she3Δ*) and absence (*slr1-6SA-GFP/SLR1 she3Δ/she3Δ*) of She3 were grown and visualized as in Fig. 8. Arrows indicate the most distal slr1-6SA-GFP focus in each hypha. Scale bar = 5 μm.
B. *Quantification of slr1-6SA-GFP hyphal tip localization.* Cells containing distal GFP foci either within 2 μm of the hyphal tip or farther than 2 μm from the hyphal tip were counted ($\geq$ 65 cells per strain). Percentages of cells with slr1-6SA-GFP at the hyphal tip were significantly different between the two strains (*$p < 0.0001$; student's *t*-test). Mean values from three independent trials and standard error of the mean are shown.

binding protein families: the Npl3/Srp2 proteins, which are essential in *S. cerevisiae* and *S. pombe*, and SpSrp1-like proteins, which have not previously been identified in the Saccharomycetale lineage (Plass *et al.*, 2008).

Fungal SR-like protein divergence

Comparison of the primary sequence of Slr1 to other fungal proteins revealed that whereas the C-terminal arginine-rich domain is most similar to Ascomycete Npl3-like proteins, the N-terminal RNA-recognition motif is homologous to that of SpSrp1 (Fig. 1). BLAST searches with the single RRM of SpSrp1 and Slr1 revealed the wider presence of potentially related proteins than initially suggested (Plass *et al.*, 2008; Supporting Information Fig. S1). The absence of the identification of these putative SpSrp1 homologs in previous work may be due in part to the divergence within a peptide found in SR proteins that overlaps with RNP-1 (Fig. 1B; Supporting Information Fig. S1; Birney *et al.*, 1993). The conservation of the 5′ splice site among the intron-containing *SRP1* homologs (after the second nucleotide of the codon for the underlined residue in Fig. 1B), however, supports an evolutionary relationship among these genes.

SR-like protein modification and localization

Although the predominance of RG dipeptides in the Slr1 arginine-rich C-terminal domain more closely resembles ScNpl3 than SpSrp1, the clustering of SR/RS dipeptides in C-terminal 20 amino acids of Slr1 (Fig. 1C) is more similar to SpSrp1 and many metazoan SR proteins (Wilson-Grady *et al.*, 2008). This clustering of SR/RS dipeptides in Slr1 raises the question of whether the regulation of Slr1 by phosphorylation may be more similar to that of SpSrp1 family proteins than that of ScNpl3. Phosphatase treatment of Slr1-GFP and slr1-6SA-GFP indicated that Slr1 is likely phosphorylated at multiple sites within the SR region (Fig. 4A). Phosphorylation of one or more residues may control additional phosphorylation events, as seen in the sequential phosphorylation of serine residues in human SR protein ASF/SF2 (Ngo *et al.*, 2008). Whereas wildtype Slr1-GFP is predominantly nuclear, the S-to-A substitutions increase cytoplasmic levels of Slr1-GFP, suggesting that phosphorylation promotes import of Slr1 (Fig. 5), potentially by facilitating interaction with a conserved Mtr10 import receptor complex, as seen for *S. cerevisiae* Npl3 (Yun and Fu, 2000). Phosphorylation of the SR domain of multiple metazoan SR proteins similarly allows binding to the importin transportin-SR (Lai *et al.*, 2000). The cytoplasmic localization of slr1-6SA-GFP in *C. albicans* decreases in the absence of arginine methyltransferase Hmt1 (Fig. 5), supporting a role for methylation in nuclear export of Slr1, as seen for ScNpl3 and CaNpl3 (Shen *et al.*, 1998; McBride *et al.*, 2007). Therefore, the impact of post-translational modification on Slr1 nucleo-cytoplasmic transport is more similar to the effects of modifications on Npl3 family proteins than on SpSrp1, correlating with greater similarity of the Npl3 and Slr1 R-rich domains rather than with the clustered arrangement of SR/RS motifs.

Interestingly, subcellular localization of slr1-6SA-GFP was also detected in cytoplasmic foci in both budding and hyphal cells, including near the bud neck and hyphal tip. These foci could reflect increased interaction of cytoplasmic unphosphorylated slr1-6SA-GFP with ribonucleoprotein complexes in subcellular domains such as RNA-processing bodies (P-bodies), stress granules (Buchan and Parker, 2009), or target regions for mRNA transport. P-bodies accumulate during *C. albicans* hyphal induction (Jung and Kim, 2011), but they are not specifically detected at the hyphal tip; the less intense slr1-6SA-GFP foci present throughout the hypha (e.g., Fig. 10A) may indicate association of slr1-6SA-GFP with these RNA-rich cytoplasmic regions. Lack of phosphorylation of an SR motif in the severe acute respiratory syndrome coronavirus (SARS CoV) nucleocapsid protein has been implicated in accumulation of this viral SR protein in stress granules (Peng *et al.*, 2008). The localization of slr1-6SA-GFP to cytoplasmic foci suggests that phosphorylation may prevent accumulation of this SR-like protein in similar mRNA-rich structures.

We hypothesize that Slr1 may aid in transport of mRNAs in *C. albicans* and that its phosphorylation may promote its dissociation from mRNP complexes in distinct cytoplasmic sites such as the bud neck and the hyphal tip. In *S. cerevisiae*, the absence of the kinase ScSky1 or the presence of an S-to-A mutation in ScNpl3 increases the binding of ScNpl3 to poly(A) RNA, indicating a role for phosphorylation in promoting cytoplasmic mRNA release as well as in nuclear ScNpl3 import (Gilbert *et al.*, 2001). CaShe3 is the primary *C. albicans* protein known to facilitate mRNA transport to the hypha (Elson *et al.*, 2009); this fungus lacks an ortholog of ScShe2, a key mRNA-binding protein in *S. cerevisiae* that couples nuclear export of *ASH1* mRNA to formation of the She3 mRNA transport complex in the cytoplasm (Bohl *et al.*, 2000). While slr1-6SA-GFP still forms cytoplasmic foci in hyphal cells lacking CaShe3, the absence of CaShe3 reduces the number of cells with foci at the hyphal tip (Fig. 10). This result suggests that slr1-6SA-GFP may travel with CaShe3 mRNA transport complexes to the hyphal tip.

The localization of the slr1-6SA-GFP focus at the hyphal tip is remarkably similar to that of the Spitzenkörper, a vesicular structure found in filamentous fungi thought to aid in transport of proteins and lipids to and from the hyphal tip (Riquelme, 2013). FM4-64 staining of the Spitzenkörper in strains expressing slr1-6SA-GFP indicated that these two structures partially overlap (Fig. 9A; Supporting Information Fig. S4). Sudbery and colleagues recently demonstrated that the *C. albicans* Sec2 protein, a Guanine Exchange Factor involved in vesicular transport to the hyphal tip, binds to the Sec2 mRNA and that wildtype Sec2 mRNA and protein colocalize in the Spitzenkörper (Caballero-Lima *et al.*, 2014). A phosphomimetic mutation in Sec2 decreases Sec2 protein binding to and colocalization with Sec2 mRNA in the Spitzenkörper (Caballero-Lima *et al.*, 2014). These results support a model in which phosphorylation of Sec2 helps regulate Sec2 mRNA transport to the hyphal tip (Caballero-Lima *et al.*, 2014). Phosphorylation of She3, Khd1 and Puf6 RNA-binding proteins in *S. cerevisiae* has also been linked to polarized *ASH1* mRNA transport and translation regulation (Paquin *et al.*, 2007; Deng *et al.*, 2008; Landers *et al.*, 2009). The colocalization of slr1-6SA-GFP with the Spitzenkörper suggests both that mRNA-binding proteins in addition to Sec2 and She3 could influence transport of mRNAs to the hyphal tip and that such mRNP complexes could be regulated similarly by phosphorylation of RNA-binding proteins including Slr1.

SR-like protein function

SR proteins have been implicated in many steps of mRNA metabolism, from linking transcription to splicing, controlling constitutive and alternative splicing, and directing mRNA nuclear export to affecting mRNA turnover and translation in the cytoplasm (Long and Caceres, 2009; Shepard and Hertel, 2009; Zhong *et al.*, 2009). The RNA-dependent interaction of Slr1 with the nuclear mRNA cap-binding complex, which affects mRNA splicing, transport, stability and translation in *S. cerevisiae* (Topisirovic *et al.*, 2011; Garre *et al.*, 2012), suggests that Slr1 may also have complex roles in *Candida* RNA metabolism. The cytoplasmic localization of bulk mRNA in *slr1Δ/Δ* cells indicates that Slr1 is not crucial for bulk mRNA transport (Fig. 6), yet the co-fractionation of wildtype Slr1-GFP with 80S and translating ribosomes on sucrose-density gradients (Fig. 7) suggests that Slr1 may have a cytoplasmic role in translation. In addition, the localization of slr1-6SA-GFP raises the question whether Slr1 might also function in mRNA transport to the bud neck (Fig. 5) or hyphal tip (Figs. 8–10).

Although deletion of *SLR1* in *C. albicans*, like the C-terminal truncation of its ortholog *SwoK* in *Aspergillus nidulans*, causes defects in polarized growth of these filamenting fungi (Shaw and Upadhyay, 2005; Ariyachet *et al.*, 2013), the six S-to-A substitutions in Slr1 do not disrupt its critical functions. Yeast cells expressing mutant and wildtype Slr1-GFP proteins have similar growth rates and the slr1-6SA-GFP mutant cells can form hyphae. These results, combined with the presence of low levels of slr1-6SA-GFP in hyphal nuclei, are consistent with a model in which Slr1 shuttles between the nucleus and the hyphal tip and Slr1 phosphorylation facilitates, but is not absolutely required for, release of mRNAs at the hyphal tip.

In conclusion, the unphosphorylated slr1-6SA protein is the first *C. albicans* protein with a defined RNA-binding domain to be found at the hyphal tip and this localization depends on the known mRNA transport protein CaShe3. The importance of Slr1 for hyphal formation and function may therefore be due in part to Slr1 having a role in hyphal mRNA transport. For example, in the absence of a *C. albicans* She2 ortholog, Slr1 might link export of mRNAs required at the hyphal tip to cytoplasmic She3 mRNP formation. The slr1-6SA mutant protein will serve as a particularly useful tool for future studies to identify the protein and mRNA components of ribonucleoprotein complexes that could impact hyphal growth and function.

Experimental procedures

C. albicans *strains and growth conditions*

Genotypes and important features of the strains, plasmids and oligonucleotides used in this study are described in Supporting Information Tables S1, S2 and S3 respectively. Most *C. albicans* strains in this study were derived from the arginine-, histidine-, uridine-auxotrophic strain BWP17 (Wilson *et al.*, 1999). The other uridine-auxotrophic parental strains with *SHE3* deletions are described in (Elson *et al.*, 2009). All oligonucleotides were synthesized at Integrated DNA Technologies. Strain construction is described in detail in Supporting Information.

C. albicans strains were grown in YPD medium (1% yeast extract, 2% bactopeptone, 2% glucose) supplemented with 80 μg ml^{-1} uridine (Uri) or in synthetic dropout media with 2% glucose and lacking the appropriate nutrients to select for integrated markers. Generation times for strains expressing wildtype *SLR1-GFP* or *slr1-6SA-GFP* as the sole copy of *SLR1* (11 replicate cultures per strain) were calculated from 24 h growth curves as described in (Ariyachet *et al.*, 2013). For optimal filamentation in broth cultures, strains were grown overnight in YPD + Uri, diluted to 3×10^6 cells ml^{-1} into pre-warmed HEPES-buffered RPMI 1640 (Life Technologies) and incubated at 37°C with shaking for 3 h.

SR-like protein sequence analysis

A BLASTP search with amino acids 5–51 of Slr1, representing the core of the RNA-recognition motif from RNP-2 through RNP-1 (Birney *et al.*, 1993), identified proteins similar to Slr1 in many fungi. The following sequences were used to align the RRMs of twelve of these representative fungal SR-like proteins: XP_002553256.1 (*L. thermotolerans*), XP_452519.1 (*K. lactis*), NP_985205.1 (*A. gossypii*), XP_500797.1 (*Y. lipolytica*), CAA22007.1 (*C. albicans*), XP_459563.2 (*D. hansenii*), XP_956575.2 (*N. crassa*), XP_663406.1 (*A. nidulans*), NP_596398.1 (*S. pombe* Srp1), XP_758616.1 (*U. maydis*) and XP_001731715.1 (*M. globosa*). A BLASTP search of the *L. kluyveri* genome also revealed a similar protein encoded by SAKL0H05192 (http://www.genolevures.org/blast.html). RNA-recognition motifs were identified using an InterProScan sequence search (HMMPfam, PF00076; http://www.ebi.ac.uk/Tools/pfa/iprscan/; Zdobnov and Apweiler, 2001) and aligned using Clustalw2 (http://www.ebi.ac.uk/Tools/msa/clustalw2/; Larkin *et al.*, 2007; Goujon *et al.*, 2010). Given the shorter length of other predicted Slr1-like RRMs, up to 5 residues were removed from the C-terminus of the predicted RRM domains of *M. globosa*, *U. maydis*, *A. nidulans*, *N. crassa* and *K. lactis* Slr1-like proteins in the alignments shown in Fig. 1B and Supporting Information Fig. S1.

Testing Slr1 R-rich domain function in S. cerevisiae Npl3

To study the functional similarity between ScNpl3 and Slr1, the R-rich domain (codons I279-R402) of ScNpl3 with or without the C-terminal heptapeptide (codons T403-R414) was replaced with that of Slr1. To take advantage of the high level of homologous recombination in *S. cerevisiae* to construct these hybrid plasmids, the coding region for the R-rich domain of Slr1 was amplified from BWP17 genomic DNA using AM322/AM323 (codons Q90-G233, lacking the Slr1 C-terminus) or oligos AM322/AM324 (codons Q90-Y263, including the Slr1 C-terminus). Each fragment was co-transformed into wildtype *S. cerevisiae* strain FY23 with ApaI/NsiI-cut pAM463 (*PrA-ScNPL3-ApaI*) (McBride *et al.*, 2007) and plasmids were rescued from Leu$^+$ cells. Resulting plasmids pAM471 (encoding ScNpl3 with the Slr1 R-rich domain and the ScNpl3 C-terminus) and pAM472 (encoding ScNpl3 with the Slr1 R-rich domain and Slr1 C-terminus) were sequenced at Geneway Research to ensure proper fusion.

To monitor the ability of the Slr1 C-terminus to support *S. cerevisiae* Npl3 function, plasmids encoding chimeric ScNpl3 proteins fused to Protein A, or the *PrA LEU2* vector pNOPPATA (Hellmuth *et al.*, 1998), were transformed into an *S. cerevisiae* npl3Δ strain bearing a wildtype *NPL3 URA3* plasmid (PSY814; *npl3Δ::HIS3 ade2 ade8 can1 ura3 leu2 his3 lys1 trp1+ YCp50-NPL3-3 MATa* (Henry *et al.*, 1996)). The ability of transformed cells to lose the *ScNPL3* plasmid was detected on plates containing 5-fluoro-orotic acid as previously described (McBride *et al.*, 2007).

Cell lysis for protein expression and purification

C. albicans cells were grown to mid-log phase at 30°C. Cells were harvested and resuspended in minimal lysis buffer. All lysis buffers contained protease inhibitors: phenylmethylsulfonyl fluoride (1 mM), pepstatin, leupeptin, aprotinin, antipain and chymostatin (2.5 μg ml^{-1} each). Lysis buffers included: RIPA buffer (radio immunoprecipitation assay buffer: 50 mM Tris-HCl (pH 8), 50 mM NaCl, 1% Triton X-100, 0.1% sodium dodecyl sulfate (SDS), 0.5% sodium deoxycholate); phosphate-buffered saline (PBS) with 2.5 mM MgCl$_2$, 3 mM KCl and 0.5% or 1% Triton X-100 (PBSMT$_{0.5\%}$ or PBSMT$_{1\%}$), TAP lysis buffer (150 mM potassium acetate, pH 7.4, 20 mM HEPES-KOH pH 7.4, 2 mM magnesium acetate, 1 mM EDTA, pH 8.0, 1 mM EGTA, pH 8.0, 0.5% or 1% Triton X-100, 2 mM dithiothreitol, 1 mM PMSF and one mini EDTA-free protease inhibitor cocktail tablet (Roche) per 50 ml; Blackwell and Brown, 2009) and UV-crosslinking lysis buffer [ULB: 20 mM Tris pH 7.5, 50 mM LiCl, 1% SDS, 1 mM EDTA, 1% ß-mercaptoethanol, 1 mg ml^{-1} heparin (Sigma-Aldrich), 20 mM ribonucleoside vanadyl complexes (New England Biolabs)]. Cells were lysed with glass beads using a Fast-Prep FP120 (Thermo Savant) cell disruptor at 4°C (speed 6.5 for 30 s for all experiments except phosphatase treatment, which used 4 cycles of 4 s disruption), then mixed with additional lysis buffer. Crude lysate was obtained by centrifugation at 16,000*g* for 10 min at 4°C, and supernatants were clarified with an additional round of centrifugation under the same conditions.

Poly(A) RNA binding assay

To test whether Slr1 binds to polyadenylated mRNA, a UV crosslinking assay developed to detect mRNA-binding proteins in *S. cerevisiae* (Marfatia *et al.*, 2003) was adapted for *C. albicans*. Briefly, Slr1-TAP-expressing cells (*SLR1-TAP/slr1Δ*; AMC94) were grown to mid-log phase in 1 L YPD, washed and irradiated in a petri dish on ice with UV light in a Stratalinker 2400. Following lysis in ULB as described above, clarified lysates were adjusted to 0.5 M LiCl and bound to oligo (dT) cellulose resin (GE Healthcare) for 2 h at 4°C. After washing, oligo (dT)-bound complexes were eluted and subjected to a second round of purification. To collect RNA–protein complexes, eluates were concentrated and precipitated prior to resuspension in RSB buffer (10 mM Tris, pH 7.4, 100 mM NaCl, 2.5 mM MgCl$_2$, 1 mM CaCl$_2$) with protease inhibitors. Following RNA digestion, the presence of Slr1-TAP in oligo (dT)-bound material was analyzed by immunoblotting with a horseradish peroxidase-conjugated anti-Protein A (PrA) antibody. Detailed methods are available in Supporting Information.

Identification of Slr1-interacting proteins

To detect Slr1-interacting proteins, *SLR1-TAP/slr1Δ* (AMC94) and *SLR1/slr1Δ* (AMC91) cells were grown in 300 ml YPD + Uri to OD$_{600}$ ∼ 2. Cells were lysed with glass beads in TAP lysis buffer as described above. Slr1-TAP and interacting proteins were precipitated with immunoglobulin G (IgG)-Sepharose (Pharmacia) at 4°C overnight, washed four times in TAP lysis buffer with 1% Triton X-100 and 0, 0.5, 1 and 1.25 M potassium acetate, respectively, eluted with tobacco etch virus (TEV) protease (Invitrogen)

(Blackwell and Brown, 2009), precipitated with trichloroacetic acid, and analyzed by SDS-10% PAGE and blue silver (Candiano *et al.*, 2004) or zinc staining (Bio-Rad). Protein bands that were not precipitated from the untagged strain were excised from the blue-silver stained gel for protein identification by mass spectrometry at The University of Texas Health Science Center at San Antonio.

To detect interactions with GFP-tagged nuclear mRNA cap-binding complex (CBC) proteins Cbc1 and Cbc2, *orf19.387-GFP/ORF19.387   SLR1-TAP/slr1Δ* (Cbc1-GFP; AMC108) and *orf19.763-GFP/ORF19.763   SLR1-TAP/slr1Δ* (Cbc2-GFP; AMC109) cells were grown in 50 ml YPD to $OD_{600} = 1–2$ and lysed in TAP lysis buffer with 1% Triton X-100 before IgG bead precipitation as described above. Following washing, Slr1-TAP and interacting proteins were eluted with 3 M $MgCl_2$, precipitated with trichloroacetic acid, and co-precipitation of CBC proteins with Slr1-TAP analyzed by anti-GFP immunoblotting. For the RNase sensitivity experiment, lysates were pretreated with 10 μg ml^{-1} RNase A (Sigma-Aldrich) for 15 min at 25°C. To test for background binding of Cbc1-GFP and Cbc2-GFP to the beads, *orf19.387-GFP/ORF19.387 SLR1/slr1Δ* (Cbc1-GFP; AMC106)   and   *orf19.763-GFP/ORF19.763   SLR1/slr1Δ* (Cbc2-GFP; AMC107) cells were employed for the pulldown experiment.

Phosphatase treatment

Cells expressing Slr1-GFP (*SLR1-GFP/slr1Δ;* AMC96) and slr1-6SA-GFP (*slr1-6SA-GFP/slr1Δ;* AMC99) as the sole copy of Slr1 were grown to mid-log phase in medium lacking uridine at 30°C. Cells were lysed with glass beads in minimal RIPA buffer prior to resuspension in PBSMT$_{0.5\%}$ buffer, as described above. Lysates (12 mg) were incubated with 4 μg anti-GFP (Roche Diagnostics) for 1 h at 4°C. GFP fusion proteins were precipitated with 40 μl Protein G PLUS-Agarose beads (Santa Cruz Biotechnology) by overnight incubation at 4°C. Beads were washed four times with PBSMT$_{0.5\%}$ and divided into three aliquots, each resuspended in 50 μl NEB3 buffer. For each strain, one aliquot was incubated with 5 U calf intestinal phosphatase (New England Biolabs) at 37°C, and two controls were incubated without phosphatase at 0°C or 37°C. All samples were incubated for 60 min with agitation every 10 min. Slr1-GFP proteins were eluted by boiling in SDS-PAGE sample buffer. Purified proteins were resolved by SDS-8% PAGE and analyzed by immunoblotting.

Identification of major arginine-methylated proteins in C. albicans

Major arginine methylated proteins in *Candida albicans* were identified by immunoprecipitation with an anti-dimethylarginine antibody. Cells from YPD cultures of *hmt1Δ/Δ* (AMC11), *hmt1Δ/Δ + HMT1* (AMC14) and *npl3Δ/Δ* (AMC18) grown at 30°C to mid-log phase were lysed in PBSMT$_{1\%}$ as described above. Lysates (5 mg total protein) were incubated with 25 μl anti-methylarginine antibody (Ab412; Abcam) overnight with rotation at 4°C. Protein G beads (40 μl packed volume; GE Lifesciences) were added

to each lysate prior to 4 h incubation at 4°C with rotation. Beads were washed with PBSMT$_{0.5\%}$ extensively prior to addition of protein sample buffer. Proteins isolated from 3 mg total protein were resolved by SDS-12% PAGE and visualized by Coomassie staining. Major proteins not detected in cell lysates lacking the arginine methyltransferase were identified by mass spectrometry at the University of Texas San Antonio Health Sciences Center.

To confirm Slr1 methylation, mid-log-phase wildtype and *hmt1Δ/Δ* cells expressing Slr1-GFP (AMC85 and AMC86) were lysed in PBSMT$_{0.5\%}$ as described above. Slr1-GFP was precipitated from lysates (2.7 mg total protein) by incubation with 5 μl of monoclonal α-GFP antibody (Roche Life Sciences) followed by protein G-agarose incubation as above. The beads were washed in lysis buffer, and bound proteins eluted in SDS-PAGE sample buffer, resolved by SDS-10% PAGE and analyzed by immunoblotting.

Immunoblot analysis

GFP-tagged proteins were recognized with a monoclonal α-GFP antibody (Roche; 1:1000) and arginine methylation was recognized with a monoclonal α-mono and dimethyl arginine antibody (Ab412, Abcam; 1:500), followed by a secondary α-mouse-horseradish peroxidase (HRP) antibody (GE Lifesciences; 1:5000). Slr1-TAP was recognized with an HRP-conjugated goat anti-Protein A (PrA) antiserum (Rockland; 1:10,000). Ribosomal protein Rps3 was recognized with a polyclonal rabbit antibody against Rps3 (1:1000). Proteins were visualized through enhanced chemiluminescence (Pierce) and autoradiography.

Anti-rabbit IgG (H + L)-HRPO and anti-mouse IgG (H + L) HRPO (Dianova) secondary antibodies were used for sucrose density gradient fraction immunoblots. The signals were detected with Amersham ECL Prime Western Blotting Detection Reagent (GE Healthcare) and the FUSION-SL chemiluminescence detection system (Peqlab) and the Western blot analyses were quantified using the Image StudioLite software (LI-COR).

Fluorescence microscopy

To visualize wildtype and mutant Slr1-GFP proteins in yeast-form cells, cells were grown to log phase in synthetic minimal medium lacking uridine (Uri$^-$) at 30°C. Cells were washed with PBS and subsequently incubated with 10 μg ml^{-1} DAPI (4′,6-diamidono-2-phenylindole; Molecular Probes) in PBS for 4 min at 30°C. Cells were washed with Uri$^-$ medium and visualized by Nomarski (differential interference contrast, DIC) and widefield epifluorescence microscopy (Olympus BX51: 100× objective, GFP and DAPI filters). Images were captured with an EvolutionVF color digital camera (noncooled, 12-bit; MediaCybernetics) and QCapture Pro 5.0 software. Exposure times were the same for cells of all genotypes in the same experiment.

To visualize Slr1-GFP in filamenting cells, cells were collected by centrifugation after 3 h growth in RPMI at 37°C, washed with PBS and visualized on agarose-coated slides. To test for nuclear localization of wildtype and mutant Slr1-GFP proteins in hyphal cells, cells were incubated for 1 min

in 10 µg ml^{-1} DAPI in PBS prior to visualization. To determine whether slr1-6SA-GFP colocalized with the Spitzenkörper, after 3 h of hyphal induction in RPMI, FM4-64 was added to *slr1-6SA-GFP/slr1Δ* (AMC99) and *MLC1-YFP/MLC1* (YJB7139) cells to a final concentration of 0.25 µg ml^{-1} and cultures incubated at 37°C for 4 min. Cells were rapidly collected by centrifugation, washed in PBS at 37°C and visualized immediately to allow detection of FM4-64 in the Spitzenkörper. A Texas Red filter was used to detect FM4-64 and a GFP filter was used to detect slr1-6SA-GFP and Mlc1-YFP. Colocalization of the Spitzenkörper and GFP/YFP proteins was determined by stacking the FM4-64 and GFP/YFP images in ImageJ v1.49 (Schneider *et al.*, 2012), selecting the hyphal tip foci and noting overlap of selections between red and green images. Given the transitory nature of Spitzenkörper staining with FM4-64, in one experiment 64–66 cells with distinct Spitzenkörper staining were analyzed and in additional experiments at least such 20 cells were analyzed. Line scans of FM4-64, slr1-6SA-GFP and Mlc1-YFP focal fluorescence that demonstrate partial colocalization of proteins with the Spitzenkörper at the hyphal tip are included in Supporting Information Fig. S4.

Fluorescence image analysis

To quantify subcellular localization of Slr1-GFP proteins, the brightness/contrast levels of all DAPI images were first adjusted equivalently in Adobe Photoshop CS5 to lower background cytoplasmic fluorescence. GFP, DAPI and DIC images were then stacked in ImageJ v1.49 (Schneider *et al.*, 2012) and cells with in-focus nuclei were identified. The method of Hood-DeGrenier (Hood-DeGrenier *et al.*, 2007) was modified to calculate two metrics of subcellular localization: percent nuclear fluorescence intensity (%N) and mean nuclear-to-cytoplasmic fluorescence intensity (N/C). For each cell, the whole cell and the nucleus were selected on DIC and DAPI images, respectively, and area and average pixel intensity (API) were measured for each selection on the GFP image. Selection was performed in triplicates for each cell using a Wacom Cintiq 13HD touch tablet; the mean of the three area and API measurements was used for subsequent calculations. For each image, the API of background regions lacking cells was subtracted from the whole-cell and nuclear API measurements. The total nuclear and whole cell pixel intensities (TPI$_N$ and TPI$_{WC}$) were calculated by multiplying the average area (A) by the background-adjusted API. Percent nuclear fluorescence (%N) was calculated by dividing TPI$_N$ by TPI$_{WC}$. The ratio of the API of the nucleus to the API of the cytoplasm (N/C) was calculated as follows: N/C = API$_N$/[(TPI$_{WC}$ − TPI$_N$)/(A$_{WC}$ − A$_N$)]. Three independent experiments were performed for each set of strains and the data analyzed in R (R Core Team, 2016). Differences among cells of different genotypes in a single experiment were evaluated by the Kruskal-Wallis rank sum test ($p < 0.0001$ for all experiments), given the non-normal distribution of the data. Pairwise Mann–Whitney–Wilcoxon tests with Bonferroni correction for multiple comparisons were then used to determine whether the localization of specific Slr1-GFP proteins differed from each other. Box plots were generated with GraphPad

Prism 7.0 software. The presence of slr1-6SA-GFP foci at the bud neck of post-mitotic cells was quantified in three trials (> 55 post-mitotic cells per genotype).

To quantify localization of slr1-6SA to the hyphal tip in cells with and without She3, two independent cultures each of *she3Δ/SHE3 slr1-6SA-GFP/SLR1* (AMC138) and *she3Δ/she3Δ slr1-6SA-GFP/SLR1* (AMC139) were induced to filament in RPMI and prepared for microscopy as above. GFP and DIC images were overlaid and hyphal cells were divided into two categories: cells with the most distal slr1-6SA-GFP focus (a) within 2 µm (one hyphal width) of the hyphal tip or (b) farther than 2 µm from the tip. Exposure times were equivalent for all strains in a single experiment and images were overlaid using Adobe Photoshop CS5. At least 65 hyphal cells of each genotype were analyzed in three independent trials. Differences in hyphal tip localization of slr1-6SA-GFP between cells with and without She3 were evaluated by an unpaired student's *t*-test.

Fluorescence in situ *mRNA hybridization*

A protocol to detect localization of bulk mRNA in *S. cerevisiae* was adapted for use in *C. albicans* cells (Green *et al.*, 2002). Wildtype (AMC79) and *slr1Δ/Δ* (AMC89) cells were collected from 1 mL synthetic dropout culture (OD$_{600}$ ∼ 0.2) grown at 30 or 37°C. For heat shock, cells were grown at 30°C to ∼ 0.2 OD$_{600}$ and shifted to 42°C for 30 min. Cells were then fixed in 5% formaldehyde for 1 h, washed twice in P solution (1.2 M sorbitol in 0.1 M potassium phosphate buffer, pH 6.8), and resuspended in 1 ml P solution. Cells from 20 µl suspension were placed on a multiwell slide coated with 0.1% poly-L-lysine (Sigma-Aldrich), spheroplasted in P solution containing 500 µg ml^{-1} Zymolyase (100T, US Biological) and 1% β-mercaptoethanol, permeabilized by addition of 0.5% Triton X-100 in P solution for 10 min, equilibrated with 0.1 M triethanolamine (pH 8.0), and polar groups blocked with 0.25% acetic anhydride. Cells were incubated in prehybridization buffer (1 mg ml^{-1} yeast tRNA (Sigma-Aldrich), 0.005% BSA, 10% dextran sulfate, 25% deionized formamide and 2× SSC) and hybridized overnight with 250 nM digoxigenin-labeled oligo(dT) probe (IDT). Cells were washed with 2× and 4× SSC, incubated with FITC-conjugated anti-digoxigenin antibody (Roche; 1:200 dilution in 2× SSC) at room temperature for 1–2 h, and briefly stained with DAPI and washed with 2× SSC. Cells were examined by Nomarski (DIC) and fluorescence microscopy as described above.

Sucrose-density fractionation experiments

The preparation and fractionation of sucrose-density gradients was carried out in three replicate experiments following published protocols for *S. cerevisiae*, modified for use with *C. albicans* (Gross *et al.*, 2007; Baierlein *et al.*, 2013). Briefly, 300 ml *SLR1-GFP/slr1Δ* (AMC96) yeast cell cultures were grown to log phase in YPD at 30°C. Cycloheximide (Sigma-Aldrich) was added to a final concentration of 100 µg ml^{-1} and cells were incubated for 15 min on ice. After harvesting, the cell pellets were lysed with the same amount of glass beads in lysis buffer (20 mM HEPES-KOH

pH7.5, 10 mM KCl, 2.5 mM $MgCl_2$, 1 mM EGTA, 1 mM DTT, 100 μg ml^{-1} cycloheximide) supplemented with Complete, EDTA-free protease inhibitor cocktail (Roche). Cells were lysed with 5 cycles of 1.5 min in a BeadBeater (Biospec) followed by 2 min on ice. The lysates were centrifuged at 4°C once for 5 min at 16,000g and the supernatant cleared by additional centrifugation for 10 min at 16,000g. If indicated, the lysates were treated with 0.25 mg ml^{-1} RNase A (AppliChem) for 20 min on ice. For protein and ribosomal profile analyses 30 $OD_{260\ nm}$ units of lysates were loaded onto a linear 7%–47% (w/v) sucrose gradients (20 mM HEPES-KOH pH 7.5, 10 mM KCl, 2.5 mM $MgCl_2$, 1 mM EGTA) poured with the Gradient Master machine (Biocomp) and centrifuged for 3 h at 40,000 rpm and 4°C in a TH-641 rotor and Sorvall WX80 ultracentrifuge (Thermo Scientific). The gradients were fractionated with a density-gradient fractionator (Teledyne Isco) while the absorbance at 254 nm was documented.

Protein fractions were precipitated with 10% trichloroacetic acid (TCA), washed two times with 70% acetone and subjected to SDS-PAGE and Western blotting. To be able to load the whole gradient on one gel and to increase the signal strength, some fractions were pooled as indicated.

Acknowledgements

Author contributions

C.A. and A.M. made major contributions to the conception and design of this study. C.A., A.M., C.B., X.L., S.L., O.M., P.M., K.O., T.P., S.S. and H.K. contributed to the acquisition, analysis and interpretation of the data. A.M., C.A., C.B. and X.L. contributed to the writing of the manuscript.

References

Ariyachet, C., Solis, N.V., Liu, Y., Prasadarao, N.V., Filler, S.G., and McBride, A.E. (2013) SR-like RNA-binding protein Slr1 affects *Candida albicans* filamentation and virulence. *Infect Immun* **81**: 1267–1276.

Baierlein, C., Hackmann, A., Gross, T., Henker, L., Hinz, F., and Krebber, H. (2013) Monosome formation during translation initiation requires the serine/arginine-rich protein Npl3. *Mol Cell Biol* **33**: 4811–4823.

Baker, B.S., Burtis, K., Goralski, T., Mattox, W., and Nagoshi, R. (1989) Molecular genetic aspects of sex determination in *Drosophila melanogaster*. *Genome* **31**: 638–645.

Becht, P., Vollmeister, E., and Feldbrugge, M. (2005) Role for RNA-binding proteins implicated in pathogenic development of *Ustilago maydis*. *Eukaryot Cell* **4**: 121–133.

Becht, P., Konig, J., and Feldbrugge, M. (2006) The RNA-binding protein Rrm4 is essential for polarity in *Ustilago maydis* and shuttles along microtubules. *J Cell Sci* **119**: 4964–4973.

Birney, E., Kumar, S., and Krainer, A.R. (1993) Analysis of the RNA-recognition motif and RS and RGG domains: conservation in metazoan pre-mRNA splicing factors. *Nucleic Acids Res* **21**: 5803–5816.

Blackwell, C., and Brown, J.D. (2009) The application of tandem-affinity purification to *Candida albicans*. *Methods Mol Biol* **499**: 133–148.

Bohl, F., Kruse, C., Frank, A., Ferring, D., and Jansen, R.P. (2000) She2p, a novel RNA-binding protein tethers *ASH1* mRNA to the Myo4p myosin motor via She3p. *Embo J* **19**: 5514–5524.

Bossie, M.A., DeHoratius, C., Barcelo, G., and Silver, P. (1992) A mutant nuclear protein with similarity to RNA-binding proteins interferes with nuclear import in yeast. *Mol Biol Cell* **3**: 875–893.

Bruno, V.M., Wang, Z., Marjani, S.L., Euskirchen, G.M., Martin, J., Sherlock, G., and Snyder, M. (2010) Comprehensive annotation of the transcriptome of the human fungal pathogen *Candida albicans* using RNA-seq. *Genome Res* **20**: 1451–1458.

Buchan, J.R., and Parker, R. (2009) Eukaryotic stress granules: the ins and outs of translation. *Mol Cell* **36**: 932–941.

Bucheli, M.E., and Buratowski, S. (2005) Npl3 is an antagonist of mRNA 3′ end formation by RNA polymerase II. *Embo J* **24**: 2150–2160.

Caballero-Lima, D., Hautbergue, G.M., Wilson, S.A., and Sudbery, P.E. (2014) In *Candida albicans* hyphae, Sec2p is physically associated with *SEC2* mRNA on secretory vesicles. *Mol Microbiol* **94**: 828–842.

Candiano, G., Bruschi, M., Musante, L., Santucci, L., Ghiggeri, G.M., Carnemolla, B., *et al.* (2004) Blue silver: a very sensitive colloidal Coomassie G-250 staining for proteome analysis. *Electrophoresis* **25**: 1327–1333.

Crampin, H., Finley, K., Gerami-Nejad, M., Court, H., Gale, C., Berman, J., and Sudbery, P. (2005) *Candida albicans* hyphae have a Spitzenkorper that is distinct from the polarisome found in yeast and pseudohyphae. *J Cell Sci* **118**: 2935–2947.

Dalle, F., Wachtler, B., L'ollivier, C., Holland, G., Bannert, N., Wilson, D., *et al.* (2010) Cellular interactions of *Candida albicans* with human oral epithelial cells and enterocytes. *Cell Microbiol* **12**: 248–271.

De Groot, P.W., Bader, O., de Boer, A.D., Weig, M., and Chauhan, N. (2013) Adhesins in human fungal pathogens: glue with plenty of stick. *Eukaryot Cell* **12**: 470–481.

Deng, Y., Singer, R.H., and Gu, W. (2008) Translation of *ASH1* mRNA is repressed by Puf6p-Fun12p/eIF5B interaction and released by CK2 phosphorylation. *Genes Dev* **22**: 1037–1050.

Dermody, J.L., Dreyfuss, J.M., Villen, J., Ogundipe, B., Gygi, S.P., Park, P.J., *et al.* (2008) Unphosphorylated SR-like protein Npl3 stimulates RNA polymerase II elongation. *PLoS One* **3**: e3273.

Elson, S.L., Noble, S.M., Solis, N.V., Filler, S.G., and Johnson, A.D. (2009) An RNA transport system in *Candida albicans* regulates hyphal morphology and invasive growth. *PLoS Genet* **5**: e1000664.

Filler, S.G., Swerdloff, J.N., Hobbs, C., and Luckett, P.M. (1995) Penetration and damage of endothelial cells by *Candida albicans*. *Infect Immun* **63**: 976–983.

Flach, J., Bossie, M., Vogel, J., Corbett, A., Jinks, T., Willins, D.A., and Silver, P.A. (1994) A yeast RNA-binding protein shuttles between the nucleus and the cytoplasm. *Mol Cell Biol* **14**: 8399–8407.

Garre, E., Romero-Santacreu, L., De Clercq, N., Blasco-Angulo, N., Sunnerhagen, P., and Alepuz, P. (2012) Yeast mRNA cap-binding protein Cbc1/Sto1 is necessary for the rapid reprogramming of translation after hyperosmotic shock. *Mol Biol Cell* **23**: 137–150.

Gilbert, W., Siebel, C.W., and Guthrie, C. (2001) Phosphorylation by Sky1p promotes Npl3p shuttling and mRNA dissociation. *rna* **7**: 302–313.

Goujon, M., McWilliam, H., Li, W., Valentin, F., Squizzato, S., Paern, J., and Lopez, R. (2010) A new bioinformatics analysis tools framework at EMBL-EBI. *Nucleic Acids Res* **38**: W695–W699.

Green, D.M., Marfatia, K.A., Crafton, E.B., Zhang, X., Cheng, X., and Corbett, A.H. (2002) Nab2p is required for poly(A) RNA export in *Saccharomyces cerevisiae* and is regulated by arginine methylation via Hmt1p. *J Biol Chem* **277**: 7752–7760.

Gross, T., Richert, K., Mierke, C., Lutzelberger, M., and Kaufer, N.F. (1998) Identification and characterization of srp1, a gene of fission yeast encoding a RNA binding domain and a RS domain typical of SR splicing factors. *Nucleic Acids Res* **26**: 505–511.

Gross, T., Siepmann, A., Sturm, D., Windgassen, M., Scarcelli, J.J., Seedorf, M., *et al.* (2007) The DEAD-box RNA helicase Dbp5 functions in translation termination. *Science* **315**: 646–649.

Gui, J.F., Lane, W.S., and Fu, X.D. (1994) A serine kinase regulates intracellular localization of splicing factors in the cell cycle. *Nature* **369**: 678–682.

Hacker, S., and Krebber, H. (2004) Differential export requirements for shuttling serine/arginine-type mRNA-binding proteins. *J Biol Chem* **279**: 5049–5052.

Hellmuth, K., Lau, D.M., Bischoff, F.R., Kunzler, M., Hurt, E., and Simos, G. (1998) Yeast Los1p has properties of an exportin-like nucleocytoplasmic transport factor for tRNA. *Mol Cell Biol* **18**: 6374–6386.

Henry, M.F., and Silver, P.A. (1996) A novel methyltransferase (Hmt1p) modifies poly(A)+-RNA-binding proteins. *Mol Cell Biol* **16**: 3668–3678.

Henry, M., Borland, C.Z., Bossie, M., and Silver, P.A. (1996) Potential RNA binding proteins in *Saccharomyces cerevisiae* identified as suppressors of temperature-sensitive mutations in *NPL3*. *Genetics* **142**: 103–115.

Hood-DeGrenier, J.K., Boulton, C.N., and Lyo, V. (2007) Cytoplasmic Clb2 is required for timely inactivation of the mitotic inhibitor Swe1 and normal bud morphogenesis in *Saccharomyces cerevisiae*. *Curr Genet* **51**: 1–18.

Jung, J.H., and Kim, J. (2011) Accumulation of P-bodies in *Candida albicans* under different stress and filamentous growth conditions. *Fungal Genet Biol* **48**: 1116–1123.

Kadosh, D., and Johnson, A.D. (2005) Induction of the *Candida albicans* filamentous growth program by relief of transcriptional repression: a genome-wide analysis. *Mol Biol Cell* **16**: 2903–2912.

Kadowaki, T., Chen, S., Hitomi, M., Jacobs, E., Kumagai, C., Liang, S., *et al.* (1994) Isolation and characterization of *Saccharomyces cerevisiae* mRNA transport-defective (*mtr*) mutants. *J Cell Biol* **126**: 649–659.

Kress, T.L., Krogan, N.J., and Guthrie, C. (2008) A single SR-like protein, Npl3, promotes pre-mRNA splicing in budding yeast. *Mol Cell* **32**: 727–734.

Lai, M.C., Lin, R.I., Huang, S.Y., Tsai, C.W., and Tarn, W.Y. (2000) A human importin-beta family protein, transportin-SR2, interacts with the phosphorylated RS domain of SR proteins. *J Biol Chem* **275**: 7950–7957.

Landers, S.M., Gallas, M.R., Little, J., and Long, R.M. (2009) She3p possesses a novel activity required for *ASH1* mRNA localization in *Saccharomyces cerevisiae*. *Eukaryot Cell* **8**: 1072–1083.

Larkin, M.A., Blackshields, G., Brown, N.P., Chenna, R., McGettigan, P.A., McWilliam, H., *et al.* (2007) Clustal W and Clustal X version 2.0. *Bioinformatics* **23**: 2947–2948.

Lasko, P. (2011) Posttranscriptional regulation in Drosophila oocytes and early embryos. *Wiley Interdiscip Rev RNA* **2**: 408–416.

Lee, M.S., Henry, M., and Silver, P.A. (1996) A protein that shuttles between the nucleus and the cytoplasm is an important mediator of RNA export. *Genes Dev* **10**: 1233–1246.

Lewis, J.D., Gorlich, D., and Mattaj, I.W. (1996) A yeast cap binding protein complex (yCBC) acts at an early step in pre-mRNA splicing. *Nucleic Acids Res* **24**: 3332–3336.

Lo, H.J., Kohler, J.R., DiDomenico, B., Loebenberg, D., Cacciapuoti, A., and Fink, G.R. (1997) Nonfilamentous *C. albicans* mutants are avirulent. *Cell* **90**: 939–949.

Long, J.C., and Caceres, J.F. (2009) The SR protein family of splicing factors: master regulators of gene expression. *Biochem J* **417**: 15–27.

Lutzelberger, M., Gross, T., and Kaufer, N.F. (1999) Srp2, an SR protein family member of fission yeast: *in vivo* characterization of its modular domains. *Nucleic Acids Res* **27**: 2618–2626.

Marfatia, K.A., Crafton, E.B., Green, D.M., and Corbett, A.H. (2003) Domain analysis of the *Saccharomyces cerevisiae* heterogeneous nuclear ribonucleoprotein, Nab2p. Dissecting the requirements for Nab2p-facilitated poly(A) RNA export. *J Biol Chem* **278**: 6731–6740.

McBride, A.E., Cook, J.T., Stemmler, E.A., Rutledge, K.L., McGrath, K.A., and Rubens, J.A. (2005) Arginine methylation of yeast mRNA-binding protein Npl3 directly affects its function, nuclear export, and intranuclear protein interactions. *J Biol Chem* **280**: 30888–30898.

McBride, A.E., Zurita-Lopez, C., Regis, A., Blum, E., Conboy, A., Elf, S., and Clarke, S. (2007) Protein arginine

methylation in *Candida albicans*: role in nuclear transport. *Eukaryot Cell* **6**: 1119–1129.

McBride, A.E., Conboy, A.K., Brown, S.P., Ariyachet, C., and Rutledge, K.L. (2009) Specific sequences within arginine-glycine-rich domains affect mRNA-binding protein function. *Nucleic Acids Res* **37**: 4322–4330.

Nantel, A., Dignard, D., Bachewich, C., Harcus, D., Marcil, A., Bouin, A.P., *et al.* (2002) Transcription profiling of *Candida albicans* cells undergoing the yeast-to-hyphal transition. *Mol Biol Cell* **13**: 3452–3465.

Ngo, J.C., Giang, K., Chakrabarti, S., Ma, C.T., Huynh, N., Hagopian, J.C., *et al.* (2008) A sliding docking interaction is essential for sequential and processive phosphorylation of an SR protein by SRPK1. *Mol Cell* **29**: 563–576.

Paquin, N., Menade, M., Poirier, G., Donato, D., Drouet, E., and Chartrand, P. (2007) Local activation of yeast *ASH1* mRNA translation through phosphorylation of Khd1p by the casein kinase Yck1p. *Mol Cell* **26**: 795–809.

Peng, T.Y., Lee, K.R., and Tarn, W.Y. (2008) Phosphorylation of the arginine/serine dipeptide-rich motif of the severe acute respiratory syndrome coronavirus nucleocapsid protein modulates its multimerization, translation inhibitory activity and cellular localization. *FEBS J* **275**: 4152–4163.

Plass, M., Agirre, E., Reyes, D., Camara, F., and Eyras, E. (2008) Co-evolution of the branch site and SR proteins in eukaryotes. *Trends Genet* **24**: 590–594.

R Core Team (2016) R: A language and environment for statistical computing. R Foundation for Statistical Computing, Vienna, Austria. URL: https://www.R-project.org/.

Riquelme, M. (2013) Tip growth in filamentous fungi: a road trip to the apex. *Annu Rev Microbiol* **67**: 587–609.

Saavedra, C., Tung, K.S., Amberg, D.C., Hopper, A.K., and Cole, C.N. (1996) Regulation of mRNA export in response to stress in *Saccharomyces cerevisiae*. *Genes Dev* **10**: 1608–1620.

Saville, S.P., Lazzell, A.L., Monteagudo, C., and Lopez-Ribot, J.L. (2003) Engineered control of cell morphology *in vivo* reveals distinct roles for yeast and filamentous forms of *Candida albicans* during infection. *Eukaryot Cell* **2**: 1053–1060.

Schaller, M., Borelli, C., Korting, H.C., and Hube, B. (2005) Hydrolytic enzymes as virulence factors of *Candida albicans*. *Mycoses* **48**: 365–377.

Schneider, C.A., Rasband, W.S., and Eliceiri, K.W. (2012) NIH Image to ImageJ: 25 years of image analysis. *Nat Methods* **9**: 671–675.

Sellam, A., Hogues, H., Askew, C., Tebbji, F., van Het Hoog, M., Lavoie, H., *et al.* (2010) Experimental annotation of the human pathogen *Candida albicans* coding and noncoding transcribed regions using high-resolution tiling arrays. *Genome Biol* **11**: R71.

Sen, S., Jumaa, H., and Webster, N.J. (2013) Splicing factor SRSF3 is crucial for hepatocyte differentiation and metabolic function. *Nat Commun* **4**: 1336.

Senger, B., Simos, G., Bischoff, F.R., Podtelejnikov, A., Mann, M., and Hurt, E. (1998) Mtr10p functions as a nuclear import receptor for the mRNA-binding protein Npl3p. *Embo J* **17**: 2196–2207.

Shaw, B.D., and Upadhyay, S. (2005) *Aspergillus nidulans swoK* encodes an RNA binding protein that is important for cell polarity. *Fungal Genet Biol* **42**: 862–872.

Shen, E.C., Henry, M.F., Weiss, V.H., Valentini, S.R., Silver, P.A., and Lee, M.S. (1998) Arginine methylation facilitates the nuclear export of hnRNP proteins. *Genes Dev* **12**: 679–691.

Shen, E.C., Stage-Zimmermann, T., Chui, P., and Silver, P.A. (2000) The yeast mRNA-binding protein Npl3p interacts with the cap-binding complex. *J Biol Chem* **275**: 23718–23724.

Shepard, P.J., and Hertel, K.J. (2009) The SR protein family. *Genome Biol* **10**: 242.

Shepard, K.A., Gerber, A.P., Jambhekar, A., Takizawa, P.A., Brown, P.O., Herschlag, D., *et al.* (2003) Widespread cytoplasmic mRNA transport in yeast: identification of 22 bud-localized transcripts using DNA microarray analysis. *Proc Natl Acad Sci U S A* **100**: 11429–11434.

Singleton, D.R., Chen, S., Hitomi, M., Kumagai, C., and Tartakoff, A.M. (1995) A yeast protein that bidirectionally affects nucleocytoplasmic transport. *J Cell Sci* **108**: 265–272.

Spingola, M., and Ares, M. Jr. (2000) A yeast intronic splicing enhancer and Nam8p are required for Mer1p-activated splicing. *Mol Cell* **6**: 329–338.

Tang, Z., Tsurumi, A., Alaei, S., Wilson, C., Chiu, C., Oya, J., and Ngo, B. (2007) Dsk1p kinase phosphorylates SR proteins and regulates their cellular localization in fission yeast. *Biochem J* **405**: 21–30.

Tani, T., Derby, R.J., Hiraoka, Y., and Spector, D.L. (1996) Nucleolar accumulation of poly (A)+ RNA in heat-shocked yeast cells: implication of nucleolar involvement in mRNA transport. *Mol Biol Cell* **7**: 173–192.

Thandapani, P., O'connor, T.R., Bailey, T.L., and Richard, S. (2013) Defining the RGG/RG motif. *Mol Cell* **50**: 613–623.

Topisirovic, I., Svitkin, Y.V., Sonenberg, N., and Shatkin, A.J. (2011) Cap and cap-binding proteins in the control of gene expression. *Wiley Interdiscip Rev RNA* **2**: 277–298.

Vida, T.A., and Emr, S.D. (1995) A new vital stain for visualizing vacuolar membrane dynamics and endocytosis in yeast. *J Cell Biol* **128**: 779–792.

Whiteway, M., and Bachewich, C. (2007) Morphogenesis in *Candida albicans*. *Annu Rev Microbiol* **61**: 529–553.

Wilson, R.B., Davis, D., and Mitchell, A.P. (1999) Rapid hypothesis testing with *Candida albicans* through gene disruption with short homology regions. *J Bacteriol* **181**: 1868–1874.

Wilson-Grady, J.T., Villen, J., and Gygi, S.P. (2008) Phosphoproteome analysis of fission yeast. *J Proteome Res* **7**: 1088–1097.

Windgassen, M., Sturm, D., Cajigas, I.J., Gonzalez, C.I., Seedorf, M., Bastians, H., and Krebber, H. (2004) Yeast shuttling SR proteins Npl3p, Gbp2p, and Hrb1p are part of the translating mRNPs, and Npl3p can function as a translational repressor. *Mol Cell Biol* **24**: 10479–10491.

Wisplinghoff, H., Bischoff, T., Tallent, S.M., Seifert, H., Wenzel, R.P., and Edmond, M.B. (2004) Nosocomial bloodstream infections in US hospitals: analysis of 24,179 cases from a prospective nationwide surveillance study. *Clin Infect Dis* **39**: 309–317.

Yun, C.Y., and Fu, X.D. (2000) Conserved SR protein kinase functions in nuclear import and its action is

counteracted by arginine methylation in *Saccharomyces cerevisiae*. *J Cell Biol* **150**: 707–718.

Zdobnov, E.M., and Apweiler, R. (2001) InterProScan–an integration platform for the signature-recognition methods in InterPro. *Bioinformatics* **17**: 847–848.

Zhong, X.Y., Ding, J.H., Adams, J.A., Ghosh, G., and Fu, X.D. (2009) Regulation of SR protein phosphorylation and alternative splicing by modulating kinetic interactions of SRPK1 with molecular chaperones. *Genes Dev* **23**: 482–495.

Supporting information

Additional supporting information may be found in the online version of this article at the publisher's web-site.

Translation termination depends on the sequential ribosomal entry of eRF1 and eRF3

Christian Beißel[1], Bettina Neumann[1], Simon Uhse[1], Irene Hampe[1], Prajwal Karki[2] and Heike Krebber[1,*]

[1]Abteilung für Molekulare Genetik, Institut für Mikrobiologie und Genetik, Göttinger Zentrum für Molekulare Biowissenschaften (GZMB), Georg-August Universität Göttingen, Germany and [2]Department of Physical Biochemistry, Max Planck Institute for Biophysical Chemistry, Göttingen, Germany

ABSTRACT

Translation termination requires eRF1 and eRF3 for polypeptide- and tRNA-release on stop codons. Additionally, Dbp5/DDX19 and Rli1/ABCE1 are required; however, their function in this process is currently unknown. Using a combination of *in vivo* and *in vitro* experiments, we show that they regulate a stepwise assembly of the termination complex. Rli1 and eRF3-GDP associate with the ribosome first. Subsequently, Dbp5-ATP delivers eRF1 to the stop codon and in this way prevents a premature access of eRF3. Dbp5 dissociates upon placing eRF1 through ATP-hydrolysis. This in turn enables eRF1 to contact eRF3, as the binding of Dbp5 and eRF3 to eRF1 is mutually exclusive. Defects in the Dbp5-guided eRF1 delivery lead to premature contact and premature dissociation of eRF1 and eRF3 from the ribosome and to subsequent stop codon readthrough. Thus, the stepwise Dbp5-controlled termination complex assembly is essential for regular translation termination events. Our data furthermore suggest a possible role of Dbp5/DDX19 in alternative translation termination events, such as during stress response or in developmental processes, which classifies the helicase as a potential drug target for nonsense suppression therapy to treat cancer and neurodegenerative diseases.

INTRODUCTION

When a ribosome arrives at a stop codon on the mRNA, protein synthesis is terminated and the peptide is released (1). In eukaryotes, two essential release factors are well known to mediate translation termination. The eukaryotic release factor 1 (eRF1), in *Saccharomyces cerevisiae* encoded by *SUP45*, is the only class I termination factor in eukaryotes that recognizes all three different stop codons (UAG, UAA, UGA) and subsequently mediates the hydrolysis of the peptidyl-tRNA in the ribosomal peptidyl-transferase center (PTC). In addition, the class II eukaryotic release factor 3 (eRF3), in *S. cerevisiae* encoded by *SUP35*, enhances translation termination efficiency with its GTPase activity (2,3). Most termination models (Supplementary Figure S1A) anticipate that eRF1 and eRF3–GTP enter the ribosome together as a ternary complex once the stop codon is reached (1,2,4), as both factors strongly interact with each other via their C-terminal domains (5,6). Supposedly, successful stop codon recognition by eRF1 induces GTP-hydrolysis of eRF3, which in turn leads to a conformational rearrangement in eRF1 resulting in its active form, which positions its GGQ-motif in the PTC and mediates hydrolysis of the ester bond of the peptidyl-tRNA (7–9).

In light of these mostly *in vitro* studies, nothing seems to be missing; however, novel factors essential for translation termination *in vivo* were discovered and need to be incorporated into a comprehensive model: The DEAD-box RNA helicase Dbp5, encoded by *RAT8* (human DDX19) (10), its stimulating co-factors Gle1 plus inositol hexakisphosphate IP_6 (11,12), the iron-sulfur containing ATP-binding cassette protein Rli1 (human ABCE1) (13,14) and the initiation factor eIF3, including Hcr1 (15). Dbp5 and Gle1 are well known for their function in mRNA-export through nuclear pore complexes (NPCs) (16). Using its regulated ATPase cycle, Dbp5 remodels RNA–protein complexes at the cytoplasmic side of the NPC on emerging mRNAs (17). By dissociation of the export receptor Mex67-Mtr2 (human TAP-p15) from the arriving mRNAs, its backsliding is prevented and directionality of the transport event established. Its co-factors Gle1 and IP_6 stimulate ATP-hydrolysis leading to RNP-release and binding of Dbp5-ADP to the NPC-protein Nup159 (human Nup214). Importantly, this binding leads to ADP-release, a conformational change and the binding of ATP (16,17). The ATPase activity of Dbp5 is also essential for efficient translation termination (10,12).

In addition to these functions, Dbp5 plays also a role in the export of both ribosomal subunits (18). However, in contrast, to mRNA export and translation termination, Dbp5 acts independently of its ATPase activity in ribosome export (18).

Rli1 functions in biogenesis and nuclear export of pre-ribosomal subunits (19–21), translation initiation (22), termination (13) and in particular in ribosome recycling (23). Rli1 is a soluble member of the ATP-binding cassette (ABC) protein superfamily that contains two nucleotide-binding domains (NBDs) and two N-terminal iron-sulfur clusters. A hinge domain connects both NBDs forming a cleft, which is open in the ADP-bound state, while ATP-binding induces its closure with a concomitant movement of the iron-sulfur domain allowing ATP-hydrolysis. This ATP-dependent tweezers-like motion converts chemical energy into mechanical power, which is important for splitting the ribosome into its ribosomal subunits (24). The protein is highly conserved in eukaryotes and essential in all organisms tested (22). Interestingly, Rli1 acts ATP-hydrolysis independent during translation termination (13,25). It was suggested that Rli1 associates with the termination complex upon dissociation of eRF3–GDP, taking over its position to keep eRF1 in its favourable position to facilitate peptidyl-tRNA hydrolysis (4,26).

The initiation factor eIF3 has recently been associated with translation termination, because mutations in its subunits reduce the rate of stop codon readthrough (15). Interestingly, deletion of the substoichiometric component *HCR1* shows an increased readthrough activity and this phenotype was suppressed by high copy *RLI1*. A model was proposed in which Hcr1 is not a bona fide translation initiation factor, but rather acts in termination by promoting GDP–eRF3 ejection from the ribosomes (15).

So far, no translation termination model is available that includes all of these factors that support termination and many results were obtained from *in vitro* assays with purified components. Therefore, we analysed the process in *S. cerevisiae in vivo* and *in vitro* with all participating factors and uncovered a sequential recruitment mechanism, in which Rli1 and eRF3 wait at the ribosome for the entry of Dbp5 that delivers eRF1 and at the same time shields it from premature access of eRF3. Upon proper positioning Dbp5 dissociates, allowing eRF3 to contact and stimulate eRF1 activity. This stepwise entry of the termination factors and in particular the Dbp5 controlled eRF1–eRF3 interaction, prevents premature and inefficient translation termination.

MATERIALS AND METHODS

Yeast strains and plasmids

All *S. cerevisiae* strains, plasmids and oligonucleotides used in this study are listed in the Expanded View Supplementary Tables S1, S2 and S3, respectively. For growth analyses, cells were spotted in 10-fold serial dilutions onto selective agar plates and grown for 3 days at the indicated temperatures.

The strains, HKY1622 and HKY1623, were generated by crossing HKY1271 (*RLI1-GFP*) and HKY446 (*sup45-2*). Crossing the strains HKY445 (WT of HKY446) or HKY446 with the strain HKY1122 (Prt1-GFP) produced the strain HKY1915 and the corresponding WT

HKY1914. The strain HKY1921 was generated by crossing the strains HKY477 (*rat8-2-myc*) and HKY1907 (*trp5Δ*) and exchange of pHK629 with pHK693. For the generation of plasmid pHK1292, the GFP ORF was amplified by polymerase chain reaction using the primers HK1194 and HK1195 and inserted via Xh*o*I and PstI sites into pHK887 (*2µ Rli1-HA LEU2*) replacing the HA-tag. To create pHK1474 and pHK1475, the *RLI1-GFP* ORF with promoter and terminator was amplified from pHK1292 with the primers HK2136 and HK2137 and inserted via Gibson assembly reaction into pHK86 and pHK87, respectively, which were linearized by SacI and SalI digestion. The *GLE1* ORF was amplified from gDNA with HK1398 and HK1399 and inserted via BamHI site into pHK825 (*CEN P_{ADH1}3xMYC URA3*) to generate pHK1323. For the generation of pHK1283, the *SUP35* ORF was amplified with the primers HK1109 and HK1110 and inserted via EcoRI and XhoI sites into pGEX-4T-1. The *SUP45* ORF was amplified with the primers HK1144 and HK1156 and inserted via NdeI and XhoI sites into pET28a to create pHK1280. The *SUP45Δ1237-1311* ORF was amplified with the primers HK1146 and HK1147 and inserted via BamHI and XhoI sites into pET15b to generate pHK1278. To generate pHK1394, the *GLE1* ORF was amplified with the primers HK1613 and HK1614 and inserted via Gibson assembly reaction into pETMBP1_1a that was linearized by SacI and NcoI digestion.

Co-immunoprecipitation experiments

In vivo interactions studies were carried out following the protocols published previously (18,27). For immunoprecipitation of GFP-tagged proteins, 10 µl slurry of GFP-Trap_A beads (Chromotek) and for TAP-tagged proteins, 20 µl slurry of IgG-Sepharaose beads (GE Healthcare) were used per reaction and incubated with 200 (high abundant proteins) and up to 2000 µl (for low abundant proteins) of the clarified lysate for 3 h rotating at 4°C. If indicated, the samples were treated with 0.2 mg/ml RNase A (AppliChem) for additional 30 min at 4°C. Finally, the eluted proteins were separated on 10% SDS-polyacrylamide gels and analysed by western blotting.

Sucrose-density gradient fractionation

The experiments were essentially performed as described previously (18) with the following modifications. For elongation factor mutants, no cycloheximide treatment was performed meaning that cells were directly harvested upon 1 h temperature shift, cycloheximide was omitted from the lysis buffer. For protein analyses, 15 OD_{260nm} units of lysates were loaded onto the top of linear 7–47% (w/v) sucrose gradients and centrifuged for 2 h and 40 min at 40 000 rpm and 4°C in a TH-641 rotor and Sorvall WX80 ultracentrifuge (Thermo Scientific). After gradient fractionation, protein fractions were precipitated with 10% trichloroacetic acid, washed twice with 80% aceton and subjected to sodium dodecylsulphate-polyacrylamide gel electrophoresis (SDS-PAGE) and western blotting.

Western blot analyses and quantification

Polyclonal rabbit antibodies against Dbp5 (dilution 1:1000), eRF1 and eRF3 (kindly provided by D. Bedwell, dilution for both 1:1000), uL29 = Rpl35 and uS3 = Rps3 (kindly provided by M. Seedorf, dilution 1:5000 and 1:10 000 respectively, or anti-Rps3 peptide antibody 1:500), Aco1, Hem15, Por1 and Zwf1 (kindly provided by R. Lill, dilution 1:1000, 1:7000, 1:2000, and 1:4000, respectively), Asc1 (kindly provided by G. Braus, dilution 1:2000) and Cdc28 (sc-28550; Santa Cruz, dilution 1:2000) were used. GFP-tagged proteins were detected with anti-GFP antibodies (sc-8334; Santa Cruz, dilution 1:1000), or GF28R (Pierce Protein Biology, 1:5000), or (ab183734; Abcam; 1:10 000), MYC-tagged proteins with an anti-MYC antibody (sc-789; Santa Cruz, dilution 1:750) and HA-tagged proteins with an anti-HA antibody (sc-57592 and sc-7392; Santa Cruz, dilution 1:750) and GST-tagged proteins with an anti-GST antibody (sc-138; Santa Cruz, dilution 1:2000). Secondary anti-rabbit IgG (H+L)-HRPO and anti-mouse IgG (H+L)-HRPO (Dianova) antibodies were used and detected with Amersham ECL Prime Western Blotting Detection Reagent (GE Healthcare) or WesternBright Chemilumineszenz Substrat Quantum (Biozym) and the FUSION-SL chemiluminescence detection system (Peqlab). Quantification of western blot signals was performed with the Bio1D software (Peqlab) or with ImageStudio Lite (Li-COR Biosciences). For statistical analyses of co-immunoprecipitation studies, the intensity of co-precipitated bands was related to that of the pull-down and finally, the ratio of the mutant or treated strains was compared to the wild typical ratio. For quantification of the sucrose density gradient fractionation experiments, the intensity of each fraction was measured and the polysomal fractions were compared to the sum of the 80S, 60S, 40S and non-ribosomal fractions.

In vitro binding studies

GST-Dbp5, GST-eRF1 and GST-eRF3ΔN65, a more stable version of eRF3 that has a truncated C-terminus, were expressed in *Escherichia coli* Rosetta 2 cells, purified by affinity chromatography with GSTrap 4B Glutathione Sepharose (GE Healthcare) and stored at −80°C in elution buffer (for GST-Dbp5: 50 mM Tris pH 7.5, 150 mM NaCl, 30 mM Glutathione reduced) (for GST-eRF1 and GST-eRF3: 20 mM HEPES pH 7.5, 500 mM NaCl, 5% glycerol, 4 mM β-MeOH, 30 mM Glutathione reduced). To obtain untagged Dbp5, eRF1 and eRF3, the purified GST-tagged proteins were cleaved with PreScission protease overnight at 4°C. Afterwards, GST was removed by performing a second affinity chromatography with GSTrap 4B Glutathione Sepharose (GE Healthcare). The proteins were further purified by running the collected flow through over a gel filtration chromatography. Purified GST–Dbp5 and Dbp5 were stored in 50 mM Tris pH 7.5, 150 mM NaCl, 10% glycerol at −80°C, whereas GST-eRF1, eRF1, GST- eRF3 and eRF3 were stored in 50 mM NaCl pH 7.5, 20 mM HEPES, 5% glycerol and 4 mM β-MeOH at 80°C.

For binding studies either purified proteins as indicated above were used or Rosetta II (DE3) cells were transformed with pET15b-HIS$_6$-SUP45 delta 25 (eRF1 lacking 25aa at the C-terminus), pET28a-HIS$_6$-SUP45, pGEX4T1-GST-SUP35, pGEX-6P-1-GST-RLI1 and pGEX6P1-GST. Overexpression was induced by growing the cells for 3 days in auto-inducing media (LB media with 0.5% (v/v) glycerol, 0.05% (v/v) Ggucose and 0.2% (v/v) lactose plus 25 mM K$_2$HPO$_4$, 25 mM NaH$_2$PO$_4$, 50 mM NH$_4$Cl and 0.5 mM Na$_2$SO$_4$) at 16°C. Cells were harvested and resuspended in lysis buffer (50 mM Tris–HCl, pH 7.5, 150 mM NaCl, 2 mM MgCl, 5% (v/v) glycerol, 1 mM Dithiothreitol (DTT), 0.2% (v/v) NP-40 and ethylenediaminetetraacetic acid (EDTA)-free protease inhibitor mix (Roche)). After cell lysis by sonication and centrifugation, the supernatant was used for further analysis. The used GSTrap 4B Glutathione Sepharose (GE Healthcare) beads were pre-incubated with 3% Albumin Fraction V (Roche) and mixed with lysis buffer. Next, the GST tagged proteins or only GST were incubated with 15 μl slurry of GSTrap for 2 h at 4°C. After several washing steps with buffer (excluding protease inhibitor), the beads were incubated with the protein lysates for additional 2 h at 4°C. For the competition assay, the eRF1 lysate was first incubated with GST-Dbp5 bound to the GSTrap for 20 min at 4°C, before adding purified eRF3ΔN65 in the indicated amounts and further incubation for 1 h at 4°C. After five washing steps with lysis buffer, the proteins that were bound to the beads were analysed by SDS-PAGE and western blot.

Prt1-GFP and Nip1-GFP were purified from yeast cells before the *in vitro* binding assay was carried out with recombinantly expressed GST-Rli1.

Readthrough assay

The dual reporter β-galactosidase luciferase assay was basically performed as described previously (10,28). Briefly, all analysed yeast strains were transformed with the reporter plasmids pHK607 or pHK608, respectively. Yeast cells were grown at 25°C to mid-log phase, shifted for 30 min to 37°C and afterward divided: 20 OD$_{600}$ were used for the luciferase assay and 50 ml that were split for triplicates for the β-galactosidase assay,

The luciferase assay was performed with the 'Beetle-Juice Luciferase Assay Firefly' kit (p.j.k GmbH) according to the manufacturer's protocol. For that, cell pellets were lysed with 300 μl glass beads in a FastPrep-24 machine (MP Biomedical) in 400 μl lysis buffer (77 mM K$_2$HPO$_4$, 23 mM KH$_2$PO$_4$, 0.2% Triton X-100, 1 mM DTT) supplemented with Complete, EDTA-free protease inhibitor cocktail (Roche). The lysates were centrifuged twice for 5 min at 21 000 × *g* and 4°C. Afterwards, 20 μl of the cleared lysate was transferred in triplicate into a white 96-well plate, supplemented with always 50 μl substrate and measured with the luminometer (Victor X3 2030 multilabel reader from Perkin Elmer).

For the β-galactosidase assay, all cell pellets were resuspended in 300 μl of Z-buffer (100 mM phosphate buffer pH 7.0, 10 mM KCl, 1 mM MgSO$_4$) and lysed with the freeze-and-thaw method (1 min in liquid nitrogen, 2 min in 37°C water bath, four times repeated). Afterwards, 700 μl of Z-buffer with 1 mM DTT and 160 μl of the substrate ONPG (4 mg/ml of o-Nitrophenyl-β-D-galactopyranosid in Z-buffer) were added and incubated at 30°C until colour changes into yellow. The reaction was stopped by the addi-

tion of 1 M Na$_2$CO$_3$ and the OD$_{420nm}$ was measured with a spectrophotometer (UV-1601 from Shimadzu). The relative readthrough activity was calculated from the ratio of luciferase to β-galactosidase activity measured with the stop codon-containing reporter related to the ratio from the in-frame control.

Statistical analysis

Quantification was performed for at least three independent experiments. Quantification of co-immunoprecipitation experiments shown in Figures 1D, 2C, E, 3C, E, 4B, C, E, G 6D, G and I were analysed for significance by Student's two-tailed, two-sample, unequal variance *t*-test. In all cases, each dataset was normalized and only compared to wild-type. The mean ± standard deviations are displayed. The same was done for Figures 1G, 2H and 6B, with the exception that the differences were analysed by a Student's one-tailed, two-sample, unequal variance *t*-test. In Figures 1G and 6B, the signal intensity of the analysed proteins in the polysomal fraction of the *tef2-9* strain was subtracted from the wild-type signals in the polysoms of the respective protein and normalized to the Asc1/uS3 protein content that reflected the amount of polysomes. All data were finally analysed for significance by Student's two tailed, two-sample, unequal variance *t*-test. Significance *P*-values below 0.05 were indicated by asterisks (*$P < 0.05$; **$P < 0.01$; ***$P < 0.001$).

RESULTS

Binding of Dbp5, but not Rli1, to the termination complex depends on eRF1

Previous studies of the translation termination process have not revealed, how and when Rli1 and Dbp5 are recruited to the terminating ribosome. Crystal structure and *in vitro* analyses with purified proteins proposed that Rli1 and eRF3 bind to the same position on the terminating ribosome so that their association seemed to be mutually exclusive and it was suggested that Rli1 might take over the binding site of eRF3 after its dissociation to catalyse the subsequent ribosome recycling (4,29) (Supplementary Figure S1B). However, a potentially earlier association of Rli1 with the ribosome before ribosome recycling has not been investigated. The same is unclear for Dbp5. The helicase might already be associated with elongating ribosomes or it could be recruited at a later step together with eRF1 upon arrival of the ribosome at the stop codon. To address these questions, we analysed the ribosomal association of Rli1 and Dbp5 in the temperature-sensitive eRF1 mutant *sup45-2* that is defective in translation termination and in ribosome binding. Upon a temperature shift to 37°C, ribosome binding of the mutated eRF1 protein sup45-2 is disturbed, resulting in stop codon recognition defects and subsequent readthrough activity in which near-cognate tRNAs are incorporated at the termination codon and translation elongation continues to the next stop codon (30). If Rli1 would enter the termination process after eRF1 has entered, one would expect to see a reduced binding of Rli1 to ribosomes in that mutant. However, co-immunoprecipitation experiments (co-IPs) show that the binding of Rli1 to the large ribosomal protein uL29 (yeast Rpl35) is unchanged and

its association with the small ribosomal protein uS3 (yeast Rps3) is even increased in *sup45-2* cells (Figure 1A and D). These results indicate that Rli1 binds ribosomal particles without functional eRF1 and that it is possibly associated with ribosomes before eRF1 enters. The increased binding of Rli1 to the 40S subunit in *sup45-2* might represent an enhanced presence of 43S pre-initiation complexes, which are stabilized by Rli1 (22). In contrast to Rli1, the interaction of Dbp5 and the mutated eRF1 protein with both ribosomal proteins is reduced in *sup45-2* (Figure 1B–D) suggesting that Dbp5 requires functional eRF1 for its association with terminating ribosomes. This reduced ribosomal association might be due to the fact that mutant eRF1 is rather unstable and only ∼50% of the protein amount is detectable in lysates on western blots (Figure 1C). Thus, while the association of Rli1 with the ribosome rather increases in *sup45-2* cells, the association of Dbp5 and mutant eRF1 decreases. These results might indicate that Rli1 associates with the ribosome before Dbp5 and eRF1.

To verify this sequential recruitment, we analysed whether Rli1, but not Dbp5 associates with ribosomes arrested in translation elongation and found that this is indeed the case (Figure 1E–G). Mutations in eEF1A (such as in *tef2-9*) lead to defects in translation elongation (31), which is reflected in polysomal profiles of sucrose-density gradient fractionations that were prepared without the usual addition of cycloheximide. Under such conditions, wild-type cells continue elongation, leading to a complete polysome run-off, while elongation factor mutants stall ribosomes during elongation on the mRNA, thereby preventing their arrival at the stop codon (Figure 1E) (32). Western blot analyses of the corresponding protein fractions show that high amounts of Rli1 are present in the mono- and polysomal factions in *tef2-9* cells, similar to the ribosome-bound protein Asc1 (Figure 1G). This finding is in agreement with structural analyses of the human homolog of Rli1, ABCE1 at the ribosome, which show that the protein binds to the intersubunit space of the ribosome where aEF1 also associates (29), suggesting that their binding is mutually exclusive. However, as stalled ribosomes have free A-sites when the elongation factor is inactivated as in the *tef2-9* mutant, different factors can stochastically go there, among them Rli1. These findings suggest that Rli1 can bind to the ribosome as soon as the A-site is free and thus might be the first termination factor that enters the ribosome, which is clearly earlier than anticipated. In contrast to that, Dbp5 is almost absent in the polysome fractions of *tef2-9* cells (Figure 1F and G), indicating that Dbp5 is recruited to ribosomes only after translation elongation. Thus, our results suggest that the ribosomal association of Dbp5 not only requires a free A-site like this is the case for Rli1, because in contrast to Rli1 Dbp5 is not associated with ribosomes in an elongation mutant, but Dbp5 recruitment also seems to depend on a stop codon and functional eRF1.

Dbp5 and Rli1 interact with each other during translation termination

Although both Rli1 and Dbp5 were identified as translation termination factors (10,13), it is unclear whether they interact with each other. To answer that question, we co-
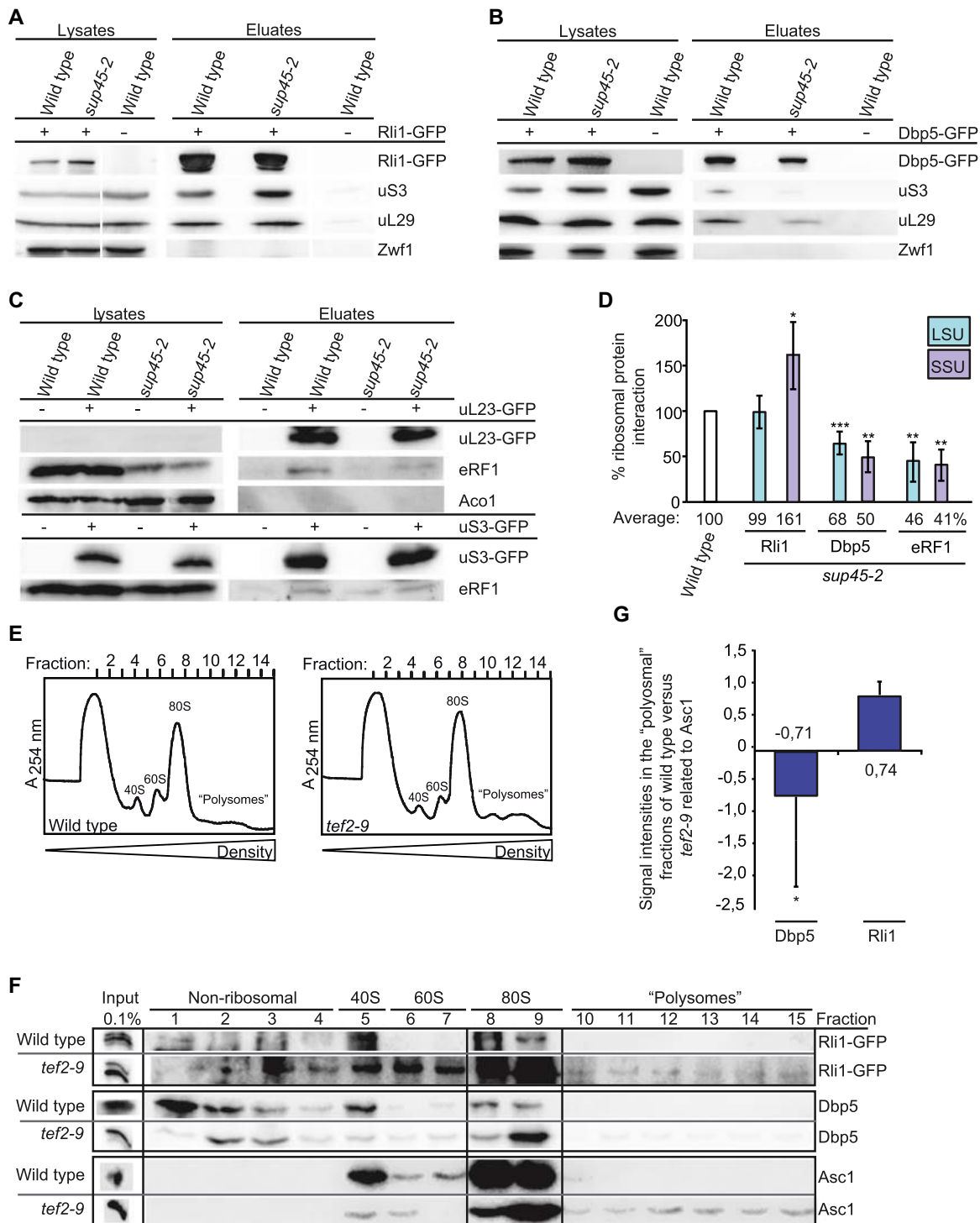
Figure 1. Dbp5, but not Rli1, requires eRF1 to associate with the ribosome at a stop codon. (**A**) The interaction of Rli1 with the ribosome is not dependent on eRF1. Western blot analysis of Rli1 co-IPs in wild-type and *sup45-2* cells shifted to 37°C for 1 h reveal co-precipitation of the small ribosomal protein uS3 (= Rps3) and the large ribosomal protein uL29 (= Rpl35). Detection of Zwf1 served as non-binding control. (**B**) The interaction of Dbp5 with ribosomal subunits is decreased in *sup45-2*. Western blot analysis shows co-precipitation of uS3 and uL29 with Dbp5 IPs in wild-type and *sup45-2* cells, shifted to 37°C for 1 h. (**C**) The interaction of mutant eRF1 with the ribosome is decreased. Western blot analysis of the co-precipitation of mutant eRF1 (sup45-2) with uL23 (top) or with uS3 (bottom) is shown. Aco1 served as a negative control. (**D**) Quantification of at least three independent experiments, one of which is shown in panels (A–C), which determine the amount of the co-precipitated proteins, measured with the Fusion SL detection system. (**E**) Ribosome profiles of wild-type and the translation elongation defective strain *tef2-9* reflects the translational run-off in wild-type and a translational arrest in the elongation mutant. Wild-type and *tef2-9* cells were shifted to 37°C for 1 h before the lysates were analysed in linear sucrose-density gradients without cycloheximide. (**F**) Rli1, but not Dbp5, is bound to ribosomes during translation elongation. Western blot analysis of the fractions, representing the total cellular amount of the indicated proteins, reveals their ratio in the 80S, polysomal or non-ribosomal, 40S and 60S fractions. Asc1 as a ribosome binding protein served as a positive control. (**G**) Quantification of four different western blot analyses shown in panel (F); $*P < 0.05$; $**P < 0.01$; $***P < 0.001$.
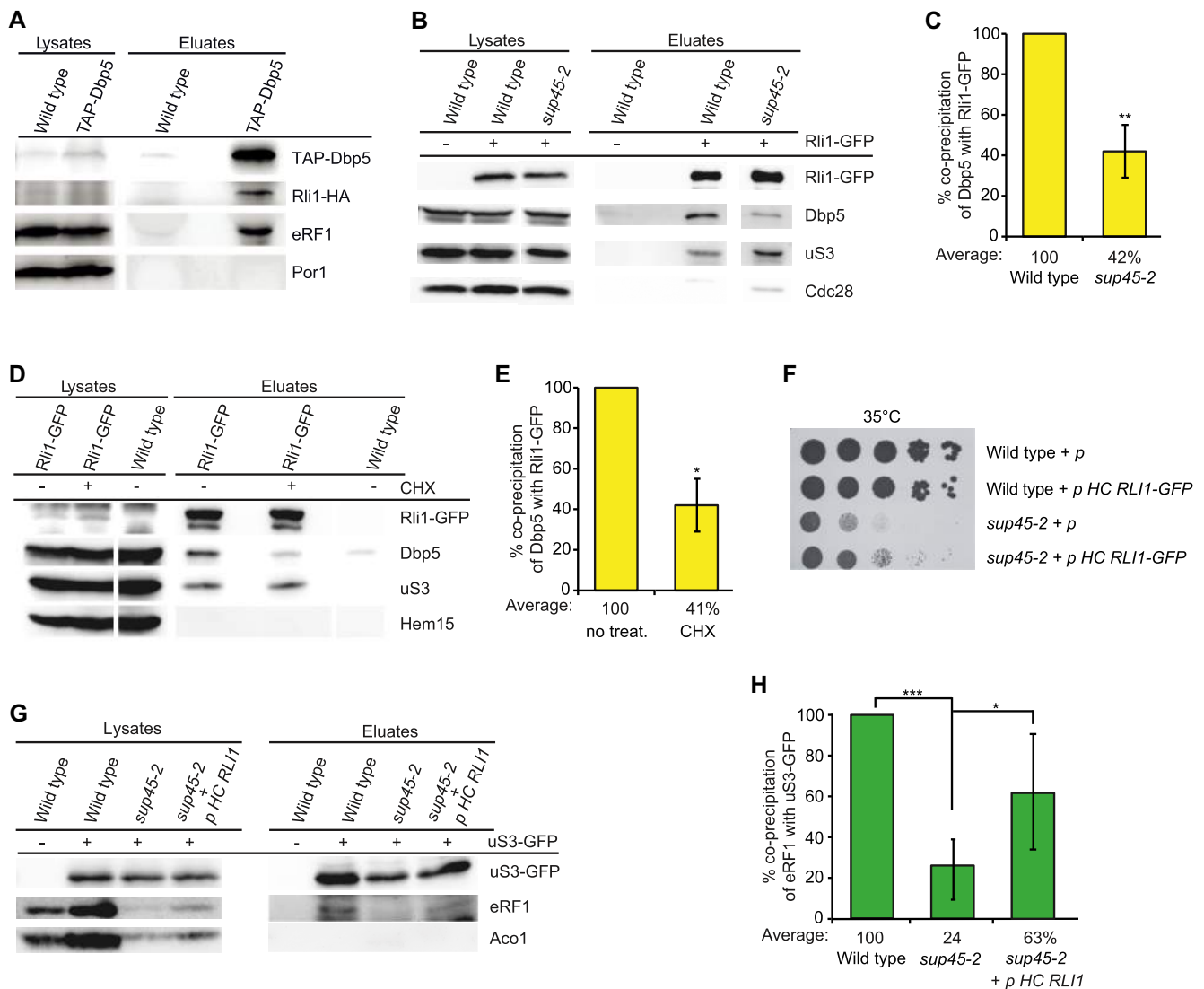
Figure 2. Rli1 supports the recruitment of Dbp5 and eRF1 to the ribosome. (**A**) Dbp5 interacts RNA-independently with Rli1. Immunoprecipitation of TAP-Dbp5 in the presence of RNase A shows co-precipitation of Rli1-HA in western blot analysis. Detection of eRF1 served as positive and of Por1 as negative control. (**B**) The interaction between Rli1 and Dbp5 is decreased in *sup45-2*, shifted to 37°C for 1 h. Western blot analyses of Rli1-IPs reveal less co-precipitation of Dbp5, but no reduction of the ribosomal protein uS3 in *sup45-2* compared to wild-type. Cdc28 served as negative control. (**C**) Quantification of four different experiments shown in panel (B). (**D**) Inhibition of translation elongation leads to a reduced interaction between Rli1 and Dbp5. Western blot analyses of co-IPs of Dbp5 with Rli1 upon treatment with 0.5 mg/ml cycloheximide (CHX) for 30 min are shown. Hem15 was detected as non-binding control. (**E**) Quantification of three different experiments shown in panel (D). (**F**) Overexpression of *RLI1* partially rescues the growth defects of *sup45-2*, while the wild-type growth is not influenced. Serial dilutions of the indicated strains are shown upon growth on selective plates for 3 days at 35°C. (**G**) Overexpression of *RLI1* suppresses the binding defect of eRF1 to the ribosome in *sup45-2* cells. Co-IPs of eRF1 with uS3-GFP are shown in the indicated strains with or without high copy (HC) *RLI1*. (**H**) Quantification of four different experiments shown in panel (G); *$P < 0.05$; **$P < 0.01$; ***$P < 0.001$.

precipitated Rli1 with Dbp5 *in vivo* (Figure 2A) and vice versa Dbp5 as well as its co-factor Gle1 with Rli1 (Supplementary Figure S1B) unrevealing a physical interaction between Dbp5 and Rli1 that might be direct or mediated by other proteins. To verify that this interaction actually occurs during translation termination and not for instance during pre-ribosomal subunit export from the nucleus in which Rli1 and Dbp5 are both involved (18,19,21), we compared their interaction in *sup45-2* cells in which the termination process is inhibited and Dbp5 does not enter the ribosome.

Our results show that in *sup45-2* the interaction of Rli1 and Dbp5 is indeed reduced to more than half, while its interaction to the ribosome is not decreased (Figure 2B and C). Moreover, we treated wild-type cells with the antibiotic cycloheximide, which inhibits translation elongation and thus, prevents ribosomes from arriving at stop codons, reflected in the ribosomal profiles. Also in this case the prevention of translation termination leads to a significantly decreased association of Rli1 and Dbp5 (Figure 2D and E). These results suggest that an interaction of Dbp5 and Rli1 takes place
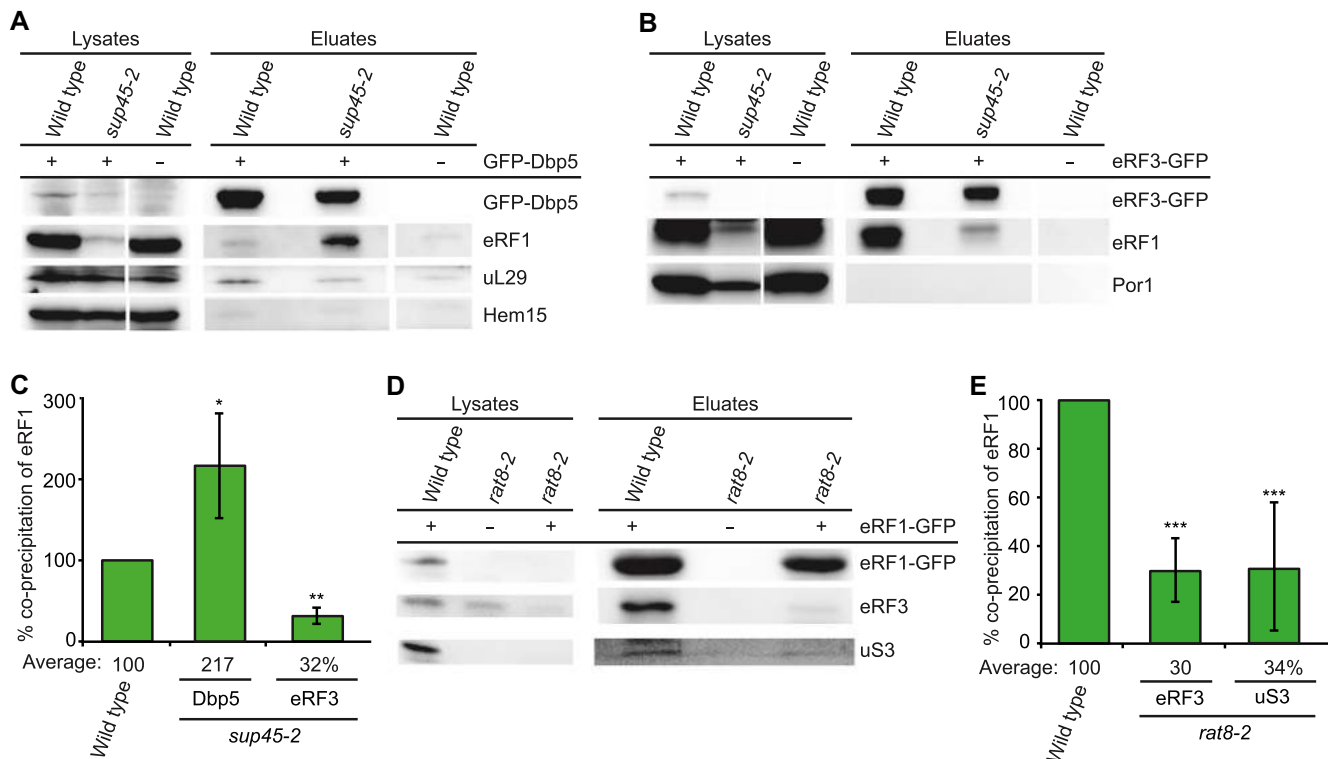
Figure 3. Not eRF1 and eRF3 enter the ribosome together, but eRF1 and Dbp5. (**A**) The binding of Dbp5 with the ribosome-binding defective protein sup45-2 is increased, while its ribosome association is decreased. Western blot analyses of co-IPs with mutated eRF1 (sup45-2) and Dbp5 or uL29 are shown. Detection of Hem15 served as a non-binding control. (**B**) The interaction between eRF3 and eRF1 is decreased in the *sup45-2* strain as shown in western blots of the eRF1 co-IP with eRF3. Por1 served as negative control. (**C**) Quantification of three different experiments shown in panels (A) and (B). (**D**) The interaction of eRF1 and eRF3 is decreased in a *DBP5* mutant. Western blot analysis of eRF3 co-IPs with eRF1 in wild-type and the *rat8-2* stain is shown. (**E**) Quantification of three different experiments shown in (D); *$P < 0.05$; **$P < 0.01$; ***$P < 0.001$.

during translation termination and that both proteins bind simultaneously to the termination complex, possibly during stop codon recognition. This finding contradicts older models, in which Rli1 binds only for ribosome recycling.

An *in vivo* interaction of Dbp5 and eRF1 was shown earlier (10). However, as Rli1 most likely binds to the ribosome before Dbp5 and eRF1 have entered (Figure 1), we wondered whether Rli1 might support their recruitment to the ribosome. We therefore investigated if an overexpression of *RLI1* would suppresses the *sup45-2* mutant, which has defects in ribosome binding (Figure 1C and D), (30). Indeed, growth analyses show at least a partial rescue of the *sup45-2* growth defects in the presence of high copy *RLI1* (Figure 2F). The reason for this suppression might be that an increased amount of Rli1 proteins leads to their faster ribosome binding, which supports the defective sup45 protein in associating with the ribosome. This seems indeed to be the case as shown by co-IPs (Figure 2G). While the association of the mutated eRF1 protein with the ribosome is reduced to a quarter, increased Rli1 concentrations support the binding of sup45-2 to more than 60% (Figure 2H). These findings suggest that the initial presence of Rli1 at the ribosome could support the subsequent eRF1 recruitment to the stop codon.

eRF1 and eRF3 do not enter the termination complex together

In contrast to Rli1, Dbp5 requires intact eRF1 for its binding to the ribosome (Figure 1). From previous studies, it was suggested that Dbp5 might help to position eRF1 at the stop codon and dissociate before eRF3 enters the termination complex (10). Thus, it seems conceivable that eRF1 and eRF3 are not recruited as a complex, but rather individually, which challenges current models. To analyse whether Dbp5 and eRF1 form a complex already in the cytoplasm, we took again advantage of the *sup45-2* mutant, in which the mutated eRF1 protein sup45-2 has a ribosome-binding defect and is thus detached and freely present in the cytoplasm at the non-permissive temperature (Figure 1C and D) (30) and analysed its binding to Dbp5. Indeed, co-IPs revealed an increased binding of the cytoplasmic sup45-2 to Dbp5 (Figure 3A and C), while at the same time its interaction to eRF3 is decreased (Figure 3B and C). Remarkably, despite the fact that the sup45-2 protein is less stable as compared to wild-type eRF1, as reflected in the lysate lanes, its binding to Dbp5 is significantly increased. These results could suggest that a pre-formed complex of Dbp5 and eRF1 in the cytoplasm approaches the terminating ribosome, while eRF3 enters separately upon Dbp5-dissociation. As Dbp5 and eRF3 do not interact *in vivo* (10),
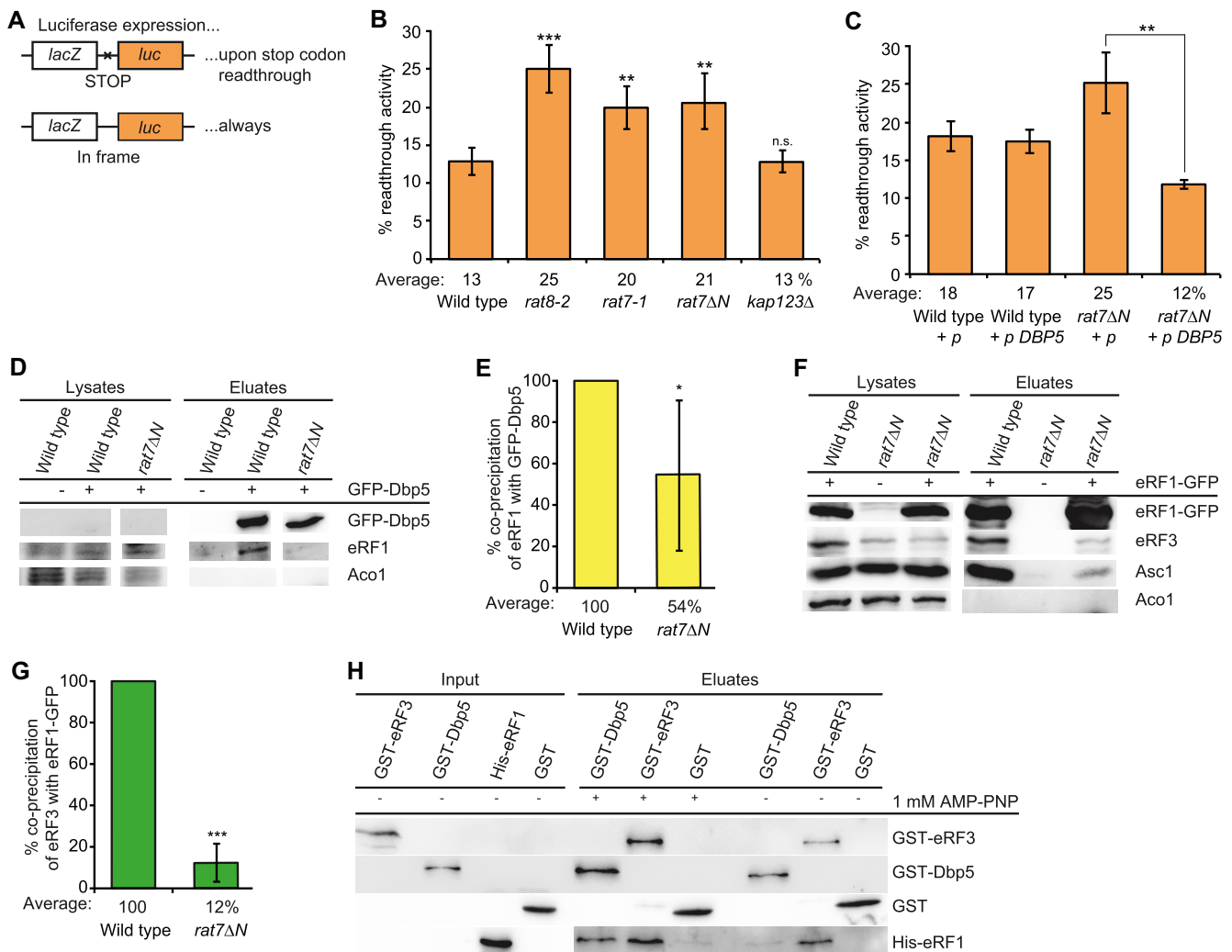
Figure 4. Nup159 recycles Dbp5-ATP also for translation termination. (**A**) Scheme of the reporter plasmids used in the dual reporter β-galactosidase luciferase assay. The *lacZ* gene, expressing β-galactosidase and the *luc* gene, expressing luciferase is either separated by the stop codon UAG or in frame. In the upper case, luciferase will only be expressed in case the stop codon is readthrough. The in-frame reporter serves as control to monitor basal expression levels and relate it to the stop codon containing construct. (**B**) Mutants of *NUP159* show increased readthrough of the stop codon. The average readthrough activity of at least three independent experiments is shown after shift of all indicated strains to 37°C for 30 min. (**C**) High copy *DBP5* rescues the increased stop codon readthrough of *rat7ΔN*. All strains were shifted to 37°C for 30 min. (**D**) The interaction of Dbp5 and eRF1 is disturbed in the recycling defective mutant *rat7ΔN*. Western blot analysis of a co-IP with Dbp5 and eRF1 is shown. Aco1 served as a negative control. (**E**) Quantification of three different experiments shown in panel (D). (**F**) The interaction of eRF1 and eRF3 and the ribosome is diminished in *rat7ΔN* cells. Western blot analysis of a co-IP with eRF1-GFP and eRF3 or the ribosome bound protein Asc1 is shown. (**G**) Quantification of three different experiments shown in panel (F). (**H**) Dbp5 and eRF1 directly interact in the presence of a non-hydrolysable ATP-analogue. An *in vitro* binding study with recombinant proteins in which GST-tagged Dbp5 or eRF3 were used in pull-down experiments in the presence of His-eRF1 and if indicated 1 mM AMP–PNP is shown in western blot analysis. GST alone served as a non-binding control; $*P < 0.05$; $**P < 0.01$; $***P < 0.001$.

a complex formation between the three termination factors is unlikely or their potential contact is very short.

To further investigate whether Dbp5 might indeed deliver eRF1 to the ribosome and eRF1 and eRF3 do not enter the ribosome together, we analysed if mutations in *DBP5* would lead to a reduced binding of eRF1 to eRF3 and to the ribosome. For this purpose, we used the *rat8-2* strain that produces instable Dbp5 protein due to a leucine to proline exchange at position 267 (33) (Figure 6H). Indeed, *in vivo* interaction studies of eRF1 and eRF3 in *rat8-2* mutants reveal a ~70% reduction of eRF1 binding to the ribosome and to eRF3 upon a 1 h temperature shift to 37°C (Figure 3D and E). The reduced eRF1 and eRF3 interaction was also de-

tected earlier and seems to happen immediately, already after a 20 min temperature shift of the *rat8-2* strain. However, the ribosomal binding of eRF1 was less obviously decreased after this short shifting time (10). But the longer 1 h shift produces a clear ribosome binding defect of eRF1 (Figure 3D and E). Together, our findings suggest that Dbp5 might deliver eRF1 to the ribosome without eRF3.

Nup159 recycles Dbp5–ADP for export and translation termination

The ATPase activity of Dbp5 is essential not only for mRNA transport, but also for translation termination

(10,16,17). During termination, we suggest that the helicase might deliver eRF1 and it seems possible that it could use its ATPase-dependent activity to position eRF1 properly on the stop codon. In particular, because we have shown earlier that its ATPase activity is necessary not only for its function in mRNA export, but also for its role in translation termination (10). In both cases, upon ATP-hydrolysis, the enzyme needs to be recycled. During mRNA export, the nucleoporin Nup159/Rat7 is the ADP-release factor of Dbp5 (17). Thus, it is conceivable that recycling from termination also occurs at the NPC via Nup159, rather than at the ribosome. In particular, because Dbp5 must return to the cytoplasm to capture a new molecule of eRF1 as they first interact in the soluble fraction of the cytosol (Figure 1). Indeed, readthrough experiments with a dual β-galactosidase luciferase reporter system show an increased readthrough activity in different *nup159* mutants, very similar to the *dbp5* mutant *rat8-2* (Figure 4A and B), (10). As both *nup159* mutants, *rat7-1* and *rat7ΔN*, the latter of which specifically lacks the interaction domain for Dbp5 (34), exhibit increased readthough activities as compared to wild-type (Figure 4B), Nup159 seems to be the recycling factor for Dbp5 not only for mRNA export, but also for translation termination. In support of this model, we found that overexpression of *DBP5* leads to a rescue of the high readthrough activity in *rat7ΔN* cells (Figure 4C) indicating that less recycling by Nup159 is needed when more Dbp5–ATP is present.

These results suggest that Nup159 recycles Dbp5–ADP also upon its action in translation termination, which is quite attractive, because in this way Dbp5 might couple two important cellular processes—nuclear mRNA export and translation. When the translation rate is low, Dbp5 is free to increasingly act in mRNA export to raise the mRNA amount in the cytoplasm and vice versa, high translation rates could reduce mRNA export. To verify a dependence of the eRF1–Dbp5 interaction on Nup159, because their contact should only be established when Dbp5 is ATP-bound, we performed co-IPs with these proteins in *rat7ΔN*. Indeed, while the interaction of Dbp5 and eRF1 was clearly detectable in wild-type, it was significantly reduced in *rat7ΔN* (Figure 4D and E), supporting a model in which Dbp5 is recycled at the NPC with ATP. These findings further suggest that Dbp5–ATP can bind eRF1, while Dbp5–ADP might release the termination factor. As Dbp5 could not be re-charged in *rat7ΔN* and thus cannot deliver eRF1 to the ribosome anymore, the interaction of eRF1 with eRF3 should also be decreased in this mutant, which is indeed the case as shown by co-IPs (Figure 4F and G).

The switch in eRF1 binding and release through ATP-hydrolysis of Dbp5 was further investigated in *in vitro* experiments with purified recombinantly expressed proteins. We show that Dbp5 only binds to eRF1 in the presence of the non-hydrolysable ATP-analogue AMP–PNP, whereas eRF3 interacts also ATP-independently with eRF1 (Figure 4H). Together, these *in vivo* and *in vitro* studies support a model in which eRF1 associates with Dbp5–ATP in the cytoplasm and dissociates from Dbp5–ADP at the ribosome, where Dbp5 possibly uses its ATP-dependent helicase activity to place eRF1 properly on the stop codon. Moreover

it becomes evident that eRF1 and Dbp5 form a complex in the cytoplasm, from which eRF3 is absent.

Binding of Dbp5 and eRF3 to eRF1 is mutually exclusive

As Dbp5 and eRF1 enter termination complexes together, and Dbp5 does not interact with eRF3 (10), it seems possible that the binding of Dbp5 and eRF3 with eRF1 is mutually exclusive. It was shown that the eRF3-interaction domain of eRF1 comprises the last 25 amino acid residues of its C-terminus (5). *In vitro* binding studies with recombinant proteins were carried out to investigate whether this domain is also the Dbp5-interaction domain. Indeed, while full-length eRF1 interacts with both, eRF3 and Dbp5, no interaction was detectable with eRF1Δ25C (Figure 5A), indicating that both termination factors share the same binding site on eRF1. Interestingly, although also the middle domain of eRF1 was reported to contribute to the eRF1–eRF3 interaction (35), we found that the deletion of the C-terminal domain is sufficient to abrogate the interaction of eRF1 with eRF3 and Dbp5 *in vitro*. Moreover, a preformed interaction of Dbp5 and eRF1 was not disrupted by the addition of increasing amounts of eRF3 in a competition assay (Figure 5B). Intriguingly, these findings suggest indeed a sequential and mutually exclusive binding of Dbp5 and eRF3 to eRF1 with a first complex formation between Dbp5 and eRF1. Thus, a model is possible, in which during the progress of termination, Dbp5–ATP prohibits the access of eRF3 to eRF1 until eRF1 was placed properly in the ribosomal A-site. Such a mechanism would prevent a premature access of eRF3 and a consequent premature GTP-hydrolysis. Because as soon as eRF3 contacts its guanine exchange factor eRF1 at the ribosome, eRF3 binds GTP, which is subsequently hydrolysed, resulting in the immediate dissociation of eRF3 from the ribosome (36,37). The suggested sequential entry of the termination factors would have the advantage that the contact of eRF3 with eRF1 is controlled, which will prevent premature GTP-hydrolysis of eRF3 and its subsequent premature dissociation before the stop codon is successfully recognized.

eRF3 binds to the ribosome prior to eRF1

Protection of eRF1 from premature eRF3 access would only be necessary if eRF3 would already be present at the ribosome when eRF1 enters. Therefore, we analysed its ribosomal association in the *tef2-9* mutant that arrests in translation elongation as shown in Figure 1E and F. Strikingly, eRF3, but almost no eRF1 is detectable in the polysomal fractions of this elongation mutant, suggesting that eRF3 can independently bind ribosomes before they arrive at a stop codon and is therefore already present when eRF1 enters (Figure 6A and B). These findings are supported by co-immunoprecipitation analyses of eRF3 with ribosomal proteins in the mutant *sup45-2*. In the situation in which this mutant eRF1 protein accumulates with Dbp5 in the cytoplasm (Figure 1), the binding of eRF3 to the ribosomal protein uS3 is not reduced, but rather increases as its eRF1 mediated GTP-hydrolysis and release is prevented (Figure 6C and D).

Because Rli1 is also present at that early time point, we investigated a potential direct interaction of eRF3 and Rli1.
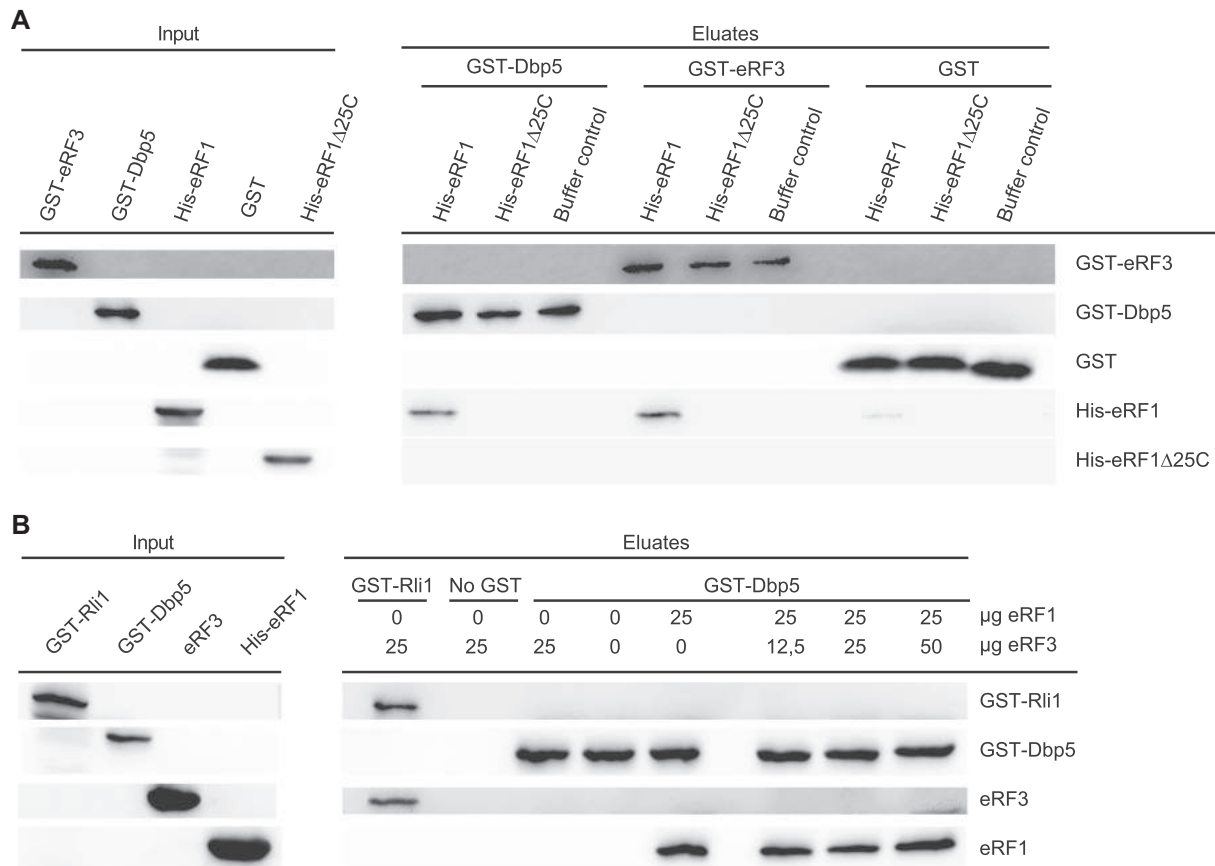
Figure 5. Dbp5 and eRF3 interaction with eRF1 is mutually exclusive. (**A**) The interaction site of eRF1 with Dbp5 and eRF3 overlap. Western blot analyses of pull-downs experiments with GST–Dbp5, GST–eRF3 or GST and His-eRF1 or His-eRF125 lacking the last C-terminal amino acid residues are shown. All binding buffers contained 1 mM AMP–PNP. (**B**) A preformed complex of eRF1 and Dbp5 cannot be disrupted by eRF3. Western blot analysis of a competition assay of the indicated recombinantly expressed proteins is shown. Increasing amounts of eRF3 were added to the preformed complex of GST–Dbp5 and His-eRF1. Rli1 served as a positive control for eRF3 binding. All binding buffers for Figure 5 contained 1 mM AMP–PNP.

In vitro binding studies revealed that either nucleotide free eRF3, or GDP-bound but not GTP-bound eRF3 directly interacts with Rli1 (Figure 6E), (23), suggesting that Rli1 might bind to eRF3–GDP at the ribosome, where they wait for the arrival of eRF1. Furthermore, Rli1 interacts with eRF3 without the addition of ATP (Figure 6E), supporting a model in which nucleotide-free Rli1 binds to the ribosome and eRF3 and the recruitment of ATP to Rli1 occurs later. As this nucleotide-free state of Rli1 was shown to result in a rather weak association with the ribosome (23), it is conceivable that Rli1 might change its position on the ribosome during the stepwise assembly of all termination factors. Upon eRF1 entry, eRF3 most likely binds to GTP, as its affinity to the triphosphate increases upon eRF1 contact (36,37), which would trigger its dissociation from Rli1, because it interacts only with eRF3–GDP (Figure 6E). These rearrangements in the termination complex through eRF3–GTP-hydrolysis stimulate the eRF1-mediated polypeptide- and tRNA-release by moving eRF1 into its favourable position to terminate translation (37). The poly(A) binding protein Pab1 might further support this early association of eRF3 to the ribosome and Rli1 as eRF3 and Pab1 were shown to interact (38,39).

Dbp5 enables a stable contact of eRF1 and eRF3 at the ribosome

In a model in which Dbp5 delivers eRF1 and prevents premature excess of eRF3, one would expect that in a situation in which the Dbp5 binding to eRF1 is inhibited, the release factor might be able to access the ribosome alone and immediately contact eRF3. This situation should result in the immediate dissociation of eRF1 and eRF3 from each other and from the ribosome, because their contact would not be prevented until eRF1 was properly positioned by Dbp5. This is indeed the case. In a mutant of the Dbp5 recycling factor Nup159, *rat7ΔN*, Dbp5 remains ADP-bound, which prevents its complex formation with eRF1 (Figure 4D), or in mutant *DBP5*, such as *rat8-2*, in which the protein is detached from the NPC at 37°C and not re-charged with ATP (40), eRF1 is not Dbp5 bound. In both cases, the freely available eRF1 leads to the reduced presence of eRF1 and eRF3 at the ribosome as reflected in uS3 co-IPs (Figure 6F–I). Possibly eRF1 and eRF3 are less present at the ribosome, because both release factors instantly dissociate upon their uncontrolled contact, because their contact initiates the GTP-binding of eRF3, its subsequent hydrolysis, which triggers the dissociation of eRF1 and eRF3. Such
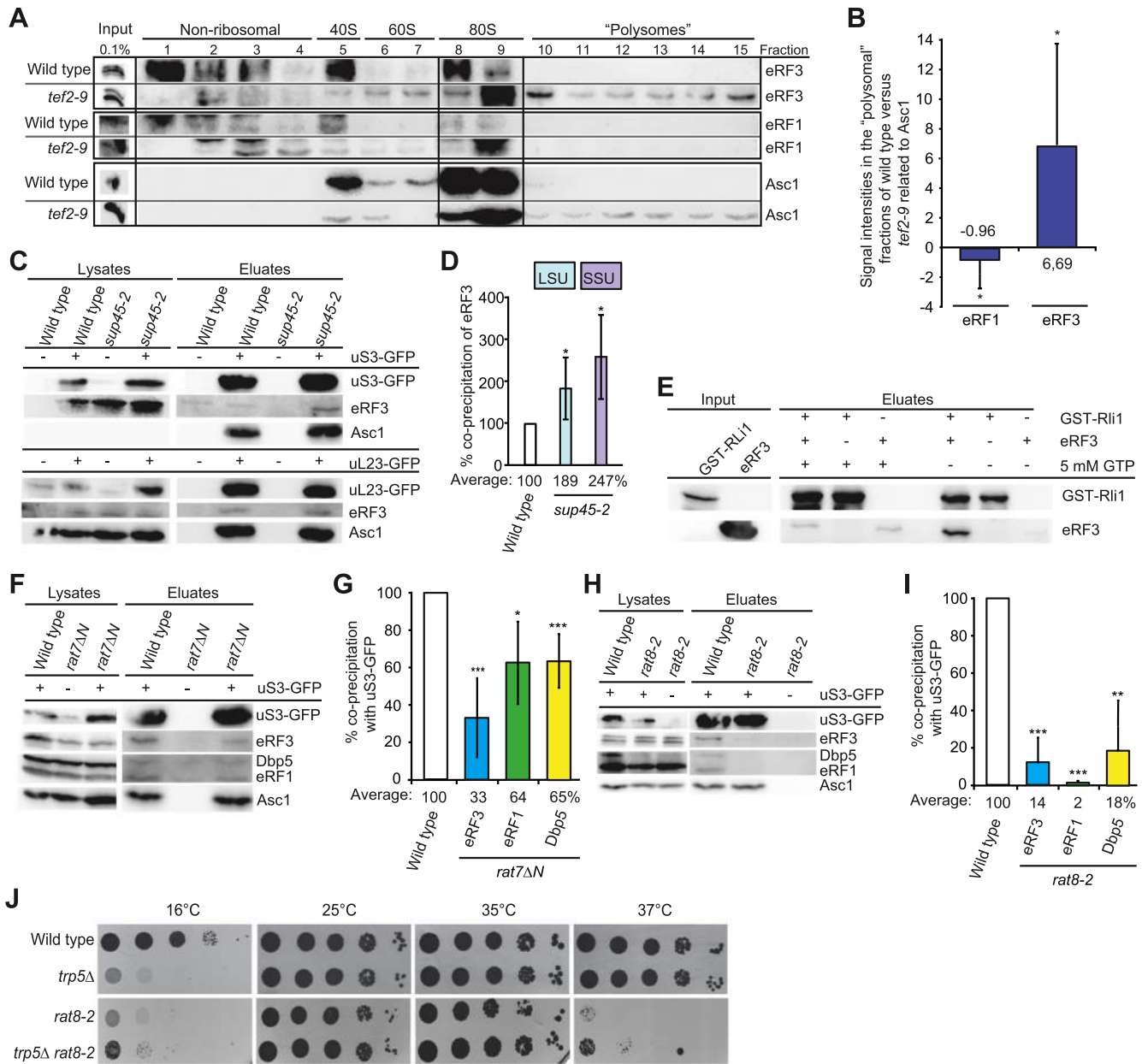
Figure 6. eRF3–GDP binds Rli1 prior to the entry of Dbp5 and eRF1. (**A**) eRF3 is present on ribosomes stalled in translation elongation. Western blot analysis of the collected fractions of the *tef2-9* gradient shown in Figure 1E with antibodies against eRF3, eRF1 and Asc1 are displayed. (**B**) Quantification of four different western blot analyses shown in panel (A). (**C**) Ribosome binding of eRF3 in *sup45-2* is increased. Western blot analysis of co-IPs of eRF3 and the positive control Asc1 with uS3 (top) and uL29 (bottom) are shown. (**D**) Quantification of four different IPs shown in (C). (**E**) Rli1 binds nucleotide free eRF3 directly and releases eRF3-GTP. Western blot analysis of *in vitro* pull-down experiments with Rli1 is shown. (**F–I**) The ribosomal association of eRF1, eRF3 and Dbp5 is decreased in *nup159* (F and G) or *dbp5* (H and I) mutants. Western blot analyses of the uS3-co-precipitated proteins in the indicated strains are shown. (**G and I**) Quantification of four (G) and three (I) different IPs shown in panels (F) and (H), respectively. (**J**) Defects in eRF1 delivery partially suppresses the growth defects of *trp5Δ*. Serial dilutions of the indicated strains are shown upon growth on full medium agar plates at the indicated temperatures; *P < 0.05; **P < 0.01; ***P < 0.001.

premature contact would support the observed increased readthrough activity (Figure 4B and C).

It is quite intriguing that Dbp5 controls the entry of eRF1 into termination reactions. However, this novel function might have an impact not only at termination codons on readthrough activity, but also on termination events at near cognate codons, such as the UGG tryptophan codon that is similar to the stop codon UGA. In such situation it is observed that mRNA translation is not continued and instead translation termination occurs. To investigate whether Dbp5 would genetically interact with the tryptophan synthetase mutant *trp5Δ*, we generated the *rat8-2 trp5Δ* double mutant and monitored the growth at different temperatures. We found that the double mutant partially suppresses both single mutants at 16°C and *rat8-2* strain also at higher temperatures. This suppression phenotype suggests that mu-

tations in *DBP5* indeed affect termination events at near cognate codons and the deleterious effect of the trp5 deletion stems from inefficient decoding of UGG codons, and increased eRF1-catalysed mistermination events on such codons. This effect appears suppressed in *rat8-2* mutants where the delivery of eRF1 to such codons would be reduced (Figure 6J).

eIF3 enters translation termination after the Dbp5-mediated delivery of eRF1

In addition to eRF1, eRF3, Rli1 and Dbp5, the translation initiation factor, eIF3 with its subunit Hcr1 were shown to participate in translation termination (15). Mutations in eIF3 reduce the rate of stop codon readthrough, while *hcr1Δ* shows an increased readthrough activity and this phenotype was suppressed by high copy Rli1. A model was proposed in which Hcr1 is not a bona fide translation initiation factor, but rather acts in termination by promoting GDP–eRF3 ejection from the ribosomes (15). In such a model Dbp5 would not bind to Hcr1, because it would dissociate before Hcr1 would contact eRF3. To investigate this, we carried out co-IPs with Hcr1 and Dbp5 and could confirm the Hcr1 eRF3 interaction, while no interaction between Hcr1 and Dbp5 was visible (Figure 7A). Interestingly, also the interaction of Hcr1 with the ribosome is less strong as that of eRF1, supporting the model that Hcr1 ejects eRF3 from the ribosome. eIF3 was suggested to promote ribosome recycling after termination. As such, one would expect the complex to bind after translation termination. Indeed, one of the eIF3 subunits Prt1 clearly interacts with Rli1, eRF3, eRF1 and the ribosome, represented by Asc1 in wild-type cells, but these interactions were abrogated in *sup45-2* cells, in which the termination reaction does not occur (Figure 7B). A Dbp5 Prt1 interaction was not detected, which might suggest that a potential interaction is either rather short or Prt1 associates only after Dbp5 has delivered eRF1. We further show in co-IPs that the interaction of eIF3 with Rli1 and the ribosome is independent on the ATP-binding of Rli1, because both eIF3 subunits, Prt1 and Nip1 interact without or with the addition of AMP–PNP (Figure 7C).

These data support the following stepwise entry model for translation termination in yeast (Figure 8). Nucleotide-free Rli1 binds to the ribosome as soon as the A-site is unoccupied. eRF3–GDP associates with Rli1 and waits for the entrance of eRF1. Rli1 furthermore supports the entry of eRF1 into the ribosome, which is delivered and positioned at the stop codon by the helicase Dbp5. The contact of eRF3 and eRF1 is controlled by the dissociation of Dbp5, which occurs upon hydrolysis of its ATP through Gle1- and IP$_6$-stimulation. ADP–Dbp5 recycling is mediated at the NPC through Nup159, which couples translation to mRNA-export. Dissociation of Dbp5 allows contact of eRF1 and eRF3, which stimulates eRF3 to associate with GTP and induces a stronger binding to Rli1, which might indicate that Rli1 changes its position. The subsequent GTP-hydrolysis of eRF3 results in the final positioning of eRF1, dissociation of eRF3–GDP by Hcr1, which is delivered by eIF3 to the ribosome and to peptidyl-tRNA hydrolysis and polypeptide chain release from the ribosome.

Subsequent recycling of the ribosomal subunits is mediated by Rli1 (4,23,26).

DISCUSSION

Translation termination depends on the two key factors eRF1 and eRF3, but also on Dbp5 and Rli1 (10,13). However, their function and the order in which the termination complex assembles, was unclear. Current models suggest that eRF1 and eRF3 enter the ribosome together as a complex (1,2,4), but we show here that this is very unlikely and propose a new translation termination model in which the termination complex assembles stepwise (Figure 8).

Polysomal gradients and co-IPs indicate that nucleotide-free Rli1 and eRF3–GDP binds to the ribosome prior to eRF1 and Dbp5 entry (Figures 1 and 6). Our data support a function of Rli1 in promoting the recruitment of the other termination factors. In particular, it promotes the binding of the Dbp5–eRF1 complex leading to the formation of a ternary complex with Rli1 (Figures 2F–H and 6E). For such a function, Rli1 would not require its ATPase activity, which is in agreement with earlier studies in which it was shown that ATP-hydrolysis by Rli1 does not take place during the termination process (4,13). It was furthermore suggested earlier that Rli1 associates with the termination complex upon dissociation of eRF3–GDP, taking over its position to lock eRF1 in its favourable position to facilitate peptidyl-tRNA hydrolysis (4,26). In contrast to this model, we present evidence that Rli1 and eRF3–GDP are the initial components of the termination complex that bind to the ribosome. However, our data are in agreement with a model in which in the course of the stepwise assembly, Rli1 could take over the position of eRF3, because initially eRF3 binds to Rli1 in its GDP bound form and dissociates upon GTP binding and hydrolysis (Figure 6E), which could allow the remodelling of the complex and enable Rli1 to occupy the eRF3 position upon its release. Because Rli1 is most likely nucleotide-free in this early stage of translation termination (Figure 6E), it is conceivable that the rearrangements upon eRF3 dissociation might be supported by its binding to ATP, which is later on required for the splitting of the ribosomal subunits (23,24). However, it is also possible that the entry of eIF3 and/or the dissociation of eRF3 through Hcr1 (Figure 7A–C) induce these rearrangements.

In contrast to earlier models, our results furthermore indicate that Dbp5–ATP captures eRF1 in the cytoplasm (Figures 3A,C and 4D) and delivers it to the stop codon-bound ribosome on which eRF3–GDP and Rli1 are already present (Figures 1F,G and 6A,B). The interaction between Rli1 and Dbp5 might thereby support the Dbp5–eRF1 recruitment (Figure 2). Upon placing eRF1 properly on the stop codon, Dbp5–ADP dissociates and is recycled at the NPC via Nup159 (Figure 4). In this way, the two key processes of mRNA export and translation are coupled via Dbp5. How the duty of Dbp5 in both processes is divided and how Dbp5 captures eRF1 is currently unclear and needs further investigation. Interestingly, the overall cellular protein abundance estimates suggest an intracellular Dbp5:eRF1:eRF3 ratio of ∼1:2:4 (https://www.yeastgenome.org/). Dbp5 as a limiting factor further qualifies itself as a regulator of the interaction between eRF1 and
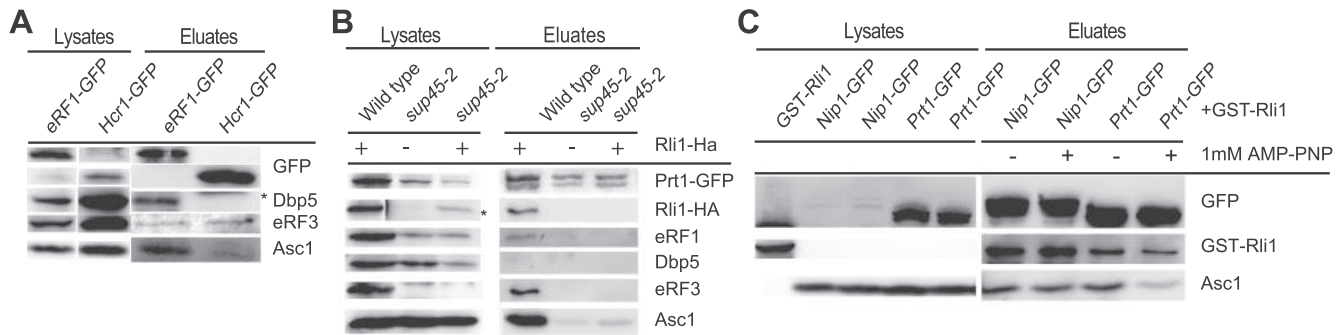
Figure 7. The eIF3 complex binds to the ribosome after the Dbp5-mediated delivery of eRF1. (**A**) The eRF3 release factor Hcr1 does not bind to Dbp5 and only weakly to the ribosome. Co-IPs with GFP-tagged Hcr1 and as a control eRF1–GFP with Dbp5, eRF3 and the ribosomal protein Asc1 are shown. The asterisk indicates Hcr1–GFP. (**B**) Defects in the eRF1 delivery result in the absence of the eIF3 subunit Prt1 at the ribosome. Co-IPs of GFP-tagged Prt1 with HA-tagged Rli1, eRF1, Dbp5, eRF3 and the ribosomal protein Asc1 are shown in wild-type and *sup45-2* strains. The asterisk indicates that the *sup45-2* lysate lanes were exposed four times as long as the wild-type lanes. (**C**) The binding of the eIF3 subunits Prt1 and Nip1 are independent of the nucleotide association of Rli1. The GFP-tagged eIF3 subunits were precipitated and the co-precipitated GST-tagged Rli1 and Asc1 are shown.

eRF3, because only the Dbp5-delivered eRF1 can engage in proper termination events. Excess of eRF1 over Dbp5 might be required, because it participates also in ribosome recycling (4,23,26) and thus remains bound for a longer time. The high amounts of eRF3 might be required, because it waits on every ribosome at late stages of elongation (Figure 6A and B) for eRF1 to enter. In support of this view, it is interesting to note that a 20% decrease of the basal cellular protein levels of Dbp5 or eRF1 already negatively impact protein biosynthesis, while a 60% decrease of eRF3 has no effect (14). Thus, the Dbp5-mediated delivery of eRF1 is the rate-limiting step, supporting a view that Dbp5 controls the termination event.

Interestingly, our *in vivo* results clearly show that Dbp5 is not bound to the ribosome during elongation (Figures 1F, G, 2D and E), although its human homolog DDX19 has been shown to stabilize translation elongation *in vitro* (14). This might either be a difference between the human and the yeast helicase, but it is also conceivable that in the *in vivo* situation a contact of Dbp5 with the elongating ribosome is prevented and its recruitment is only possible when bound to eRF1.

Importantly, the simultaneous entry of Dbp5 and eRF1 in a complex has the advantage that Dbp5 protects eRF1 from premature access to eRF3, because Dbp5 occupies the binding domain of eRF3, located at the last 25 amino acid residues of the C-terminal domain (Figure 5). This is particularly important, because eRF3 is already present at the ribosome, when Dbp5–eRF1 enters (Figure 6A and B). In fact, a separated entry of eRF1 and eRF3 is actually supported by earlier studies, showing that a reduced eRF3 expression does not lead to a decreased ribosomal association of eRF1 (3).

In situations of defective Dbp5 or Dbp5–ATP recycling, as in the *rat8-2* and *nup159ΔN* mutants, respectively, the protected eRF1 delivery to the ribosome cannot occur and eRF1 can contact eRF3 prior to its proper positioning and stop codon recognition. This contact would induce eRF3 to release GDP and bind GTP, because the affinity of eRF3 to GTP strongly increases upon eRF1 contact (36,37). This in turn can trigger the premature GTP-hydrolysis and subsequent dissociation of eRF3–GDP and eRF1 from each

other and the ribosome (Figure 6F–I), as evident in these mutants (Figures 3D, E, 4F and G). In support of such a model, it is interesting to note that a reduced binding of eRF3 to polysomes was already detected in *rat8-2* cells upon a very short, 20 min temperature shift to the non-permissive temperature and in mutants of the co-factor of Dbp5, *GLE1* (10,12). As eRF1 would not have been properly positioned when Dbp5 cannot deliver it, stop codon recognition, polypeptide chain- and tRNA-release would be unsuccessful and translation might be continued with near-cognate tRNAs, resulting in the observed readthrough activity in *nup159* and *dbp5* mutants (Figure 4B and C). Longer temperature shifts of both mutants and thus constant defects in stop codon recognition and mRNA transport cannot be tolerated and are lethal to cells (33,34).

Dbp5 not only impacts stop codon readthrough, but also controls the delivery of eRF1 to near-cognate codons, such as the UGG tryptophan codon, suggested by its suppression of the *trp5Δ* strain (Figure 6J). This supports a view, in which Dbp5 controls the delivery of eRF1. This discovery further suggests that cells may use this system to trigger stop codon readthrough in particular situations. Stress for example changes the expression program of cells, as it blocks bulk mRNA export, while it allows the uncontrolled export of stress specific mRNAs (41,42). Such massive changes in the cellular expression program might also involve Dbp5. Intriguingly, it was reported that Dbp5 mislocalizes to the nucleus upon ethanol stress (43), which would circumvent the helicase to support efficient termination and rather promote the readthrough of stop codons. Also during glucose starvation, in which the ATP-production is reduced, Dbp5 is most likely not efficiently re-charged with ATP, which in turn should reduce the Dbp5-mediated eRF1 delivery and result in an increased readthrough of stop codons.

Generally, stop codon readthrough has the potential to create proteins with new or additional functions. Extended C-termini could for instance add nuclear localization signals to normally cytoplasmic proteins and in this way redirect them to the nucleus. It is also possible that the longer protein is unstable and quickly degraded. Moreover, when no additional stop codon is present in an mRNA upon readthrough, the ribosome subsequently decodes the
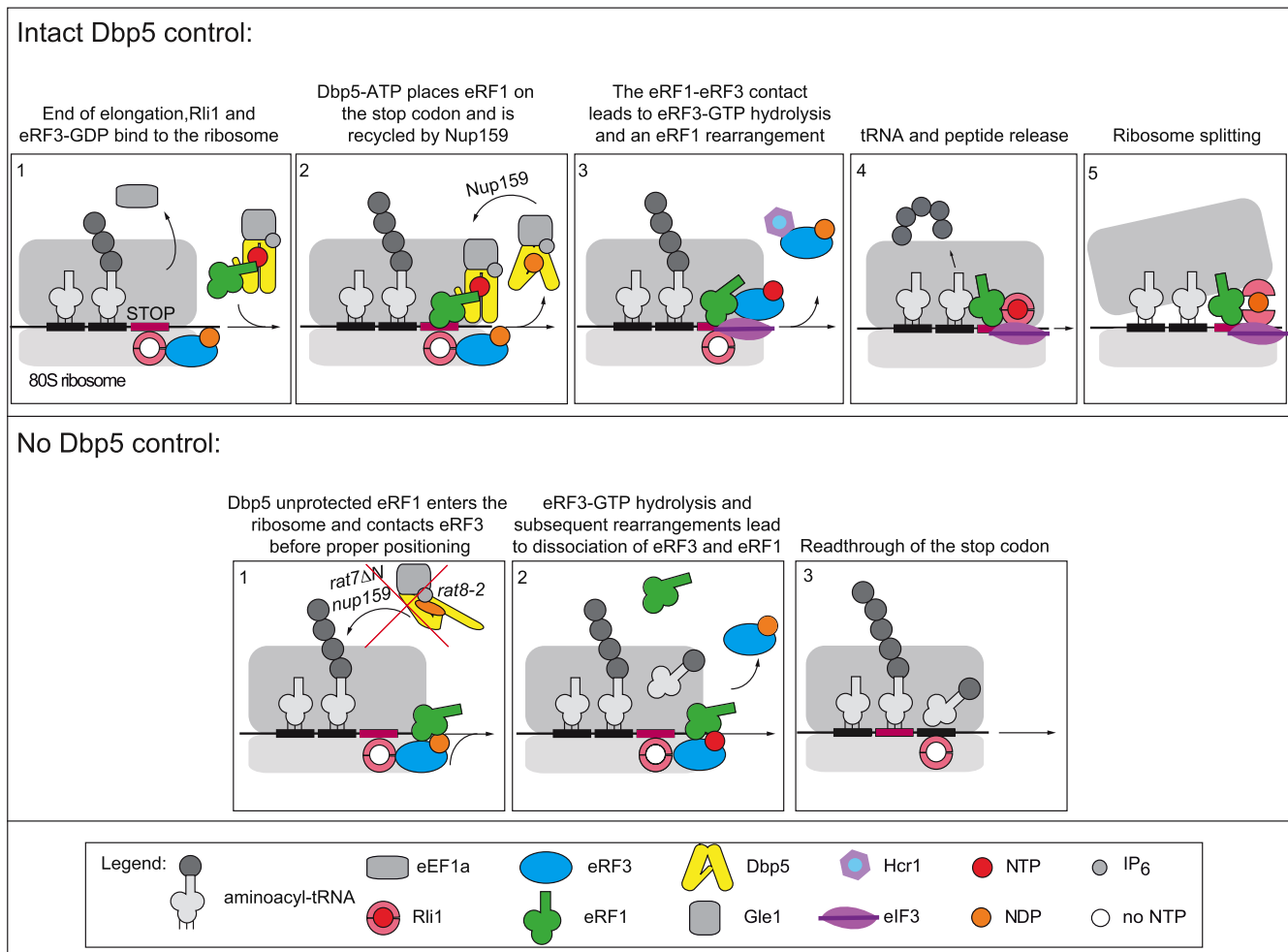
Figure 8. Stepwise entry model for translation termination. (Top) Step 1: Nucleotide-free Rli1 associates with the ribosomes as soon as the A-site is free. It binds to eRF3–GDP. Step 2: Rli1 supports the entry of Dbp5–ATP bound eRF1. Gle1/IP$_6$ stimulated ATP-hydrolysis of Dbp5–ATP leads to the proper positioning of eRF1 on the stop codon. Dbp5–ADP dissociates and is recycled at the nuclear pore complex by Nup159. Step 3: Dissociation of Dbp5–ADP allows the controlled interaction of eRF1 with eRF3. This in turn triggers the GTP recruitment of eRF3. Subsequent GTP hydrolysis leads to conformational changes in eRF1 allowing adjustments in its positioning in the ribosomal peptidyl-transferase center. eRF3–GDP dissociates in a complex with Hcr1, which was delivered by eIF3. Step 4: eRF3–GDP dissociation allows change of position and strong binding of Rli1–ATP that locks eRF1 in the position necessary to mediate peptidyl-tRNA hydrolysis. Step 5: Upon peptide release, ATP-hydrolysis of Rli1–ATP recycles the ribosomal subunits, which is supported by eRF1. (Bottom) Situation in which Dbp5 cannot deliver eRF1 to the ribosome that consequently results in the stop codon readthrough. Step1: Rli1 associates and binds eRF3–GDP. Step 2: eRF1 is not protected by Dbp5 and contacts eRF3 before being properly positioned, leading to premature GTP-binding, hydrolysis and the subsequent release of eRF1 and eRF3–GDP from the ribosome before the polypeptide chain and the tRNA are released. Because eRF1 had contact to eRF3 before it was placed in the optimal position, it dissociates at the same time as eRF3. Step3: A near-cognate tRNA gets access to the A-site, the stop codon is suppressed and translation elongation continues until the next stop codon is reached.

mRNA into the poly(A) tail. In such cases, the consequence is the degradation of the protein and the mRNA by the no-stop decay (NSD) system (44). In higher eukaryotes e.g. in Drosophila or mammals, stop codon readthrough occurs also during developmental processes and is called functional translational readthrough (FTR) (45,46). In these cases, the stop codons are suppressed and treated as sense codons due to the competition between eRF1 and near-cognate tRNAs at the A-site. It is tempting to speculate that Dbp5/DDX19 might be involved in regulating such processes.

Most interestingly, one-third of all inherited disorders are caused by protein truncating pre-termination mutations that lead to non-functional proteins or cause dominant neg-

ative effects, leading to cancer and neurodegenerative diseases (47,48). Nonsense suppression therapies comprise approaches aiming at suppressing translation termination at in-frame premature stop codons to restore the deficient protein function. Using Dbp5/DDX19 as a drug target to decrease its function and increase readthrough at premature stop codons for suppression therapy might be a novel starting point for therapies.

SUPPLEMENTARY DATA

Supplementary Data are available at NAR Online.

REFERENCES

1. Jackson,R.J., Hellen,C.U. and Pestova,T.V. (2012) Termination and post-termination events in eukaryotic translation. *Adv. Protein Chem. Struct. Biol.*, **86**, 45–93.
2. Alkalaeva,E.Z., Pisarev,A.V., Frolova,L.Y., Kisselev,L.L. and Pestova,T.V. (2006) In vitro reconstitution of eukaryotic translation reveals cooperativity between release factors eRF1 and eRF3. *Cell*, **125**, 1125–1136.
3. Salas-Marco,J. and Bedwell,D.M. (2004) GTP hydrolysis by eRF3 facilitates stop codon decoding during eukaryotic translation termination. *Mol. Cell. Biol.*, **24**, 7769–7778.
4. Shoemaker,C.J. and Green,R. (2011) Kinetic analysis reveals the ordered coupling of translation termination and ribosome recycling in yeast. *Proc. Natl. Acad. Sci. USA*, **108**, E1392–E1398.
5. Eurwilaichitr,L., Graves,F.M., Stansfield,I. and Tuite,M.F. (1999) The C-terminus of eRF1 defines a functionally important domain for translation termination in Saccharomyces cerevisiae. *Mol. Microbiol.*, **32**, 485–496.
6. Merkulova,T.I., Frolova,L.Y., Lazar,M., Camonis,J. and Kisselev,L.L. (1999) C-terminal domains of human translation termination factors eRF1 and eRF3 mediate their in vivo interaction. *FEBS Lett.*, **443**, 41–47.
7. Cheng,Z., Saito,K., Pisarev,A.V., Wada,M., Pisareva,V.P., Pestova,T.V., Gajda,M., Round,A., Kong,C., Lim,M. *et al.* (2009) Structural insights into eRF3 and stop codon recognition by eRF1. *Genes Dev.*, **23**, 1106–1118.
8. des Georges,A., Hashem,Y., Unbehaun,A., Grassucci,R.A., Taylor,D., Hellen,C.U., Pestova,T.V. and Frank,J. (2014) Structure of the mammalian ribosomal pre-termination complex associated with eRF1.eRF3.GDPNP. *Nucleic Acids Res.*, **42**, 3409–3418.
9. Taylor,D., Unbehaun,A., Li,W., Das,S., Lei,J., Liao,H.Y., Grassucci,R.A., Pestova,T.V. and Frank,J. (2012) Cryo-EM structure of the mammalian eukaryotic release factor eRF1-eRF3-associated termination complex. *Proc. Natl. Acad. Sci. USA*, **109**, 18413–18418.
10. Gross,T., Siepmann,A., Sturm,D., Windgassen,M., Scarcelli,J.J., Seedorf,M., Cole,C.N. and Krebber,H. (2007) The DEAD-box RNA helicase Dbp5 functions in translation termination. *Science* , **315**, 646–649.
11. Alcazar-Roman,A.R., Bolger,T.A. and Wente,S.R. (2010) Control of mRNA export and translation termination by inositol hexakisphosphate requires specific interaction with Gle1. *J. Biol. Chem.*, **285**, 16683–16692.
12. Bolger,T.A., Folkmann,A.W., Tran,E.J. and Wente,S.R. (2008) The mRNA export factor Gle1 and inositol hexakisphosphate regulate distinct stages of translation. *Cell*, **134**, 624–633.
13. Khoshnevis,S., Gross,T., Rotte,C., Baierlein,C., Ficner,R. and Krebber,H. (2010) The iron-sulphur protein RNase L inhibitor functions in translation termination. *EMBO Rep.*, **11**, 214–219.
14. Mikhailova,T., Shuvalova,E., Ivanov,A., Susorov,D., Shuvalov,A., Kolosov,P.M. and Alkalaeva,E. (2017) RNA helicase DDX19 stabilizes ribosomal elongation and termination complexes. *Nucleic Acids Res.*, **45**, 1307–1318.
15. Beznoskova,P., Cuchalova,L., Wagner,S., Shoemaker,C.J., Gunisova,S., von der Haar,T. and Valasek,L.S. (2013) Translation initiation factors eIF3 and HCR1 control translation termination and stop codon read-through in yeast cells. *PLoS Genet.*, **9**, e1003962.
16. Tieg,B. and Krebber,H. (2013) Dbp5 - From nuclear export to translation. *Biochim. Biophys. Acta*, **1829**, 791–798.
17. Noble,K.N., Tran,E.J., Alcazar-Roman,A.R., Hodge,C.A., Cole,C.N. and Wente,S.R. (2011) The Dbp5 cycle at the nuclear pore complex during mRNA export II: nucleotide cycling and mRNP remodeling by Dbp5 are controlled by Nup159 and Gle1. *Genes Dev.*, **25**, 1065–1077.
18. Neumann,B., Wu,H., Hackmann,A. and Krebber,H. (2016) Nuclear export of Pre-Ribosomal subunits requires Dbp5, but not as an RNA-Helicase as for mRNA export. *PLoS One*, **11**, e0149571.
19. Kispal,G., Sipos,K., Lange,H., Fekete,Z., Bedekovics,T., Janaky,T., Bassler,J., Aguilar Netz,D.J., Balk,J., Rotte,C. *et al.* (2005) Biogenesis of cytosolic ribosomes requires the essential iron-sulphur protein Rli1p and mitochondria. *EMBO J.*, **24**, 589–598.
20. Strunk,B.S., Novak,M.N., Young,C.L. and Karbstein,K. (2012) A translation-like cycle is a quality control checkpoint for maturing 40S ribosome subunits. *Cell*, **150**, 111–121.
21. Yarunin,A., Panse,V.G., Petfalski,E., Dez,C., Tollervey,D. and Hurt,E.C. (2005) Functional link between ribosome formation and biogenesis of iron-sulfur proteins. *EMBO J.*, **24**, 580–588.
22. Dong,J., Lai,R., Nielsen,K., Fekete,C.A., Qiu,H. and Hinnebusch,A.G. (2004) The essential ATP-binding cassette protein RLI1 functions in translation by promoting preinitiation complex assembly. *J. Biol. Chem.*, **279**, 42157–42168.
23. Pisarev,A.V., Skabkin,M.A., Pisareva,V.P., Skabkina,O.V., Rakotondrafara,A.M., Hentze,M.W., Hellen,C.U. and Pestova,T.V. (2010) The role of ABCE1 in eukaryotic posttermination ribosomal recycling. *Mol. Cell*, **37**, 196–210.
24. Barthelme,D., Dinkelaker,S., Albers,S.V., Londei,P., Ermler,U. and Tampe,R. (2011) Ribosome recycling depends on a mechanistic link between the FeS cluster domain and a conformational switch of the twin-ATPase ABCE1. *Proc. Natl. Acad. Sci. USA*, **108**, 3228–3233.
25. Shoemaker,C.J., Eyler,D.E. and Green,R. (2010) Dom34:Hbs1 promotes subunit dissociation and peptidyl-tRNA drop-off to initiate no-go decay. *Science*, **330**, 369–372.
26. Preis,A., Heuer,A., Barrio-Garcia,C., Hauser,A., Eyler,D.E., Berninghausen,O., Green,R., Becker,T. and Beckmann,R. (2014) Cryoelectron microscopic structures of eukaryotic translation termination complexes containing eRF1-eRF3 or eRF1-ABCE1. *Cell Rep.*, **8**, 59–65.
27. Baierlein,C., Hackmann,A., Gross,T., Henker,L., Hinz,F. and Krebber,H. (2013) Monosome formation during translation initiation requires the serine/arginine-rich protein Npl3. *Mol. Cell. Biol.*, **33**, 4811–4823.
28. Bidou,L., Stahl,G., Hatin,I., Namy,O., Rousset,J.P. and Farabaugh,P.J. (2000) Nonsense-mediated decay mutants do not affect programmed -1 frameshifting. *RNA* , **6**, 952–961.
29. Becker,T., Franckenberg,S., Wickles,S., Shoemaker,C.J., Anger,A.M., Armache,J.P., Sieber,H., Ungewickell,C., Berninghausen,O., Daberkow,I. *et al.* (2012) Structural basis of highly conserved ribosome recycling in eukaryotes and archaea. *Nature*, **482**, 501–506.
30. Stansfield,I., Kushnirov,V.V., Jones,K.M. and Tuite,M.F. (1997) A conditional-lethal translation termination defect in a sup45 mutant of the yeast Saccharomyces cerevisiae. *Eur J Biochem.*, **245**, 557–563.
31. Dinman,J.D. and Kinzy,T.G. (1997) Translational misreading: mutations in translation elongation factor 1alpha differentially affect programmed ribosomal frameshifting and drug sensitivity. *RNA* , **3**, 870–881.
32. Anand,M., Chakraburtty,K., Marton,M.J., Hinnebusch,A.G. and Kinzy,T.G. (2003) Functional interactions between yeast translation eukaryotic elongation factor (eEF) 1A and eEF3. *J. Biol. Chem.*, **278**, 6985–6991.
33. Snay-Hodge,C.A., Colot,H.V., Goldstein,A.L. and Cole,C.N. (1998) Dbp5p/Rat8p is a yeast nuclear pore-associated DEAD-box protein essential for RNA export. *EMBO J.*, **17**, 2663–2676.
34. Hodge,C.A., Colot,H.V., Stafford,P. and Cole,C.N. (1999) Rat8p/Dbp5p is a shuttling transport factor that interacts with Rat7p/Nup159p and Gle1p and suppresses the mRNA export defect of xpo1-1 cells. *EMBO J.*, **18**, 5778–5788.
35. Kononenko,A.V., Mitkevich,V.A., Dubovaya,V.I., Kolosov,P.M., Makarov,A.A. and Kisselev,L.L. (2008) Role of the individual domains of translation termination factor eRF1 in GTP binding to eRF3. *Proteins*, **70**, 388–393.

36. Frolova,L., Le Goff,X., Zhouravleva,G., Davydova,E., Philippe,M. and Kisselev,L. (1996) Eukaryotic polypeptide chain release factor eRF3 is an eRF1- and ribosome-dependent guanosine triphosphatase. *RNA* , **2**, 334–341.

37. Pisareva,V.P., Pisarev,A.V., Hellen,C.U., Rodnina,M.V. and Pestova,T.V. (2006) Kinetic analysis of interaction of eukaryotic release factor 3 with guanine nucleotides. *J. Biol. Chem.*, **281**, 40224–40235.

38. Jacobson,A. (2005) The end justifies the means. *Nat. Struct. Mol. Biol.*, **12**, 474–475.

39. Uchida,N., Hoshino,S., Imataka,H., Sonenberg,N. and Katada,T. (2002) A novel role of the mammalian GSPT/eRF3 associating with poly(A)-binding protein in Cap/Poly(A)-dependent translation. *J. Biol. Chem.*, **277**, 50286–50292.

40. Scarcelli,J.J., Viggiano,S., Hodge,C.A., Heath,C.V., Amberg,D.C. and Cole,C.N. (2008) Synthetic genetic array analysis in Saccharomyces cerevisiae provides evidence for an interaction between RAT8/DBP5 and genes encoding P-body components. *Genetics*, **179**, 1945–1955.

41. Zander,G., Hackmann,A., Bender,L., Becker,D., Lingner,T., Salinas,G. and Krebber,H. (2016) mRNA quality control is bypassed for immediate export of stress-responsive transcripts. *Nature*, **540**, 593–596.

42. Zander,G. and Krebber,H. (2017) Quick or quality? How mRNA escapes nuclear quality control during stress. *RNA Biol.*, **14**, 1642–1648.

43. Takemura,R., Inoue,Y. and Izawa,S. (2004) Stress response in yeast mRNA export factor: reversible changes in Rat8p localization are caused by ethanol stress but not heat shock. *J. Cell Sci.*, **117**, 4189–4197.

44. Shoemaker,C.J. and Green,R. (2012) Translation drives mRNA quality control. *Nat. Struct. Mol. Biol.*, **19**, 594–601.

45. Schueren,F. and Thoms,S. (2016) Functional translational Readthrough: A systems biology perspective. *PLoS Genet.*, **12**, e1006196.

46. von der Haar,T. and Tuite,M.F. (2007) Regulated translational bypass of stop codons in yeast. *Trends Microbiol.*, **15**, 78–86.

47. Bordeira-Carrico,R., Pego,A.P., Santos,M. and Oliveira,C. (2012) Cancer syndromes and therapy by stop-codon readthrough. *Trends Mol. Med.*, **18**, 667–678.

48. Keeling,K.M., Xue,X., Gunn,G. and Bedwell,D.M. (2014) Therapeutics based on stop codon readthrough. *Annu. Rev. Genomics Hum. Genet.*, **15**, 371–394.

Review

Dbp5/DDX19 between Translational Readthrough and Nonsense Mediated Decay

Christian Beißel †, Sebastian Grosse † and Heike Krebber *

Abteilung für Molekulare Genetik, Institut für Mikrobiologie und Genetik, Göttinger Zentrum für Molekulare Biowissenschaften (GZMB), Georg-August Universität Göttingen, 37077 Göttingen, Germany; christian.beissel@biologie.uni-goettingen.de (C.B.); sgrosse@gwdg.de (S.G.)

* Correspondence: heike.krebber@biologie.uni-goettingen.de

† These authors contributed equally.

check for updates

Abstract: The DEAD-box protein Dbp5 (human DDX19) remodels RNA-protein complexes. Dbp5 functions in ribonucleoprotein export and translation termination. Termination occurs, when the ribosome has reached a stop codon through the Dbp5 mediated delivery of the eukaryotic termination factor eRF1. eRF1 contacts eRF3 upon dissociation of Dbp5, resulting in polypeptide chain release and subsequent ribosomal subunit splitting. Mutations in *DBP5* lead to stop codon readthrough, because the eRF1 and eRF3 interaction is not controlled and occurs prematurely. This identifies Dbp5/DDX19 as a possible potent drug target for nonsense suppression therapy. Neurodegenerative diseases and cancer are caused in many cases by the loss of a gene product, because its mRNA contained a premature termination codon (PTC) and is thus eliminated through the nonsense mediated decay (NMD) pathway, which is described in the second half of this review. We discuss translation termination and NMD in the light of Dbp5/DDX19 and subsequently speculate on reducing Dbp5/DDX19 activity to allow readthrough of the PTC and production of a full-length protein to detract the RNA from NMD as a possible treatment for diseases.

Translational control is an organized and adaptable mechanism, which is vital for all organisms in life. The expression level and the quality of the protein expressed from a protein-coding gene depend both on the stability and on the quality of the expressed mRNA. Eukaryotic cells have evolved nuclear and cytoplasmic mRNA surveillance systems. Nuclear quality control captures transcripts that experience problems in 5'-capping, 3' polyadenylation and/or intron splicing, prevents their nuclear export and initiates their degradation [1–3]. In contrast to that, the cytoplasmic quality control system ensures integrity of the mRNA open reading frame by monitoring ribosomal decoding. If this is not the case and the ribosome stalls without encountering a stop codon, those transcripts are eliminated by the no-go decay (NGD) and no-stop decay (NSD). When a premature termination codon (PTC) is detected, mRNA degradation occurs via the nonsense mediated decay (NMD) [4,5].

In this review we will summarize the process of translation termination with a focus on Dbp5/DDX19. We will then introduce the principles of NMD and explain the role of Dbp5/DDX19 between these two events. Finally, we will discuss why we think that Dbp5/DDX19 might be an interesting drug target to manipulate these processes and use this for potential treatments of diseases.

1. Translation Termination

On normal mRNAs, translation initiation is followed by elongation and ends with termination. Subsequently the ribosomes are split, which is termed ribosome recycling. These processes are linked

through proteins that act comprehensively to maintain the homeostasis of the 40S and 60S ribosomal subunits, important for repeated rounds of translation. Initiation and elongation involve multiple players and several excellent reviews exist that describe the earlier phases of translation in detail [6–8]. Translation termination comprises three key events: (1) Recognition of the stop codon, (2) hydrolysis of the terminal peptidyl-tRNA bond and polypeptide chain release, and (3) ribosome recycling and disassembly of the termination complex. As soon as one of the three stop codons is reached on the RNA, the eukaryotic release factor eRF1 (encoded by *SUP45* in yeast) binds to the ribosomal A-site. eRF1 interacts with the GTPase eRF3 (encoded by *SUP35* in yeast), leading to polypeptide chain release and ribosome recycling [9]. eRF1 consists of three domains, which structurally mimic the shape of tRNAs with which it competes for binding to the ribosome. The N terminal domain, which comprises the YxCxxxF and TASNIKS motifs, is most important for recognition and binding to the stop codon [10–12]. The central domain on the other hand, especially the methylated GGQ motif, is necessary for the hydrolysis of the peptidyl-tRNA bond [13]. The C-terminal domain of eRF1 finally contacts eRF3, leading to its GTP-binding and subsequent hydrolysis and results in a conformational change important for proper termination [14,15]. Importantly, GTP hydrolysis of eRF3 leads to the dissociation of eRF1 and eRF3, allowing eRF1 to interact with Rli1 (ABCE1 in human) [6]. Rli1 not only functions in translation termination but also has an important function in ribosome splitting by forcing the ribosomal subunits apart through a tweezers-like movement upon NTP-hydrolysis. However, in termination the ordered binding of Rli1 to eRF1 after eRF3 release leads to conformational changes of eRF1, resulting in the aminoacyl bond hydrolysis [16–19].

During ribosome recycling, the ribosomes are split, resulting in free 60S subunit and a 40S subunit bound to mRNA and the deacylated tRNA, and subsequently, the post-termination complexes are disassembled. Recycling requires Rli1 to free the subunits and the eukaryotic initiation factors (eIF) 1, 1A and 3 to prevent reformation of the ribosome through occupying the post-recycled ribosomal subunits [20].

Most of the knowledge about termination and recycling was gained through in vitro assays and kinetic analyses in which nothing seemed to be missing. However, the situation in vivo must be different and regulation of these processes more complex because additional termination factors were discovered. Defects in termination, detected in termination readthrough assays, identified mutations in eIF5A and Pub1 that affect translation termination. Pub1 seems to fine tune termination in different nucleotide surroundings and eIF5A supports eRF1 activity in polypeptide chain release [21,22]. Research, mostly with *Sachharomyces cerevisiae*, identified additional important termination factors. Readthrough defects were furthermore detected in mutants of the initiation factors eIF3 and Hcr1 [23,24] and the DEAD-box RNA helicase Dbp5 [25]. The initiation factors eIF3 and Hcr1 function in the release of the termination complex, which is why Hcr1 is not only considered as bona fide initiation factor anymore. It was shown, that Hcr1, which is delivered by eIF3, releases eRF3-GDP from the ribosome after termination [16,23,24]. The function of Dbp5 in translation termination was surprising. Not only because it has an additional well-known function in mRNA export but also because identification of its function abrogated the prior view that eRF1 and eRF3 would enter the ribosome together.

2. The Function of Dbp5 in Translation Termination

The DEAD-box protein Dbp5 has a well-established function in mRNA export from the nucleus to the cytoplasm [25–29]. Dbp5 (encoded by *RAT8* in yeast and DDX19 in humans) is conserved and essential in all eukaryotes. It acts as an RNA helicase with an ATP dependent RNA- and protein complex remodeling activity [27,30]. Dbp5 belongs to the helicase superfamily 2 (SF2) and contains 13 characteristic sequence motifs and the eponymous sequence Asp-Glu-Ala-Asp (DEAD) in motif 2 (Figure 1) [31]. Dbp5 is localized in the nucleus, in the cytoplasm and concentrated around the nuclear rim [27,32]. A nuclear export signal and a nuclear import signal were identified in the N-terminus of the protein, enabling shuttling between the compartments [33]. The helicase core of Dbp5 is composed

of two highly conserved RecA-like domains linked by a hinge region [34]. The unique N-terminal extension of Dbp5 is important for its autoregulation and determines the specificity of the enzyme [35].
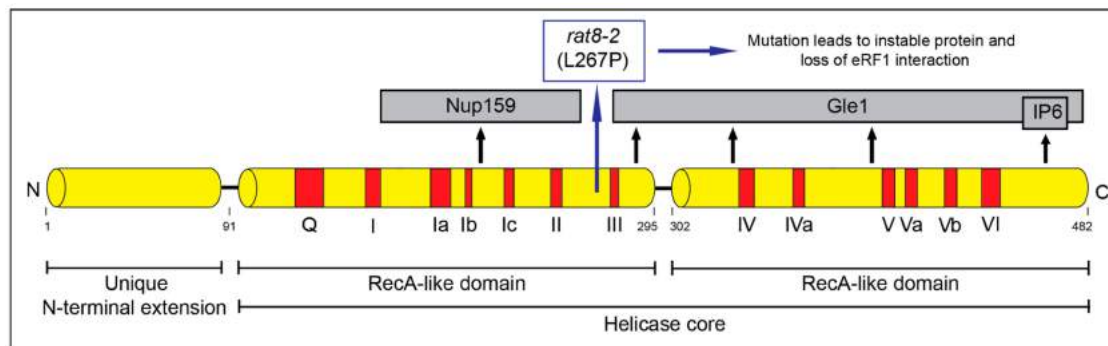

Figure 1. Scheme of the domain structure of Dbp5. Indicated are the domains important for RNA- and ATP binding (red) and the domains important for the interaction partners and co-factors (grey).

In mRNA export, Dbp5 displaces the mRNA export receptor heterodimer Mex67-Mtr2 from the appearing transcript on the cytoplasmic side of the nuclear pore complex (NPC) [36]. Located at the cytoplasmic filaments of the NPC, Dbp5 interacts with the N-terminal domain of its ADP release factor NUP159/Rat7 for recycling, enabling multiple rounds of Mex67-dissociation [27,37,38]. Under physiological conditions, Nup159 is not the only co-factor required for Dbp5 activity but also Gle1-IP$_6$ [38,39]. Gle1-IP$_6$ preferentially binds to ATP-Dbp5 and causes a conformational change to initiate ATPase activity [40,41]. ATP bound Dbp5 shows the highest affinity for single stranded RNA, and the presence of a non-hydrolysable ATP analog leads to tightly bound RNA in vitro [38,42]. Thus, by binding to Gle1, the ATPase- and remodeling-activity of Dbp5 is triggered and the subsequent conformational change allows Nup159 binding and recycling of the helicase [29,40,43,44]. Besides mRNA export, Dbp5 was identified to participate in the nuclear export of pre-ribosomal subunits and tRNA; however, its role in these processes is less well understood [33,45].

The function of Dbp5 in translation termination was first identified in 2007 [25]. Dbp5 was detected in polysomes and mutants of *DBP5* were shown to be hypersensitive to translational inhibitors. In addition, physical interaction of Dbp5 and eRF1 was shown [25]. Subsequently, also Gle1 was identified to co-localize with translating ribosomes and identified as an interaction partner of eRF1 [40,46]. Most importantly, mutations in *DBP5* and *GLE1* caused severe stop codon readthrough defects [25,40]. Likewise, it was recently shown that the human protein DDX19 stabilizes translation termination complexes and participates in termination [47].

Subsequent in vivo and in vitro studies suggest that Dbp5 regulates a stepwise assembly of the termination complex (Figure 2) and [16]. Although not all details are clear and established, the following model suggests the most likely mechanism for translation termination. Unlike what was anticipated in older models, eRF1 and eRF3 presumably do not enter termination together as a complex, but rather Rli1 and eRF3-GDP associate with the ribosome first as soon as the A-site is unoccupied. Subsequently, nucleotide free Rli1 promotes the binding of the Dbp5-eRF1 complex, which formed before in the cytoplasm. After delivery of eRF1 through the helicase Dbp5 and its proper positioning in the A-site of the ribosome, which requires ATP hydrolysis, Dbp5-ADP dissociates. For its recycling Dbp5 moves to the NPC, where it releases the ADP and re-binds to ATP through the actions of Nup159 and Gle1-IP6. Dbp5-ATP then captures a new eRF1 molecule, preparing for the next round of translation termination [16]. The double duty of Dbp5 in mRNA export and in termination, not only couples these important processes but also shows how efficient nature uses one factor for several functions. Remarkably, Gle1 seems to stay longer at the ribosome than Dbp5 and presumably has an additional function in ribosome recycling or translation initiation. This is independent of Dbp5 and IP$_6$, as Gle1 interacts with the eIF3, which was not seen for Dbp5 [16,43,46].
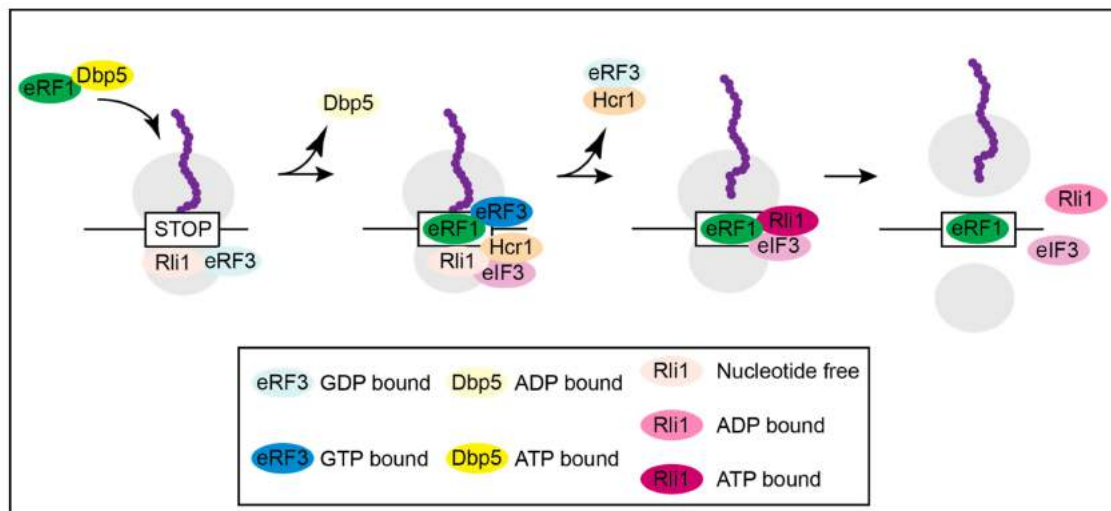
Figure 2. Model for translation termination. The yeast DEAD-box RNA helicase Dbp5 delivers eRF1 to the ribosome located on a stop codon. Its function is to prevent an early contact of eRF1 with eRF3. As soon as eRF1 was placed properly, the ATP-hydrolysis of Dbp5 dissociates the helicase. Free eRF1 subsequently contacts eRF3 that waited in its GDP-bound form attached to Rli1. This contact triggers GTP-binding of eRF3 and subsequent hydrolysis causing polypeptide chain and tRNA release. At the same time, eIF3 delivers Hcr1, which eliminates eRF3 from the complex. Removal of eRF3 enables contact of eRF1 with Rli1-ATP and through ATP-hydrolysis the ribosomal subunits are split.

The scenario at the ribosome after Dbp5 has delivered eRF1 and has left the termination complex continues with the interaction of eRF1 and eRF3 (Figure 2). Their interaction is prevented as long as Dbp5 is bound, because both proteins bind to the C-terminus of eRF1, and their binding is mutually exclusive. In fact, competition experiments revealed that eRF3 is not able to dissociate a preformed Dbp5-eRF1 complex [16]. In this way, the interaction of eRF1 and eRF3 is prevented until eRF1 was properly positioned. This is most important to prevent a premature contact, because as soon as these proteins interact with each other, eRF3 has a higher affinity to GTP, which instantly triggers GTP hydrolysis and dissociation of eRF1 and eRF3. eRF3-GDP is removed from the termination complex by Hcr1 [16,23,24]. Such a regulatory principle, the shielded delivery of eRF1 by Dbp5, makes sense, when considering the situation in mutants of *DBP5*, in which eRF1 does not bind and is therefore not delivered to the ribosome by the helicase.

3. Mutations in *DBP5* Lead to Termination Readthrough

When Dbp5 is not functional, as shown in several mutants, eRF1 approaches the ribosome on its own and contacts eRF3 before it is properly positioned for termination, resulting in the immediate dissociation of both release factors and translational readthrough [16]. Inefficient termination increases the chance of the incorporation of a near-cognate tRNA and results in ongoing translation and longer proteins (Figure 3) and [16].

In most cases, general readthrough might be problematic for cells, however, tuning readthrough also holds the possibility for regulation. Such a potential regulation is still unclear and not much is known for a possible role of Dbp5. However, for example during stress, Dbp5 localizes to the nuclei of cells [48] and is thus depleted from the cytoplasm. Its absence presumably causes translational readthrough at stop codons, allowing the synthesis of longer polypeptides. This could create proteins with new functions, such as proteins that in their longer form now contain a nuclear localization signal or a degradation signal, which can change their place of function or eliminate this protein function altogether. In multicellular organisms, Dbp5/DDX19 might even be developmentally regulated, e.g., by phosphorylation or other modifications, for such purposes under normal conditions. These aspects certainly need more research for clarification.
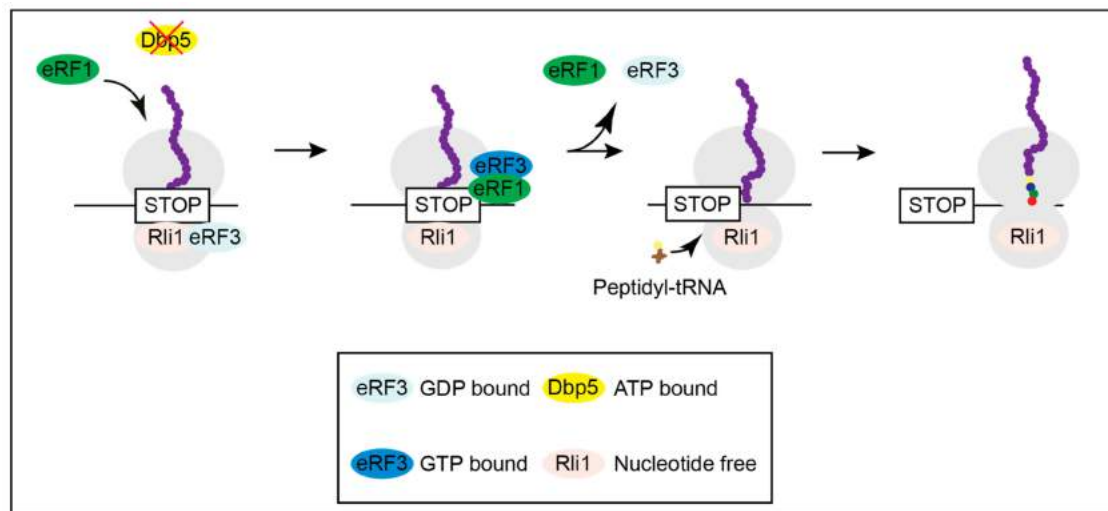
Figure 3. Lack of Dbp5 leads to translational readthrough. Mutations in Dbp5 prevent a shielded entry of eRF1 to the ribosome, resulting in an early contact of eRF1 and eRF3 and their subsequent dissociation. This increases the probability for the incorporation of a near-cognate tRNA and the continuation in translation.

4. Regulatory Principles in Nonsense Mediated Decay (NMD)

For more than 25 years, one major goal has been to understand the mechanisms underlying NMD. Although at first only considered as a cytoplasmic mRNA quality control system, current research has clearly identified its power in regulating the RNA-transcriptome beyond RNA surveillance, e.g., in biological contexts such as development [49,50]. Therefore, it is of particular interest to identify the parameters that in the cells discriminate mRNAs that should be translated from those that should be degraded. Clearly, NMD is linked to inefficient translation termination [51]. However, when and why this can occur is not fully understood. Not only the RNA sequence itself is relevant but also the proteins within the ribonucleoparticle (RNP).

Generally, in mRNA surveillance, a premature termination codon (PTC) is distinguished from a normal one as the trigger for NMD. NMD can only be initiated during translation termination as it requires the decoding of a stop codon by eRF1 and eRF3 [52]. At a PTC, the ATPase and helicase Upf1 interacts with eRF1 and eRF3 to initiate the NMD pathway (Figure 4) and [53,54]. Upf1 is activated by its less abundant co-factors Upf2 and Upf3 [55,56]. These trigger a conformational change in Upf1 to increase its ATPase and Helicase activity, which is initially inhibited by eRF1 and eRF3 [53,57]. In higher eukaryotes SMG1 (and its co-factors SMG8 and SMG9) binds to UPF1 to form the SURF (SMG1 UPF1 Release Factors) complex [58,59]. Then, the helicase DHX34 promotes the association with UPF2 and UPF3 to form the DECID (decay inducing) complex [60]. Further, SMG1 phosphorylates UPF1 [61], which is considered to be the step that commits an mRNA to NMD [62]. In *S. cerevisiae* phosphorylation of Upf1 was also described, but there the relevance is not clear [63,64]. After formation of the Upf1-2,3 complex (or DECID complex in higher eukaryotes), Upf1 triggers rapid mRNA degradation.

Of course, the NMD pathway should only be initiated when translation termination occurs prematurely. Several models have been proposed to describe the differentiation of a normal stop codon and a PTC. The two main models are the exon junction complex (EJC) induced NMD and the long 3′UTR model [65]. The former is based on the position of the EJC, a complex that is placed during splicing near the exon–exon junction [66]. Stop codons typically occur in the last exon and have no downstream EJC in the 3′UTR. If, however, translation is terminated at a stop codon that is followed by an EJC, the complex strongly promotes NMD [67–69]. It serves as a binding platform for UPF2 and UPF3 and, if downstream of a termination event, promotes their interaction with the SURF complex [58,70,71] The long 3′UTR model, which is more relevant in yeast but also described in higher eukaryotes, focuses on the distance between a stop codon and the poly(A) tail. A normal stop codon

is typically in proximity to the poly(A) tail and the poly(A) binding protein Pab1 (PABP in human). Pab1 interacts with eRF3, promotes regular termination and prevents NMD [51,72,73]. At a PTC the distance to Pab1 is increased, which allows the formation of the Upf1-2,3 complex and the initiation of NMD. Further, Upf1 ubiquitously binds any mRNA and is displaced by the translating ribosome. As a consequence, Upf1 stays bound to the 3'UTR. It was suggested that longer 3'UTRs have more bound Upf1 molecules, which might promote the Upf1 binding to the terminating ribosome [74,75]. In addition to these two models, it was found that the sequence downstream (and in a few cases upstream) of the stop codon further promotes or inhibits NMD [76–79].
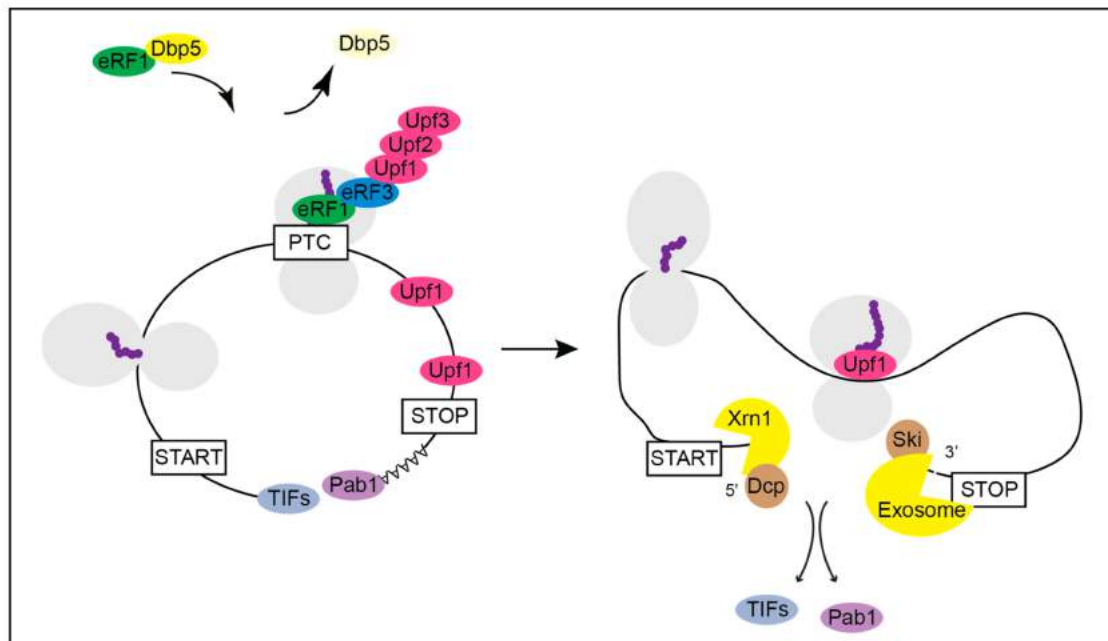

Figure 4. Termination at a premature termination codon (PTC) and the subsequent initiation of the nonsense mediated decay (NMD) of the mRNA. Under normal conditions yeast Dbp5 promotes the stop codon recognition by eRF1 and eRF3 also at a PTC. However, when recognized as premature by the NMD machinery, Upf1 binds to the release factors and assembles the Upf1-2,3 complex. Consequently, further translation is inhibited, and downstream factors are recruited to promote rapid mRNA decay. The decapping factors Dcp1 and Dcp2 and Xrn1 act from 5' to 3' and the Ski complex and the exosome degrade the PTC-containing mRNA from 3' into 5' direction.

Although there is growing insight into the mechanisms by which NMD is initiated and degrades transcripts, there are still many open questions. It is for instance unknown how PTC-detection is signaled to the ends of the transcript, where degradation is initiated. In this context, the mRNP conformation during NMD is presumably important but not yet understood. For the EJC induced NMD in humans, it was described that Upf1 interacts with the cap binding complex (CBC) in a process where the mRNA might fold back so that the Upf1 complex at the PTC can reach the 5' end [80,81]. In yeast NMD, however, where the 3' UTR length is the main determinant, the CBC is dispensable [82]. Moreover, NMD was shown to occur also on transcripts in which CBC has dissociated and instead the cap binding protein and translation initiation factor eIF4E has bound [76,83]. Presumably several proteins are involved in the required mRNP remodeling for NMD, but this is to date almost completely unknown.

In the EJC independent initiation of NMD, it is unclear how Upf2 and Upf3 join Upf1. In yeast, it is assumed that they must be specifically recruited to NMD targets, due to their low cellular abundance. However, their association with translated mRNPs is Upf1 independent [84], suggesting an involvement of other currently unknown NMD factors. The sequences that affect NMD, and proteins

that bind to these sequences are poorly understood, but these appear to affect both the EJC induced NMD and long 3' UTR induced NMD in yeast as well as in metazoans [76–79].

NMD of different targets presumably requires a different subset of proteins; even the co-factor Upf2 is not required for all NMD [65,67]. Which proteins are functioning in which instances of NMD and how this is regulated are still very hazy matters. Future research will have to identify new NMD factors and sort out their functions on different NMD targets. In particular research in simple organisms such as baker's yeast can help to untangle the underlying basic principles of NMD.

5. Termination Readthrough and Nonsense Mediated Decay (NMD)

Another aspect is important in this regard. Many inherited human diseases and cancer types are caused by the loss of a specific protein due to the elimination of its transcripts that contained a premature termination codon (PTC) [85–87]. In fact, one-third of inherited human diseases are due to PTCs, and such premature stops in translation account for up to 70% of all genetic disorders [88–90]. Such PTC containing transcripts can result from, e.g., splicing defects or mutations in the DNA. Usually, such PTC containing mRNAs are recognized and eliminated by nonsense mediated decay, so that the protein is never made. However, some PTC-containing transcripts escape NMD and produce truncated, dominant, negatively operating gene products that can also cause diseases [85,91].

It was observed that overexpressing Upf1 alleviates the negative effects in a TDP-43 induced rat model of the neurodegenerative disease ALS [92]. Thus, promoting NMD in such cases might be a valuable therapeutic approach. However, in some cases, the remaining functional allele is haploinsufficient, and NMD cannot regain the functional protein of a PTC containing transcript [93]. In these cases, readthrough of the PTC may recover the loss of function. When a PTC is read through, a near cognate tRNA is inserted at the stop codon, and translation continues until it is terminated by the correct termination codon [94]. Hence, the produced protein has, if at all, only one amino acid exchange and can, at least partially, recover the loss of function. Indeed, for several targets it was reported that nonsense suppressors increase the amount of functional protein [95]. Such an approach is also potentially interesting for cancer research as some types of cancer carry nonsense mutations in tumor suppressors [96–98], which may regain function through readthrough. Generally, nonsense suppression as a therapeutic approach is encouraged by the fact that PTCs are more susceptible to read through than normal stop codons, presumably due to reduced termination efficiency at a PTC [51,95]. Research with suppression agents revealed that global translation is unaffected at concentrations that cause read through at PTCs [95,99,100]. This does not preclude, however, the possibility of side effects of nonsense suppression therapy as NMD is also involved in regulatory mechanisms that include wild typical PTC-containing mRNAs [101].

Attempts were started to downregulate NMD, allowing the production of some of the full-length protein as treatment for diseases. Such drugs could act as nonsense suppressors (e.g., Ataluren or RTC13). These compounds can be natural or synthetic aminoglycosides and nonaminoglycosides [100,102–106]. Interestingly, several compounds have already been identified to inhibit the helicase and ATPase activities of the Plasmodium falciparum Dbp5/DDX19 homolog PfD66 [107]. Although promising, a great concern with these compounds is that they lack drug target specificity. Moreover, the many gaps and weaknesses in current NMD models urge for further research of the mechanisms and participating factors in NMD.

Further, different NMD targets do not respond similarly to one nonsense suppressor. Ataluren (also called PTC124), a therapeutic for Duchenne muscular dystrophy, was not approved for Cystic Fibrosis, as clinical trials did not show sufficient improvement [108,109]. This highlights the necessity to investigate further and for different approaches in nonsense suppression. Here Dbp5/DDX19 might serve as an interesting new drug target to fine tune translation read through, possibly in conjunction with other drugs in lower doses (Figure 5).
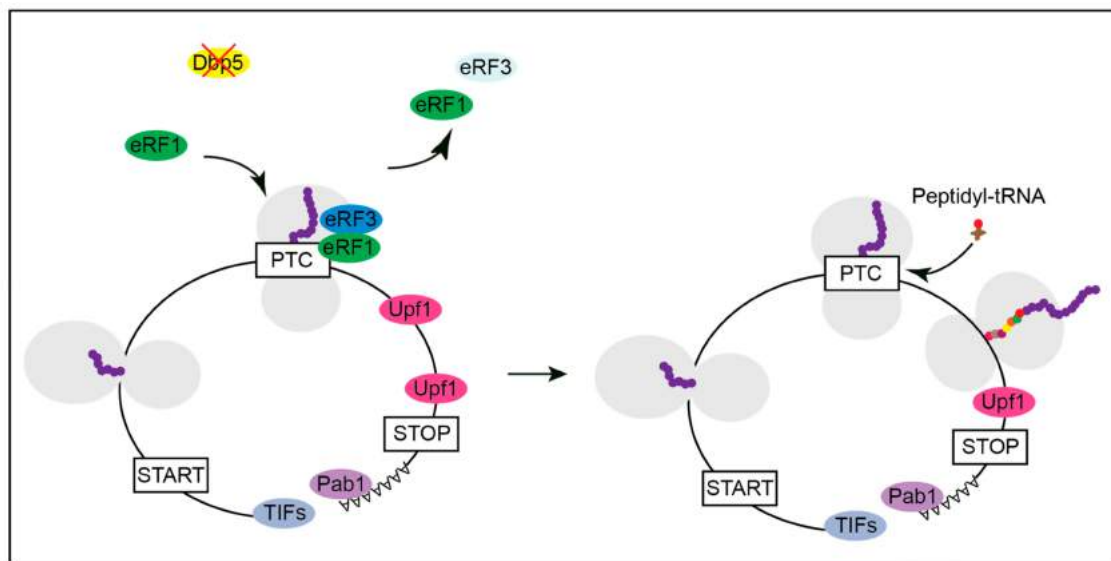
Figure 5. Affecting the availability of functional Dbp5 might generate full length proteins from PTC containing mRNAs. With a reduced function of Dbp5, the stop codon recognition of eRF1 and eRF3 is impaired. If the PTC is not recognized as a stop codon, a near cognate peptidyl-tRNA enters the ribosome, and translation elongation continues. A normal stop codon is less susceptible to translational readthrough than a PTC, presumably due to additional factors that promote translation termination, such as Pab1. Hence, there is a high probability that translation can terminate at the correct stop codon rather than at the PTC. This will most likely generate a full-length protein with only one amino acid exchange instead of a truncated polypeptide.

Strategies to repress NMD for correct protein production are one hope for therapy. Understanding the full mechanistic details of translation termination and NMD in the cellular context will be important and necessary to develop more sophisticated therapies for PTC-caused diseases.

Conflicts of Interest: The authors declare no conflict of interest.

References

1. Doma, M.K.; Parker, R. RNA quality control in eukaryotes. *Cell* **2007**, *131*, 660–668. [CrossRef] [PubMed]
2. Soheilypour, M.; Mofrad, M.R.K. Quality control of mRNAs at the entry of the nuclear pore: Cooperation in a complex molecular system. *Nucleus* **2018**, *9*, 202–211. [CrossRef] [PubMed]
3. Zander, G.; Krebber, H. Quick or quality? How mRNA escapes nuclear quality control during stress. *RNA Biol.* **2017**, *14*, 1642–1648. [CrossRef] [PubMed]
4. Lykke-Andersen, J.; Bennett, E.J. Protecting the proteome: Eukaryotic cotranslational quality control pathways. *J. Cell Biol.* **2014**, *204*, 467–476. [CrossRef] [PubMed]
5. Mühlemann, O.; Jensen, T.H. mRNP quality control goes regulatory. *Trends Genet.* **2012**, *28*, 70–77. [CrossRef] [PubMed]
6. Dever, T.E.; Green, R. The elongation, termination, and recycling phases of translation in eukaryotes. *Cold Spring Harb. Perspect. Biol.* **2012**, *4*, a013706. [CrossRef]
7. Dever, T.E.; Kinzy, T.G.; Pavitt, G.D. Mechanism and Regulation of Protein Synthesis in Saccharomyces cerevisiae. *Genetics* **2016**, *203*, 65–107. [CrossRef]
8. Sonenberg, N.; Hinnebusch, A.G. Regulation of translation initiation in eukaryotes: Mechanisms and biological targets. *Cell* **2009**, *136*, 731–745. [CrossRef]
9. Jackson, R.J.; Hellen, C.U.; Pestova, T.V. Termination and post-termination events in eukaryotic translation. *Adv. Protein Chem. Struct. Biol.* **2012**, *86*, 45–93.

10. Bertram, G.; Bell, H.A.; Ritchie, D.W.; Fullerton, G.; Stansfield, I. Terminating eukaryote translation: Domain 1 of release factor eRF1 functions in stop codon recognition. *RNA* **2000**, *6*, 1236–1247.

11. Blanchet, S.; Rowe, M.; Von der Haar, T.; Fabret, C.; Demais, S.; Howard, M.J.; Namy, O. New insights into stop codon recognition by eRF1. *Nucleic Acids Res.* **2015**, *43*, 3298–3308. [CrossRef] [PubMed]

12. Conard, S.E.; Buckley, J.; Dang, M.; Bedwell, G.J.; Carter, R.L.; Khass, M.; Bedwell, D.M. Identification of eRF1 residues that play critical and complementary roles in stop codon recognition. *RNA* **2012**, *18*, 1210–1221. [PubMed]

13. Heurgue-Hamard, V.; Champ, S.; Mora, L.; Merkulova-Rainon, T.; Kisselev, L.L.; Buckingham, R.H. The glutamine residue of the conserved GGQ motif in Saccharomyces cerevisiae release factor eRF1 is methylated by the product of the YDR140w gene. *J. Biol. Chem.* **2005**, *280*, 2439–2445. [PubMed]

14. Eyler, D.E.; Green, R. Distinct response of yeast ribosomes to a miscoding event during translation. *RNA* **2011**, *17*, 925–932.

15. Salas-Marco, J.; Bedwell, D.M. GTP hydrolysis by eRF3 facilitates stop codon decoding during eukaryotic translation termination. *Mol. Cell. Biol.* **2004**, *24*, 7769–7778. [CrossRef]

16. Beissel, C.; Neumann, B.; Uhse, S.; Hampe, I.; Karki, P.; Krebber, H. Translation termination depends on the sequential ribosomal entry of eRF1 and eRF3. *Nucleic Acids Res.* **2019**, *47*, 4798–4813. [CrossRef]

17. Brown, A.; Shao, S.; Murray, J.; Hegde, R.S.; Ramakrishnan, V. Structural basis for stop codon recognition in eukaryotes. *Nature* **2015**, *524*, 493–496. [CrossRef]

18. Khoshnevis, S.; Gross, T.; Rotte, C.; Baierlein, C.; Ficner, R.; Krebber, H. The iron-sulphur protein RNase L inhibitor functions in translation termination. *EMBO Rep.* **2010**, *11*, 214–219.

19. Preis, A.; Heuer, A.; Barrio-Garcia, C.; Hauser, A.; Eyler, D.E.; Berninghausen, O.; Green, R.; Becker, T.; Beckmann, R. Cryoelectron microscopic structures of eukaryotic translation termination complexes containing eRF1-eRF3 or eRF1-ABCE1. *Cell Rep.* **2014**, *8*, 59–65. [CrossRef]

20. Pisarev, A.V.; Skabkin, M.A.; Pisareva, V.P.; Skabkina, O.V.; Rakotondrafara, A.M.; Hentze, M.W.; Hellen, C.U.; Pestova, T.V. The role of ABCE1 in eukaryotic posttermination ribosomal recycling. *Mol. Cell* **2010**, *37*, 196–210.

21. Schuller, A.P.; Wu, C.C.; Dever, T.E.; Buskirk, A.R.; Green, R. eIF5A Functions Globally in Translation Elongation and Termination. *Mol. Cell* **2017**, *66*, 194–205. [CrossRef] [PubMed]

22. Urakov, V.N.; Mitkevich, O.V.; Safenkova, I.V.; Ter-Avanesyan, M.D. Ribosome-bound Pub1 modulates stop codon decoding during translation termination in yeast. *FEBS J.* **2017**, *284*, 1914–1930. [CrossRef] [PubMed]

23. Beznoskova, P.; Cuchalova, L.; Wagner, S.; Shoemaker, C.J.; Gunisova, S.; von der Haar, T.; Valasek, L.S. Translation initiation factors eIF3 and HCR1 control translation termination and stop codon read-through in yeast cells. *PLoS Genet.* **2013**, *9*, e1003962. [CrossRef] [PubMed]

24. Beznoskova, P.; Wagner, S.; Jansen, M.E.; von der Haar, T.; Valasek, L.S. Translation initiation factor eIF3 promotes programmed stop codon readthrough. *Nucleic Acids Res.* **2015**, *43*, 5099–5111. [CrossRef]

25. Gross, T.; Siepmann, A.; Sturm, D.; Windgassen, M.; Scarcelli, J.J.; Seedorf, M.; Cole, C.N.; Krebber, H. The DEAD-box RNA helicase Dbp5 functions in translation termination. *Science* **2007**, *315*, 646–649. [CrossRef]

26. Folkmann, A.W.; Noble, K.N.; Cole, C.N.; Wente, S.R. Dbp5, Gle1-IP6 and Nup159: A working model for mRNP export. *Nucleus* **2011**, *2*, 540–548. [CrossRef]

27. Snay-Hodge, C.A.; Colot, H.V.; Goldstein, A.L.; Cole, C.N. Dbp5p/Rat8p is a yeast nuclear pore-associated DEAD-box protein essential for RNA export. *EMBO J.* **1998**, *17*, 2663–2676. [CrossRef]

28. Stewart, M. Nuclear export of mRNA. *Trends Biochem. Sci.* **2010**, *35*, 609–617. [CrossRef]

29. Tieg, B.; Krebber, H. Dbp5—From nuclear export to translation. *Biochim. Biophys. Acta* **2013**, *1829*, 791–798.

30. Tseng, S.S.; Weaver, P.L.; Liu, Y.; Hitomi, M.; Tartakoff, A.M.; Chang, T.H. Dbp5p, a cytosolic RNA helicase, is required for poly(A)+ RNA export. *EMBO J.* **1998**, *17*, 2651–2662.

31. Fairman-Williams, M.E.; Guenther, U.P.; Jankowsky, E. SF1 and SF2 helicases: Family matters. *Curr. Opin. Struct. Biol.* **2010**, *20*, 313–324. [CrossRef] [PubMed]

32. Zhao, J.; Jin, S.B.; Bjorkroth, B.; Wieslander, L.; Daneholt, B. The mRNA export factor Dbp5 is associated with Balbiani ring mRNP from gene to cytoplasm. *EMBO J.* **2002**, *21*, 1177–1187. [CrossRef]

33. Lari, A.; Arul Nambi Rajan, A.; Sandhu, R.; Reiter, T.; Montpetit, R.; Young, B.P.; Loewen, C.J.; Montpetit, B. A nuclear role for the DEAD-box protein Dbp5 in tRNA export. *Elife* **2019**, *8*, e48410. [CrossRef] [PubMed]

34. Linder, P.; Jankowsky, E. From unwinding to clamping—The DEAD box RNA helicase family. *Nat. Rev.* **2011**, *12*, 505–516.

35. Collins, R.; Karlberg, T.; Lehtio, L.; Schutz, P.; van den Berg, S.; Dahlgren, L.G.; Hammarstrom, M.; Weigelt, J.; Schuler, H. The DEXD/H-box RNA helicase DDX19 is regulated by an {alpha}-helical switch. *J. Biol. Chem.* **2009**, *284*, 10296–10300. [PubMed]

36. Lund, M.K.; Guthrie, C. The DEAD-box protein Dbp5p is required to dissociate Mex67p from exported mRNPs at the nuclear rim. *Mol. Cell* **2005**, *20*, 645–651. [PubMed]

37. Schmitt, C.; von Kobbe, C.; Bachi, A.; Pante, N.; Rodrigues, J.P.; Boscheron, C.; Rigaut, G.; Wilm, M.; Seraphin, B.; Carmo-Fonseca, M.; et al. Dbp5, a DEAD-box protein required for mRNA export, is recruited to the cytoplasmic fibrils of nuclear pore complex via a conserved interaction with CAN/Nup159p. *EMBO J.* **1999**, *18*, 4332–4347. [CrossRef]

38. Weirich, C.S.; Erzberger, J.P.; Flick, J.S.; Berger, J.M.; Thorner, J.; Weis, K. Activation of the DExD/H-box protein Dbp5 by the nuclear-pore protein Gle1 and its coactivator InsP6 is required for mRNA export. *Nat. Cell Biol.* **2006**, *8*, 668–676.

39. Alcazar-Roman, A.R.; Tran, E.J.; Guo, S.; Wente, S.R. Inositol hexakisphosphate and Gle1 activate the DEAD-box protein Dbp5 for nuclear mRNA export. *Nat. Cell Biol.* **2006**, *8*, 711–716.

40. Alcazar-Roman, A.R.; Bolger, T.A.; Wente, S.R. Control of mRNA export and translation termination by inositol hexakisphosphate requires specific interaction with Gle1. *J. Biol. Chem.* **2010**, *285*, 16683–16692.

41. Montpetit, B.; Thomsen, N.D.; Helmke, K.J.; Seeliger, M.A.; Berger, J.M.; Weis, K. A conserved mechanism of DEAD-box ATPase activation by nucleoporins and InsP6 in mRNA export. *Nature* **2011**, *472*, 238–242. [CrossRef] [PubMed]

42. Tran, E.J.; Zhou, Y.; Corbett, A.H.; Wente, S.R. The DEAD-box protein Dbp5 controls mRNA export by triggering specific RNA:protein remodeling events. *Mol. Cell* **2007**, *28*, 850–859. [CrossRef] [PubMed]

43. Bolger, T.A.; Wente, S.R. Gle1 is a multifunctional DEAD-box protein regulator that modulates Ded1 in translation initiation. *J. Biol. Chem.* **2011**, *286*, 39750–39759. [CrossRef] [PubMed]

44. Noble, K.N.; Tran, E.J.; Alcazar-Roman, A.R.; Hodge, C.A.; Cole, C.N.; Wente, S.R. The Dbp5 cycle at the nuclear pore complex during mRNA export II: Nucleotide cycling and mRNP remodeling by Dbp5 are controlled by Nup159 and Gle1. *Genes Dev.* **2011**, *25*, 1065–1077. [CrossRef]

45. Neumann, B.; Wu, H.; Hackmann, A.; Krebber, H. Nuclear Export of Pre-Ribosomal Subunits Requires Dbp5, but Not as an RNA-Helicase as for mRNA Export. *PLoS ONE* **2016**, *11*, e0149571. [CrossRef] [PubMed]

46. Bolger, T.A.; Folkmann, A.W.; Tran, E.J.; Wente, S.R. The mRNA export factor Gle1 and inositol hexakisphosphate regulate distinct stages of translation. *Cell* **2008**, *134*, 624–633. [CrossRef] [PubMed]

47. Mikhailova, T.; Shuvalova, E.; Ivanov, A.; Susorov, D.; Shuvalov, A.; Kolosov, P.M.; Alkalaeva, E. RNA helicase DDX19 stabilizes ribosomal elongation and termination complexes. *Nucleic Acids Res.* **2017**, *45*, 1307–1318. [CrossRef]

48. Takemura, R.; Inoue, Y.; Izawa, S. Stress response in yeast mRNA export factor: Reversible changes in Rat8p localization are caused by ethanol stress but not heat shock. *J. Cell Sci.* **2004**, *117*, 4189–4197. [CrossRef]

49. Nasif, S.; Contu, L.; Muhlemann, O. Beyond quality control: The role of nonsense-mediated mRNA decay (NMD) in regulating gene expression. *Semin. Cell Dev. Biol.* **2018**, *75*, 78–87. [CrossRef]

50. Nickless, A.; Bailis, J.M.; You, Z. Control of gene expression through the nonsense-mediated RNA decay pathway. *Cell Biosci.* **2017**, *7*, 26. [CrossRef]

51. Amrani, N.; Ganesan, R.; Kervestin, S.; Mangus, D.A.; Ghosh, S.; Jacobson, A. A faux 3'-UTR promotes aberrant termination and triggers nonsense-mediated mRNA decay. *Nature* **2004**, *432*, 112–118. [CrossRef] [PubMed]

52. Keeling, K.M.; Lanier, J.; Du, M.; Salas-Marco, J.; Gao, L.; Kaenjak-Angeletti, A.; Bedwell, D.M. Leaky termination at premature stop codons antagonizes nonsense-mediated mRNA decay in S. cerevisiae. *RNA* **2004**, *10*, 691–703. [PubMed]

53. Czaplinski, K.; Ruiz-Echevarria, M.J.; Paushkin, S.V.; Han, X.; Weng, Y.; Perlick, H.A.; Dietz, H.C.; Ter-Avanesyan, M.D.; Peltz, S.W. The surveillance complex interacts with the translation release factors to enhance termination and degrade aberrant mRNAs. *Genes Dev.* **1998**, *12*, 1665–1677. [CrossRef] [PubMed]

54. Ivanov, P.V.; Gehring, N.H.; Kunz, J.B.; Hentze, M.W.; Kulozik, A.E. Interactions between UPF1, eRFs, PABP and the exon junction complex suggest an integrated model for mammalian NMD pathways. *EMBO J.* **2008**, *27*, 736–747. [CrossRef]

55. Dehecq, M.; Decourty, L.; Namane, A.; Proux, C.; Kanaan, J.; Le Hir, H.; Jacquier, A.; Saveanu, C. Nonsense-mediated mRNA decay involves two distinct Upf1-bound complexes. *EMBO J.* **2018**, *37*, e99278. [CrossRef]

56. Maquat, L.E.; Serin, G. Nonsense-mediated mRNA decay: Insights into mechanism from the cellular abundance of human Upf1, Upf2, Upf3, and Upf3X proteins. *Cold Spring Symp. Quant. Biol.* **2001**, *66*, 313–320. [CrossRef]

57. Chakrabarti, S.; Jayachandran, U.; Bonneau, F.; Fiorini, F.; Basquin, C.; Domcke, S.; Le Hir, H.; Conti, E. Molecular mechanisms for the RNA-dependent ATPase activity of Upf1 and its regulation by Upf2. *Mol. Cell* **2011**, *41*, 693–703. [CrossRef]

58. Kashima, I.; Yamashita, A.; Izumi, N.; Kataoka, N.; Morishita, R.; Hoshino, S.; Ohno, M.; Dreyfuss, G.; Ohno, S. Binding of a novel SMG-1-Upf1-eRF1-eRF3 complex (SURF) to the exon junction complex triggers Upf1 phosphorylation and nonsense-mediated mRNA decay. *Genes Dev.* **2006**, *20*, 355–367. [CrossRef]

59. Yamashita, A.; Izumi, N.; Kashima, I.; Ohnishi, T.; Saari, B.; Katsuhata, Y.; Muramatsu, R.; Morita, T.; Iwamatsu, A.; Hachiya, T.; et al. SMG-8 and SMG-9, two novel subunits of the SMG-1 complex, regulate remodeling of the mRNA surveillance complex during nonsense-mediated mRNA decay. *Genes Dev.* **2009**, *23*, 1091–1105. [CrossRef]

60. Hug, N.; Caceres, J.F. The RNA helicase DHX34 activates NMD by promoting a transition from the surveillance to the decay-inducing complex. *Cell Rep.* **2014**, *8*, 1845–1856. [CrossRef]

61. Yamashita, A.; Ohnishi, T.; Kashima, I.; Taya, Y.; Ohno, S. Human SMG-1, a novel phosphatidylinositol 3-kinase-related protein kinase, associates with components of the mRNA surveillance complex and is involved in the regulation of nonsense-mediated mRNA decay. *Genes Dev.* **2001**, *15*, 2215–2228. [CrossRef] [PubMed]

62. Kurosaki, T.; Li, W.; Hoque, M.; Popp, M.W.; Ermolenko, D.N.; Tian, B.; Maquat, L.E. A post-translational regulatory switch on UPF1 controls targeted mRNA degradation. *Genes Dev.* **2014**, *28*, 1900–1916. [CrossRef] [PubMed]

63. Lasalde, C.; Rivera, A.V.; Leon, A.J.; Gonzalez-Feliciano, J.A.; Estrella, L.A.; Rodriguez-Cruz, E.N.; Correa, M.E.; Cajigas, I.J.; Bracho, D.P.; Vega, I.E.; et al. Identification and functional analysis of novel phosphorylation sites in the RNA surveillance protein Upf1. *Nucleic Acids Res.* **2014**, *42*, 1916–1929. [CrossRef] [PubMed]

64. Wang, W.; Cajigas, I.J.; Peltz, S.W.; Wilkinson, M.F.; Gonzalez, C.I. Role for Upf2p phosphorylation in Saccharomyces cerevisiae nonsense-mediated mRNA decay. *Mol. Cell. Biol.* **2006**, *26*, 3390–3400. [CrossRef]

65. Kurosaki, T.; Popp, M.W.; Maquat, L.E. Quality and quantity control of gene expression by nonsense-mediated mRNA decay. *Nat. Rev.* **2019**, *20*, 406–420. [CrossRef]

66. Le Hir, H.; Izaurralde, E.; Maquat, L.E.; Moore, M.J. The spliceosome deposits multiple proteins 20–24 nucleotides upstream of mRNA exon-exon junctions. *EMBO J.* **2000**, *19*, 6860–6869. [CrossRef]

67. Gehring, N.H.; Kunz, J.B.; Neu-Yilik, G.; Breit, S.; Viegas, M.H.; Hentze, M.W.; Kulozik, A.E. Exon-junction complex components specify distinct routes of nonsense-mediated mRNA decay with differential cofactor requirements. *Mol. Cell* **2005**, *20*, 65–75. [CrossRef]

68. Lykke-Andersen, J. mRNA quality control: Marking the message for life or death. *Curr. Biol.* **2001**, *11*, 88–91. [CrossRef]

69. Nagy, E.; Maquat, L.E. A rule for termination-codon position within intron-containing genes: When nonsense affects RNA abundance. *Trends Biochem. Sci.* **1998**, *23*, 198–199. [CrossRef]

70. Le Hir, H.; Gatfield, D.; Izaurralde, E.; Moore, M.J. The exon-exon junction complex provides a binding platform for factors involved in mRNA export and nonsense-mediated mRNA decay. *EMBO J.* **2001**, *20*, 4987–4997. [CrossRef]

71. Kim, V.N.; Kataoka, N.; Dreyfuss, G. Role of the nonsense-mediated decay factor hUpf3 in the splicing-dependent exon-exon junction complex. *Science* **2001**, *293*, 1832–1836. [CrossRef]

72. Eberle, A.B.; Stalder, L.; Mathys, H.; Orozco, R.Z.; Muhlemann, O. Posttranscriptional gene regulation by spatial rearrangement of the 3′ untranslated region. *PLoS Biol.* **2008**, *6*, e92. [CrossRef]

73. Ivanov, A.; Mikhailova, T.; Eliseev, B.; Yeramala, L.; Sokolova, E.; Susorov, D.; Shuvalov, A.; Schaffitzel, C.; Alkalaeva, E. PABP enhances release factor recruitment and stop codon recognition during translation termination. *Nucleic Acids Res.* **2016**, *44*, 7766–7776. [CrossRef] [PubMed]

74. Hurt, J.A.; Robertson, A.D.; Burge, C.B. Global analyses of UPF1 binding and function reveal expanded scope of nonsense-mediated mRNA decay. *Genome Res.* **2013**, *23*, 1636–1650. [CrossRef]

75. Kurosaki, T.; Maquat, L.E. Rules that govern UPF1 binding to mRNA 3′ UTRs. *Proc. Natl. Acad. Sci. USA* **2013**, *110*, 3357–3362. [CrossRef] [PubMed]

76. Hoek, T.A.; Khuperkar, D.; Lindeboom, R.G.H.; Sonneveld, S.; Verhagen, B.M.P.; Boersma, S.; Vermeulen, M.; Tanenbaum, M.E. Single-Molecule Imaging Uncovers Rules Governing Nonsense-Mediated mRNA Decay. *Mol. Cell* **2019**, *75*, 324–339. [CrossRef] [PubMed]

77. Peltz, S.W.; Brown, A.H.; Jacobson, A. mRNA destabilization triggered by premature translational termination depends on at least three cis-acting sequence elements and one trans-acting factor. *Genes Dev.* **1993**, *7*, 1737–1754. [CrossRef]

78. Ruiz-Echevarria, M.J.; Gonzalez, C.I.; Peltz, S.W. Identifying the right stop: Determining how the surveillance complex recognizes and degrades an aberrant mRNA. *EMBO J.* **1998**, *17*, 575–589. [CrossRef]

79. Toma, K.G.; Rebbapragada, I.; Durand, S.; Lykke-Andersen, J. Identification of elements in human long 3′ UTRs that inhibit nonsense-mediated decay. *RNA* **2015**, *21*, 887–897.

80. Hosoda, N.; Kim, Y.K.; Lejeune, F.; Maquat, L.E. CBP80 promotes interaction of Upf1 with Upf2 during nonsense-mediated mRNA decay in mammalian cells. *Nat. Struct. Mol. Biol.* **2005**, *12*, 893–901. [CrossRef]

81. Hwang, J.; Sato, H.; Tang, Y.; Matsuda, D.; Maquat, L.E. UPF1 association with the cap-binding protein, CBP80, promotes nonsense-mediated mRNA decay at two distinct steps. *Mol. Cell* **2010**, *39*, 396–409. [CrossRef] [PubMed]

82. Gao, Q.; Das, B.; Sherman, F.; Maquat, L.E. Cap-binding protein 1-mediated and eukaryotic translation initiation factor 4E-mediated pioneer rounds of translation in yeast. *Proc. Natl. Acad. Sci. USA* **2005**, *102*, 4258–4263. [CrossRef] [PubMed]

83. Rufener, S.C.; Muhlemann, O. eIF4E-bound mRNPs are substrates for nonsense-mediated mRNA decay in mammalian cells. *Nat. Struct. Mol. Biol.* **2013**, *20*, 710–717. [CrossRef] [PubMed]

84. Atkin, A.L.; Schenkman, L.R.; Eastham, M.; Dahlseid, J.N.; Lelivelt, M.J.; Culbertson, M.R. Relationship between yeast polyribosomes and Upf proteins required for nonsense mRNA decay. *J. Biol. Chem.* **1997**, *272*, 22163–22172. [CrossRef] [PubMed]

85. Bordeira-Carrico, R.; Pego, A.P.; Santos, M.; Oliveira, C. Cancer syndromes and therapy by stop-codon readthrough. *Trends Mol. Med.* **2012**, *18*, 667–678. [CrossRef] [PubMed]

86. Holbrook, J.A.; Neu-Yilik, G.; Hentze, M.W.; Kulozik, A.E. Nonsense-mediated decay approaches the clinic. *Nat. Genet.* **2004**, *36*, 801–808. [CrossRef] [PubMed]

87. Mort, M.; Ivanov, D.; Cooper, D.N.; Chuzhanova, N.A. A meta-analysis of nonsense mutations causing human genetic disease. *Hum. Mutat.* **2008**, *29*, 1037–1047.

88. Frischmeyer, P.A.; Dietz, H.C. Nonsense-mediated mRNA decay in health and disease. *Hum. Mol. Genet.* **1999**, *8*, 1893–1900.

89. Lee, H.L.; Dougherty, J.P. Pharmaceutical therapies to recode nonsense mutations in inherited diseases. *Pharmacol. Ther.* **2012**, *136*, 227–266.

90. Linde, L.; Kerem, B. Introducing sense into nonsense in treatments of human genetic diseases. *Trends Genet.* **2008**, *24*, 552–563.

91. Keeling, K.M.; Xue, X.; Gunn, G.; Bedwell, D.M. Therapeutics based on stop codon readthrough. *Annu. Rev. Genom. Hum. Genet.* **2014**, *15*, 371–394. [CrossRef] [PubMed]

92. Jackson, K.L.; Dayton, R.D.; Orchard, E.A.; Ju, S.; Ringe, D.; Petsko, G.A.; Maquat, L.E.; Klein, R.L. Preservation of forelimb function by UPF1 gene therapy in a rat model of TDP-43-induced motor paralysis. *Gene Ther.* **2015**, *22*, 20–28. [PubMed]

93. Miller, J.N.; Pearce, D.A. Nonsense-mediated decay in genetic disease: Friend or foe? *Mutat. Res. Rev. Mutat. Res.* **2014**, *762*, 52–64. [CrossRef] [PubMed]

94. Fearon, K.; McClendon, V.; Bonetti, B.; Bedwell, D.M. Premature translation termination mutations are efficiently suppressed in a highly conserved region of yeast Ste6p, a member of the ATP-binding cassette (ABC) transporter family. *J. Biol. Chem.* **1994**, *269*, 17802–17808.

95. Keeling, K.M.; Bedwell, D.M. Suppression of nonsense mutations as a therapeutic approach to treat genetic diseases. *Wiley Interdiscip. Rev. RNA* **2011**, *2*, 837–852. [CrossRef]

96. Anczukow, O.; Ware, M.D.; Buisson, M.; Zetoune, A.B.; Stoppa-Lyonnet, D.; Sinilnikova, O.M.; Mazoyer, S. Does the nonsense-mediated mRNA decay mechanism prevent the synthesis of truncated BRCA1, CHK2, and p53 proteins? *Hum. Mutat.* **2008**, *29*, 65–73.

97. Pinyol, M.; Bea, S.; Pla, L.; Ribrag, V.; Bosq, J.; Rosenwald, A.; Campo, E.; Jares, P. Inactivation of RB1 in mantle-cell lymphoma detected by nonsense-mediated mRNA decay pathway inhibition and microarray analysis. *Blood* **2007**, *109*, 5422–5429. [CrossRef]

98. Ware, M.D.; DeSilva, D.; Sinilnikova, O.M.; Stoppa-Lyonnet, D.; Tavtigian, S.V.; Mazoyer, S. Does nonsense-mediated mRNA decay explain the ovarian cancer cluster region of the BRCA2 gene? *Oncogene* **2006**, *25*, 323–328. [CrossRef]

99. Chernikov, V.G.; Terekhov, S.M.; Krokhina, T.B.; Shishkin, S.S.; Smirnova, T.D.; Kalashnikova, E.A.; Adnoral, N.V.; Rebrov, L.B.; Denisov-Nikol'skii, Y.I.; Bykov, V.A. Comparison of cytotoxicity of aminoglycoside antibiotics using a panel cellular biotest system. *Bull. Exp. Biol. Med.* **2003**, *135*, 103–105.

100. Du, L.; Damoiseaux, R.; Nahas, S.; Gao, K.; Hu, H.; Pollard, J.M.; Goldstine, J.; Jung, M.E.; Henning, S.M.; Bertoni, C.; et al. Nonaminoglycoside compounds induce readthrough of nonsense mutations. *J. Exp. Med.* **2009**, *206*, 2285–2297. [CrossRef]

101. Lykke-Andersen, S.; Jensen, T.H. Nonsense-mediated mRNA decay: An intricate machinery that shapes transcriptomes. *Nat. Rev.* **2015**, *16*, 665–677. [CrossRef] [PubMed]

102. Du, M.; Liu, X.; Welch, E.M.; Hirawat, S.; Peltz, S.W.; Bedwell, D.M. PTC124 is an orally bioavailable compound that promotes suppression of the human CFTR-G542X nonsense allele in a CF mouse model. *Proc. Natl. Acad. Sci. USA* **2008**, *105*, 2064–2069. [CrossRef] [PubMed]

103. Gonzalez-Hilarion, S.; Beghyn, T.; Jia, J.; Debreuck, N.; Berte, G.; Mamchaoui, K.; Mouly, V.; Gruenert, D.C.; Deprez, B.; Lejeune, F. Rescue of nonsense mutations by amlexanox in human cells. *Orphanet J. Rare Dis.* **2012**, *7*, 58. [CrossRef] [PubMed]

104. Nakamura, K.; Du, L.; Tunuguntla, R.; Fike, F.; Cavalieri, S.; Morio, T.; Mizutani, S.; Brusco, A.; Gatti, R.A. Functional characterization and targeted correction of ATM mutations identified in Japanese patients with ataxia-telangiectasia. *Hum. Mutat.* **2012**, *33*, 198–208. [CrossRef]

105. Shalev, M.; Baasov, T. When Proteins Start to Make Sense: Fine-tuning Aminoglycosides for PTC Suppression Therapy. *Medchemcomm* **2014**, *5*, 1092–1105. [CrossRef]

106. Welch, E.M.; Barton, E.R.; Zhuo, J.; Tomizawa, Y.; Friesen, W.J.; Trifillis, P.; Paushkin, S.; Patel, M.; Trotta, C.R.; Hwang, S.; et al. PTC124 targets genetic disorders caused by nonsense mutations. *Nature* **2007**, *447*, 87–91. [CrossRef]

107. Mehta, J.; Tuteja, R. Inhibition of unwinding and ATPase activities of Plasmodium falciparum Dbp5/DDX19 homolog. *Commun. Integr. Biol.* **2011**, *4*, 299–303.

108. Aslam, A.A.; Higgins, C.; Sinha, I.P.; Southern, K.W. Ataluren and similar compounds (specific therapies for premature termination codon class I mutations) for cystic fibrosis. *Cochrane Database Syst. Rev.* **2017**. [CrossRef]

109. DeFrancesco, L. Drug pipeline: 1Q17. *Nat. Biotechnol.* **2017**, *35*, 400. [CrossRef]